Lateral extrusion and exhumation of orogenic crust during indentation by rigid Adriatic continental lithosphere – tectonic evolution of the eastern Tauern Window (Eastern Alps, Austria)

Kumulative Dissertation

von

Andreas Scharf

Zur

Erlangung des Doktorgrades der Naturwissenschaften

im Fachbereich Geowissenschaften

an der

Freien Universität Berlin

Freie Universität Berlin

Berlin, Januar 2013

Diese Arbeit wurde von dem Promotionsausschuss des Fachbereiches Geowissenschaften am 08. November 2010 genehmigt.

……

Prof. Dr. Mark R. Handy (Erstgutachter)
Freie Universität Berlin

Prof. Dr. Roland Oberhänsli (Zweitgutachter)
Universität Potsdam

Die Disputation erfolgte am 10.05.2013

Erklärung

Hiermit erkläre ich, Andreas Scharf, dass diese Arbeit ausschließlich auf Grundlage der angegebenen Hilfsmittel und Hilfen selbstständig von mir verfasst wurde. Diese Arbeit wurde nicht in einem früheren Promotionsverfahren eingereicht.

Berlin, den 7. Januar 2013

Andreas Scharf

Zusammenfassung

Das östliche Ende des Tauern Fensters besteht aus einem paläogenen Deckenstapel, welcher im Miozän senkrecht zum Orogen verkürzt wurde und gleichzeitig parallel zum Orogen nach Osten extrudierte. Diese Exhumierungsstruktur wird als Katschberg Shear Zone System (KSZS) bezeichnet. Das bedeutenden Scherzonensystem ist gekennzeichnet durch einen 5 km breiten Gürtel aus amphibolit- bis obere grünschieferfaziellen Myloniten, welche im zentralen Bereich der KSZS (die Katschberg Normal Fault, KNF) moderat bis flach nach Ost bis Südost abtauchen. Die NNO-SSW streichende KNF kurvt nach Norden und Süden parallel zu dem Europäischen Gneisdom des Tauern Fensters ab. Die Hauptfoliation entlang der beiden orogen-parallelen Äste versteilt sich mit dextralen (im nördlichen Ast) und sinistralen (im südlichen Ast) Schersinnindikatoren. Weiterhin werden die zwei Äste der KSZS als „stretching faults“ interpretiert. Der Versatz der stretching faults nimmt zu ihrem westlichen Ende hin ab. Die größte tektonische Ausdünnung wurde im südlichen Bereich der KNF ermittelt, dabei ist der vertikale- und horizontale Versatz 13.5 beziehungsweise 26 km.

Die Miozäne adriatischen Indentation führte zu einer Fragmentierung der Austroalpinen Einheiten südlich des Tauern Fensters und nördlich der Periadriatischen Störung, in zwei Blöcke: Den Rieserferner Block westlich der Zwischenbergen-Wöllatratten-Drau (ZWD) Störung und den Drau-Möll Block östlich dieser Störung. Der Drau-Möll Block hat einen zusätzlichen 12 km nordwärts-gerichteten horizontalen Versatz erfahren und ist der Auslöser für die ausgeprägten Entwicklung des KSZS.

Ramanmikrospektroskopie an organischem Material (RSCM) wurde angewendet um die Höchsttemperaturen der Gesteine im Arbeitsgebiet zu ermitteln. Die große Probenanzahl (200 Proben) ermöglichte ein Vergleich von vier verschiedenen Höchsttemperaturkalibrierungen. Zwei der Kalibrierungen (Beyssac et al. 2002b und Aoya et al. 2010, Kalibration d in Tabelle 3.1) zeigen überzeugende Ergebnisse im Vergleich mit Höchsttemperaturbestimmungen durch Mineralparagenesen aus dem Untersuchungsgebiet. Alpidische Höchsttemperaturen im Kern der Subpenninischen Einheiten des Östlichen Tauern Subdoms (ETD) lagen bei ca. 612° C. Am Rand des Subdomes hin zu dem Kontakt mit den Penninischen Einheiten lagen die Höchsttemperaturen bei ca. 500° C. Die Höchsttemperaturen der Penninischen Einheiten an der Basis der Austroalpinen Einheiten überschreiten nicht 450° C. Zusätzlich zeigen diese neuen RSCM-Daten, dass es wahrscheinlich kein tektonisches hoch-druck Ereignis in den Penninischen Einheiten nördlich, östlich und südlich des ETD gab. Im Gegensatz dazu gibt es Beweise für eine Hochdruckmetamorphose in den Penninischen Einheiten im Großglockner Gebiet, westlich des ETD. Das Muster von Höchsttemperaturkonturen in den Penninischen Einheiten nördlich des ETD ist schräg zu den Höchsttemperaturkonturen innerhalb des Subdoms und lässt deshalb auf eine unterschiedliche thermische Entwicklung schließen. Weiterhin zeigen die RSCM-Untersuchungen, dass alle Subpenninische Decken des ETD der Oligozänen Barrow-artigen Metamorphose (Tauernkristallisation) ausgesetzt war. Zusätzlich erreichten nur lokale

Bereiche der strukturell tiefsten Penninischen Einheiten am nördlichen und südlichen Ast der KSZS ihre Höchsttemperaturen durch die Tauernkristallisation. Paläogene Höchsttemperaturen in Penninische- und Subpenninische Einheiten entlang des zentralen Bereichs der KSZS, der Katschberg Normal Fault (KNF), wurden nicht von diesen Barrow-artigen Metamorphose überprägt. Die Raman Daten zeigen, dass die Höchsttemperaturkonturen und das Streichen der KNF parallel zueinander sind. Der Feldgradient innerhalb der KNF erreicht Werte von bis zu 70° C/km in dem Bereich mit der größten tektonischen Ausdünnung. In Gebieten die nicht beeinflusst sind von der Miozänen extensionellen Scherung erreicht der Feldgradient Werte von 7-8° C/km.

Weiterhin wurden $^{40}Ar/^{39}Ar$ Laser Ablations Alter an Hellglimmern aus den Subpenninischen- und Penninischen Decken aus der footwall der KSZS bestimmt. Ich interpretiere diese Alter (20-16 Ma) als Alter, wann die Gesteine die Schließtemperatur im $^{40}Ar/^{39}Ar$-System unterschritten haben (400-470° C). Eine mikrostrukturelle Untersuchung dieser Proben zeigt, dass die meiste Bewegung entlang der KSZS älter ist als 17 Ma. Eventuell gab es noch vereinzelt duktile Bewegung entlang der KSZS bis vor ca. 15 Ma. Eine Probe aus den Austroalpine Einheiten wurde analysiert, sie stammt aus der hangingwall der KSZS. Diese Probe unterschritt die Schließtemperatur vom $^{40}Ar/^{39}Ar$-System in der Oberkreide vor ca. 76 Ma.

Der westliche Tauern Subdom (WTD) und der ETD haben eine unterschiedliche Exhumierung erfahren. Die rasche Exhumierung begann im ETD vor 21 Ma oder früher. Im WTD begann die schnelle Exhumierung bei 20 Ma. Die schnelle Abkühlentwicklung beider Tauern Dome ist auch unterschiedlich. Im ETD begann die rasche Abkühlung vor 21 Ma oder früher während die schnelle Abkühlung im WTD vor 18 Ma begann. Es ist noch nicht geklärt wann genau die rasche Exhumierung im ETD begann. Wenn sie älter ist als 21 Ma würde das bedeuten, dass die Indentation von der Adriatischen Mikroplatte in Europa nicht überall gleichzeitig geschah. Indentation würde zuerst im Osten (südlich des ETD's) erfolgen und dann nach Westen (südlich des WTD's) migrieren. Die Indentation südlich des WTD's erfolgte vor ca. 21 Ma.

Ein Grund für eine möglicherweise unterschiedliche Exhumierung/Abkühl Entwicklung beider Tauern Subdome wäre wahrscheinlich in der gegen-den-Uhrzeigersinn verlaufende Rotation von Adria im Vergleich zum stabilen Europa zu finden. Zusätzlich zeigen tomographische Untersuchungen, dass sich die Länge und die Richtung des Europäischen Slabs unterhalb des westlichen bis zentralen Tauern Fensters ändert. Weiterhin ändern sich im selben Bereich des Tauern Fensters die Neogen-deformierten Subpenninischen Einheiten drastisch. Das würde bedeuten dass, Oberflächenstrukturen direkt mit Mantelstrukturen vernetzt sind.

Diese Doktorarbeit unterstützt die These, dass die nordwärts gerichtete Bewegung der Adriatischen Mikroplatte in das stabile Europa, der treibende Motor für die Oligozäne bis Miozäne Aufdomung und der lateralen Extrusion im Tauern Fenster und Teilen der Ostalpen ist. Ost-West streichende Extensionelle Strukturen, ausgelöst durch die ostwärts gerichteten Slab-roll back Subduktion unterhalb der Karpaten, erreichte das Arbeitsgebiet vor ca. 17 Ma. Diese Strukturen

können daher nicht der Auslöser für die Aufdomung und Extension im Tauern Fenster sein. Während dieser Zeit gab es keine oder nur noch geringe Bewegung entlang der KSZS. Eventuell hat diese Ost-West streichende Bewegung die nach Osten gerichtete Entweichung der Ostalpen unterstützt. Diese Interpretation wird gestützt durch verfügbare radiometrische und sedimentäre Alter, eigenen strukturellen Untersuchungen entlang des KSZS, Höchsttemperaturbestimmungen mit Hilfe der RSCM Methode und $^{40}Ar/^{39}Ar$ Laser Ablations Alter Bestimmungen an Hellglimmern.

Abstract

The eastern end of the Tauern Window exposes a Paleogene nappe stack, which became coevally shortened perpendicular to the orogen and extended eastward in the Neogene. Structures related to orogen-parallel extension are referred as being part of the Katschberg Shear Zone System (KSZS). This shear zone system is marked by an up to 5 km wide belt of amphibolite-to-upper-greenschist-facies mylonites which moderately dips towards E-SE in the central part of the KSZS; the so-called Katschberg Normal Fault (KNF). In map view this NNE-SSE striking central segment of the KSZS bends into an orogen-parallel orientation at its northern and southern ends, thereby curving around the gneiss dome of the Tauern Window. Along these two orogen-parallel branches the foliation related to the KSZS becomes steep to subvertical, sense of shearing being dextral (in the north) and sinistral (in the south), respectively. In addition, the two steep dipping branches of the KSZS are interpreted as stretching faults with decreasing amounts of displacement towards their western ends. The greatest tectonic omission is manifested at the southern central part of the shear zone with a vertical throw of c. 13.5 km and a horizontal displacement of c. 26 km.

Miocene Adriatic indentation leads to fragmentation of the Austroalpine units south of the Tauern Window and north of the Periadriatic Fault into two blocks: the Rieserferner Block west of the Zwischenbergen-Wöllatratten-Drau (ZWD) Fault and the Drau-Möll Block east of this fault. This fragmentation contributes to extra 12 km horizontal northward displacement across the eastern end of the Eastern Tauern Subdome north of the Drau-Möll Block that leads to the pronounced development of the KSZS.

To determine peak temperatures in the study area the Raman microspectroscopy on organic matter (RSCM) technique was adopted. The large amount of amount of samples (200) allows comparing four different calibrations. Two of them (Beyssac et al. 2002b and Aoya et al. 2010, calibration d in Table 3.1) yield convincing data, when compared with peak temperatures derived from the observed mineral assemblages. Peak-Alpine thermal conditions of c. 612° C were reached in the core of Subpenninic units of the Eastern Tauern Subdome (ETD), c. 500° C at its rim in contact with the Penninic nappes. Peak temperatures at the contact of the Penninic units with the Austroalpine nappes are ≤ 450° C. Furthermore, the new RSCM data indicate a lack of a high-pressure tectonic event in the Penninic units north, east and south of the ETD. This contrasts with the high-pressure mineral assemblages of the Penninic units in the Grossglockner area, west of the ETD. The oblique pattern of peak temperatures in map view provides evidence for a different thermal evolution of the Penninic nappes with respect to the Subpenninic units within the ETD. In addition, my RSCM investigation reveals that all Subpenninic nappes of the ETD were affected by an Oligocene Barrow-type metamorphism (Tauernkristallisation). Additionally, only minor parts of the structurally lowermost Penninic nappes at the northern and southern branch of the KSZS reached their peak temperature during the aforementioned Tauernkristallisation. Paleogene peak temperatures in Penninic

and Subpenninic nappes along the KNF, where not overprinted by those Barrow-type event. Furthermore, the peak-temperature contours along the KNF are parallel to the striking of the KNF. The field gradient within the KNF attain 70° C/km in the area of greatest tectonic omission, while they only reach 7-8° C/km in areas unaffected by Miocene extensional shearing.

$^{40}Ar/^{39}Ar$ Laser ablation ages on white micas were obtained from the northeastern part of the ETD and the adjacent Penninic units in the footwall of the KSZS. These ages are interpreted to date the time (20-16 Ma) when the rocks passed the closure temperature of the $^{40}Ar/^{39}Ar$ white mica system (400-470° C). Microstructural investigations of these samples clearly indicate that most of the motion along the KSZS did not outlast 17 Ma. Probably, minor displacements occurred until some 15 Ma. Furthermore, one sample is derived from Austroalpine units in the hangingwall of the KSZS and yield Upper Cretaceous ages (76 Ma).

The Western Tauern Subdome (WTD) and the ETD have a different exhumation history. The rapid exhumation in the ETD starts before 21 Ma or earlier. In the WTD the rapid exhumation began at 20 Ma. The rapid cooling development of both Subdoms is different as well. In the ETD the rapid cooling starts at 21 Ma or earlier, whereas the rapid cooling in the WTD starts at 18 Ma. It is not solved when rapid exhumation starts in the ETD, yet. If the exhumation predates 21 Ma, than indentation of the Adriatic microplate would not be coeval. Indentation would start first south of the ETD and then migrates further to the west (e.g., south of the WTD) at around 21 Ma.

My preliminary explanation for a possible different geodynamic evolution of both Tauern Subdoms might be the overall counter-clock wise rotation of Adria with respect to Europe. This happened in Oligocene to Miocene times additionally to the general northward motion of Adria with respect to stable Europe. Therefore areas further to the east (e.g., were the ETD is located) with respect to the rotation pole (beneath the western Po-plain) exhumed earlier than areas further to the west (e.g., were the WTD is located). In addition, tomographic investigations formidable point out a change of length and switch of the European slab polarity beneath the western to central Tauern Window. This coincides at the surface and at the upper crust where the style of Miocene deformed Subpenninic nappes changes. Thus, the expression of the deformed continental crust is directly linked to mantel structures.

The present Ph.D. thesis strongly supports the idea that northward motion and Miocene indentation of the Adriatic microplate is primarily responsible for the Oligocene to Miocene doming and lateral extrusion in the Tauern Window and in parts of the Eastern Alps, rather than the east-ward directed slab roll-back beneath the Carpathians. Extension related tectonics affect the study area at about 17 Ma, i.e. at a time when motion along the KSZS was in its final stages. However, it is important to note that slab roll-back subduction beneath the Carpathians may facilitate the eastward escape of the whole Eastern Alps. This interpretation is analyzed under the light of available radiometric and sedimentary ages, own structural investigations along the KSZS, peak-temperature estimates using the RSCM method and the $^{40}Ar/^{39}Ar$ Laser ablation ages on white micas.

Acknowledgements

This study would not been finished without the help of many co-authors and supporting hands. First of all my supervisors **Prof. Dr. Mark Handy** and **Prof. Dr. Claudio Rosenberg**, the initiators of this thesis and the whole greater Tauern Window project, must be thanked. Prof. Dr. Mark Handy are always welcomed me in his office and home, we spend hundreds of hours with fruitful discussion. Within this study three additional Ph.D. these are involved, the studies of Audrey Bertrand, Silvia Favaro and Susanne Schneider. Always efficient discussions during the four years of studying were essential for the success of our theses. Additional, **Prof. Dr. Stefan Schmid**, who joints the Freie Universität Berlin from 2008 to 2010, is thanked in a very special way! In my eyes, he taught me the most important thing - how to solve complex geological problems in general and never believe anything before it is proven. For the incredible detailed field knowledge and shearing this to me, I would thank **Dr. Ralf Schuster** from the Geologische Bundesanstalt Wien. In addition, Prof. Dr. Roland Oberhänsli, Dr. Martin Ziemann, Dr. Masafumi Sudo, Dr. Martin Timmermann from the Universität Potsdam; Dr. Konrad Hammerschmidt, Prof. Dr. Frank Mattern, Dr. Kamil Ustaszweski, Dr. Ekkehard Scheuber, Dr. Ralf Mielke, Peter Gipper, Friedrich Hawemann from the Freie Universität Berlin, Prof. Dr. Bernhard Fügenschuh from the Univerität Innsbruck and Prof. Dr. Walter Kurz from the Universität Graz are explicit thanked. All of them are specialist in their own field and supports me in every imaginable way. However, without the support of Martina Grundmann (IT-assistance), Anna Giribaldi, Sandra Wollnik (both thin-section preparation) and Christine Fischer (boreholes drilling for the $^{40}Ar/^{39}Ar$ analyses at the Universität Potsdam) I would not been finished. Indeed, I would be busy with preparation of one of the over 300 thin-sections in microprobe quality, right now. An extraordinary thank must be taken into account to all colleagues and friends of the department of sedimentology and tectonics at the Freie Universität Berlin. They improved my non-Tauern Window-knowledge horizon significant and showed me that there is more than the Tauern Window. All in all, I will never miss the time spend in Berlin, in Potsdam, in the field and during the numerous congresses. This point out to me that to study geology was the best solution I have done ever (with exception of knowing my girlfriend, of course!).

My family and friends gave me always backup during the last years. Therefore, Katharina Hester my fiancé and my parents are thanked in a way I cannot express. Not only because of the financial thinks, also the feeling of never be alone and have someone behind yourself is awesome. Unfortunately, my grandmother could not see my ending my thesis. My friends, especially Alexander Groß, Regine Pagel, Lennart Pagel, Franziska Frütsch and Andreas Franz are thanked for the good time we have had.

I will never forget the really good time I had, and that's because of you all. Thanks a lot!!!

Organization of this thesis

Seven chapters, four of them as single manuscripts, which will be published in peer-reviewed journals are the outcome of this cumulative thesis. Three manuscripts (Chapter 2, 3 and 5) are submitted, one manuscripts (Chapter 4) will be submitted soon in Journal of Metamorphic Geology. In Chapter 5 Stefan Schmid is the first author. An outline of all chapters (1-7) will be revealed in the following.

Chapter 1

Introduction

The framework, previous studies, aims, incorporation into other projects and a methodological approach are the scope of this chapter. Finally, a time schedule of this thesis will be presented.

Chapter 2

Modes of orogen-parallel stretching and extensional exhumation in response to microplate indentation and roll-back subduction (Tauern Window, Eastern Alps)

Andreas Scharf, Mark R. Handy, Silvia Favaro, Stefan M. Schmid

Submitted to International Journal of Earth Science. The original publication is available at www.springerlink.com.

This chapter detailed describes the ductile and brittle structures at the eastern end of the Eastern Tauern Subdome, especially along the Katschberg Shear Zone System (KSZS). This includes the Neogene motion along this shear zone system. Metamorphic conditions and timing of deformation in the study are shown as well. Additional, the kinematic partitioning between folding and faulting including a geodynamic evolution of the eastern Tauern Window are discussed in this chapter. Structural and available geochronological data are investigated with respect to northward Adriatic indentation and eastward Carpathian slab roll-back subduction. Finally, a model of the geodynamic evolution of the whole Eastern Alps including adjacent areas is presented.

The first author (Andreas Scharf) carried out by extensive fieldwork the structures at the eastern end of the Tauern Window, usefully attended by the second (Mark Handy) and fourth (Stefan Schmid) authors. The metamorphic and structural conditions in and around the Tauern Window, including the concept of stretching faults and fragmentation of the Adriatic microplate, were carried out by all authors during progress work and compilation from the literature. The model of the

geodynamic evolution of the Eastern Alps (Fig. 2.11) were introduced by the second author (Mark Handy) and assisted by all authors. Finally, the second and forth authors (Mark Handy and Stefan Schmid) substantially helped writing of this manuscript, they leading the discussions and they draws the initial stage of figures 2.9 and 2.11. The first author (Andreas Scharf) draw most of the figures, significant helped by all other authors (especially by Mark Handy).

Chapter 3

Peak temperature patterns of accretion, subduction and collision preserved in the eastern subdome of the Tauern Window (Eastern European Alps) – A study with Raman microspectroscopy on carbonaceous material (RSCM)

Andreas Scharf, Mark R. Handy, Martin A. Ziemann, Stefan M. Schmid

Submitted to Journal of Metamorphic Geology. The definitive version is available at www.blackwell-synergy.com.

This chapter presents Alpine peak-temperatures estimates using Raman microspectroscopy on carbonaceous material at the eastern end of the Tauern Window. The aims of this chapter are first: Identify the thermal regime by peak-temperature contours in map- and cross-section view in three different fabric domains with respect to their geodynamic evolution of the eastern Tauern Window. These domains a related to Paleogene accretion/nappe stacking, Eocene subduction/exhumation and Early Oligocene Barrow-type thermal overprinting combined with Late Oligocene to Early Miocene coeval doming and lateral extrusion. The difficulty of this technique is an attribution of the peak temperatures with respect to their age; Second: to discuss the comparison between four available peak-temperature calibrations and points out the comparability with mineral assemblages associations in the study area.

The first author (Andreas Scharf) analyzed all samples in the Raman Laboratory at the Universität Potsdam, collected from the study area and wrote a first version of this manuscript. The third author (Martin Ziemann) supervised the analytic treatment and introduced the first author in this method. All authors together developed the discussion and interpretation of the data with respect to their age and tectonic conditions. The second author (Mark Handy) significant improved the manuscript. In addition, the fourth author (Stefan Schmid) enhanced the manuscript by a detailed review. The first author (Andreas Scharf) draw all figures and tables, he was inspired by concepts of the third author and the work of Wiederkehr et al. (2011).

Chapter 4

Thermal evolution from orogenic doming to extensional exhumation - new perspectives from in-situ $^{40}Ar/^{39}Ar$ laser-probe ages of white mica (Tauern Window, Eastern Alps)

Andreas Scharf, Mark R. Handy, Stefan M. Schmid, Masafumi Sudo

Will be submitted in Journal of Metamorphic Geology. The definitive version is available at www.blackwell-synergy.com.

This chapter described $^{40}Ar/^{39}Ar$ Laser ablation dating on white micas with respect to their microstructure at the northeastern end of the Eastern Tauern Subdome and adjacent areas. These new data clearly reveals Early Miocene ages related to cooling below the closure temperature at the eastern end of the Tauern Window and brackets the ending of motion along the Katschberg Shear Zone System. Peak temperature estimates presented in Chapter 3 helps to interpret the obtained ages in light of cooling, formation and deformation.

The first author (Andreas Scharf) analyzed all samples in the $^{40}Ar/^{39}Ar$ Laboratory at the Universität Potsdam and was introduced and supervised by the fourth author (Masafumi Sudo). This author helps writing the section about the $^{40}Ar/^{39}Ar$ Laser ablation method. The first-author wrote a first version of this manuscript and drew all figures and tables. The third author (Stefan Schmid) revised the manuscript and substantially improved it.

Chapter 5

The Tauern Window (Eastern Alps, Austria) – A new tectonic map, cross-sections and teconometamorphic synthesis

Stefan M. Schmid, Andreas Scharf, Mark R. Handy, Claudio L. Rosenberg

Submitted to Swiss Journal of Geosciences. The original publication is available at www.springerlink.com.

This chapter provides the regional and local geology and introduces the tectonic units in and around the Tauern Window. It reveals the Late Alpine Faults and debates the kinematic evolution of the Tauern Window in the framework of the Alps. All these aspects were manifested by a compiled tectonic map, cross sections across of the entire Tauern Window and sketches of the Cenozoic tectonic evolution. To complete this chapter, a tomographic image with respect to slab polarity beneath the greater study area is shown.

The first author (Stefan Schmid) wrote the text and leads the discussion about the drawing of the figures and cross-sections. The second author (Andreas Scharf) draws most of the maps, parts of

the cross sections and compiled the table. The third author (Mark Handy) introduces the sketches of the Cenozoic evolution, whereas the forth author (Claudio Rosenberg) improves this manuscript by constructing cross section along the western Tauern Window by envisage alternatives in the interpretation of the cross sections 1 and 2 of Plate 2. All co-authors significant improved the text.

Chapter 6
Outlook and future work

Resulting on my Ph.D. thesis attached scientific projects could be started. This chapter provides a proposal for five individual studies in and around the Tauern Window, inspired by this thesis. Thus, these projects would help to answer the unsolved questions, left in this Ph.D. thesis.

Chapter 7
Summary and conclusions

This chapter summarizes the main results and conclusion presented in this entire thesis.

Table of content

Chapter 1 **1**

Introduction

1.1 Framework, previous studies, aims and incorporation in related projects 1

1.2 Methological approach 3

1.3 Schedule 4

Chapter 2 **5**

Modes of orogen-parallel stretching and extensional exhumation in response to microplate indentation and roll-back subduction (Tauern Window, Eastern Alps)

Abstract 5

Keywords 7

2.1 Introduction 7

2.2 Tectonic Setting 8

2.3 Katschberg Shear Zone System 10

2.3.1 Ductile shearing the Katschberg Shear Zone System 10

2.3.2 Brittle Faulting 14

2.3.3 Displacement along the KSZS 16

2.4 Metamorphic conditions in the ETD and the timing of Katschberg-related deformation 17

2.4.1 Pressure and temperature conditions 17

2.4.2 Constraints on the ages of exhumation of Tauern subdomes and activity of the KSZS 20

2.5 Strain partitioning between folding, normal faulting and strike-slip faulting in the eastern Tauern Window 24

2.5.1 Coeval folding, normal faulting and stretching 24

2.5.2 The northern and southern branches of the KSZS as stretching faults 24

2.5.3 Faults in the Austroalpine basement and their bearing on indentation of the ETD 25
2.5.4 Comparison with the WTD and strain partitioning at the scale of the entire Tauern Window 27

2.6 Relationship of lateral extrusion to Adria-Europe convergence 29
2.6.1 Timing constraints 29
2.6.2 Kinematics and amount of lateral extrusion during indentation 32

2.7 Summary and implications for the driving forces of lateral extrusion 37

Acknowledgments 38

Chapter 3 **39**

Peak temperature patterns of accretion, subduction and collision preserved in the eastern subdome of the Tauern Window (Eastern European Alps) – A study with Raman microspectroscopy on carbonaceous material (RSCM)

Abstract 39

Keywords 40

3.1 Introduction 40

3.2 Lithologies and structural provenance of the samples 42

3.2.1 Lithologies and sampling strategy 42
3.2.2 Fabric domains sampled 46

3.3 Raman microspectroscopy on carbonaceous material (RSCM) 48
3.3.1 The method 48
3.3.2 Measurement of Raman spectra on carbonaceous material 49
3.3.3 Peak-temperature calibration of Raman spectra on carbonaceous material 50

3.4 Results 51
3.4.1 Contouring of peak temperatures in different fabric domains 51
3.4.2 Domain 1 52
3.4.3 Domain 2 52
3.4.4 Domain 3 53

3.5 Discussion 56
3.5.1 Multiple peak temperatures in a given sample 56
3.5.2 Age constraints for the inferred peak temperatures 56
3.5.3 Interpretation of peak temperatures in a geodynamic context 57

3.6 Conclusions 61
Acknowledgment 62

Chapter 4 **63**

Thermal evolution from orogenic doming to extensional exhumation - new perspectives from in-situ $^{40}Ar/^{39}Ar$ laser-probe ages of white mica (Tauern Window, Eastern Alps)

Abstract 63

Keywords 64

4.1 Introduction 64

4.2 Geological setting 65
4.2.1 Tectonic overview 65
4.2.2 Sample locations 68
4.2.3 Previous $^{40}Ar/^{39}Ar$ dating 68

4.3 The method 69

4.4 Results 69
4.4.1 Sample strategy 69
4.4.2 Geochemistry of white micas 72
4.4.3 $^{40}Ar/^{39}Ar$ dating 73
4.4.4 Relationship between ages and microstructural setting of the analyzed grains 76

4.5 Discussion 79
4.5.1 Errors 79
4.5.2 Interpretation of age data presented in this study 79
4.5.3 Comparison with other radiometric age data from the eastern end of the Tauern Window 82

4.5.4 Exhumation rates 84
4.5.5 Did indentation of the Southern Alps east of the Giudicarie Belt also trigger the exhumation of the Eastern Tauern Window? 85
4.6 Conclusions 86
Acknowledgment 86

Chapter 5 **89**

The Tauern Window (Eastern Alps, Austria) – A new tectonic map, cross-sections and teconometamorphic synthesis

Abstract 89
Keywords 90
5.1 Introduction 90
5.2 Major tectonic units of the Tauern Window and its surroundings 91
5.2.1 Subpenninic nappes of the Venediger Duplex (or Venediger Nappe System) 91
5.2.1.1 Variscan basement 92
5.2.1.2 Permo-Carboniferous intrusions 94
5.2.1.3 Post-Variscan cover 94
5.2.2 Subpenninic nappes in the hangingwall of the Venediger Duplex 96
5.2.2.1 Wolfendorn Nappe 96
5.2.2.2 Eclogite Zone 96
5.2.2.3 Modereck Nappe System 97
5.2.3 Stratigraphical and paleogeographical considerations regarding the Mesozoic cover of the Subpenninic nappes 98
5.2.4 Ophiolitic units 100
5.2.4.1 Glockner Nappe System 100
5.2.4.2 Reckner Ophiolitic Complex 101
5.2.4.3 Matrei Zone 101
5.2.5 Lower Austroalpine Nappes 103
5.2.5.1 Hippold and Hochfeind nappes 103
5.2.5.2 Reckner and Main Nappe Group 104
5.2.5.3 Lower Austroalpine south of the Tauern Window 104

5.2.6 Upper Austroalpine basement-cover nappes 104
5.2.6.1 Silvretta-Seckau Nappe System 104
5.2.6.2 Koralpe-Wölz Nappe System 106
5.2.6.3 Ötztal-Bundschuh Nappe System 107
5.2.6.4 Drauzug-Gurktal Nappe System 107
5.2.7 Upper Austroalpine: far travelled cover nappes 108
5.2.7.1 Grauwackenzone 108
5.2.7.2 Northern Calcareous Alps 108
5.2.7.3 Southern Alps and Periadriatic plutons 109

5.3 Major Late Alpine fault zones 110

5.4 Large scale structure of the Tauern Window 114

5.5 Discussion: Kinematic evolution of the Tauern Window in the framework of the Alps 118
5.5.1 Subduction of the Piemont-Ligurian Ocean and accretion of oceanic relics in front of the Austroalpine nappe stack 119
5.5.2 Subduction of the Valais Ocean and parts of the distal-most European margin 119
5.5.3 Exhumation of the high-pressure units and incipient accretion of the European crust 120
5.5.4 Formation of the Venediger Duplex and Tauern "Kristallisation" 120
5.5.5 Indentation, doming and lateral extrusion 121

5.6 Conclusions and unanswered questions 124

Acknowledgements 125

Chapter 6 **127**

Outlook and future work

6.1 Projects related to different exhumation/cooling history of the Tauern subdomes 127

6.2 Project related to processes in a subduction/exhumation channel 128

Chapter 7 **131**

Summary and conclusions

7.1 Structural and petrological evolution of the Tauern Window 131

7.2 The Katschberg Shear Zone System (KSZS) 132

7.3 Timing of exhumation and orogen-parallel stretching at the KSZS 132

7.4 Kinematic and driving forces for the evolution of the KSZS 133

References **135**

Appendix **163**

A-1 Additional information to Chapter 3 163

A-1.1 Samples used in the RSCM study 163
A-1.2 Method 172
A-1.3 Compilation of observations used to draw the isograde and peak-temperature contours 173
A-1.4 Comparison of the calibrations 174
A-1.4.1 Beyssac et al. 2002b vs. Rahl et al. 2005 174
A-1.4.2 Beyssac et al. 2002b vs. Aoya et al. 2010, c 175
A-1.4.3 Beyssac et al. 2002b vs. Aoya et al. 2010, d 176
A-1.5 Alternative RSCM peak-temperature contours 177

A-2 Additional information to Chapter 4 180

A-2.1 Microprobe analyses of white micas 180

List of figures, tables and plates

Figure 2.1 Tectonic map of the Eastern Alps 9

Figure 2.2 Structure of the Eastern Tauern Subdome 12-13

Figure 2.3 Cross sections across the easternmost Tauern Window 14

Figure 2.4 Structures of the Katschberg Shear Zone System 16

Figure 2.5 Alpine metamorphism and sample locations 18

Figure 2.6 Microstructures of the KSZS 19

Figure 2.7 Temperature-time evolutions of the Eastern- and Western Tauern subdomes 23

Figure 2.8 Tectonic map showing the major folds and faults within and around the Tauern Window 26

Figure 2.9 Semi-quantitative evaluation of the Eastern Tauern Window 29

Figure 2.10 Age of events related to exhumation and lateral extrusion in the Eastern Alps 30

Figure 2.11 Indentation and lateral extrusion in the Alps 34-35

Figure 3.1 Tectonic map of the Tauern Window 41

Figure 3.2a Tectonic map of the study area 44

Figure 3.2b Fabric domains 45

Figure 3.3 Sample location 47

Table 3.1 Raman peak-temperature calibrations and conditions 51

Figure 3.4 Peak-temperature contours (Beyssac et al. 2002b) 54

Figure 3.5 Cross sections (a-h) 55

Figure 3.5 Schematic peak temperatures versus time curves and tectonic stages 60

Figure 4.1 Tectonic map of the investigated area 67

Table 4.1 Isotopic analyses from $^{40}Ar/^{39}Ar$ dating with respect to their microstructure 70-71

Figure 4.2 Composition of the white micas 73

Figure 4.3 Microstructural fabrics of white micas from microprobe 75

Figure 4.4 Microstructural fabrics of white micas from optical microscope 76

Figure 4.5 Probability versus age distribution of samples in the footwall of the KSZS 78

Figure 4.6 Probability versus age distribution of a sample in the hangingwall of the KSZS 79

Figure 4.7 Temperature-time evolutions of the Eastern- and Western Tauern subdomes 83

Figure 5.1 Stratigraphic columns 102

Table 5.1 Nappe correlations 110

Figure 5.2 Tectonic map showing the hinge lines of post-duplex (D5) antiforms 115

Figure 5.3 Horizontal depth section at 150 km depth through the 3-D Vp model 118

Figure 5.4 Kinematic evolution of the Tauern Window 124

Table A-1 List of RSCM samples 163-171

Figure A-1 Typical first-order Raman bands 173

Figure A-2 Comparison of the calibrations – Beyssac et al. (2002b) vs. Rahl et al. (2005) 174

Figure A-3 Comparison of the calibrations – Beyssac et al. (2002b) vs. Aoya et al. (2010, c) 175

Figure A-4 Comparison of the calibrations – Beyssac et al. (2002b) vs. Aoya et al. (2010, d) 176

Figure A-5 Peak-temperature contours (Rahl et al. 2005) 177

Figure A-6 Peak-temperature contours (Aoya et al. 2010, c) 178

Figure A-7 Peak-temperature contours (Aoya et al. 2010, d) 179

Table A-2 Summary mica compositions 180

Plate 1 Tectonic map of the Tauern Window (Eastern Alps)

Plate 2 Orogen-perpendicular and -parallel cross sections of the Tauern Window

Chapter 1
Introduction

1.1 Framework, previous studies, aims and incorporation in related projects

The field-based Ph.D. thesis is a partial result of an interdisciplinary research project, supervised and initiated by Mark R. Handy (Freie Universität Berlin) and Claudio L. Rosenberg (Université Pierre et Marie Curie, Paris). Stefan M. Schmid (Eidgenössische Technische Hochschule, ETH Zürich) co-supervised and supported this thesis. Stefan M. Schmid was associated at the Freie Universität Berlin from 2008 to 2010 for 18 months, supported by the Alexander-von-Humboldt Foundation. Many national and international collaborators were substantially involved in this project which goes beyond the Ph.D. thesis (Konrad Hammerschmidt, Freie Universität Berlin; Roland Oberhänsli, Masafumi Sudo and Martin Ziemann, all Universität Potsdam; Ralf Schuster, Geologische Bundesanstalt Wien; Bernhard Fügenschuh, Universität Innsbruck). The project in financed by the German Science Foundation (DFG) - DFG-project Ha 2403/10.

The Eastern Alps formed in the plate convergent tectonic frame of the collision between Adria and Europe in the end (e.g., Trümpy 1960, Schmid et al. 1996), in a non-cylindrical extensive fashion. Nevertheless, orogen-parallel extension is a wide-spread phenomenon in this mountain belt, especially in the Eastern Alps (Ratschbacher et al. 1991a, Frisch et al. 2000, Rosenberg et al. 2007). The thesis will help to understand the relationship between orogen-perpendicular shortening and orogen-parallel extension with respect to north-ward directed indentation and east-ward directed roll-back subduction. The key area to study such mountain-shaping processes in the Eastern Alps is the Tauern Window (Termier 1903). There, the window sheds light on these matters through the absence of elsewhere present Africa-derived thrust units on the tectonically lower European-derived units (e.g., Schmid et al. submitted, Chapter 5).

My work focuses on the eastern part of the Tauern Window, which is characterized by a low-angle normal shear zone at its eastern end (the Katschberg Normal Fault; KNF, Genser and Neubauer 1989). This normal fault is part of a much larger shear zone system – the Katschberg Shear Zone System (KSZS). The KSZS is characterized by the KNF in its central part and a northern (dextral) and southern (sinistral) strike-slip faults at the KNF's continuation (Scharf et al. submitted a, Chapter 2).

The geodynamic Cenozoic history of the European-derived and overlaying Penninic units (sandwiched between the underlying European units [Subpenninic] and overlaying Austroalpine units) involves accretion, subduction, exhumation, thickening (Venediger Duplex formation, Schmid et al. submitted, Chapter 5) and intense orogen-parallel shearing (e.g., Schmid et al. submitted, Chapter 5). However, a structural and metamorphic zonation represents all describes geodynamic stages at different locations along-strike the Tauern Window. Hence, not all units suffer the same tectonic and metamorphic conditions. European-derived units underwent Cenozoic subduction in parts of their

distal margin. Penninic units are partitioned in two tectonic and metamorphic domains. One domain at the vicinity of the Grossglockner preserves high-pressure mineral assemblages whereas Penninic units at the eastern end of the Tauern Window lack such mineralogical evidence (e.g., Scharf et al. submitted b, Chapter 3). The first domain underwent Cenozoic subduction and exhumation, while the other units were probably never subducted and exhumed. Hence, those units experienced accretion during the Paleogene. A significant Early Oligocene thermal overprint affected most of the European-derived units, in contrast to most of the Penninic units. Late Oligocene to Early Miocene shearing and large-amplitude folding affected all European units and most of the Penninic units, especially at the western- and eastern margin of the Tauern Window (e.g., Schmid et al. submitted, Scharf et al. submitted a, Chapter 2, Chapter 5).

Previous studies, focused on the geodynamic evolution of the western Tauern Window, were carried out by e.g., Frisch (1980), Selverstone et al. (1988), Axen et al. (1995), Selverstone et al. (1995), Rosenberg et al. (2004) and Rosenberg and Schneider (2008). Geochronological investigations in this area were done by several authors (e.g., Selverstone et al. 1983, von Blanckenburg et al. 1989, Christensen et al. 1994, Fügenschuh et al. 1997, Luth and Willingshofer 2008 and references therein). Genser and Neubauer (1989) and Kurz and Neubauer (1996) target their research on the tectonic evolution of the eastern Tauern Window. Additionally, e.g., Cliff et al. (1985), Droop (1985), Dunkl et al. (2003) and Luth and Willingshofer (2008 and reference therein) focused on the geochronological development of the eastern Tauern Window. The geodynamic evolution of the Tauern Window and its surroundings as a whole with respect to the Adriatic indentation and the Carpathian slab-roll back is treated by e.g., Ratschbacher et al. (1991a, b), Selverstone (1995), Kurz et al. (1999) and Rosenberg et al. (2007).

This work will add new structural and geochronological information from the eastern Tauern Window and considers the previous studies to describe and quantify the orogen-perpendicular shortening, orogen-parallel extension with respect to indentation and roll-back subduction. Furthermore, the geodynamic development of the entire Tauern Window is another important aspect of this thesis.

The thesis is part of a wider research project covering the Oligocene to Miocene exhumation and formation of the Tauern Window and adjacent areas with respect to northward Adriatic indentation and eastward Carpathian subduction. Three additional Ph.D. theses are incorporated with this project: (1) Susanne Schneider - western and central Tauern Window, structural investigations and high-temperature thermochronology; (2) Audrey Bertrand - entire Tauern Window, research on mostly brittle structures and low-temperature thermochronology; and (3) Silvia Favaro – Sonnblick- and Hochalm area in the southern part of the Eastern Tauern Subdome, structural investigations and high-temperature thermochronology. Additionally, the Master theses of Peter Gipper and Friedrich Hawemann (both structural and metamorphic research near Mallnitz, in the southern Eastern Tauern Subdome) are born out of the overall project.

1.2 Methological approach

For a comprehensive investigation only a multi-disciplinary way of research can quantify (in time and space) the amounts of northward indentation and eastward Neogene extension of the Tauern Window. Therefore, four different methods are applied in this study and must be regarded in combination with existing studies.

(1) Structural fieldwork: Map-view to thin section structures are investigated in detail. The most attention was dedicated to a low-angle ductile normal fault with adjacent strike-slip faults (the KSZS; Scharf et al. submitted a, Chapter 2) at the eastern end of the Tauern Window. These were carefully carried out by outcrop-scale investigations, confirmed in map-view as well as by over 300 thin sections. Mostly ductile structures on metapelites and metagneisses were analyzed with respect to tectonic relationships, the metamorphic conditions and kinematic indicators. Brittle structures where rarely found due to a lack of outcrops.

(2) Petrological investigations: In the field, beneath the microscope and the electron microprobe, closer looks at the petrological features were executed, with special attention to high-pressure mineral associations or pseudomorphism after those. The petrological research was the key to evaluate the four different calibrations of the Raman microspectroscopy on carbonaceous material with respect to the field area (3).

(3) Raman microspectroscopy on carbonaceous material (RSCM, Chapter 3): Carefully adopted peak temperatures on 200 samples in metapelites are interpreted in the light of four available calibrations and the petrological mineral assemblages in the field area (2). The peak temperature ranges from c. 350-612° C. Most of the data are from Penninic rocks which suffer Alpine metamorphism. Some of these data are from a high-pressure nappe in the central Tauern Window near the Grossglockner. This method, in concert with structural and mineralogical data, allows the subdivision of the Penninic nappes into a high-pressure- and a non-high-pressure nappe. Furthermore, the pattern of peak temperatures remarkably represents the normal shear zone at the eastern end of the Tauern Window and allows comparison field of gradients in the normal shear zone with those outside the normal shear zone.

(4) $^{40}Ar/^{39}Ar$ Laser ablation ages on white micas (Chapter 4): Eight samples at the northeastern end of the Eastern Tauern Subdome in the footwall of the KSZS and one sample from the Austroalpine units in the hangingwall of the KSZS were accurately analyzed, with respect to their microstructures. White micas in the normal shear zone are oriented in different ways. They are oriented with respect to the main foliation either parallel or refolded or oblique (newly growing) or in shear bands. In contrast, the

minerals structurally below this shear zone system display no preferred orientation. The combination of the RSCM method and the $^{40}Ar/^{39}Ar$ Laser ablation technique on white micas allows for the interpretation of the ages with respect to cooling, formation and deformation. Moreover, the interpretation of white mica ages with regard to different microfabrics constrains the timespan and duration of motion along the KSZS.

1.3 Schedule

After a brief introduction into the geology at the eastern end of the Tauern Window, I describe the kinematically linked system consisting of a low-angle normal fault, two strike-slip faults (interpreted as stretching faults) and domes that allow the Eastern Tauern Subdome to expand some 20-30 km to the ESE while undergoing coeval north-south shortening - The KSZS (Chapter 2). Afterwards I demonstrate that stretching and normal faulting as integral to the process of eastward lateral extrusion in the Eastern Alps (Chapter 2). In addition, the RSCM method bring light into the style and shape of the orogen-parallel extensional system at the eastern end of the Tauern Window and envisages the tectonic evolution in this particular area (Chapter 3). Moreover, the style of the Eastern Tauern Subdome based on absolute- and pattern of peak temperatures, strengthen all the previously quoted aspects of the orogen-parallel extensional history. Furthermore, I describe that parts of the Penninic nappes in the study area probably do not exhibit any high-pressure tectonic evolution. Data obtained by using the RSCM technique allow for the comparison of four different peak-temperature calibrations with the mineralogy of my field area (Chapter 3). In this thesis, I present new $^{40}Ar/^{39}Ar$ Laser-ablation ages on white micas in light of their microstructure, showing that rapid lateral extrusion of basement nappes in the Tauern Window was triggered by Neogene northward indentation of the Adriatic microplate (Chapter 4). In the same chapter I use available petrological and thermochronological data with respect to my own new $^{40}Ar/^{39}Ar$ Laser ablation ages on white micas to constrain the exhumation history of the deformed nappe stack during lateral extrusion at the eastern end of the Tauern Window. A compilation of the overall tectonic, metamorphic and geodynamic evolution of the entire Tauern Window and adjacent areas is presented in Chapter 5. This is supported by several maps and cross sections of the whole Tauern Window. Finally, I introduce an outlook for possible new projects of research related to my results and open questions of this thesis (Chapter 6) and provide a summary of the main results and their importance for the Cenozoic Alpine geodynamic evolution (Chapter 7).

Chapter 2

Modes of orogen-parallel stretching and extensional exhumation in response to microplate indentation and roll-back subduction (Tauern Window, Eastern Alps)

This chapter is submitted in International Journal of Earth Sciences as: Scharf, A., Handy, M.R., Favaro, S. & Schmid, S.M. (submitted, a) Modes of orogen-parallel stretching and extensional exhumation in response to microplate indentation and roll-back subduction (Tauern Window, Eastern Alps). The original publication is available at www.springerlink.com , http://dx.doi.org/doi:10.1007 /s00531-013-0894-4.

Abstract

The Tauern Window exposes a Paleogene nappe stack consisting of oceanic (Alpine Tethys) and continental (distal European margin) thrust sheets. In the eastern part of this window, a Neogene system of orogen-parallel ductile normal fault and lateral strike-slip shear zones - the Katschberg Shear Zone System (KSZS) - bounds this highly metamorphosed nappe stack -the Eastern Tauern Subdome- from the surrounding Austroalpine units derived from the upper plate (Adria). The KSZS comprises a $\leq$ 5 km wide belt of retrograde mylonite that accommodated Neogene exhumation and orogen-parallel stretching of the nappe complex. Its central segment is a southeast-dipping, low-angle ductile shear zone with a brittle overprint (Katschberg Normal Fault, KNF). At the northern and southern ends of this central segment, the KSZS loses its brittle overprint and swings around both corners of the eastern Tauern gneiss dome to become subvertical dextral and sinistral strike-slip faults. The latter represent stretching faults whose displacements decrease westwards to near-zero. The kinematic continuity of top east to -southeast ductile shearing along the central, low-angle extensional part of the KSZS with strike-slip shearing along its steep ends, combined with maximum tectonic omission of nappes in the Eastern Tauern Subdome in the footwall of the KNF, indicate that north-south-shortening, orogen-parallel stretching and normal faulting were coeval. Stratigraphic and radiometric age constraints indicate that the KSZS was active between some 21 Ma and 17 Ma. Rapid exhumation of the nappe complex in the footwall of this shear zone system involved a combination of extensional shearing that caused tectonic unroofing on the one hand, and upright folding that resulted in erosional denudation on the other. The contribution of tectonic unroofing is greatest along the central segment of the KSZS, and decreases westward to the central part of the Tauern Window.

The KSZS formed in response to the indentation of wedge-shaped blocks of semi-rigid Austroalpine basement located in front of the Southern-Alpine Indenter that was part of the Adriatic microplate. Northward motion of this indenter along the sinistral Giudicarie Belt offset the Periadriatic

Fault and triggered rapid exhumation of orogenic crust in the entire Tauern Window. Pannonian extension related to roll-back subduction in the Carpathians began at 20 Ma but was not felt in the Eastern Alps before about 17 Ma. Its effect was to reduce the lateral resistance to eastward crustal flow away from the zone of greatest thickening in the Tauern area. Therefore, we propose that roll-back subduction temporarily enhanced rather than triggered exhumation and orogen-parallel motion in the Eastern Alps. Lateral extrusion and orogen-parallel extension continued after 12-10 Ma to the present-day, and are driven by Adria push, even after inversion in the Pannonian Basin.

Keywords

Tauern Window, Katschberg Shear Zone System, stretching fault, indentation, roll-back subduction, lateral extrusion

2.1 Introduction

Understanding how Alpine-type mountain belts grow is an elusive endeavor due to their often strongly arcuate and non-cylindrical structure. Controversy centers on the relative contributions of shortening, extension and erosion to this growth, as discussed, for example, for the Alps-Carpathian segment of the Adria-Europe collision zone (inset to Fig. 2.1; e.g., Royden and Burchfield 1989, Selverstone 2005) and the India-Asia collision zone (e.g., Johnson 2002). In the latter case, lithospheric thickening due to thrusting and folding accommodated only 40-50% of the collisional plate convergence, with most of this shortfall accommodated by lateral motion of upper-plate lithosphere away from the zone of plate indentation (e.g., Tapponnier et al. 1986, Royden et al. 1997) and/or by erosion-along the accretionary front of the Himalayan Orogen (e.g., Beaumont et al. 2001).

The eastern part of the Alps with its core of exhumed Cenozoic basement nappes in the Tauern Window (Fig. 2.1) is part of a much smaller, three-dimensional kinematic system where orogenic crust and lithosphere (ALCAPA Unit in Fig. 2.1) thin eastward over a distance of only 200 km, from maximum values of 50 and 220 km, respectively, in the Eastern Alps to 25 and 60 km, respectively, in the Miocene Pannonian Basin (Praus et al. 1990, Horváth 1993, Lenkey 1999, Waldhauser et al. 2002, Horváth et al. 2006 and references therein, Kissling et al. 2006). This orogen-parallel reduction in thickness of crust and lithosphere is linked to syn-orogenic extension and basin formation within the ALCAPA- and Tisza units during Carpathian roll-back subduction (Fig. 2.1, Ustaszewski et al. 2008). This raises the issue of whether eastward, lateral extrusion of thickened orogenic crust was caused by "push" of the impinging Adriatic microplate (Ratschbacher et al. 1991b, Rosenberg et al. 2007), or alternatively, by "pull" of the eastwardly retreating European subduction slab beneath the Carpathians (Fodor et al. 1999), or by some combination of these two forces. A related debate concerns whether north-south shortening during Adria-Europe convergence was accommodated primarily by upright folding and erosion with only modest east-west orogen-parallel extension (e.g., Laubscher 1988, Rosenberg et al. 2007) or by conjugate strike-slip faulting and low-angle normal faulting towards the Pannonian Basin (Ratschbacher et al. 1989, 1991b, Frisch et al. 1998, Linzer et al. 2002).

The Tauern Window holds key information to resolve these dilemmas. Its topographic relief of more than 3000 m provides excellent three-dimensional exposure of large-scale folds, shear zones and faults (Fig. 2.1) that substantially modify the Paleogene nappe stack formed during south-directed

subduction of the Mesozoic Alpine Tethys Ocean and distal parts of the European margin. The Subpenninic-Penninic nappe stack derived from this lower plate is the same as that exposed in the Western Alps and found to the east in boreholes and/or imaged seismically beneath the northern part of the Pannonian Basin (Schmid et al. 2008). In contrast, the overlying Austroalpine nappes that frame the Tauern Window are derived from the continental margin of the Adriatic upper plate and can also be traced eastward to the subsurface of the Pannonian Basin. These nappes formed at an earlier stage of Adria-Europe convergence, i.e. during Late Cretaceous orogeny (e.g., Froitzheim et al. 2008, Handy et al. 2010), so their subdivision is not pertinent to our study of Neogene lateral extrusion. Following Ratschbacher et al. (1991b), we use the term lateral extrusion to refer to a combination of conjugate strike-slip faulting ("lateral escape", Tapponnier et al. 1986), low-angle normal faulting ("lateral extension", Dewey et al. 1988) and lower crustal flow (Royden et al. 1997) which, acting alone or in concert, move orogenic lithosphere at high angles to the convergence vector and subparallel to the orogen.

In this paper, we present new structural data showing that rapid lateral extrusion of basement nappes in the Tauern Window were triggered by Neogene northward indentation of Adriatic lithosphere. After a brief introduction to the geology in the eastern part of the Tauern Window (section 2.2), we describe a kinematically linked system of low-angle normal faults, strike-slip faults and domes that allowed the Alpine orogenic edifice to expand some 20-30 km to the ESE while undergoing north-south shortening (section 2.3). We then use available petrological and thermochronological data to constrain the exhumation history of the deformed nappe stack during lateral extrusion (section 2.4). We show that stretching and normal faulting (section 2.5) is integral to the process of eastward lateral extrusion in the Eastern Alps (section 2.6). We conclude by comparing the importance of Adria indentation and Carpathian slab retreat in driving lateral orogenic escape (section 2.7).

2.2 Tectonic Setting

The Tauern Window exposes Penninic and Subpenninic nappes that individuated during Paleogene imbrication of Alpine Tethyan oceanic units (Matrei Zone, Glockner Nappe System) with units of the distal European continental margin (e.g., Kurz et al. 2008, Schmid et al. submitted, Chapter 5, Fig. 2.2). Two basement subdomes at either end of the Tauern Window expose these continental units in duplex structures that formed at around 30 Ma ago (Fig. 2.1, Eastern and Western tauern subdomes, ETD and WTD). These duplex structures characterize the Venediger Nappe System (Lammerer and Weger 1998, Schmid et al. submitted, Chapter 5) which were subsequently deformed by upright, double-plunging folds. This folded nappe system is bounded at both ends by low-angle extensional shear zones, the Brenner and Katschberg shear zones (Fig. 2.1). These are kinematically linked to

conjugate strike-slip shear zones to form what we refer to as the Brenner and Katschberg shear zone systems (BSZS and KSZS). Both systems separate the Cenozoic metamorphic units in the Tauern Window from the overlying Late Cretaceous Austroalpine nappes (Fig. 2.1). Here, we focus on the kinematics of folding and shearing within the ETD, in particular along the KSZS.

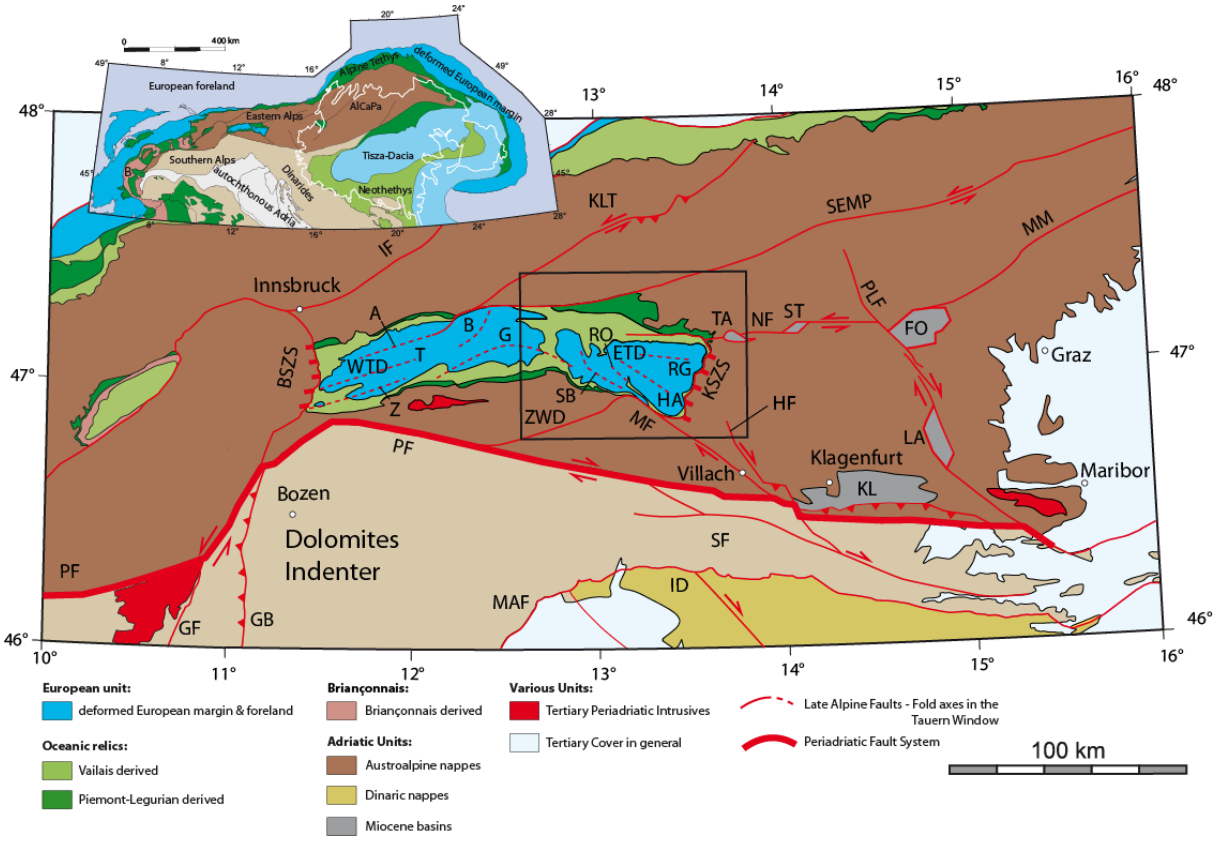

Figure 2.1: Tectonic map of the Eastern Alps, with box showing study area. Faults and shear zones: BSZS - Brenner Shear Zone System; HF - Hochstuhl Fault; GF - Giudicarie Fault; IF - Inntal Fault; KLT - Königsee-Lammertal-Traunsee Fault; KSZS - Katschberg Shear Zone System; ID - Idrija Fault; MF - Mölltal Fault; MM - Mur-Mürz Fault; NF - Niedere Tauern Southern Fault; MT Maniago Thrust; PF - Periadriatic Fault; PLF - Pöls-Lavantal Fault System; SEMP - Salzach-Ennstal-Mariazell-Puchberg Fault; SF - Sava Fault; ZWD - Zwischenbergen-Wöllatratten-Drau Fault. Fold- and thrust-belt: GB - sinisitrally transpressive Giudicarie Belt. Fold axes within the Tauern Window: A - Ahorn; B - Breitfuss; G - Granatspitz; HA - Hochalm; RG - Rotgülden; RO - Romate; SB - Sonnblick; T - Tux; Z - Zillertal. Neogene basins: FO - Fohnsdorf; KL - Klagenfurt; LA - Lavanttal; ST - Seetal; TA - Tamsweg; ETD - Eastern Tauern Subdome; WTD - Western Tauern Subdome. Inset map shows major units of Alps and Carpathians and the major tectonic plates (Europe, Adria), B - Briançonnais. White line delimits the Pannonian Basin. Maps modified from Nussbaum (2000), Schmid et al. (2004, 2008, submitted, Chapter 5), Wölfler et al. (2011).

2.3 Katschberg Shear Zone System

2.3.1 Ductile shearing the Katschberg Shear Zone System

Genser and Neubauer (1989) first described a normal fault at the eastern end of the Eastern Tauern Subdome, which they referred to as the Katschberg Normal Fault (KNF). At first glance, the KNF appears to be a classical low-angle normal fault comprising a 30-45° southeast-dipping mylonitic shear zone capped to the east by a brittle normal fault. This fault exhumed Penninic units in its footwall parallel to a southeast-plunging stretching lineation. However, our mapping revealed that the mylonites in the footwall of the KNF only represent the central part of a much larger and thicker belt of ductile shearing that envelops the entire eastern perimeter of the Tauern Window (Fig. 2.2). We refer to this arcuate mylonitic belt, including brittle overprint along the KNF, as the Katschberg Shear Zone System (KSZS). We emphasize, however, that only the central, normal-fault segment, i.e. the KNF, is capped by cataclasites. The KSZS deforms the underlying Venediger Nappe System, particularly in the vicinity of the major thrust which emplaced the Austroalpine nappes onto the Penninic and Subpenninic units in Early Tertiary time (Fig. 2.1). The KSZS is therefore a late-orogenic feature that post-dates structures dating from latest Cretaceous to Paleogene subduction, accretion, collision and nappe stacking.

The KNF comprises a wide (≤ 5 km thick) belt of retrograde amphibolite- to greenschist-facies mylonite (Figs. 2.3b, c) that affects primarily calcschist of the Penninic oceanic units as well as a broad zone in underlying Variscan gneisses of the Subpenninic basement and cover sequences. As shown in Figure 2.2, this ductile shear zone swings continuously around the ETD and connects with two subvertical shear zones that carry subhorizontal stretching lineations: a northern dextral shear zone that strikes east-west and ends near Bad Hofgastein, and a southern sinistral shear zone that trends WNW-ESE, parallel to the dextral and brittle Mölltal Fault (Fig. 2.2a). The cataclasites capping the KNF gradually disappear towards the arcuate parts of the KSZS where the KNF swings into the subvertical shear zones (Fig. 2.2a). Near the termination of the northern branch at Bad Hofgastein, the steep mylonitic foliation gradually becomes indistinguishable from older Alpine foliations and loses its subhorizontal stretching lineation. The southern branch of the KSZS ends in the vicinity of Obervellach (Fig. 2.2a). Northwest of this locality, the sinistral southern branch of the KSZS broadens, subhorizontal lineations become rare and the shear zone grades into a series of km-scale folds (Romate Antiform, Mallnitz Synform and Sonnblick Antiform, Fig. 2.2a). Yet further to the northwest, these folds become open and eventually die out. The Mallnitz Synform, for example, extends all the way to the western end of the Sonnblick Dome before acquiring a northwest trend and losing its amplitude entirely (Exner 1964, Favaro et al. 2012, in prep.). All these transitions document a kinematic link, and hence contemporaneity of dextral and sinistral shearing along the northern and southern branches of the KSZS during north-south shortening.

The low-angle, central segment of the KSZS (the KNF) is characterized by E-to-SE-dipping foliated mylonites carrying a down-dip stretching lineation. This ESE-dipping mylonitic foliation overprints variably oriented pre-Alpine and Paleogene schistosities in the Subpenninic and Penninic units, as well as a Late Cretaceous schistosity in the Katschberg Quartzphyllite Unit forming the base of the Austroalpine units (Fig. 2.2b).

Km-scale upright folds (axial traces in Fig. 2.2a) deform the duplex structure of the Venediger Nappe System in the footwall of the KSZS. Upright folding of an antiformal stack was first observed in the WTD (Lammerer and Weger 1998), where the amplitude of the folds is much larger than in east and where the axial planes trend subparallel to the strike of the thrust sheets within the duplex (Fig. 2.1). In the Eastern Tauern Subdome, the angle between duplex-related structures and the NW-SE and WSW-ENE striking fold axes (Hochalm, Rotgülden, respectively) is greater, yielding complex interference patterns in map view. Note that the southeastern lobe of the ETD mimics the shape of the southeast-plunging Hochalm Antiform (Fig. 2.2a). This is also where the KNF shows the greatest amount of tectonic omission in its footwall (area D in Fig. 2.2b). These features support the idea that north-south shortening is not only contemporaneous with dextral and sinistral shearing along northern and southern branches of the KSZS, but also with top-southeast extensional shearing across the KNF.

The stretching lineation on the mylonitic foliation of the KSZS trends ESE-WNW and plunges to the ESE, irrespective of the orientation of this foliation around the ETD. A host of kinematic indicators (Fig. 2.4) confirms that sense of shear is top-E-to-SE along the KNF (Figs. 2.4a, b), dextral in map view along the steep to moderately dipping northern branch of the KSZS (Fig. 2.4c) and sinistral along the subvertical southern branch (Fig. 2.4d). The scatter in the orientation of the lineation in fabric domains A, B and C (Fig. 2.2b) can be attributed to a strong coaxial component of mylonitic shearing and/or to the local preservation of older mylonitic fabrics related to nappe stacking. A component of coaxial shearing is recorded by c-axis textures of dynamically recrystallized quartz and calcite aggregates in the Sonnblick Dome and Sonnblick Lamellae (Kurz and Neubauer 1996). Near the western terminations of the KSZS, kinematic indicators become rare or are equivocal, with both dextral and sinsistral shear senses recorded.

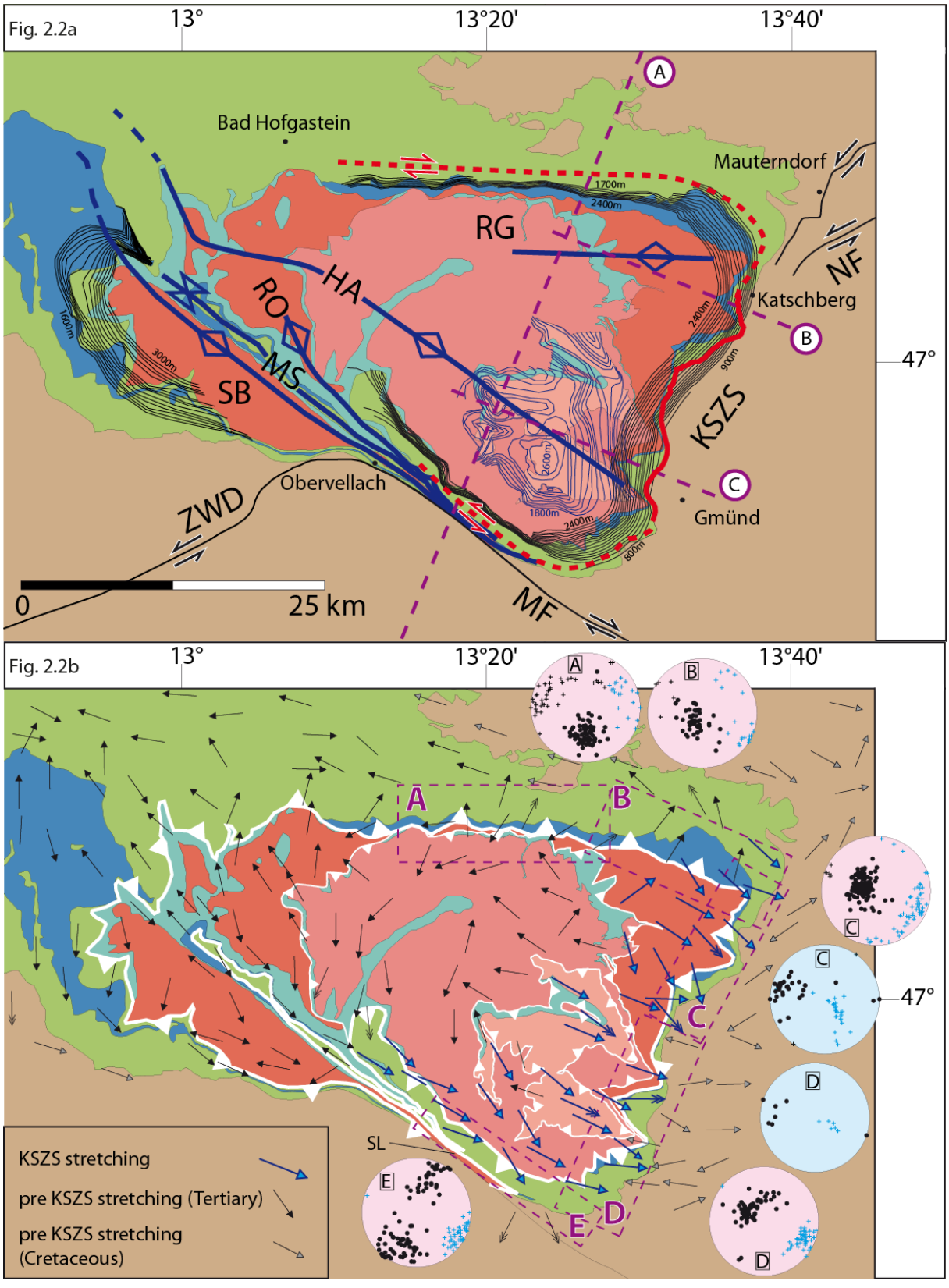
Fig. 2.2a
13°
13°20'
13°40'
47°
A
B
C
Bad Hofgastein
Mauterndorf
Katschberg
Obervellach
Gmünd
RG
HA
RO
MS
SB
KSZS
ZWD
NF
MF
1700m
2400m
1600m
3000m
2600m
1800m
900m
800m
0
25 km
Fig. 2.2b
13°
13°20'
13°40'
47°
A
B
C
D
E
SL
KSZS stretching
pre KSZS stretching (Tertiary)
pre KSZS stretching (Cretaceous)

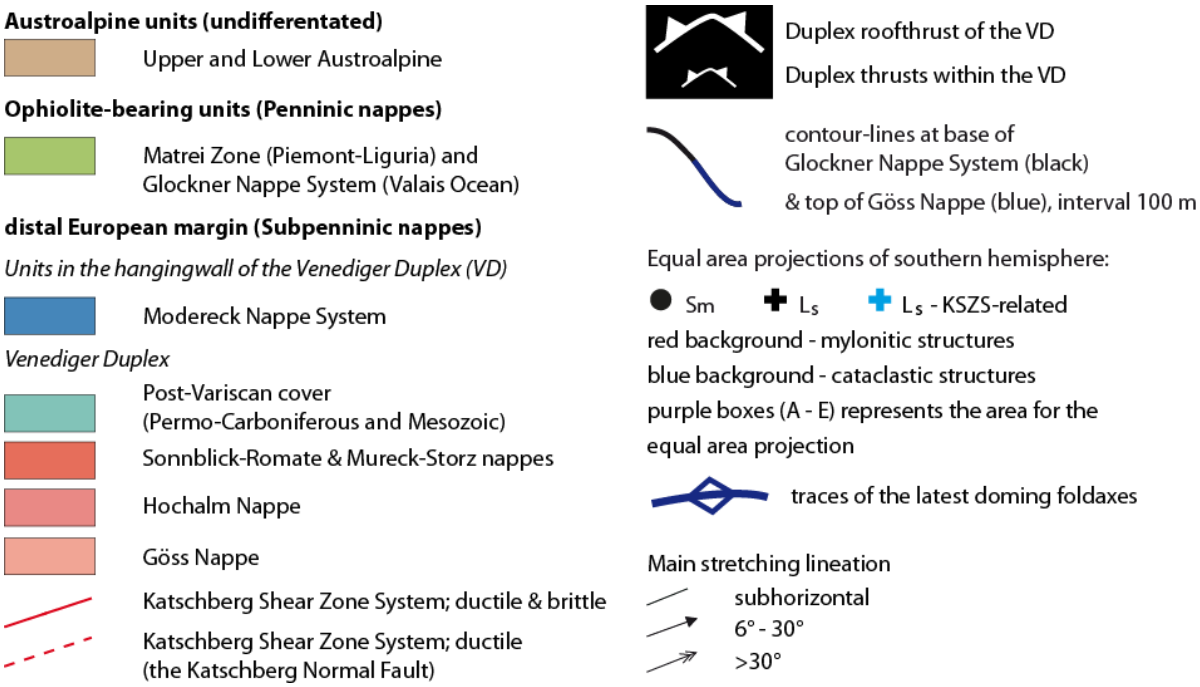

Figure 2.2: Structure of the Eastern Tauern Subdome: (a) Contours: black - basal thrust of the Glockner Nappe System, blue - top of the Göss Nappe in the Venediger Nappe System; Post-nappe folds and dome axes: HA - Hochalm Dome; RG - Rotgülden Dome; RO - Romate Fold; SB - Sonnblick Dome; MS - Mallnitz Synform. Brittle faults: MF - Mölltal Fault; NF - Niedere Tauern Southern Fault; ZWD - Zwischenbergen-Wöllatratten-Drau Fault. Purple dashed lines show traces of cross sections in Fig. 2.3; (b) Stretching lineations, Ls compiled from own measurements and Angel and Staber (1950), Becker (1993), Exner (1956, 1962a, 1980, 1983, 1989), Frank (1965). Equal-area plots show orientations of Sm (black dots) and Ls (blue dots) of the KSZS in fabric domains A-E (own measurements). SL - Sonnblick Lamellae. Tectonic map simplified from Schmid et al. (submitted, Chapter 5).

We emphasize that our determination of a sinistral shear sense along the southern branch of the KSZS, including the Sonnblick Gneiss Lamellae, is a radical departure from previous interpretations that postulate predominantly dextral shear parallel to the northwest-southeast striking southeastern margin of the Tauern Window (e.g., Kurz and Neubauer 1996). A sinistral shear sense is a key to our interpretation of the steep strike-slip branches of the KSZS as stretching faults (section 2.5.1). Note that the Mölltal Fault, immediately adjacent to and south of the mylonites of the KSZS, is indeed dextral as claimed by Kurz and Neubauer (1996). However, this fault is entirely brittle (section 2.3.2).

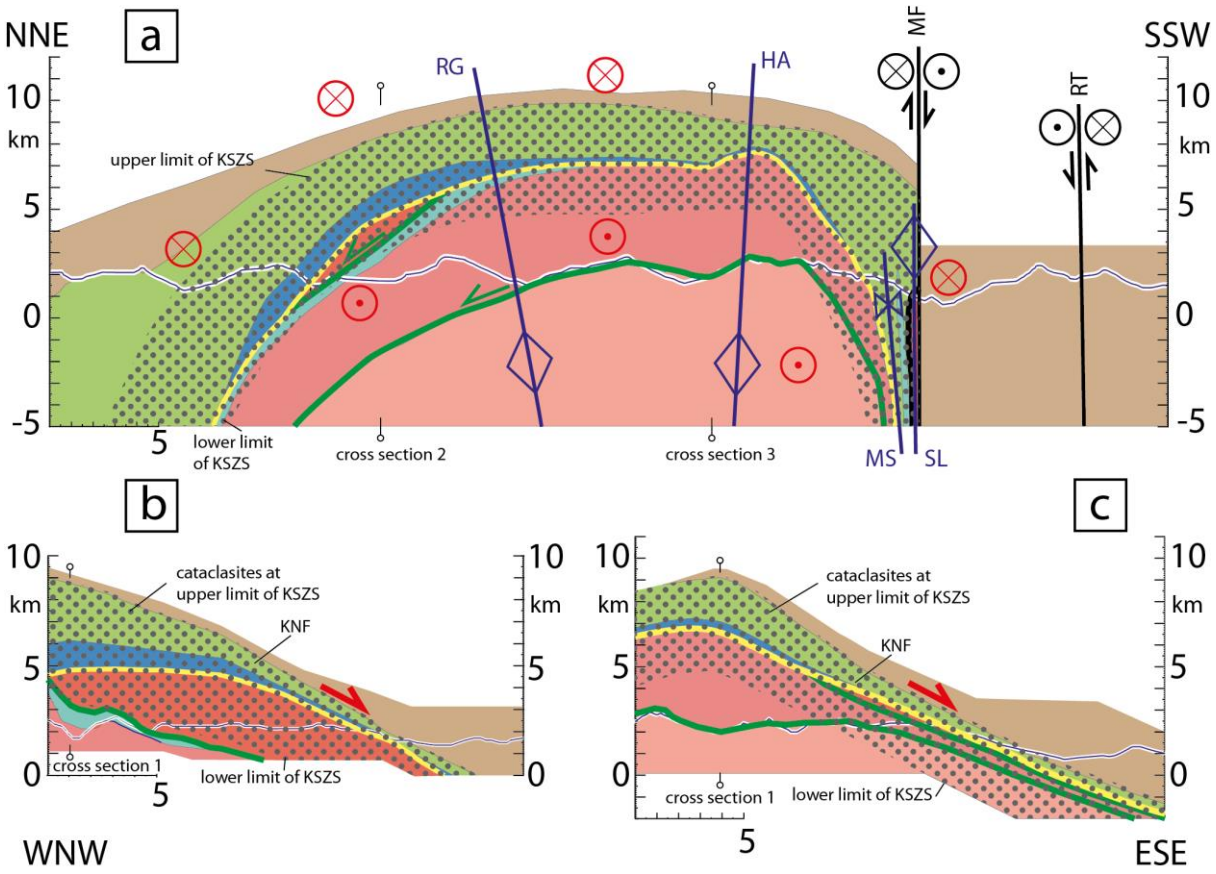

Figure 2.3: Cross sections across the easternmost Tauern Window along profile traces shown in Fig. 2.2a: (a) Section normal to the Katschberg-transport direction showing the northern and southern branches of the KSZS straddling the Hochalm- (HA) and Rotgülden (RG) Domes that shorten the underlying Venediger Nappe System. Other structures include the Mallnitz Synform (MS), Sonnblick Gneiss Lamellae (SL), Mölltal Fault (MF) and the Ragga-Teuchl Fault (RT); (b) and (c): Cross sections parallel to the ESE-directed transport direction of the KSZS and perpendicular to the KNF, respectively. Grey stippled pattern indicates mylonitic Katschberg shearing; the mylonite belt is capped by cataclasite. Green lines are nappe contacts within the Venediger Duplex; the yellow line outlines the roof thrust. Major nappe contacts and fault boundaries were constructed with the aid of structural contour maps. Legend for tectonic units as in Fig. 2.2.

2.3.2 Brittle Faulting

The brittle lid of the KNF consists of a zone of cataclasites underlain by a 10-100 m wide zone with closely spaced semi-brittle shear zones that overprint mylonite of the KNF. Semi-brittle shearing below the cataclasites is associated with small-scale drag of the earlier formed mylonitic foliation, which it overprints in kinematic continuity (Fig. 2.4b, Genser and Neubauer 1989, their Fig. 2d). The semi-brittle shears dip c. 45° to the southeast, parallel to the cataclasites of the KNF. They contain retrograde white micas and chlorites indicative of lower greenschist-facies conditions during shearing. Both mylonites and semi-brittle shears indicate top-E-to -SE displacement of the Austroalpine units in the hangingwall (Genser and Neubauer 1989). Identical kinematics and similar mineralogy indicating retrogression of fabrics at the top of the KNF suggest that brittle shearing was continuous with and outlasted mylonitic shearing.

We emphasize that the brittle lid of the KNF is restricted to the central, normal-fault segment of the KSZS and that we were unable to map a northern or southern continuation of these cataclasites along the KSZS. As mentioned above, tectonic omission of the footwall of the KNF reaches a maximum where it exhumes the Hochalm Dome in its footwall, strengthening our interpretation that Katschberg shearing and faulting were coeval with doming and upright folding. Brittle faulting is also known from the "Niedere Tauern Southern Fault" (NF in Fig. 2.1, Reinecker 2000, Wölfler et al. 2011, Schmid et al. submitted, Chapter 5). However, we were unable to map a continuous zone of cataclasites connecting the KNF and the NF in this poorly exposed area. Such a connection is not expected anyway, because the NF bounds several pull-apart basins located within the hangingwall of the KNF rather than at its base. The sedimentary fill of these basins postdates much of the activity of the KNF and serves to constrain the age of late-stages of the lateral extrusion in the Austroalpine units (section 2.6.1).

The brittle dextral Mölltal Fault only affects Austroalpine basement rocks located immediately south of, hence in the hangingwall of the KSZS. Cataclasites are beautifully exposed in outcrops along the new southern ramp of the Tauern Railroad (e.g., town of Pusarnitz, 20 km to the ESE of Obervellach in Fig. 2.2a, N 46°50'42.2" E 13°22'49.5"). There, the kinematics and crosscutting relationships of shear surfaces indicate conjugate strike-slip motion sub-parallel to the Mölltal Fault, followed by SW-down normal faulting (Favaro et al. in prep.).

The Mölltal Fault locally overprints the sinistral southern mylonitic branch of the KSZS that is best exposed north of the Mölltal Fault along the steep northern side of the Möll Valley. This indicates that brittle dextral motion on the Mölltal Fault syn- to post-dated sinistral mylonitic shearing along the southern branch of the KSZS. We found no evidence for the continuation of the Mölltal Fault into the Mallnitz Synform, as previously reported (Kurz and Neubauer 1996, Wölfler et al. 2011). Instead, the northwestern end of the Mölltal Fault broadens into a diffuse zone of cataclasites near Obervellach (Fig. 2.2a), that skirts, but does not enter the Sonnblick Dome. We suspect that this is where the Mölltal Fault conjoins with the conjugate Zwischenbergen-Wöllatratten-Drautal (ZWD) Fault (Figs. 2.1, 2.2a). These two strike-slip faults are interpreted to bound a wedge-shaped piece of Austroalpine basement, which we will refer to as the "Drau-Möll Block" (see section 2.5.3). Note that further to the southeast the Mölltal Fault does not link with the KSZS either (Fig. 2.2). Whereas the KSZS swings around to form the KNF, the Mölltal Fault continues straight to the southeast where it is covered by Plio-Pleistocene deposits of the Drau Valley before merging with, and slightly offsetting, the Periadriatic Fault (Fig. 2.1, Bigi et al. 1989). The dextral Hochstuhl Fault (Fig. 2.1) is yet another young (post-Sarmatian to recent) dextral Riedel fault that also offsets the Periadriatic Fault and delimits Late Neogene-to-Recent North Karawanken dextral transpressive overprint of the Periadriatic Fault to the west (Polisnski and Eisbacher 1992, Vrabec and Fodor 2006).

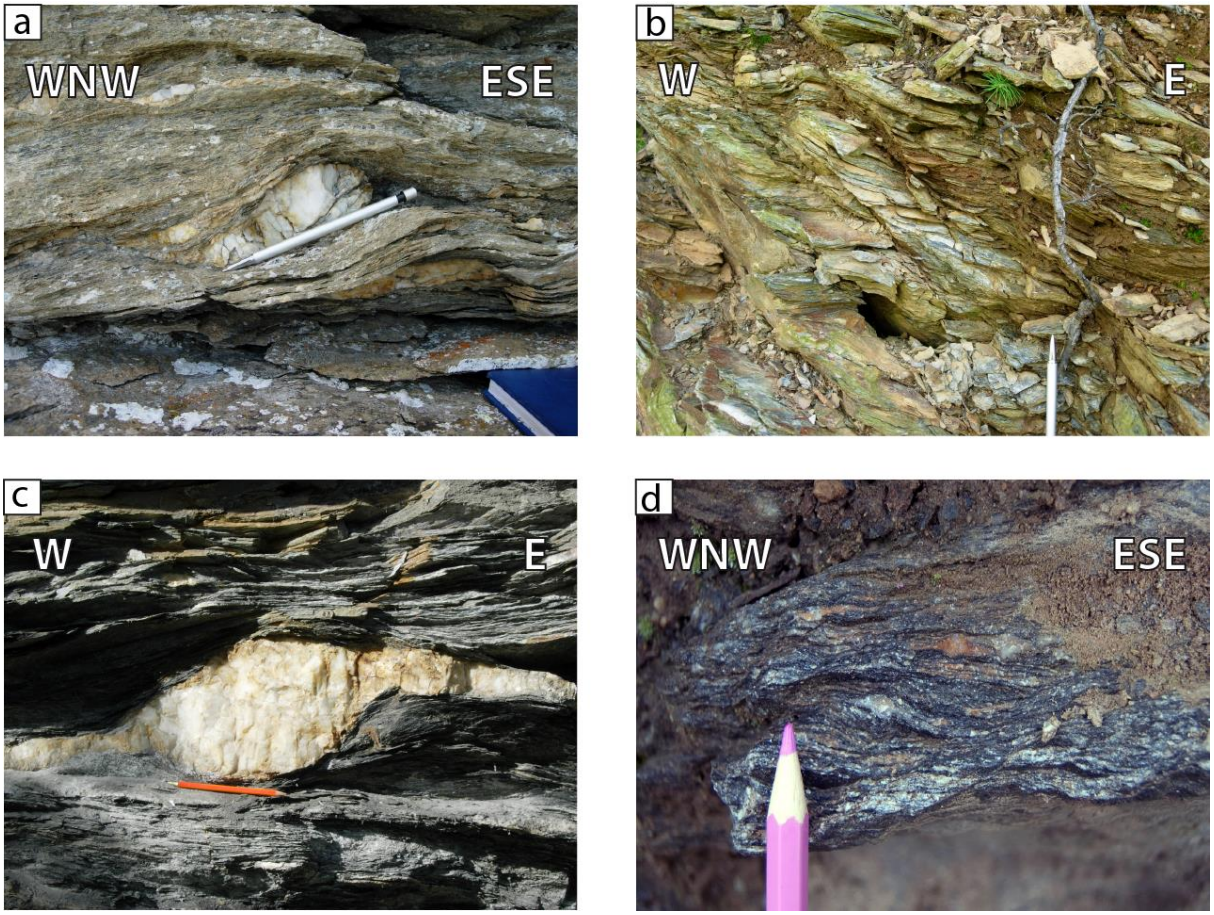

Figure 2.4: Structures of the Katschberg Shear Zone System: (a) Rotated quartz clast indicating top-ESE shear sense in calc-schist of the Glockner Nappe System along the KNF (N 47°01'11.1" E 13°32'26.9", elevation 2469 m); (b) Semi-brittle shear planes overprinting mylonites of the KNF derived from the Austroalpine Katschberg Quartzphyllite Unite located a few tens of meters below the brittle lid of the KNF (N 47°02'13.9" E 13°35'54.5", elevation 1491 m); (c) Sigma clast indicating dextral shear sense along the northern branch of the KSZS in calc-schist of the Glockner Nappe System (upper Muhr Valley, N 47°08'46.1" E 13°23'06.2", elevation 1722 m); (d) Sinistral shear bands along the southern branch of the KSZS in the Sonnblick orthogneisses from the southeastern tip of the Sonnblick Gneiss Lamellae (Möll Valley, N 46°53'17" E 13° 18'19.1" 800 m).

2.3.3 Displacement along the KSZS

We calculated a maximum throw of 13.5 km across the southern part of the central low-angle segment of the KSZS by comparing the geometry and thickness of Penninic and Subpenninic nappes where their tectonic omission is greatest (near Gmünd in Fig. 2.2, cross sections in Figs. 2.3 b, c) with those of the same nappe contacts away from the KSZS (Chapter 5, cross sections 7-10 in Plate 2). There, the deepest Subpenninic unit (Göss Nappe) in the footwall is juxtaposed in map view with the lowest Austroalpine unit in the hangingwall. Given the current 25-30° dip of the mylonites of the KNF in this area, the throw of 13.5 km corresponds to a heave (horizontal displacement) of 23-29 km. Obviously, the displacement may exceed 29 km if the dip of the KSZS at the time of shearing was less than that presently observed; doming of the hot Penninic units during Katschberg shearing may have steepened the KSZS during the late stages of extensional shearing. In fact, apatite Fission Track (AFT) and (U-Th)/He ages along a north-south transect of the Hochalm Dome indicate that the cooling rate of

9-12° C/Ma has increased since 6 Ma (Foeken et al. 2007) and leveling surveys along the Tauern railroad tunnel reveal ongoing uplift at 1-2 mm/a in the core of the Hochalm Dome below the KNF (Senftl and Exner 1973). Taken together, this suggests that the eastern margin of the KSZS has steepened during the later stages of its evolution, and, indeed, continues to steepen today.

Our estimates of displacement on the KNF are comparable to those of Genser and Neubauer (1989) who calculated a throw of 10 km from the difference in the peak temperatures of Alpine metamorphism in the hangingwall (Austroalpine units at 300° C) and footwall (Göss Nappe at 600° C) for an assumed syntectonic geothermal gradient of 30° C/km (Grundmann and Morteani 1985). This gradient must be regarded as an absolute minimum value in light of data indicating a transient, syntectonic field gradient of much as 70° C/km across the KSZS (Scharf et al. submitted b, Chapter 3). Most of the displacement must have been taken up by the mylonites of the KNF as it is the mylonites only that bend around the eastern margin of the Tauern Window into the strike-slip segments of the KSZS. The horizontal offset along these segments at the points of greatest curvature of the KSZS in map view must be equivalent to the heave (minimum 23-29 km) on the central, low-angle part of the KSZS. However, in view of the westward termination of the KSZS discussed above, offset gradually decreased westwards, as expected for stretching faults (section 2.5.1).

2.4 Metamorphic conditions in the ETD and the timing of Katschberg-related deformation

2.4.1 Pressure and temperature conditions

Figure 2.5 shows the distribution of isograds and isotemperature contours related to the thermal peak of metamorphism, the so-called “Tauernkristallisation” (Sander 1911), an amphibolite-facies event in both subdomes of the Tauern Window at around 30-28 Ma (Rb/Sr on garnet-bearing assemblages, Rb/Sr white mica of von Blanckenburg et al. 1989, Christensen et al. 1994, Inger and Cliff 1994, U-Pb allanite ages of Cliff et al. 1998, Kurz et al. 2008). The concentric isotemperature contours in Figure 2.5 cut across nappe contacts below the KSZS and coincide with the culmination of the Hochalm Dome, where peak conditions of 630 ± 40° C (Droop 1985, Scharf et al. 2012, submitted b, Chapter 3) and 0.76 ± 0.12 GPa (Droop 1985) indicate a total exhumation of 25 km.

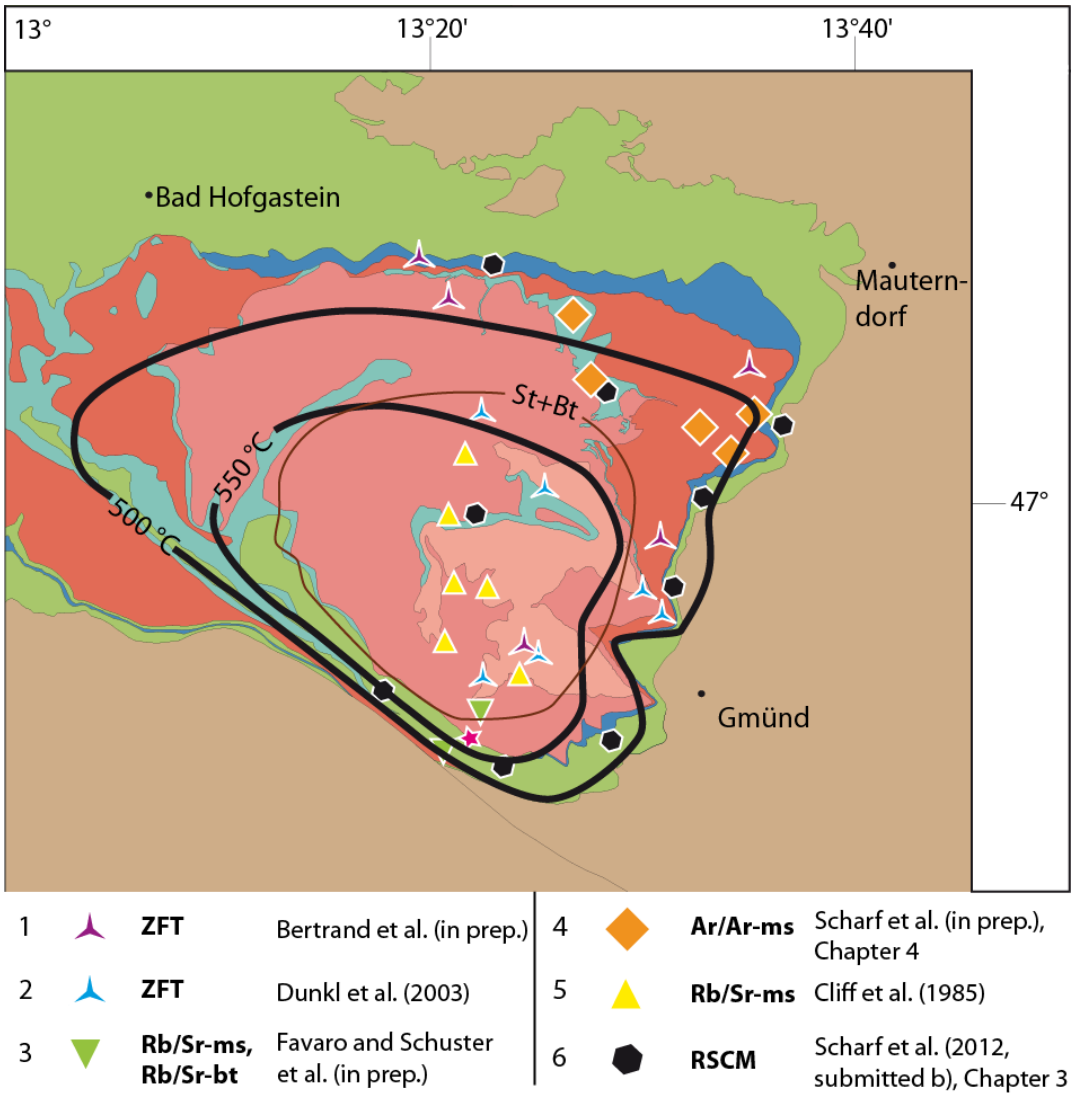

Figure 2.5: Alpine metamorphism and sample locations for thermochronology in the Eastern Tauern Subdome. Contours of peak metamorphic temperature (T_{max}) from Raman microspectroscopy on carbonaceous material (Scharf et al. 2012,submitted b, Chapter 3), the staurolite + biotite (St+Bt) isograde from Droop (1981, 1985), and the iso-cooling-temperature contours for the Rb/Sr and K/Ar biotite systems compiled in Handy and Oberhänsli (2004, and references therein). Note that the Tmax-contours and the St+Bt isograde cut the nappe contacts. Symbols show localities of samples used in Fig. 2.7. AFT, ZFT - apatite and zircon fission track, RSCM - Raman microspectroscopy on carbonaceous material. Legend for tectonic units as in Fig. 2.2.

Syntectonic metamorphism in the KSZS decreases from amphibolite-facies along its base in the Subpenninic units to lower greenschist-facies in mylonite just below the brittle top of the KNF (stippled domains in Figs. 2.3, 6a). This shearing occurred during and/or after the attainment of peak temperatures in the ETD as indicated by the closer spacing of the 500° and 550° C contours in areas of tectonic omission along the central, low-angle part of the KSZS (Fig. 2.5). We attribute this to thinning of the previously equilibrated isotherms during Katschberg shearing under retrograde conditions. The narrow spacing of the 500° and 550° C isotemperature contours along the southern branch of the KSZS and in the Mallnitz Synform is likewise attributed to mylonitic thinning and related post-nappe folding.

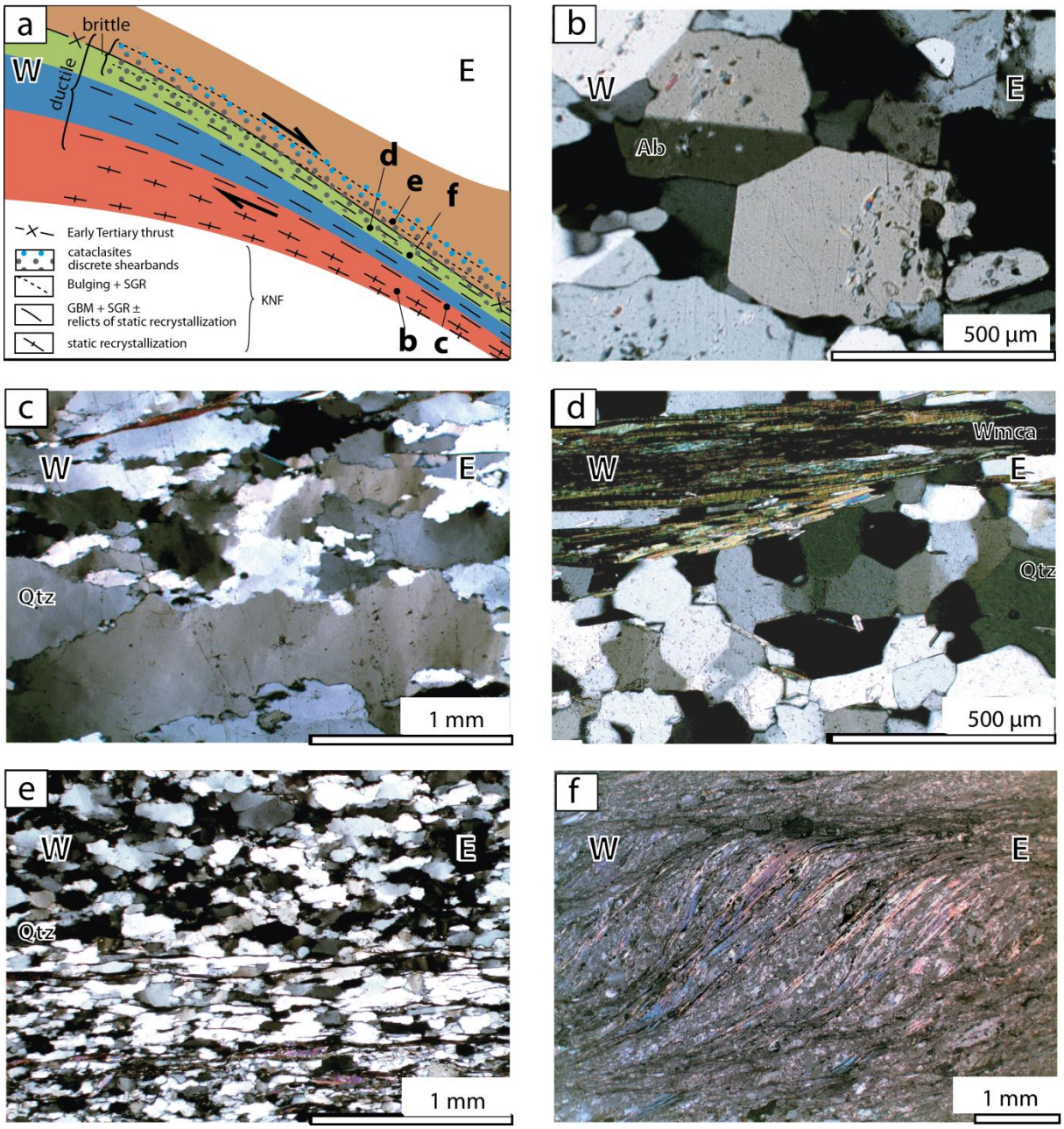

Figure 2.6: Microstructures of the Katschberg Shear Zone System: (a) cross section of the KNF with sample locations for b-f. Quartz fabric domains: SGR - subgrain rotation, GBM – grain boundary migration. Note that fabric domains overprint nappe boundaries. Legend for tectonic nappes as in Fig. 2.2; (b) Static recrystallization and 120° triple junctions in albite aggregates at the base of the KSZS some 3 km below the brittle top of the KNF (sample AS 100: N 47°08'19.4" E 13°33'46.6", elevation 2284 m); (c) Fast migration in quartz aggregates from high-temperature mylonite of the KNF (sample AS101: N 47°08'15,4" E 13°34'02,6" 2249 m; (d) Statically recrystallized quartz in upper greenschist-facies KNF mylonite along the central/upper part about 1 km below the top of the KNF (sample AS1: N 47°03'14.4" E 13°35'12.7", elevation 1959 m); (e) Dynamically recrystallized quartz in greenschist-facies mylonite towards the top of the KNF (sample AS43: N 47°02'13,9" E 13°35'54,5" 1491 m); (f) S-C fabric indicating top-E sense of shear in calc-schist (Glockner Nappe System) located 2 km below the top of the KNF (sample AS38: N 47°00'58,5" E 13°32'36,9", elevation 2219 m). All photos were taken with crossed nichols. Mineral abbreviations from Siivola and Schmid (2007)

Mylonitic gneisses from the KNF show different mechanisms of dynamic recrystallization in quartz (Fig. 2.6a). The fabric transition downwards from the base of the KNF to the underlying

Venediger Nappe System is gradational and marked by late-stage static recrystallization of quartz and albite aggregates (Fig. 2.6b) under amphibolite-facies conditions. Higher up within the mylonites of the KNF, quartz grains have arcuate and lobate grain boundaries that are indicative of fast grain-boundary migration recrystallization (Fig. 2.6c, Stipp et al. 2002, 2004). However, annealed quartz structures are still preserved between microlithons of these mylonites (Fig. 2.6d).

Within the mylonites near the brittle top of the KNF, progressive subgrain rotation becomes the dominant mode of dynamic recrystallization in quartz (Fig. 2.6e) and is in turn replaced by bulging recrystallization immediately beneath the cataclasites of the KNF. Micaceous mylonite in calc-schist of the Glockner Nappe System typically contains shear bands indicative of top-E motion (Fig. 2.6f). Taken together, these quartz microstructures are interpreted to reflect a syntectonic thermal gradient characterized by a temperature of at least 500° C at the base of the KNF to about 300-270° C (Stipp et al. 2002, their Fig. 5) along its top, where the mylonites are cataclastically overprinted.

2.4.2 Constraints on the ages of exhumation of Tauern subdomes and activity of the KSZS

Temperature-time data for both the Western and Eastern tauern subdomes are compiled in Figure 2.7 from published data and new thermochronological work. Note that we do not discuss the thermal evolution related to Late Cretaceous to Early Cenozoic subduction, nappe stacking and early exhumation (Ratschbacher et al. 2004, Kurz et al. 2008 and references therein). Instead we focus on the post-collisional exhumation of the nappe stack after the thermal peak of metamorphism at 30-28 Ma (Selverstone et al. 1995), the so-called Tauernkristallisation, that affected Subpenninic and Penninic units in the Tauern Window as described above.

To begin with, we emphasize the difficulty of dating exhumation and calculating exhumation rates in the Tauern Window, partly because reliable data from high-retentivity, high-temperature systems are sparse, particularly in the ETD, and partly due to the inherent difficulty of dating changes in pressure with thermochronometers, especially during rapid exhumation. Moreover, the conversion of cooling rates into exhumation rates is not simple and calls for sophisticated modeling and/or additional information. Rapidly exhuming rocks initially rise adiabatically because, given the slow rate of most erosion (< 2 mm/a, Burbank 2002), they do not begin to cool until they have already undergone significant exhumation (England and Thompson 1984).

In the WTD, thermobarometric data and thermal modeling for a point about 5 km horizontal distance from the Brenner Normal Fault indicate that exhumation was slow (< 1 mm/a) until about 20 Ma (blue curve in Fig. 2.7, Fügenschuh et al. 1997). Thereafter, the exhumation rate of this point near the base of the Brenner Shear Zone System (BSZS) increased rapidly to about 4 mm/a and remained high (2-4 mm/a) until about 15 Ma, when it decreased to 1 mm/a. However, rapid cooling did not begin until about 18 Ma and continued well beyond 15 Ma (Fügenschuh et al. 1997). The proposed onset of rapid exhumation at 20 Ma fits well with stratigraphic evidence that indentation of the Eastern Alps began at 21 Ma (Schmid et al. submitted, Chapter 5), as discussed in section 2.6.1 cooling and

exhumation to conditions below the viscous-frictional transition in quartz-rich rocks of the BSZS occurred at 13-12 Ma (Fig. 2.7).

The core of the Eastern Tauern Subdome beneath the KSZS cooled from 400° to 300° C between 20 and 17 Ma (solid part of red curve in Fig. 2.7, Scharf et al. in prep., Chapter 4) if one assumes that the $^{40}Ar/^{39}Ar$ white-mica and Rb/Sr biotite systems closed successively and uses the zircon fission track (ZFT) data of Dunkl et al. (2003). The spread of $^{40}Ar/^{39}Ar$ white mica ages is limited (20-17 Ma, Scharf et al., in prep., Chapter 4), in contrast to the KSZS at the eastern margin of this subdome (Fig. 2.7), where the spread of $^{40}Ar/^{39}Ar$ white mica ages is considerably larger (31-13 Ma). The youngest ages within this spectra (Scharf et al. 2012, in prep., Chapter 4) coincide with recently obtained ZFT ages of Bertrand et al. (in prep.) which, if taken at face value, would document cooling from 400° C to 270° C between 15 and 12.5 Ma. Caution is required concerning the interpretation of ZFT ages in the eastern Tauern Window in light of the anomalous and consistent differences in ages obtained by Bertrand et al. (in prep.) and Dunkl et al. (2003) for the same localities. Following Scharf et al. (in prep., Chapter 4), we interpret the broad range of $^{40}Ar/^{39}Ar$ white-mica ages from the KSZS to reflect argon loss after mylonitization or to significant lowering of the closuretemperature do to grain size reduction (Harrison et al. 2009).

We are inclined to interpret the KSZS a 20-17 Ma cooling ages for two reasons: (1) the $^{40}Ar/^{39}Ar$ age spectra of white mica oriented both parallel and oblique to the main foliation of the KSZS coincides at about 19-17 Ma, indicating that mylonitic shearing stopped no later than 17 Ma (Scharf et al. in prep., Chapter 4); (2) extensional exhumation along the KSZS rules out younger ages of shearing at the margins of the exhuming subdome than in its core. This is because heat advection along an extensional shear zone like the KSZS is expected to be greatest where the exhuming rocks are directly juxtaposed with the cool hangingwall (Ruppel et al. 1988).

Unfortunately, the onset of cooling and the early stages of exhumation are poorly constrained for the ETD. We therefore depict two hypothetical cooling curves for the high-temperature history of the ETD in Figure 2.7 (red dashed lines). Curve 1 uses the aforementioned systems from the core of the subdome, but ignores the Rb/Sr white mica ages of Cliff et al. (1985), which do not necessarily represent cooling ages since they show a very wide spread (19-27 Ma, excluding one anomalous age of 226 Ma). We tentatively interpret them as mixed ages, as discussed in Handy and Oberhänsli (2004, see Villa 1998 for a discussion of the pitfalls of this thermochronometer). The onset of rapid cooling along curve 1 is constrained by extrapolating the linear part of the cooling curve for the 17-19 Ma interval back in time to 500° C at 20 Ma. This would leave only 1 Ma between the stratigraphically constrained onset of indentation of the Southern Alps at 21 Ma and the onset of cooling in the ETD. Curve 2 passes through the center of the Rb/Sr white mica ages which Cliff et al. (1985) interpreted as formational ages at or near the thermal peak of metamorphism. According to Cliff et al. (1985), these ages are roughly coincident with the onset of rapid cooling. The average of this range of white mica ages is 22 Ma, equivalent to the average of two recently obtained Rb/Sr white mica ages (Favaro and

Schuster et al. in prep.). In this case, the onset of cooling, and hence, also exhumation, would predate indentation of the Southern Alps along the Giudicarie Belt.

Curve 1, although poorly constrained, would imply that the onset of cooling of the Eastern Tauern Subdome at 20 Ma started only 1 Ma before the onset of rapid exhumation at 21 Ma provided one is inclined to assume that all exhumation and cooling is related to such indentation and none of it to earlier periods of exhumation that followed 30-28 Ma Tauernkristallisation. If 20-40% of the exhumation across the KSZS occurred during such a short period of near-isothermal decompression (England and Thompson 1984), then exhumation rates would have been very high at a time (20-21 Ma) when the Western Tauern Subdome was still exhuming slowly, as discussed above (von Blanckenburg et al. 1989, Fügenschuh et al. 1997). Subsequent exhumation during rapid cooling from 20-17 Ma would have been almost as fast, which is incompatible with thermal models showing slow cooling at high rates of exhumation (e.g., Fügenschuh et al. 1997). Curve 2 is also poorly constrained and suggests that rapid exhumation of the ETD began much earlier than 21 Myr, possibly already at the end of the Tauernkristallisation some 30-28 Ma (Fig. 2.7). Although we cannot entirely rule out this scenario, we regard it as unlikely in view of evidence that the South-Alpine Indenter in the Eastern Alps moved N- to NNE-wards as a rigid unit no earlier than 21 Ma (Ratschbacher et al. 1991a, b, Rosenberg et al. 2007, Schmid et al. submitted, Chapter 5).

A possible explanation for this dilemma may be that although rapid exhumation in the Western and Eastern parts of the Tauern Window were broadly coeval starting at 21-20 Ma, they involved very different relative contributions of folding, normal faulting and erosion. Thus, exhumation in the west involved predominantly high-amplitude folding and rapid erosion, whereas in the east the fold amplitudes are much less, suggesting that the normal faulting along the KSZS was more important. Thermal modeling has shown that tectonic denudation primarily by extensional faulting increases the cooling rate of the exhuming footwall and therefore decreases the time lag between rapid exhumation and rapid cooling (Ruppel et al. 1988).

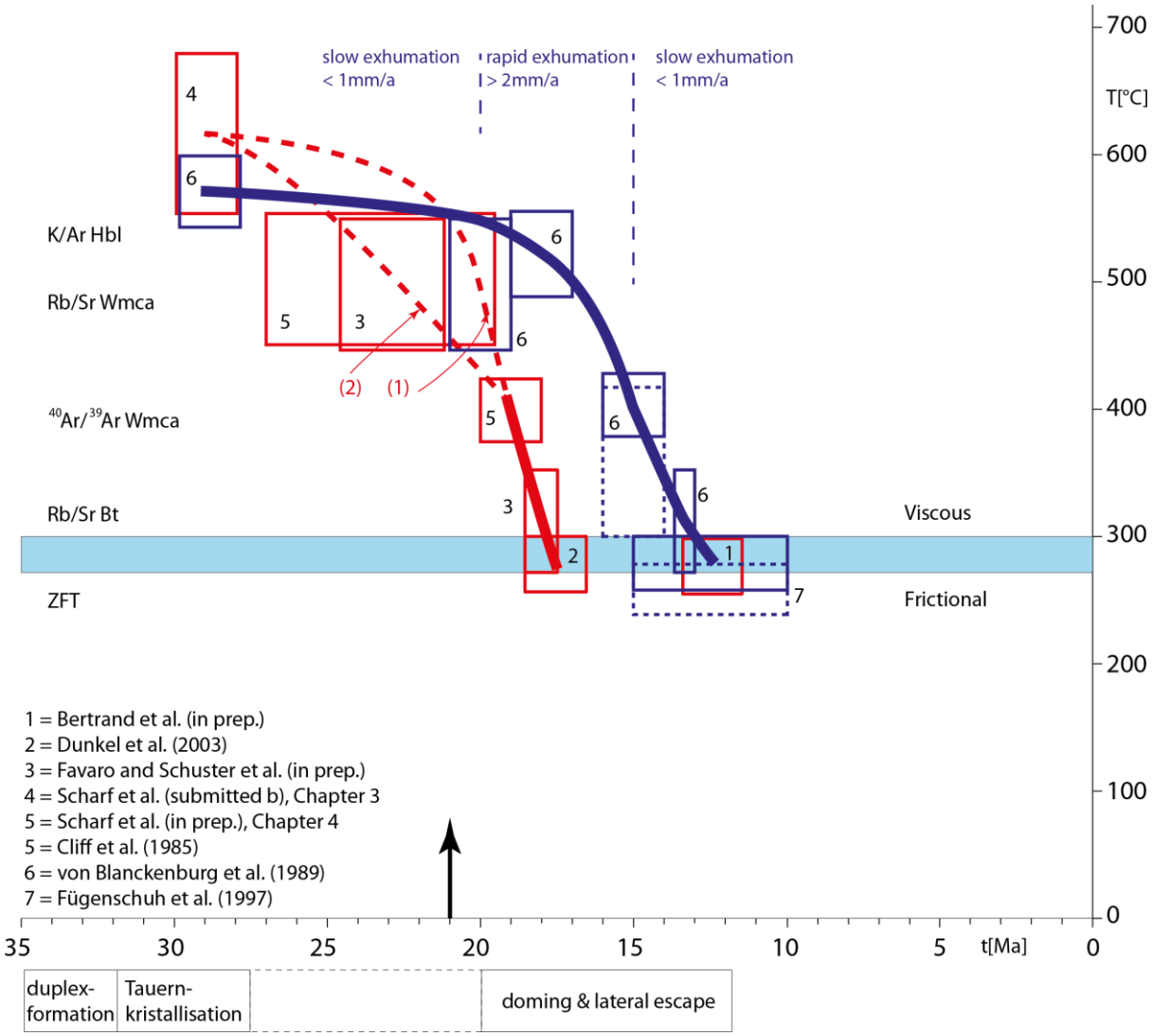

Figure 2.7: Temperature-time evolutions of the Eastern- and Western Tauern subdomes. Blue curve, boxes and letters: Cooling curve based on thermal modeling for a point in the Western Tauern Subdome located near the Brenner Normal Fault (from Fügenschuh et al. 1997). Red curves, boxes and letters: cooling curves for the Eastern Tauern Subdome. The solid red curve at low temperatures is valid for the core of the Eastern Tauern Subdome below the KSZS. Dashed red curves indicate possible cooling paths at higher temperatures for the Eastern Tauern Subdome below the KSZS, as discussed in text. Solid boxes indicate range of conditions assuming closure temperatures listed below. Dashed blue boxes indicate conditions assuming closure temperatures of von Blanckenburg et al. (1989) and Fügenschuh et al. (1997). Temperature interval of frictional-viscous transition in quartz-rich rocks taken from Handy et al. (1999) and Stipp et al. (2002). Upper left boxes indicate peak temperature (in east, from Raman microspectroscopy on carbonaceous material – RSCM, Scharf et al. 2012,submitted b, Chapter 3, in west from von Blanckenburg et al. 1989) at 30-28 Ma (Christensen et al. 1994). Sample localities and acronyms listed in Fig. 2.5. Closure temperatures used: Rb/Sr white mica 500 ± 50° C (Purdy and Jäger 1976); K/Ar hornblende 530 +33/-40° C (Harris 1981); $^{40}Ar/^{39}Ar$ white mica 350 ± 50° C (Purdy and Jäger 1976; used in von Blanckenburg et al. 1989), 400 ± 20° C (Reiners and Brandon 2006; used in Scharf et al. 2012, in prep., Chapter 4); Rb/Sr biotite 300 ± 50° C (Jäger et al. 1967; used in von Blanckenburg et al. 1989 and Favaro and Schuster et al. in prep.); ZFT 260 ± 20° C (Foster et al. 1996; used in Fügenschuh et al. 1997), 280 ± 20° C (Reiners and Brandon 2006; used in Bertrand et al. in prep.). Arrow at 21 Ma indicates earliest age of South-Alpine indentation, as discussed in text and shown in Fig. 2.10.

To summarize this section, the nappe stack in the entire Tauern Window probably underwent slow exhumation (< 1 mm/a) and cooling at high temperatures (630-500° C) from 30 Ma to about 21 Ma (Selverstone 1998). Faster exhumation from 20 Ma to about 17 Ma involved doming, erosion and extensional shearing along both the BSZS and the KSZS at the ends of the Tauern Window. In the east, rapid cooling began and ended earlier than in the west, where temperatures reached 300-270° C at about 12.5 Ma.

2.5 Strain partitioning between folding, normal faulting and strike-slip faulting in the eastern Tauern Window

2.5.1 Coeval folding, normal faulting and stretching

At first glance, the arcuate trend and variable dip of the KSZS around the perimeter of the Eastern Tauern Subdome seem to indicate that extensional shearing preceded folding. However, later folding of the KSZS can be ruled out because the KNF is not folded (undeformed contours in Fig. 2.2a). Moreover, the coincidence of maximum tectonic omission of footwall units along the KNF with the broad hinge of the ETD (Fig. 2.3) indicates that folding and extensional shearing must have been coeval. This interpretation is also consistent with the asymmetrical, concentric pattern of peak temperature isotherms (Fig. 2.5) and Miocene mineral cooling ages (Luth and Willingshofer 2008) in the ETD. In the following, we show how the normal faulting along the KNF and strike-slip faulting along the two orogen-parallel branches of the KSZS is kinematically linked to the formation of the ETD.

2.5.2 The northern and southern branches of the KSZS as stretching faults

We interpret the steeply dipping northern and southern branches of the KSZS as stretching faults in the sense of Means (1989, 1990). Stretching faults are characterized by different displacement gradients on either side of the fault, such that the offset of markers increases from zero at one end to a maximum value at the other. Kurz and Neubauer (1996) already proposed that a branch of their dextral "Mölltal Valley Fault" (not identical with our Mölltal Fault) is a stretching fault whose offset increases southeastward along the Sonnblick Gneiss Lamellae (Fig. 2.2) to a total of 24 km as estimated from the dextral offset of Austroalpine basal thrust (see their Fig. 12). Expanding on this concept, we propose that the steep northern and southern branches of the KSZS are stretching faults that accommodated some 26 km of orogen-parallel extension along the KNF (section 2.3.3).

As shown in section 2.3, these two branches are marked by orogen-parallel strain gradients as manifested by an increase in width and decrease in spacing of mylonitic structures (foliation, stretching lineation) going from the ends of these branches in the west to where they bend into the KNF in the east (Fig. 2.2). We note that sinistral shear along the southern branch including the

Sonnblick Gneiss Lamellae is unrelated to dextral shear along the Mölltal Fault. This is contrary to the interpretation of Kurz and Neubauer (1996) who regarded the Sonnblick Gneiss Lamellae as an integral part of their dextral "Mölltal Valley Fault". Further to the northwest in the vicinity of the Sonnblick Dome, the coexistence of sinistral and dextral kinematic indicators indicates that the component of flattening is more pronounced there. The analogous observations made along the dextral northern branch of the KSZS (section 2.3) suggest that this branch is also a stretching fault. Together, these branches accommodated orogen-parallel extension and shortening of the core of the ETD with respect to the un- or less-deformed Austroalpine units north and south. These units only accommodated eastward lateral extrusion further to the east, as discussed below.

2.5.3 Faults in the Austroalpine basement and their bearing on indentation of the ETD

At first sight, dextral offset across the brittle Mölltal Fault appears to have post-dated sinistral mylonitic shearing along the southern branch of the KSZS. However, a closer inspection of the large-scale kinematics of the Tauern Window (Fig. 2.8), particularly of the eastern Tauern Window, indicates that this faulting and shearing must have been contemporaneous, as discussed below and shown in Figure 2.9.

During northward motion of the Southern-Alps Indenter east of the Giudicarie Belt, the Austroalpine units located between the Tauern Window and the Periadriatic Fault were fragmented into two relatively rigid, wedge-shaped blocks (the Rieserferner Block in the west and the Drau-Möll Block in the east, Fig. 2.8). These are separated by strike-slip faults that accommodated moderate orogen-parallel extension (Fig. 2.8, Frisch et al. 1998, Linzer et al. 2002). According to Schmid et al. (submitted, Chapter 5), the Miocene Zwischenbergen-Wöllatratten (Exner 1962c) and Drautal Faults (Heinisch and Schmidt 1984) were originally a single sinistral strike-slip fault (ZWD in Fig. 2.8) that offsets the Defferegen-Antholz-Vals (DAV) Fault. The DAV- and Ragga-Teuchel (RT) faults are interpreted as segments of the same pre-Miocene fault because they juxtapose identical Austroalpine units (labeled 1 and 2 in Fig. 2.8) and define the southern boundary of Late Cretaceous Eo-alpine metamorphism (SAM of Hoinkes et al. 1999). The RT was active in pre-Miocene time as indicated by undeformed dykes with intrusive ages of 30-40 Ma (Deutsch 1984) that cut its fault plane (Hoke 1990). Thus, the available data indicate that the Rieserferner- and Drau-Möll blocks individuated in Miocene time, i.e., during doming and extensional exhumation of the Eastern and Western Tauern subdomes.

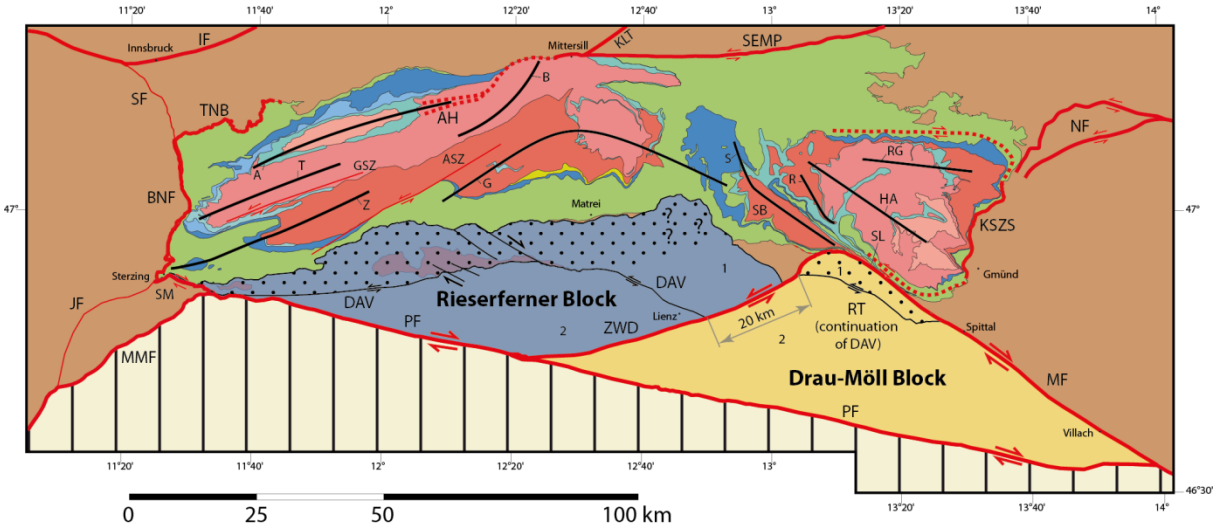

Figure 2.8: Tectonic map simplified from Figure 2.1 and Plate 1 showing the major folds and faults within and around the Tauern Window, in particular, the fragmented triangular zone of Upper Austroalpine units south of the Tauern Window made up of the Drau-Möll Block (yellow) and the Rieserferner Block (blue). Thick red lines indicate strike slip zones that were instrumental for indentation and exhumation of the Tauern Window. Dotted pattern: areas affected by Tertiary temperatures > 375° C in the Rieserferner Block (Rb/Sr, K/Ar biotite cooling ages, compiled in Luth and Willingshofer (2008) and > 270-300° C in the Drau-Möll Block (Zircon Fission Track, Wölfler et al. (2008). Tectonic units: 1 - Koralpe-Wölz Nappe System; 2 - Drauzug-Gurktal Nappe System. Folds and Domes: A - Ahorn; B - Breitfuss; G - Granatspitz; HA – Hochalm; R - Romate; RG - Rotgülden; SB - Sonnblick; SL - Sonnblick Gneiss Lamellae; T - Tux, Z - Zillertal. Faults and shear zones: AH - Ahorn Shear Zone; ASZ - Ahrntal Shear Zone; BNF - Brenner Normal Fault; DAV - Defferegen-Antholz-Vals Fault; GSZ - Greiner Shear Zone; IF - Inntal Fault; JF - Jaufen Fault; KLT - Königsee-Lammertal-Traunsee Fault; KSZS - Katschberg Shear Zone System; MF - Mölltal Fault; MMF - Meran-Mauls Fault; NF - Niedere Tauern Southern Fault; PF - Periadriatic Fault; RT - Ragga-Teuchel Fault; SEMP - Salzach-Ennstal-Mariazell-Puchberg Fault; SF - Silltal Fault; SM - Sterzing-Mauls Fault; TNB - Tauern Northern Boundary Fault; ZWD - Zwischenbergen-Wöllatratten and Drautal Faults.

The sinistral ZWD Fault is conjugate with respect to the dextral Mölltal Fault and both merge with the Periadriatic Fault along the northern margin of the Southern-Alps Indenter. These conjugate faults must be considered as co-genetic because our structural data show that they meet in a broad zone of cataclasites at their point of intersection near Obervellach (Fig. 2.2). We found no trace of the Mölltal Fault west of Obervellach within or along the northern margin of the Sonnblick Dome, so we propose that the western end of the Mölltal Fault at its junction with the ZWD Fault marks a point of zero fault displacement (Fig. 2.9). This point at the apex of the wedge-shaped Drau-Möll Block is close to the northwestern end of the sinistral southern branch of the KSZS, where we have shown that displacement related to Katschberg shearing and extension is also at or near zero. This coincidence is compounded by almost identical amounts of northwest to southeast directed displacement for the KSZS and the Mölltal Fault (Fig. 2.9): The Mölltal Fault accommodated some 24 km dextral offset of the Austroalpine basal thrust (vector v in Fig. 2.9, Kurz and Neubauer 1996), while the southern KSZS accommodated about 26 km of extension across the KNF (vector w in Fig. 2.9) according to our estimates above (section 2.3.3). These are strong kinematic arguments that northward indentation of the Drau-Möll Block caused orogen-parallel stretching of the exhuming

Eastern Tauern Subdome and that the Mölltal Fault and southern KSZS behaved collectively as a stretching fault. In this scenario, units in the footwall of the KSZS extruded eastward with respect to the apex of the indenting Drau-Möll Block (inset in Fig. 2.9). Lateral extrusion provided room for extension and exhumation of the ETD during north-south shortening. If the present-day width of the eastern margin of the ETD is assumed to approximate its original width (line x in Fig. 2.9) and the length of the KNF when it nucleated is a line connecting points of zero displacement at the ends of the northern and southern KSZS (line y in Fig. 2.9), then the ETD is estimated to have undergone about 12 km of shortening during orogen-parallel stretching. This is certainly a minimum estimate because line x includes the Hochalm- and Rotgülden folds. However, 12 km corresponds to the shortening vector in the same direction obtained from the offset along the ZWD Fault (vector z in Fig. 2.9), suggesting that the contribution of folding and erosion was modest compared to that of extension across the KNF. Note, however, that the total amount of orogen-perpendicular shortening caused by indentation of the Adriatic microplate is significantly greater and increases to the east, reaching 80 km along a line parallel to the Giudicarie Belt (Linzer at al. 2002).

2.5.4 Comparison with the WTD and strain partitioning at the scale of the entire Tauern Window

Orogen-parallel stretching and folding have also been shown to be coeval in the Western Tauern Subdome (e.g., Fügenschuh et al. 1997, Rosenberg and Schneider 2008). This area is framed by the Brenner Shear Zone System (BSZS) consisting of the Brenner Normal Fault, the sinistral Tauern Northern Boundary Fault (Töchterle et al. 2011) and the dextral Sterzing-Mauls Fault (Stöckli 1995, see Fig. 2.8). However, unlike the Eastern Tauern Subdome, the Western Tauern Subdome accommodated most orogen-parallel extension by normal faulting along the BSZS and sinistral strike slip shearing along several faults that emanate eastward from the Tauern Window (Fig. 2.8). Their combined strike-slip displacement increases from near-zero in the folded footwall of the BSZS to an estimated 66 km along the Salzach-Ennstal-Mariazell-Puchberg (SEMP) Fault and Königsee-Lammertal-Traunsee (KLT) Fault (Fig. 2.8; Linzer et al. 2002, Rosenberg and Schneider 2008, Schmid et al. submitted, Chapter 5). Hence, they represent stretching faults as well (Fig. 2.8). If the 10 km of dextral displacement along the dextral Sterzing-Meran (SM) Fault (Fig. 2.8) are included, the total amount of orogen-parallel stretch in the Western Tauern Subdome amounts to 70-80 km. This stretch was contemporaneous with some 32 km of orogen-perpendicular north-south shortening in the Tauern Window (Schmid et al. submitted, Chapter 5).

Most of this orogen-parallel stretch must be seen in the context of sinistral transpression in front of the Southern-Alps Indenter, more specifically, at the western edge of the Rieserferner Block (Fig. 2.8) as observed in analogue indentation experiments (Ratschbacher et al. 1991b, Rosenberg et al. 2007). Folds and shear zones in the Western Tauern Subdome form a predominantly sinistral, transpressional shear system that is continuous at both ends with the Giudicarie- and SEMP faults (Fig. 2.1). The similarity of 80 km of NNE-directed displacement on the Giudicarie Belt, including the

Meran-Mauls Fault (Frisch et al. 2000, Linzer et al. 2002), and the estimated 66 km of east-west extension accommodated by strike-slip faults suggests that the western Tauern Subdome served as a bridge structure in transferring much of the motion of the South-Alpine Indenter to eastward lateral extrusion in the Tauern Window (Rosenberg and Schneider 2008).

The situation in the Eastern Tauern Subdome is different in that the orogen-parallel stretch is more modest (26 km, Fig. 2.9). Also, there is no kinematic link to the SEMP Fault, indicating that dextral transpression predominated in the Eastern Tauern Subdome, again in accord with the strain patterns in analogue indentation models (Ratschbacher et al. 1991b, Rosenberg et al. 2007).

Strain partitioning in the Tauern Window is intimately related to the geometry of the two, wedge-shaped blocks of Austroalpine basement between the Tauern Window and the Periadriatic Fault (Fig. 2.8): the Rieserferner- and Drau-Möll blocks. These blocks were only partly affected by penetrative Cenozoic deformation at greenschist-facies conditions (Oberhänsli et al. 2004). Low-grade Tertiary metamorphism to temperatures slightly above the frictional-viscous transition in quartz was restricted to their leading edges (dotted patterns in Fig. 2.8). Thus, these Austroalpine blocks were strong compared to the warm orogenic crust to the north, explaining why they accommodated so much less orogeny-parallel stretch (50 km = stretch associated with offsets of c. 10 km on the Sterzing-Mauls-, 16 km on the ZWD- and 24 km on the Mölltal Faults in Figs. 2.8, 2.9).than the Tauern Window (c. 100 km = 70 and 26 in the Western and Eastern Tauern subdomes, respectively, see above).

The indentation of these Austroalpine blocks also had a pronounced effect on the pattern of shortening and exhumation of orogenic crust in the Tauern Window. The apex of the Rieserferner Block coincides with the area where Miocene north-south shortening is a minimum and where no Subpenninic units were exhumed. Shortening and orogen-parallel extension in front of the northeastern side of the Drau-Möll Block further east is by far greater as indicated by the impressive thinning of the elongate Sonnblick Dome to the narrow Sonnblick Gneiss Lamellae (20 km long, 0.5 km wide, Fig. 2.8). North-south shortening is also intense at the southern margin of the Western Tauern Subdome, adjacent to the northwestern side of the Rieserferner Block, where folds is tight to isoclinal with km-scale amplitudes (Brandner et al. 2008, Rosenberg and Garcia 2011, Schmid et al. submitted, their Fig. 3, Chapter 5, Plate 2).

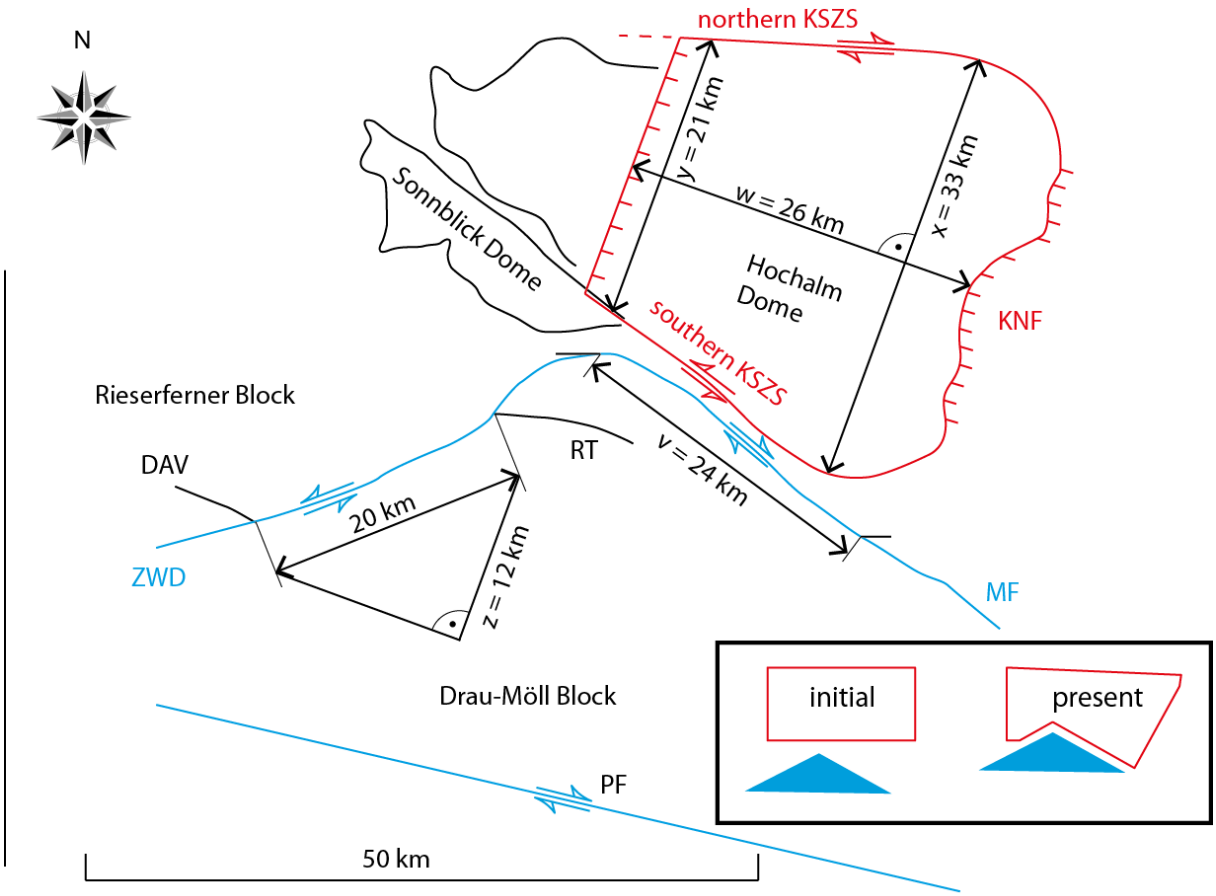

Figure 2.9: Semi-quantitative evaluation of strain partitioning during coeval shortening and orogen-parallel stretch of the Eastern Tauern Window. See Fig. 2.8 for location of the figure and text for the discussion of the vectors shown: v - Offset of the eastern margin of the Sonnblick Dome with respect to the western margin of the Hochalm Dome, achieved along the stretching segment of the Mölltal Fault that nucleated at the southern margin of the Sonnblick Dome; w - orogen-parallel stretch within the Tauern Window achieved by the KSZS; x - width of the KSZS and Eastern Tauern Subdome at its present-day eastern margin; y - width of the KSZS at the suspected site of its nucleation at about 20 Ma; z - additional component of orogen-perpendicular shortening achieved by sinistral offset between Rieserferner- and Drau-Möll Block during indentation. See Fig. 2.8 for abbreviations of faults and shear zones. Colored faults: red - branches of the KSZS, including the KNF; blue - faults bounding the Drau-Möll Block.

2.6 Relationship of lateral extrusion to Adria-Europe convergence

2.6.1 Timing constraints

Figure 2.10 summarizes the age of the main tectonic events in the Tauern Window, the sedimentary basins in the Eastern Alps and the Pannonian Basin. To place these events in a larger kinematic context, we include the age of sinistral offset along the Guidicarie Belt at the western edge of the South-Alpine Indenter, deformation within the Southern Alps and on counterclockwise rotation of the Adriatic microplate with respect to Europe. The onset of Alpine collision and breakoff of the European slab in Late Eocene to Early Oligocene time (e.g., von Blanckenburg and Davies 1995,

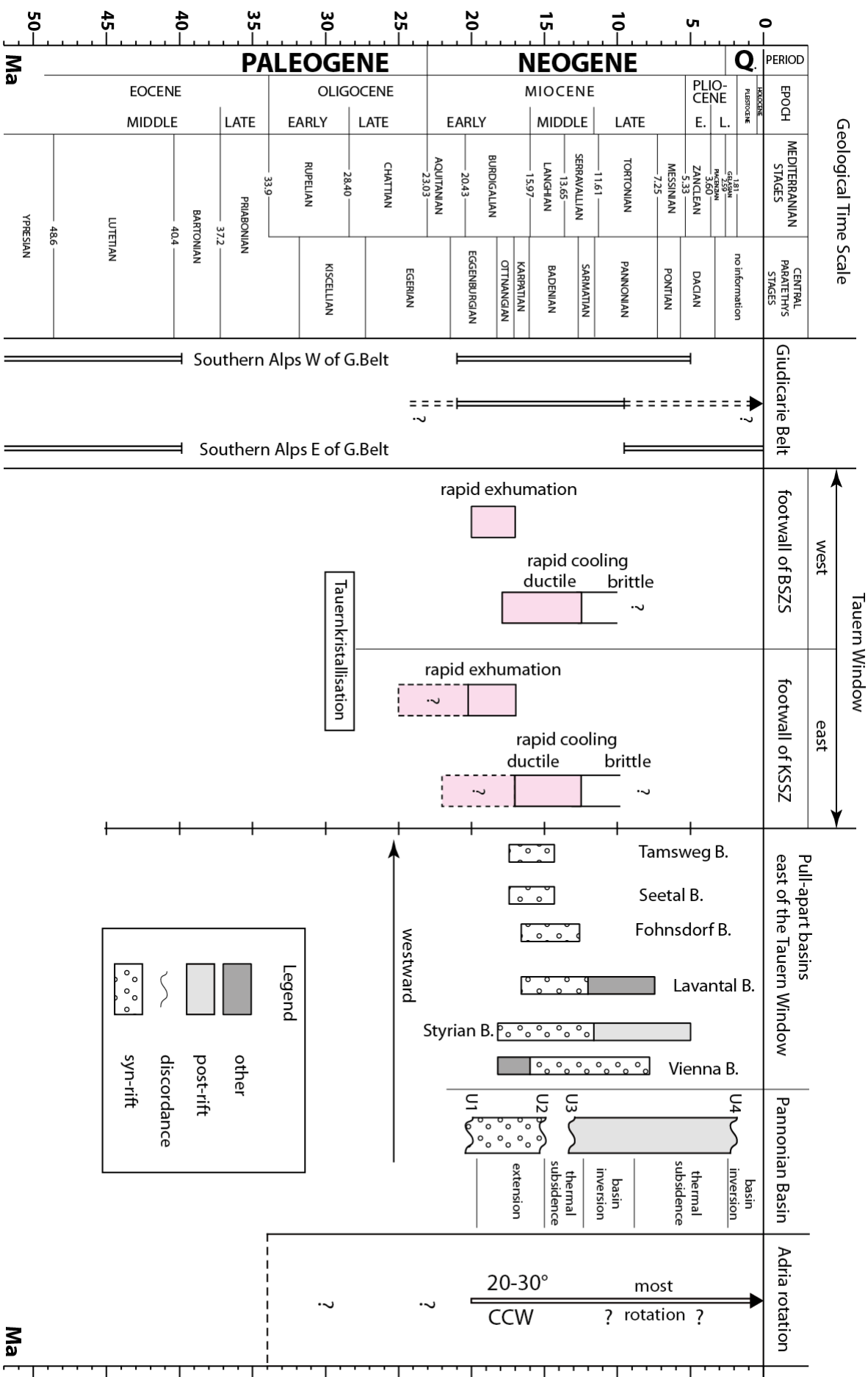
Geological Time Scale
Ma
PERIOD
EPOCH
MEDITERRANIAN STAGES
CENTRAL PARATETHYS STAGES
PALEOGENE
NEOGENE
Q.
EOCENE
OLIGOCENE
MIOCENE
PLIO-CENE
MIDDLE
LATE
EARLY
LATE
EARLY
MIDDLE
LATE
E.
L.
HOLOCENE
PLEISTOCENE
GELASIAN
PIACENZIAN
ZANCLEAN
MESSINIAN
TORTONIAN
SERRAVALLIAN
LANGHIAN
BURDIGALIAN
AQUITANIAN
CHATTIAN
RUPELIAN
PRIABONIAN
BARTONIAN
LUTETIAN
YPRESIAN
no information
DACIAN
PONTIAN
PANNONIAN
SARMATIAN
BADENIAN
KARPATIAN
OTTNANGIAN
EGGENBURGIAN
EGERIAN
KISCELLIAN
Southern Alps W of G.Belt
Southern Alps E of G.Belt
Giudicarie Belt
Tauern Window
west
east
footwall of BSZS
footwall of KSSZ
rapid exhumation
rapid cooling
ductile
brittle
Tauernkristallisation
Pull-apart basins east of the Tauern Window
Tamsweg B.
Seetal B.
Fohnsdorf B.
Lavantal B.
Styrian B.
Vienna B.
westward
Pannonian Basin
U1
U2
U3
U4
extension
thermal subsidence
basin inversion
thermal subsidence
basin inversion
Adria rotation
20-30°
CCW
most
rotation
Legend
other
post-rift
discordance
syn-rift

Figure 2.10: Age of events related to exhumation and lateral extrusion in the Eastern Alps: Sinistral motion and indentation along the Giudicarie Belt, post-nappe folding and extensional shearing in the Tauern Window, basin formation and strike-slip faulting east of the Tauern Window, subsidence and opening of the Pannonian Basin, rotation of the Adriatic microplate (see text for further discussion and references). Geological time scale: Mediterranean stages from Gradstein et al. (2004); central Paratethys stages from Piller et al. (2007) and Steininger and Wessely (2000).

Schmid et al. 1996) coincides with nappe stacking and duplex formation of the Penninic units in the Tauern Window, including units that were exhumed from high-pressure metamorphic conditions (Ratschbacher et al. 2004, Kurz et al. 2008). The Adriatic microplate moved to the northwest with respect to both Europe and Africa throughout Cenozoic time, but at about 20 Ma, i.e. at around the time when indentation of the Southern Alps began, the rate of convergence with Europe dropped from 1.3 mm/a to less than 0.5 mm/a (Handy et al. 2010).

The best constraint on the age of indentation is provided by an Oligo-Miocene pelagic sequence from the Giudicarie Belt. This thrust belt lies to the east of the Guidicarie Fault and accommodated southeast-directed thrusting and indentation (Fig. 2.1). The youngest member of the sequence below this thrust was deposited at least until 21.5 Ma ago (Monte Brione Formation, Luciani and Silvestrini 1996), indicating that thrusting post-dates 21.5 Ma (Fig. 2.10). This is consistent with the 20-5 Ma age range of south-directed thrusting in the western part of the Southern Alps that is kinematically linked with the sinistral Giudicarie Belt and that post-dates the intrusion of the Adamello Pluton; these thrusts deform Aquitanian to Tortonian sediments (Schönborn 1992, Schumacher et al. 1997, Sciunnach et al. 2010) but are themselves sealed by the Messinian unconformity beneath the Po Plain (5 Ma, Pieri and Groppi 1981). Older thrusting in the western Southern Alps preceded the Adamello intrusion and were active in Late Cretaceous and the Early to Middle Eocene time (Zanchi et al. 2012). The eastern Southern Alps, i.e., east of the Giudicarie Belt, were first affected by southwest-vergent Paleocene and Eocene thrusts of the most external Dinarides then later by S-to SSE-directed "Alpine" thrusts that have been active since Tortonian time (Venzo 1939, Doglioni and Bosselini 1987, Slejko et al. 1989, Schönborn 1999, Nussbaum 2000), i.e., after indentation along the Giudicarie Belt (Fig. 2.10). These substantial differences between western and eastern Southern Alps, particularly since Miocene time, suggest that the latter remained nearly rigid during indentation between 21 Ma and 10 Ma (see Fig. 2.10).

In Austroalpine units east of the Tauern Window, strike-slip faulting related to the opening of transtensional and pull-apart basins began in the Late Early Miocene and overlapped in time with rapid exhumation and cooling of the Eastern and Western Tauern Subdomes (Fig. 2.10). The intramontane basins along the sinistral NF Fault (Tamsweg-, Seetal-, Fohnsdorf basins, Fig. 2.1) that formed in the hangingwall of the KSZS (section 2.3.2) opened between 17.3-16.7 Ma, with sedimentation lasting to 14.3-12.8 Ma (Zeilinger 1997, Sachsenhofer et al. 2000, Strauss et al. 2001). Their opening post-dated the onset of extensional subsidence in the Styrian Basin (18.2 Ma) where synrift subsidence ended at 12 Ma (Sachsenhofer et al. 1997). Pull-apart in the Vienna Basins (16 Ma)

started even later after an earlier period of wedge-top sedimentation and ended at 7.6 Ma (Figs. 2.1, 2.10, Decker 1996, Bechtel et al. 2007, Hölzel et al. 2010, Paulissen et al. 2011). Rifting in the Styrian- and Vienna basins was related to rifting in the Pannonian Basin. (e.g., Horváth et al. 2006). The Lavanttal Basin along the dextral transtensional fault of the same name (Fig. 2.1) was initially (16.7-12 Ma) part of the Styrian Basin but became separated from the latter by the Lavanttal Fault at 12-5 Ma (Reischenbacher et al. 2007, Kurz et al. 2011, Wölfler et al. 2010).

It is important to note that the subsidence related to rifting in the Pannonian Basin located within the Intra-Carpathian Arc (inset to Fig. 2.1) started earlier (Eggenburgian, 20 Ma) than in the Austroalpine domain and lasted until Badenian time (about 15 Ma) based on intrabasinal unconformities (Horváth et al. 2006, U1-U2 in Fig. 2.10). In contrast, synrift sedimentation lasted longer in the Lavanttal-, Styrian- and Vienna basins (Fig. 2.10). The Pannonian Basin underwent post-extensional thermal subsidence until Late Serravallian time (12 Ma), and has experienced inversion, renewed thermal subsidence, and renewed basin inversion since the Late Pliocene (Horváth et al. 2006).

Taken together, the age relations in Figure 2.10 suggest that rapid exhumation and orogen-parallel extension in the Tauern Window coincided with north-directed motion of the South-Alpine Indenter along the Giudicarie Belt. Obviously, if exhumation of the Eastern Tauern Subdome began already prior to 20 Ma (curve 2 in Fig. 2.7), then this exhumation must have been triggered by more than just indentation. Most importantly, however, the strike-slip tectonics associated with the opening of intramontane basins in the Eastern Alps is somewhat younger than back-arc extension and subsidence of the Pannonian Basin. This precludes Carpathian roll-back subduction as a trigger for Neogene exhumation in the Tauern Window. We will return to this important point in our final analysis (section 2.7), but turn next to the kinematics of indentation and lateral extrusion.

2.6.2 Kinematics and amount of lateral extrusion during indentation

We envisage four stages of Tertiary convergence and lateral extrusion shown schematically in Figures 2.11a-d:

(1) Crustal thickening and formation of an Alpine orogenic root started with the onset of subduction of the European continental lithosphere at about 40 Ma (e.g., Schmid et al. 1996, Wiederkehr et al. 2009, Handy et al. 2010). In the Tauern Window, this led to the formation of km-scale duplex structures that involve Subpenninic basement nappes derived from the European continental margin at around 32-30 Ma (Schmid et al. submitted, Chapter 5). Thickening also affected the Austroalpine units north of the DAV Fault, as evidenced by Paleogene mineral cooling ages (e.g., Luth and Willingshofer 2008, Wölfler et al. 2011) and by Oligocene granitoids whose intrusive depths place a lower limit on the maximum thickness of the crust at that time (25 km in the case of the Rensen Pluton, Rosenberg et al. 2004 and references therein). This intrusive activity is interpreted to have been triggered by Late

Paleogene rupturing of the south-dipping European slab beneath the Central and Eastern Alps (von Blanckenburg and Davies 1995).

Coeval strike-slip motion on the dextral Periadriatic Fault (Schmid et al. 1989), the sinistral DAV Fault (Kleinschrodt 1987, Müller et al. 2001), the sinistral Paleo-Inntal Fault (Ortner and Stingl 2003) and the Engadine Fault (Schmid and Froitzheim 1993) may have coincided with the onset of slow exhumation of the Venediger Nappe System as early as 29 Ma (Selverstone et al. 1995). This suggests that the Alpine orogenic crust beneath the future Tauern Window already began to spread laterally in Oligocene time (Fig. 2.11a).

(2) Early Miocene indentation of the Adriatic microplate triggered coeval doming and extensional shearing of the still-thickening Venediger nappe stack in the Tauern Window (Fig. 2.11b). Rapid exhumation (2-4 mm/a) of the nappe stack in the Western Tauern Subdome, began at about 20 Ma and lasted until about 12-10 Ma in the footwall of the BSZS (Fügenschuh et al. 1997). Broadly coeval exhumation of the BSZS and KSZS seems reasonable in light of analogue models (Ratschbacher et al. 1991a, Rosenberg et al. 2007) showing that the observed pattern of north-south shortening and east-west, orogen-parallel extension in the Tauern Window (Handy et al. 2005) was established simultaneously during coherent motion of a semi-rigid South-Alpine Indenter. The exact direction of indentation, as well as the possible rotation of the South-Alpine Indenter during the counterclockwise rotation of the Adriatic microplate as a whole remains unknown. However, indentation must have been generally north-directed and oblique to the Giudicarie Fault in order to achieve transpression along the Giudicarie Belt (Fig. 2.1). The beginning of indentation at around 21 Ma (Fig. 2.10) probably coincided with the onset of counterclockwise rotation of the Adriatic microplate and a change from south- to north-directed subduction in the Eastern Alps (Horváth et al. 2006, Ustaszewski et al. 2008). As discussed earlier and shown in Figure 2.11d, the total offset along the Giudicarie Fault is about 80 km (Fig. 2.11a, e.g., Pomella et al. 2011 and references therein). We note that Miocene fragmentation of the Austroalpine basement south of the Tauern Window into two wedge-shaped blocks (Fig. 2.8 and Figs. 2.11b-d) allowed for differential north-south shortening in front of the South-Alpine Indenter while accommodating about 100 km of east-west, extension of orogenic crust in the Tauern Window as discussed above. Orogen-parallel extension of the Austroalpine units is less (some 50 km, as discussed above) and increases eastwards from the northwestern corner of the South-Alpine Indenter (Fig. 2.11b), indicating that this part of the Periadriatic Fault was a stretching fault during Miocene time. Given that this segment of the Periadriatic Fault remained straight during indentation, the wedge-shaped Austroalpine sub-indenters must have deformed somewhat in order to maintain compatibility with the South-Alpine Indenter to the south.

(a) 30 Ma

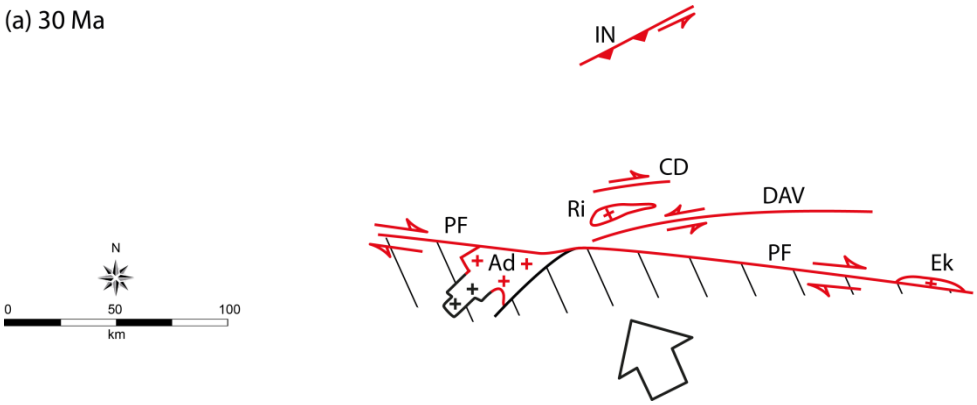

(b) 20 Ma

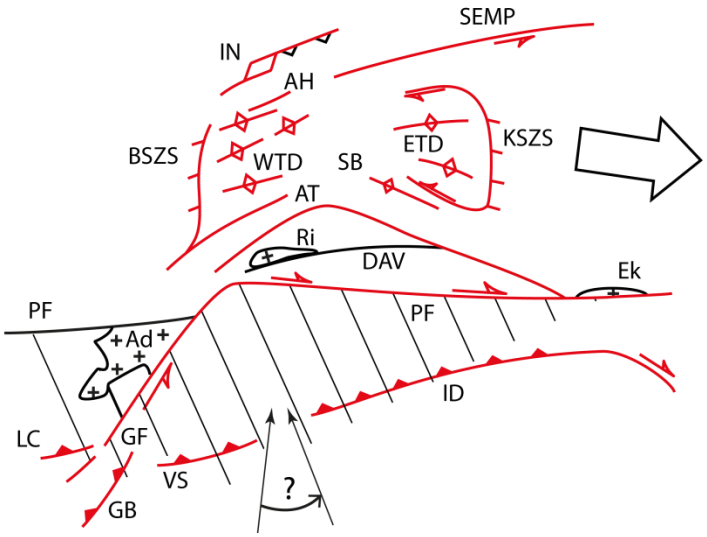

(c) 15 Ma

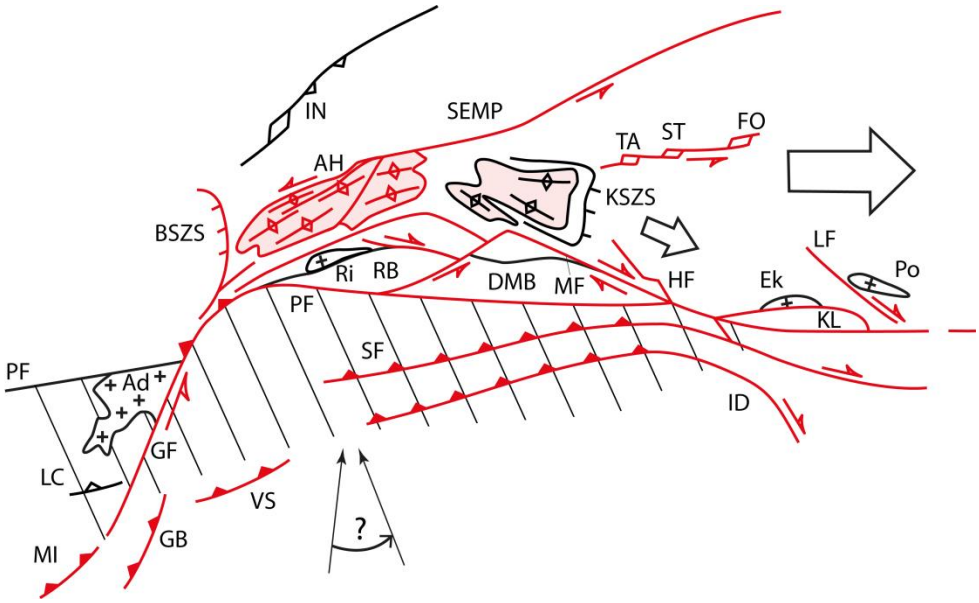

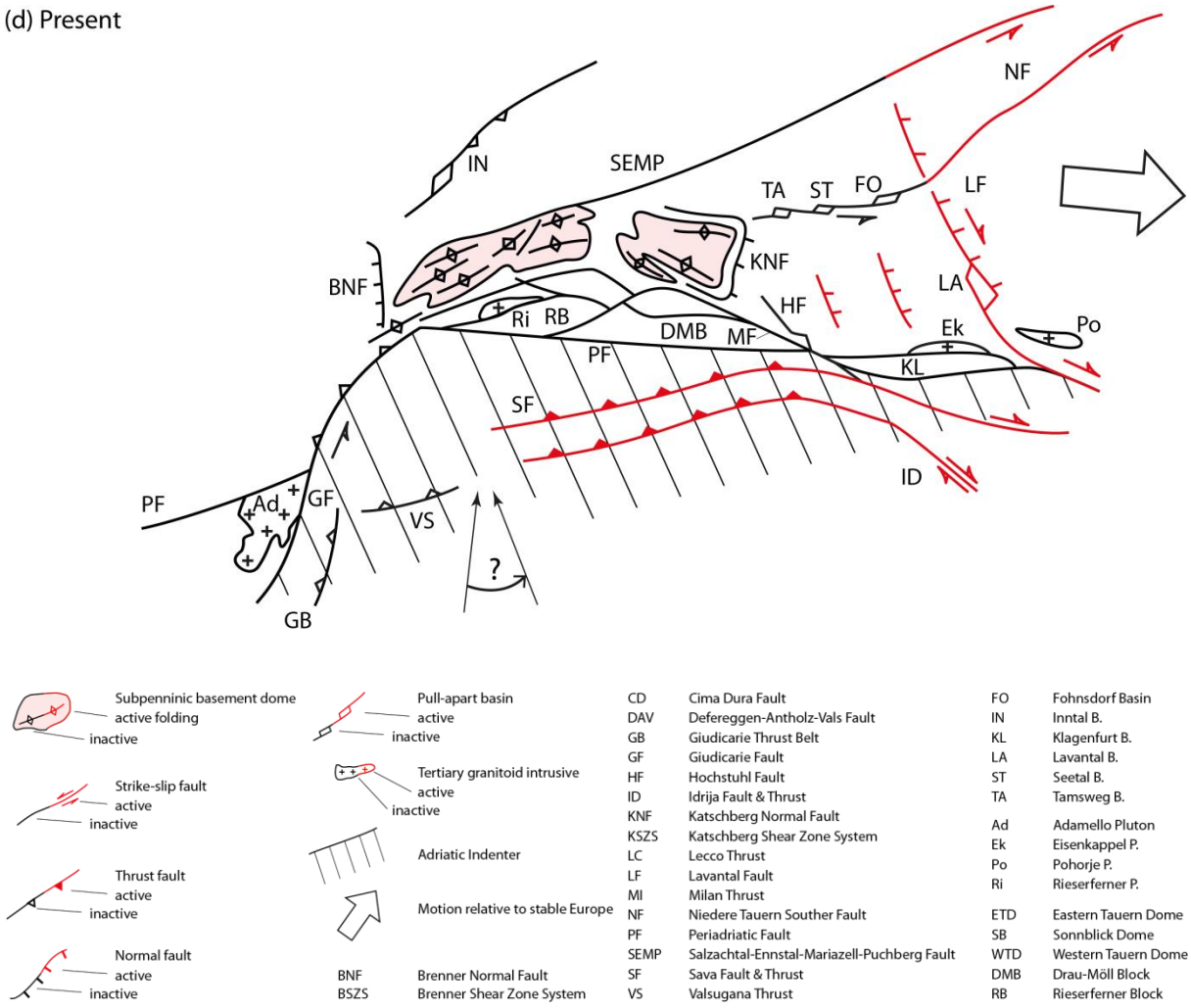

Figure 2.11: Indentation and lateral extrusion in the Alps: (a) Late Alpine collision after slab-breakoff, magmatism along Periadriatic and DAV faults, incipient doming in Tauern Window (30 Ma); (b) Onset of indentation, folding and rapid extensional exhumation of thickening orogenic crust between Katschberg- and Brenner shear zones systems, fragmentation of wedge-shaped Austroalpine units south of the Tauern Window (20 Ma); (c) Continued folding, extensional exhumation and rapid cooling in the Tauern Window, strike-slip faulting of Austroalpine units east of the Tauern Window, south-directed thrusting in Southern Alps (15 Ma); (d) Present situation involving oblique thrusting in Southern Alps, dextral strike-slip in northern Dinarides and lateral extrusion into the Pannonian Basin.

(3) By 15 Ma (Fig. 2.11c), the rate of exhumation had slowed considerably (Fügenschuh et al. 1997). Recent radiometric dating of sinistral shear zones in the Western Tauern Subdome indicates that shearing and isoclinal folding at the northern and southern margins of this subdome (Ahorn- and Ahrntal faults, Figs. 2.11b, c) stopped at 19-16 Ma as deformation focussed in the core of the subdome before ending at about 10 Ma (Schneider et al. submitted). The 100 km of orogen-parallel stretch across the BSZS and KSZS must be regarded as a minimum estimate because it does not include an unknown amount of stretching parallel to the post-nappe fold axes in the Tauern Window or, for that matter, any extension east of the Tauern Window in the hangingwall of the KSZS (e.g., along the Niedere Tauern Southern-, Mölltal- and the Lavanttal faults). Hence, the total amount of Miocene east-west extension north of the South-Alpine Indenter may well be as much as 120 km (Linzer et al. 2002). We note that the 170 km postulated by Frisch et al. (1998) also includes extension west of the

BSZS prior to indentation (Fig. 2.11a).

The opening of intramontane, pull-apart basins along strike-slip faults in the Austroalpine units east of the Tauern Window post-dated the onset of and outlasted the end of orogen-parallel extension within the Tauern Window, respectively (Fig. 2.10). All of these basins opened later than the Pannonian Basin (Fig. 2.10, not shown in Fig. 2.11) and partly outlasted synrift sedimentation in the Pannonian Basin, where intra-Carpathian back arc extension had already yielded to thermal subsidence by 15 Ma (Royden et al. 1982, Horváth et al. 2006).

(4) Inversion of the synrift and sag basins leading the present-day configuration (Fig. 2.11d) goes hand in hand with convergence due to slow counterclockwise rotation of Adria with respect to Europe (0.68°/Ma, Vrabec et al. 2006). This rotation was taken up by a system of thrusts and dextral strike-slip faults in the southernmost Eastern Alps of Carinthia and the Southern Alps of northeastern Italy and northern Slovenia (Fodor et al. 1999, Vrabec and Fodor 2006). This includes dextral transpression in the Karawanken Mountains east of the Hochstuhl Fault (Fig. 2.1, Polinski and Eisbacher 1992). Ages obtained so far for the timing of inversion of the Pannonian and intramontane basins are controversial and vary between 12 Ma (onset of sedimentation in the Klagenfurt Basin in the front of the North-Karawanken Thrust that transpressively overprints the Periadriatic Fault, Polinski and Eisbacher 1992, Nemes et al. 1997) and Late Pliocene inversion in the Pannonian Basin (Fig. 2.10, Horváth et al. 2006). In contrast, a short-lived inversion in Sarmatian time (c. 12 Ma), is also reported for the Pannonian Basin and adjacent areas (Tomljenovic and Csontos 2001, Horváth et al. 2006). Together with radiometric age constraints for the end of indentation and lateral extrusion in the Western Tauern Subdome at 10 Ma (Schneider et al. submitted), this points to the end of indentation and lateral extrusion at around 12-10 Ma. Since then, folding and faulting in the Tauern Window has stopped, with only minor seismicity recorded along the Brenner Shear Zone System (Reiter et al. 2005). East of the Tauern Window, historical and instrumentally recorded seismicity is diffuse, except for a concentration of epicenters along the Mur-Mürz strike-slip fault (Fig. 2.1) and in the Karawanken area (Reinecker and Leonhard 1999). There is also evidence that the SEMP Fault is still active in sinistral strike-slip mode (Plan et al. 2010), but the Periadriatic Fault itself is aseismic and is offset by dextral faults that merge to the east with the seismically active Hochstuhl- and Sava faults (Figs. 2.1 and 2.11d). Thus, faulting that accommodates ongoing lateral extrusion has migrated yet further to the east and south of the Periadriatic Fault, whereas the Tauern Window appears to be aseismic (Reinecker and Leonhard 1999). There is no or little evidence that the Giudicarie Belt and or the Southern Alps west of it are still active, but there is still substantial shortening ongoing in the eastern Southern Alps (e.g., Slejko et al. 1989). This can be explained partly by eastwardly increasing rates of shortening due to the counterclockwise rotation of the Adria microplate, and partly by the lateral change in present-day subduction polarity beneath the Tauern Window, i.e., near the transition from the western to the eastern parts of the Southern Alps (Lippitsch et al. 2003).

2.7 Summary and implications for the driving forces of lateral extrusion

Our data shed new light on how strain partitioned during late orogenic indentation of orogenic crust at the eastern end of the Alps. This partitioning was governed primarily by the wedge-like shape of Austroalpine blocks at the front of the South-Alpine Indenter, and by the strength contrast between these blocks and the orogenic crust presently exposed in the Tauern Window. The wedge-like shape of these semi-rigid blocks induced coeval upright folding and rapid extensional exhumation of a late Paleogene nappe complex forming the Eastern Tauern Subdome in the footwall of the Katschberg Normal Fault. The shortening during folding was accommodated by about 26 km of eastward, orogen-parallel motion of this extensional fault along two orogen-parallel stretching faults. Exhumation therefore involved a combination of tectonic unroofing by extension faulting, and erosional denudation driven by upright folding. The contribution of tectonic unroofing was greatest along the normal fault at the eastern margin of the folded nappe complex and gradually decreased away from this fault towards the central part of the Tauern Window. Compared to this situation in the east, the Western Tauern Subdome accommodated substantially more orogen-parallel extension (some 70 km) along the Brenner Shear Zone System and was kinematically linked to sinistral strike-slip motion on the SEMP Fault.

We have argued that indentation of the Southern Alps east of the Giudicarie Belt that are part of the Adriatic microplate started at about 21 Ma and triggered rapid exhumation and lateral, orogen-parallel eastward extrusion that lasted from until 12-10 Ma. Based on available data, this “push” of the advancing South-Alpine Indenter east of the Giudicarie Belt was only assisted by east-directed “pull” of the eastwardly retreating Carpathian subduction system once Pannonian extension reached the area of the Tauern Window at around 17 Ma. At that point, both mechanisms contributed to lateral extrusion, which involved a total of some 120 km orogen-parallel extension within and east of the Tauern Window since the onset of indentation. Hence we conclude that rollback subduction in the Carpathians did not pull the orogenic crust to the east, but instead facilitated its eastward expansion. Its role was similar to that of a weak lateral constraint in the indentation experiments of Ratschbacher et al. (1991a) and Rosenberg et al. (2007).

Lateral eastward escape of the Eastern Alps continued after 12-10 Ma, even after the Giudicarie Belt became inactive, and indeed continues today (1-2 mm/a; e.g., Bada et al. 2007) despite the fact that the Pannonian Basin is currently undergoing shortening. This strengthens the notion that although rollback subduction may have facilitated lateral orogenic escape in the Eastern Alps, indentation and counterclockwise rotation of the Adriatic microplate, including the Southern Alps was (and still is) the primary force driving the tectonics of the Eastern Alps and adjacent areas.

Acknowledgments

We are indebted to many colleagues for discussions, especially A. Bertrand, K. Hammerschmidt, S. Schneider and C.L. Rosenberg, all from the Freie Universität Berlin, as well as R. Schuster and G. Pestal from the Austrian Geological Survey, Wien. A. Giribaldi and S. Wollnik are thanked for preparing thin-sections and M. Grundmann for drafting figures. Finally, we acknowledge the support of the National Park Services Hohe Tauern, in particular of K. Aichhorn and the staff of the Bios Zentrum in Mallnitz. In addition, L. Ratschbacher is thanked by providing detailed diploma maps from parts of the study area. Our work was financed in part by the German Science Foundation (DFG-project Ha 2403/10). S.M Schmid acknowledges the Alexander-von-Humboldt Foundation for support of his collaborative research in Berlin from 2008-2010.

Chapter 3

Peak temperature patterns of accretion, subduction and collision preserved in the eastern subdome of the Tauern Window (Eastern European Alps) – A study with Raman microspectroscopy on carbonaceous material (RSCM)

This chapter is submitted in Journal of Metamorphic Geology: Scharf, A., Handy, M.R., Ziemann, M.A. & Schmid, S.M. (submitted, b) Peak temperature patterns of accretion, subduction and collision preserved in the eastern subdome of the Tauern Window (Eastern European Alps) – A study with Raman microspectroscopy on carbonaceous material (RSCM). The definitive version is available at www.blackwell-synergy.com.

Abstract

Raman microspectroscopy on carbonaceous material (RSCM) is applied to 200 samples from the eastern Tauern Window. We analyzed the peak temperature field in three different fabric domains characterized by distinct structural and thermal imprints during a complex poly-metamorphic evolution. Domain 1 in the northeastern Tauern Window preserves oceanic units (Glockner Nappe System, Matrei Zone) that attained peak temperatures of 350-480° C following Late-Cretaceous to Paleogene nappe stacking in an accretionary wedge. Domain 2 in the central Tauern Window includes peak temperatures of about 500-550° C that were attained either within an exhumed Paleogene subduction channel or during Barrow-type thermal overprinting due to Oligocene nappe-stacking within the Alpine collisional orogen. Domain 3 in the Eastern Tauern Subdome has a peak-temperature field that resulted from Eo-Oligocene nappe stacking of continental units derived from the distal European margin. This field was subsequently modified in Miocene time by post-nappe doming and extensional shearing along the Katschberg Shear Zone System (KSZS). The peak temperatures in the largest (Hochalm) dome range from 612° C in its core to 440° C at its rim. The highest peak temperature field gradient (≤ 70° C/km) occurs along the eastern margin of this dome where mylonitic shearing of the Katschberg Normal Fault (KNF) significantly thinned the Subpenninic- and Penninic nappe pile. All available temperature calibrations of Raman spectra yield the same pattern of peak temperatures in each fabric domain and the differences of temperature estimates from these calibrations is within the absolute error of ± 50° C. This coincidence is testimony to the robustness of the RSCM method.

Keywords

Eastern Alps, high-pressure and high-temperature metamorphism, doming, orogen-parallel extension, Raman microspectroscopy

3.1 Introduction

The Tauern Window in the Eastern Alps exposes continental and oceanic units (Subpenninic- and Penninic units, respectively) that underwent Cenozoic subduction, collision and metamorphism during convergence of the Adriatic and European Plates (e.g., Trümpy 1960, Frisch 1979, Tricart 1984, Haas et al. 1995, Stampfli et al. 2001a, Schmid et al. 2004). The structurally deepest of these units experienced upper amphibolite-facies metamorphism centered on two domes at either end of the Tauern Window (Oberhänsli et al. 2004): the Eastern and Western Tauern Subdomes (ETD and WTD in Fig. 3.1). In contrast, the center of the Window exposes higher units of the nappe pile that were less affected by doming and that contain relics of earlier high-pressure metamorphism, including blueschist- and eclogite-facies mineral assemblages (e.g., Dachs 1986, Dachs and Proyer 2001). $^{40}Ar/^{39}Ar$ dating of phengite from these assemblages (Zimmermann et al. 1994, Ratschbacher et al. 2004) combined with geodynamic arguments (see discussion in Schmid et al. submitted, Chapter 5) indicates that this high-pressure metamorphism occurred in Middle Eocene time, prior to the attainment of peak temperatures in the domes in Miocene time (Kurz et al. 2008). Previous work on the distribution and conditions of regional metamorphism based on equilibrium mineral assemblages (Cliff et al. 1985, Droop 1985, review in Hoinkes et al. 1999) and stable oxygen isotopes (Droop 1985) reveals an asymmetrical concentric pattern of peak isotherms that cuts across the nappe contacts in map view (Fig. 3.2a). This asymmetrical pattern coincides broadly with the ETD containing the structurally lowest basement nappes in its core. This dome is delimited to the east by the Katschberg Shear Zone System (KSZS, Scharf et al. submitted a, Chapter 2) which comprises an east- to southeast dipping, low-angle extensional shear zone, the Katschberg Normal Fault (KNF, Genser and Neubauer 1989) and two strike-slip shear zones in the north and south (Fig. 3.2).

Structural studies indicate that the KSZS represents a mylonitic belt up to 5 km thick that affects the surface area of the entire dome, including its deepest units (Scharf et al. submitted a, Chapter 2). This raises the possibility that the metamorphic zonation and its peak temperature distribution was modified by mylonitic deformation during extensional exhumation of the Subpenninic- and Penninic units along the KSZS. Furthermore, the occurrence of high-pressure assemblages in parts of the Glockner Nappe System in the central part of the Tauern Window (Dachs and Proyer 2001, Kurz et al. 2008, Schmid et al. submitted, Chapter 5) suggests that the peak-

temperature pattern may even be a composite of overlapping high-pressure and high-temperature events.

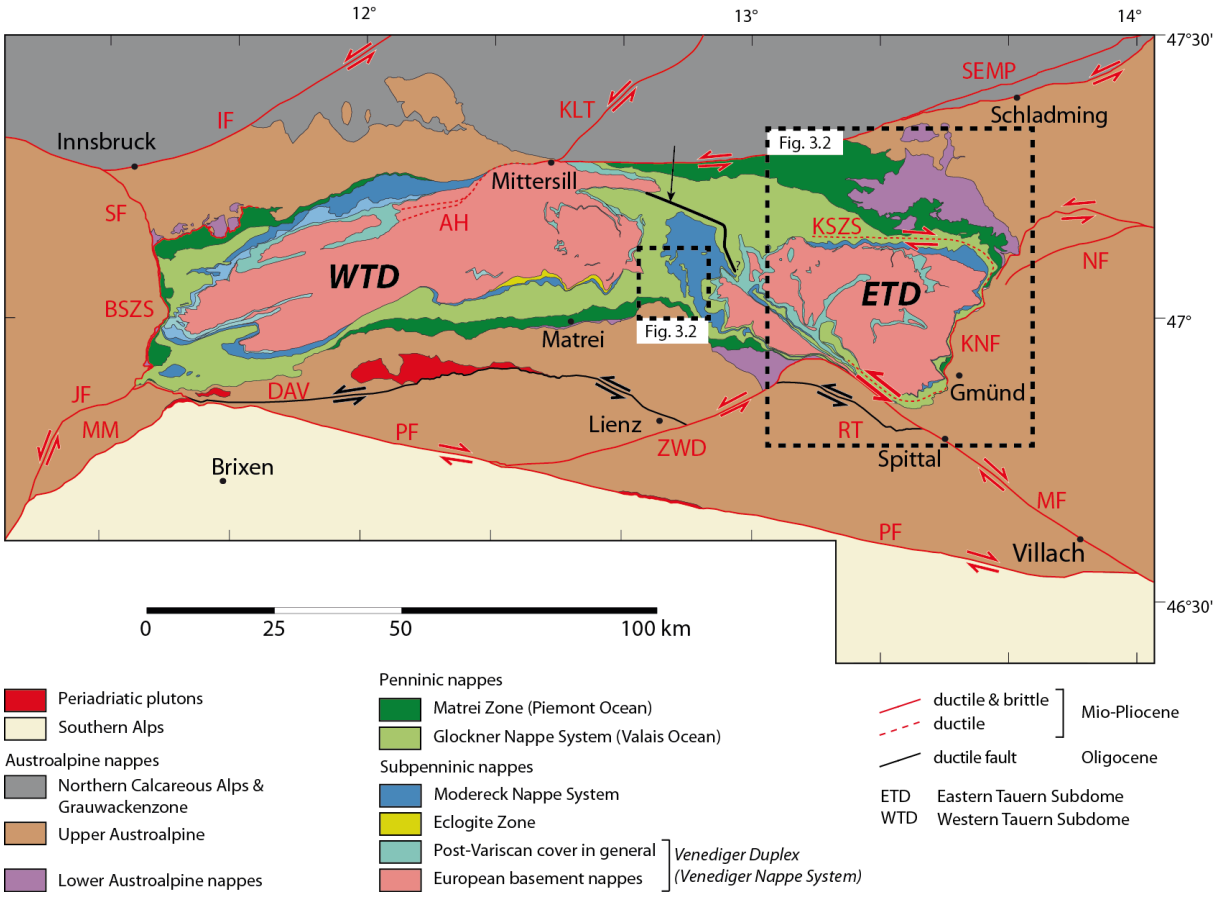

Figure 3.1: A: Tectonic map of the Tauern Window modified from Schmid et al. (submitted), Chapter 5; stippled frames indicate the investigated areas. AH – Ahorn Shear Zone; BSZS – Brenner Shear Zone System; DAV – Defereggen-Antholz-Vals Fault; IF – Inntal Fault; JF – Jaufen Fault; KLT – Königsee-Lammertal-Traunsee Fault; KNF – Katschberg Normal Fault; KSZS – Katschberg Shear Zone System; MF – Mölltal Fault; MM - Meran-Mauls Fault; NF – Niedere Tauern Southern Fault; PF – Pustertal Fault; RT – Ragga-Teuchl Fault; SEMP – Salzach-Ennstal-Mariazell-Puchberg Fault; ZWD – Zwischenbergen-Wöllatratten-Drau Fault. Arrow marks a thrust in the northern part of the central Tauern Window that separates a southern part of the Glockner Nappe System with high-pressure metamorphic relics (Glockner Nappe sensu stricto) from a northern part that was unaffected by high-pressure metamorphism (Fuscher Nappe).

To test these ideas, we applied Raman microspectroscopy of carbonaceous material (RSCM) from metapelites to obtain the distribution of peak temperature in two crucial areas: (1) the transition from the ETD across various segments of the KSZS to the Austroalpine units in the hangingwall of the KSZS (Fig. 3.2); (2) the central part of the Tauern Window affected by high-pressure metamorphism (inset in Fig. 3.2).

Our study is also a test of the RSCM method and illustrates the advantages in applying it to a large number (200) of samples in a relatively small area in order to reveal the thermal structure of a poly-metamorphic area and to test the reliability of the various available empirical calibrations (Beyssac et al. 2002b, Rahl et al. 2005, Aoya et al. 2010). Following a similar study by Wiederkehr et

al. (2011), we have demonstrated the importance of combining RSCM with a thorough structural study of the investigated area in order to understand its complex thermal history and to place this history in a geodynamic context.

In the following sections, we introduce the main tectonic units, lithologies and fabric domains that were sampled, and then describe the methods used to estimate the peak temperatures with the RSCM technique. The results presented in section 3.4 allow us to compare different peak-temperature calibrations that form the basis for our interpretations in section 3.5. We found that Katschberg shearing and doming at the eastern end of the Tauern Window substantially modified the peak-temperature pattern associated with upper greenschist- to amphibolite-facies regional metamorphism that resulted from earlier crustal thickening. In the south central part of the Tauern Window that experienced Paleogene subduction and exhumation, as well as away from the KSZS, younger Barrow-type metamorphism overprinted pre-existing high-pressure assemblages in the Subpenninic- and Penninic units. However, the Penninic units (Glockner Nappe System) at the northern, eastern and southern peripheries of the ETD probably never experienced such high-pressure metamorphism.

3.2 Lithologies and structural provenance of the samples

3.2.1 Lithologies and sampling strategy

The two hundred samples collected for RSCM from the eastern and central parts of the Tauern Window (Fig. 3.3) come from a wide range of lithologies that experienced varied metamorphic conditions at different times. Eighteen of the samples are from the Austroalpine units in the hangingwall of the KSZS. Most of these come from the Katschberg Quartzphyllite containing Silurian-age metasediments (Schönlaub et al. 1976) and retrogressed pre-Variscan micaschists and amphibolites that experienced Eo-Alpine regional metamorphism and nappe stacking in Late Cretaceous time (Schuster et al. 2006, Pestal et al. 2009). Austroalpine units sampled in the southeastern part of the area in Figure 3.2 (Koralpe-Wölz Nappe System as part of the Texel-Millstadt-Wölz Unit, sample AS-Mö191, sample 98 in Fig. 3.3 and Table A-1) underwent eclogite-facies metamorphism during Eo-Alpine subduction in Late Cretaceous time (Thöni 2006).

The largest number of samples (151) comprises calc-schists and black shales of the so-called Bündnerschiefer of the Glockner Nappe System. We use this term as a field term for schist containing white-micas, chlorite, quartz and calcite that is sometimes associated with lenses of epidote-chlorite-albite-bearing metabasic rock, known locally as “prasinite”, as well as rare pods of serpentinite. This association is interpreted to be diagnostic of oceanic lithosphere or of lithosphere formed along the ocean-continent transition of Alpine Tethys (e.g., Lemoine et al. 1987). Alpine Tethys was actually a composite of two oceans: the Piemont Ocean that opened in Early-Middle Jurassic times (Matrei Zone of Fig. 3.1) and the Valais Ocean that opened in Late Jurassic to Early Cretaceous times (Glockner

Nappe System of Fig. 3.1). Calc-schist derived from the Piemont Ocean (locally called the Matrei Zone or Nordrahmenzone) typically contains pelagic metasediment (e.g., radiolarite) and blocks of Austroalpine rock derived from the formerly adjacent Adriatic Margin, whereas the Bündnerschiefer of the Valais Ocean (the Glockner Nappe System) lack these elements and generally contain fewer ultramafic bodies (see reviews in Pestal et al. 2009, Schmid et al. submitted, Chapter 5).

In the central part of the Tauern Window, i.e., near the highest Austrian mountain, the Grossglockner (3798 m), mafic rocks of the Glockner Nappe System preserve eclogite- and blueschist-facies mineral assemblages (e.g., Dachs and Proyer 2001, Kurz et al. 2008). The peak-metamorphic conditions are described by Dachs and Proyer (2001) and Kurz et al. (2008) with 570° C and 1.7 GPa. Bündnerschiefer in this area contains lawsonite and/or albite + epidote + phengite + chlorite as pseudomorphs after lawsonite (Gleissner et al. 2007). Such high-pressure minerals are lacking in the part the Glockner Nappe System within the northern central Tauern Window (see black arrow in Fig. 3.1 marking the thrust contact between these two different metamorphic domains). Frasl and Frank (1966) therefore divided the Glockner Nappe System in two subunits: the Glockner Nappe sensu stricto with high-pressure mineral assemblages and the Fuscher Nappe with only greenschist-facies assemblages and no high-pressure minerals. No high-pressure bearing mineral assemblages have been found in the northeastern part of the Tauern Window either (Pestal et al. 2009); there the metamorphic conditions never exceeded greenschist-facies conditions (e.g., Oberhänsli et al. 2004, Bousquet et al. 2008).

A third group consisting of 35 samples was collected in Subpenninic units comprising basement and cover of the former European continental margin. Eight of these samples come from three tectonic slices (Göss, Hochalm and Sonnblick-Romate-Storz Nappes; Fig. 3.2, A-1) that make up a duplex structure in the core of the ETD (Venediger Duplex of Schmid et al. submitted, Chapter 5) These units all experienced upper greenschist- to amphibolite-facies Barrovian metamorphism ("Tauernkristallisation" of Sander 1911) at peak conditions of 630° C and 0.8 GPa (Göss Nappe; Droop 1985) about 30-28 Ma ago (Rb/Sr white mica ages; Inger and Cliff 1994, Thöni 1999, Kurz et al. 2008). The basement is variegated, with pre-Variscan metasediments and Late Paleozoic granitoid intrusive rocks overlain by a Late Paleozoic to Mesozoic cover, which experienced only Tertiary Alpine metamorphism (Pestal et al. 2009).

Another 27 of the Subpenninic samples were collected from the highest Subpenninic unit, the Modereck Nappe System (e.g., Kurz et al. 2008, Schmid et al. submitted, Chapter 5), which is infolded with part of the Glockner Nappe System (the so-called Seidlwinkl Fold at the Grossglockner area) above the roof thrust of the Venediger Duplex (Figs. 3.2 and 3.3). The units of the Modereck Nappe System originate from the most distal part of the European margin (Kurz et al. 2008, Schmid et al. submitted, Chapter 5). Their cover rocks contain mostly siliciclastic metapelite with albite, biotite and chlorite, although some horizons contain evaporite and black shale. The age of these

metasediments ranges from Upper Permian to Upper Cretaceous (Pestal et al. 2009, Schmid et al. submitted, Chapter 5), which constrains the metamorphic overprint of these rocks to be Alpine in age.

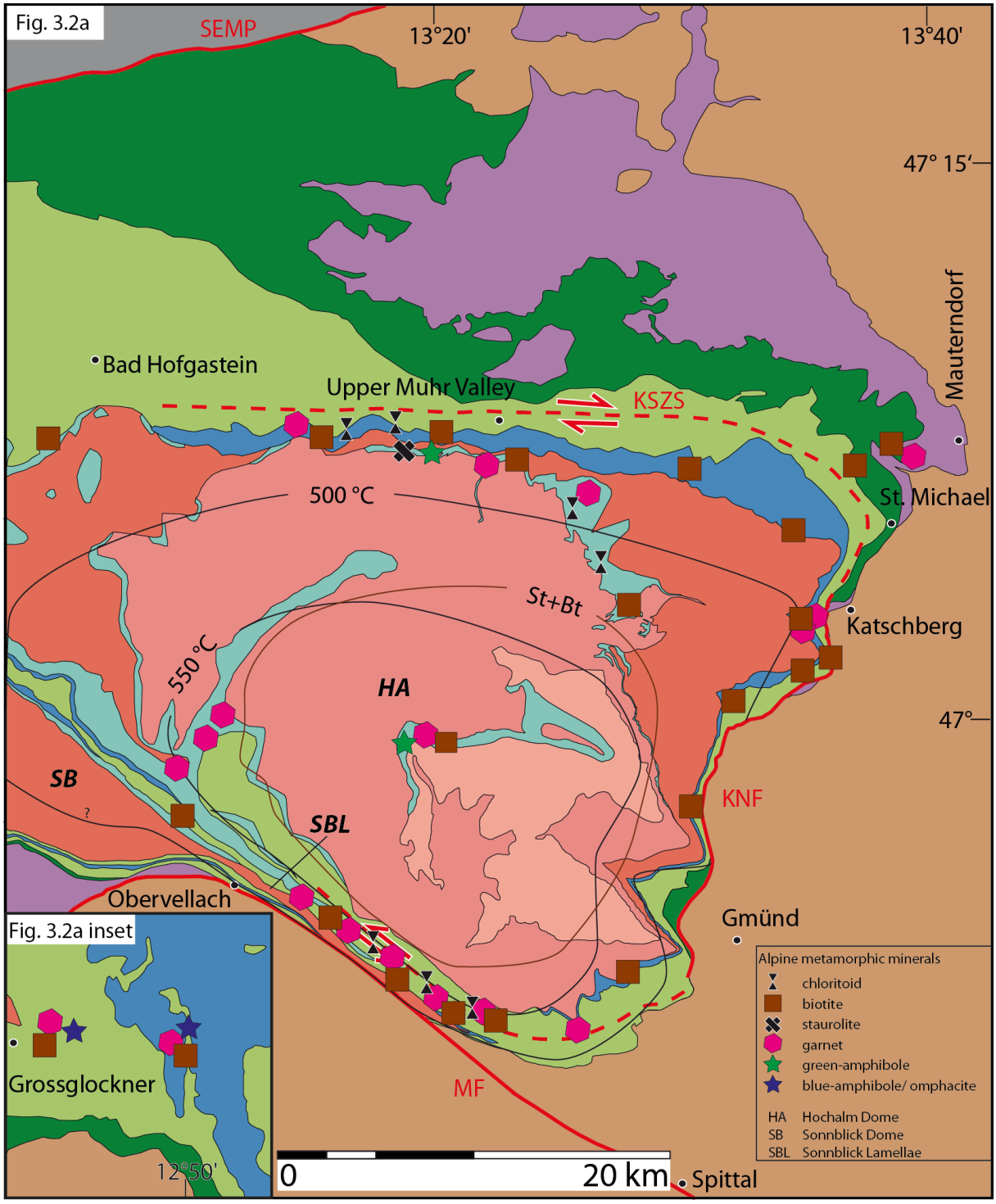

Figure 3.2: Tectonic map of the boxed areas in Figure 3.1 for the eastern Tauern Window:
(a) Map of main tectonic units, local names, metamorphic minerals and peak-metamorphic isograds; staurolite + biotite (St+Bt) from Droop (1981, 1985), isotemperature lines from Hoinkes et al. (1999) and Kurz et al. (1998) except for the Sonnblick Dome where the 500° C curve is drawn according to our own data. The legend is as in Figure 3.1, except for the basement nappes of the Venediger Duplex that are, from top to bottom (Schmid et al. submitted, Chapter 5): Sonnblick-Romate-Storz Nappe (dark red), Hochalm Nappe (intermediate red), Göss Nappe (light red).

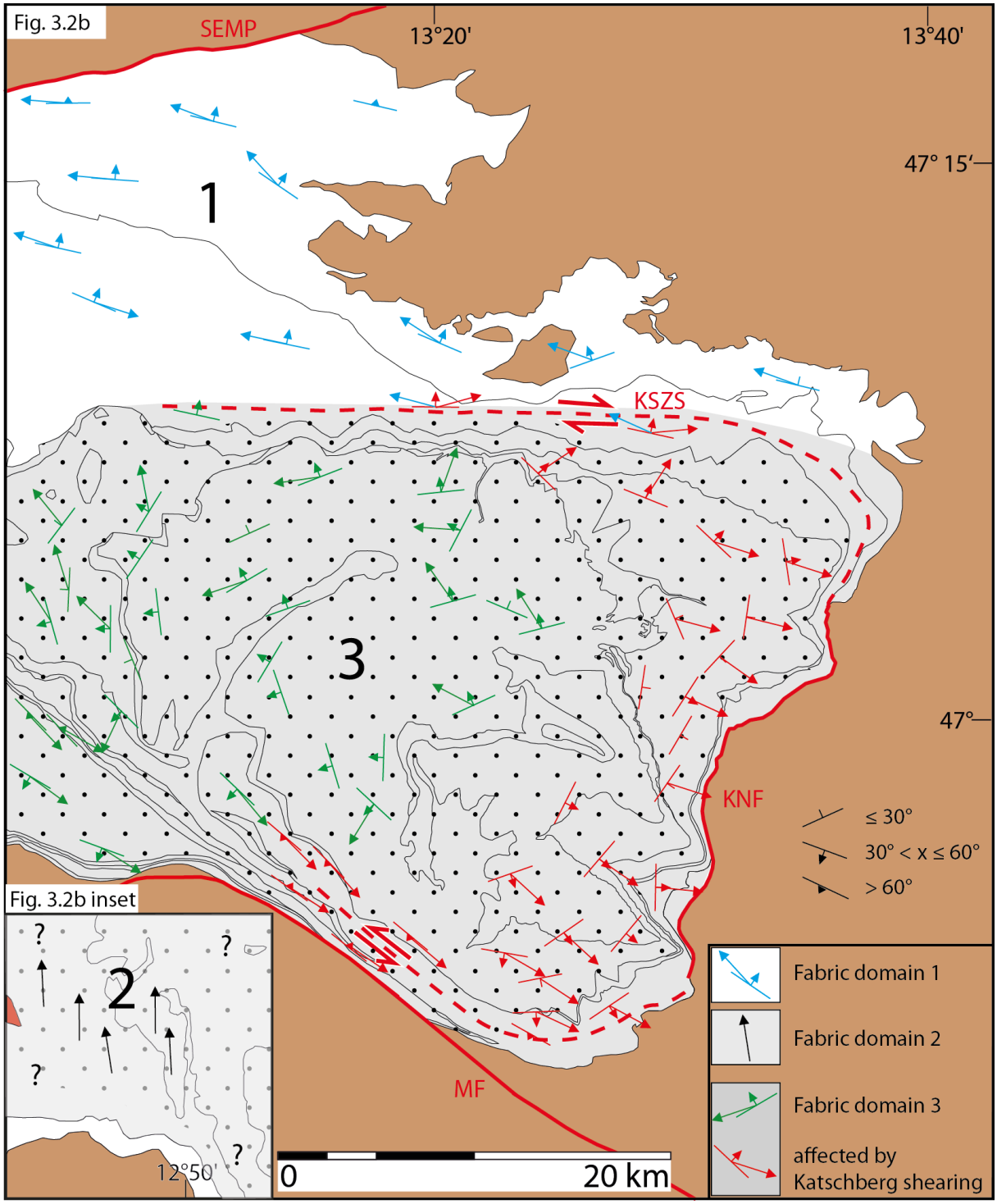

(b) Map of fabric domains 1, 2 and 3 described in text (section 3.2) and showing the orientations of the main mylonitic foliation and stretching lineation as taken from Scharf et al. (submitted a), Chapter 2. Dotted part of fabric domain 3 is where peak temperatures are clearly associated with the late-stage Barrow-type metamorphism (Tauernkristallisation).

One sample of white mica-garnet schist was taken from the cover of the Göss Nappe, the structurally lowest basement unit of the Venediger Duplex, (Fig. 3.3, light blue domain between Göss- and Hochalm basement units; sample number 196, sample AS-Gös323 in Table A-1). The protolith age of this cover, locally named the Draxel Complex (Exner 1971, 1980), is controversial; ages proposed so far range from Uppermost Devonian (Kebede et al. 2003, Lerchbauer 2008) to Lower Carboniferous (Pestal et al. 2009) and Late Carboniferous-Permian (Schmid et al. submitted, Chapter 5). In the latter case, metamorphism in these rocks would be post-Variscan and hence, of Alpine age.

3.2.2 Fabric domains sampled

We subdivided the Tauern Window into three fabric domains, based on the orientation and relative age of structures, as well as on the mineral parageneses associated with the main foliation (Fig. 3.2b):

(1) A greenschist-facies domain between the Salzach-Ennstal-Mariazell-Puchberg (SEMP) Fault (Ratschbacher et al. 1991) in the north and the northern branch of the KSZS (Scharf et al. submitted a, Chapter 2) in the south is characterized by a WNW-ESE striking main foliation (blue fabric in Fig. 3.2b). This foliation is deformed by and therefore predates the SEMP and KSZS fault structures; this older fabric deforms the base of the Lower Austroalpine nappes which are only affected by sub-greenschist-facies Alpine metamorphism (e.g., Schuster et al. 2004, Oberhänsli et al. 2004 and references therein).

(2) A blueschist- to eclogite-facies domain containing high-pressure mineral assemblages including omphacite and lawsonite (black stretching lineation in Fig. 3.2a). The main foliation in this domain carries a subhorizontal north-south trending stretching lineation associated with top-north sense of shear. This foliation is deformed by, and therefore older than, large post-nappe folds that characterizing doming in the eastern and western Tauern Window (e.g., Sonnblick- and Hochalm domes in Fig. 3.2a; D5 of Schmid et al. submitted, Chapter 5; see also Scharf et al. submitted a, Chapter 2). The boundary between domains 1 and 2 is sharp on the scale of Figure 3.2 and coincides with a major thrust contact within the Glockner Nappe System (see black arrow in Fig. 3.1 marking the thrust contact between fabric domains 1 and 2). This fabric boundary coincides with the boundary between the Glockner Nappe sensu stricto with its high-pressure mineral assemblages and the Fuscher Nappe, which shows no evidence of high-pressure metamorphism (geological map and explanations, Sheet “Salzburg”, Pestal et al. 2009). As discussed in section 3.5, we interpret this boundary to delimit a Paleogene subduction and exhumation channel.

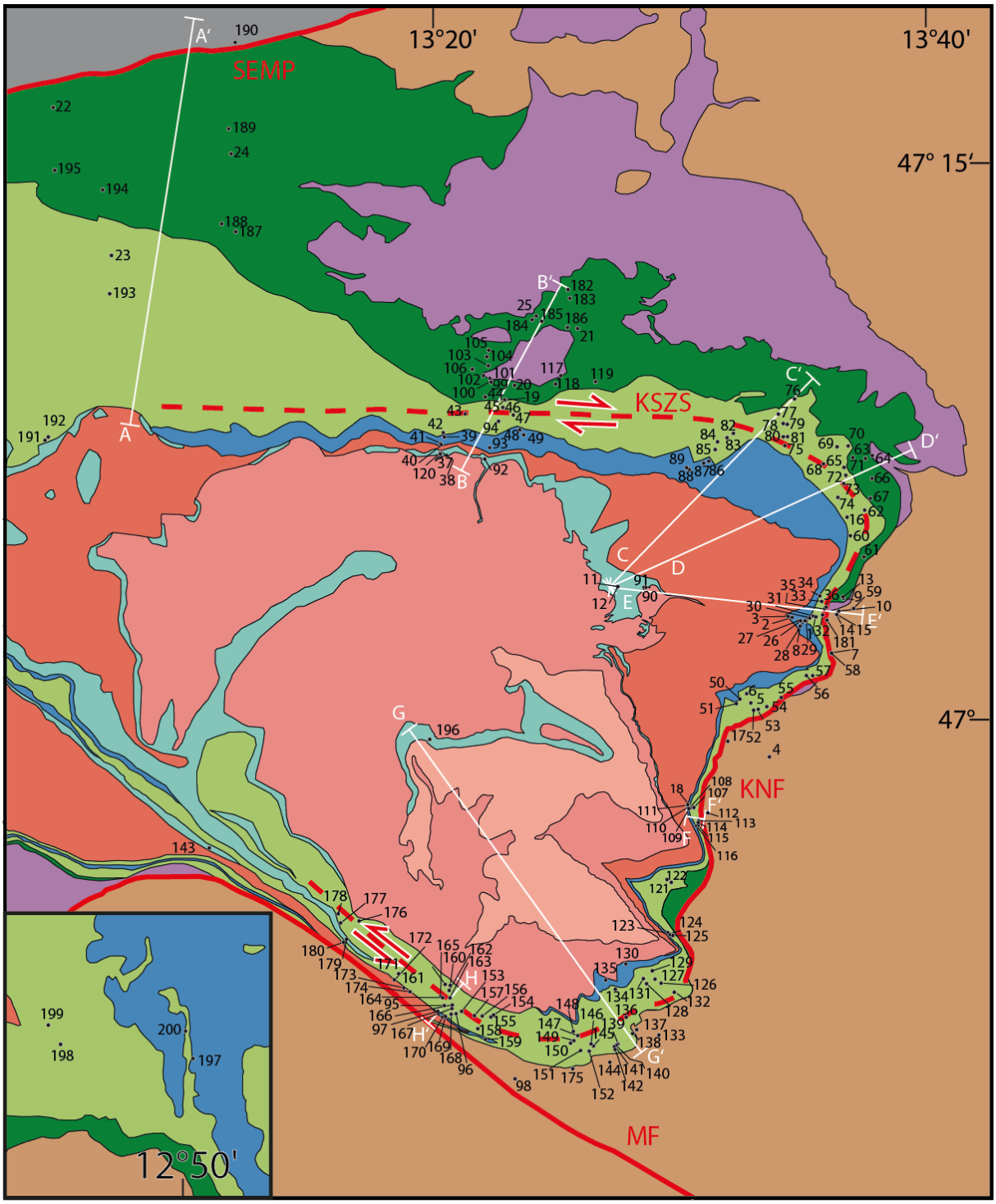

Figure 3.3: Tectonic map of the eastern part of the Tauern Window and of the Grossglockner area (inset). Numbers refer to samples and their locations (Table A-1). White lines show traces of cross sections a-h in Figure 3.5. Map modified from Schmid et al. (submitted), Chapter 5. Legend as in Figures 3.1 and 3.2.

(3) A greenschist- to amphibolite-facies domain corresponding with the ETD and the KSZS, described above, in Scharf et al. (submitted a) and Chapter 2. This domain has two main foliations: an older schistosity (green fabric in Fig. 3.2b) that is overgrown by prograde high-temperature mineral assemblages of the so-called Tauernkristallisation and deformed by the aforementioned domes, and a younger mylonitic foliation affecting the perimeter of the ETD under retrograde upper greenschist-

facies conditions (red fabric in Fig. 3.2b) and associated with the KSZS. This shear zone system accommodated east- to southeast-directed orogen-parallel motion, including top-southeast exhumation of the Subpenninic- and Penninic units sampled in the footwall of the aforementioned KNF. The northern and southern branches of the KSZS are steeply dipping, strike-slip shear zones that are interpreted as stretching faults, with decreasing amounts of displacement towards their western ends (Scharf et al. submitted a, Chapter 2).

We will return to these important distinctions in fabric when interpreting our data below, but emphasize that our strategy was to sample as many sedimentary units as possible within these fabric domains. Most of our samples were collected within domain 3. The coverage of domains 1 and 2 was more limited, but still sufficient to allow an interpretation of the geodynamic significance of pre-collisional thermal events. Samples were taken as far north as the SEMP Fault, which forms the northern limit of the Tauern Window. One sample (sample AS-GrA316, sample number 190 in Table A-1 and Fig. 3.3) was even collected in the Upper Austroalpine Grauwackenzone north of this fault.

3.3 Raman microspectroscopy on carbonaceous material

3.3.1 The method

With increasing temperature, carbonaceous material (CM) transforms from poorly ordered, highly contaminated matter to well-ordered graphite. The ordering of carbon-atoms, known as graphitization (Teichmüller 1987), is highly temperature-dependent and does not re-equilibrate or restructure with decreasing temperature during retrograde metamorphism. Therefore, graphitization is an irreversible process and the degree of carbon ordering in a natural rock by can be used as an indicator of peak metamorphic temperature (e.g., Quinn and Glass 1958, French 1964, Landis 1971, Grew 1974, Itaya 1981, Buseck and Bo-Jun 1985).

The Raman spectra of CM in a sample reflect primarily the degree of ordering of carbon atoms attained at peak temperature (e.g., Wopenka and Pasteris 1993). Several temperature calibrations based on the degree of ordering are currently available (Beyssac et al. 2002b, Rahl et al. 2005, Aoya et al. 2010). All methods rest on some basic assumptions:

(1) Only one single and distinct thermal peak affected the rocks investigated. To distinguish peak temperatures associated with different metamorphic events, a suite of samples must be collected over a sufficiently large area (some 50 km x 30 km) to ensure that only one event predominated within any given part of that area. In our study as in Wiederkehr et al. (2011) before, high-pressure metamorphism in the Glockner Nappe System was overprinted by a later Barrow-event centered in the core of the ETD (Kurz et al. 2008). Moreover, the metamorphic mineral assemblages must already be well known throughout the area and the difference in the peak temperatures of the events in this area must be greater than the relative error of the calibration (± 10-15° C, Beyssac et al. 2002b).

(2) The degree of carbon ordering in CM is exclusively temperature dependent, all other effects being negligible. Beyssac et al. (2002a) have shown that pressure effects on ordering of CM can be neglected. However, other factors that must be taken into account when interpreting CM spectra include the duration of the thermal event (Itaya 1981, Okuyama-Kusunose and Itaya 1987, Aoya et al. 2010), the differential stress (Bustin et al. 1986, Suchy et al. 1997, Ferreiro Mählmann et al. 2002, Nover et al. 2005), the host rock composition (Grew 1974, Wopenka and Pasteris 1993, Wada et al. 1994), the occurrence of catalytic minerals (Bonijoly et al. 1982, Okuyama-Kusunose and Itaya 1987 and references therein), the type of organic precursor (Kribek et al. 1994, Large et al. 1994, Bustin et al. 1995) and the composition and activity of fluids (Large et al. 1994, Guedes et al. 2005). We will return to these factors when discussing multi-peak temperature estimates from the same sample (section 3.5.1), but point out that most previous studies indicate that these effects are minor compared to that of temperature (e.g., Beyssac et al. 2002b, Rahl et al. 2005, Aoya et al. 2010, Lahfid et al. 2010, Wiederkehr et al. 2011).

The RSCM method offers several advantages when compared to other temperature indicators in metamorphic rocks (X-ray diffraction, high-resolution transmission electron microscopy (HRTEM), isotope geochemistry and vitrinite reflectance measurement). First, sample preparation is straightforward and requires only a standard polished (for microprobe) thin section which can be used for different types of investigation. Raman spectra can be acquired quickly (within 2 minutes per analysis) and several spots can be analyzed in a single sample, allowing one to identify heterogeneities. Second, the method is in-situ and does not destroy the sample. Third, the amount of CM required for an analysis is very small; 20-30 grains of 10 µm diameter are the minimum amount and size of material needed. Fourth, the range of peak temperatures that can be estimated with this method is very large, from sub-greenschist- to upper amphibolte- and granulite-facies conditions. We note that the relative peak temperatures (difference between two or more peak temperatures obtained from the same calibration) are as important for our interpretations as their absolute values. The error of relative temperature estimates is smaller (10-15° C, Beyssac et al. 2002b, Aoya et al. 2010) than the error of absolute peak temperature estimates (50° C, Beyssac et al. 2002b).

3.3.2 Measurement procedure

We used the measurement procedure of Wiederkehr et al. (2011) at a laser-wavelength of 532 nm. This wavelength is greater than the 514.5 nm used in the calibration experiments of Beyssac et al. (2002b), but nevertheless yields a difference in the estimate of peak temperature of only 5° C or less (Aoya et al. 2010). This is much less than the errors cited above in estimating the relative and absolute values of peak temperature.

Care was taken to measure CM located beneath a transparent mineral (quartz, albite or white mica) present at the sample surface (Pasteris 1989, Beyssac et al. 2002b, 2003b). We checked the effect of probing through two different transparent minerals (white mica and albite in samples

AS30ab, AS30noab; sample number 2 in Table A-1 and Fig. 3.3) and found that the peak temperatures so obtained were identical within error (CI of 95%). Where possible, the polarized laser beam was oriented perpendicular to the local mean stacking axis of the CM. Any spectra with bands from the glue (used for thin section preparation, Araldit AV 2020; refraction index of 1.553) overlying the graphite spectra were not used at all.

In each sample, 20 single spots of CM were measured, with each measurement conducted 10 times with a pulse duration of 12 s per measurement. Thus, the full acquisition time was 120 s per aggregate of CM in a sample. The position, height and width of the peaks (FWHM, full width at half maximum) beneath the single Raman spectra were determined with the program *PEAKFIT 4.12* (Seasolve Software Inc.). This program identifies the spectra with a combined Gaussian and Lorentzian function (Voigt function) and linear background correction. Error is estimated for a confidence interval (CI) of 95%.

3.3.3 Peak-temperature calibration of Raman spectra on carbonaceous material

Table 3.1 lists the four empirical temperature calibrations of the Raman spectra for carbonaceous materials used in this study. They are applicable for a temperature range of c. 350-650° C. and use the intensity ratios, R1 and R2, of the first-order Raman peaks D1-D4 and G (see Appendix). These ratios are defined as **R1 = D1/G** and **R2 = D1/(G + D1 + D2 + D3)** and are a measure of the degree of ordering of CM as a function of maximum temperature (Pasteris and Wopenka 1991, Wopenka and Pasteris 1993, Yui et al. 1996). We did not use second-order bands of the Raman spectra in our study because their relationship with the degree of carbon ordering is less clear (e.g., Beyssac et al. 2002b).

The calibrations of Beyssac et al. (2002b) and Aoya et al. (2010), i.e, calibrations a and d of Table 3.1, yield peak temperatures that are closest to the temperatures estimated from peak metamorphic mineral assemblages in the eastern Tauern Window. This is best demonstrated in two areas: (1) Along the southwestern margin of the ETD (i.e., parallel to the southern sinistral branch of the KSZS, Fig. 3.2) the coexistence of garnet, biotite and chloritoid, as well as the occurrence of the staurolite + biotite isograde (Droop 1981, 1985) constrain peak temperatures during the Tauernkristallisation to range from 500 to 550° C (Fig. 3.2). This brackets the peak-temperature estimates obtained from the two aforementioned calibrations (a and d in Table 3.1): 500° and 510° C, respectively. The other calibration methods (b and c in Table 3.1; Rahl et al. 2005 and Aoya et al. 2010) yield 475° C and 485° C, respectively; (2) In the core of the Hochalm Dome (i.e., in the Göss Nappe, Fig. 3.2), felsic gneisses contain garnet, green amphibole and biotite in the absence of evidence for partial melting. The temperature in this area therefore never exceeded 650° C, the minimum temperature for the onset of melting of water-saturated granitic rock (e.g., Holtz et al. 2001). This is corroborated by temperature estimates about 630 ± 40° C from phase equilibria (Droop 1985). All calibrations yield temperatures slightly below this value (612°, 640°, 632° C for calibrations a, c, and d in Table 3.1), except that of Rahl et al. (2005) which yields 680° C for the same locality

(Appendix, Table A-1). In general, all of the calibrations except that of Rahl et al. (2005) provide similar estimates of peak temperature for the range of c. 350-620° C; the difference in the peak temperature estimates is certainly well below the uncertainty of ± 50° C (Appendix, Figs. A-2 to A-4) and demonstrates the excellent consistency of the empirical calibrations so far.

We use Beyssac's et al. (2002b) calibration in the rest of the paper because its formula is simpler than those of the others and therefore yields a consistently lower 95% confidence interval (see Table A-1), even at peak temperatures above 575° C where the error tends to be greater. The reader is referred to the Appendix for details regarding the comparison and discussion of all the Raman calibrations applied to our area of investigation.

Table 3.1: Raman peak-temperature calibrations and conditions used in this study

	Calibration T[° C]=	**Peak temperature range [° C]**	**Laser wave-length [nm]**	**Reference**
a	-445R2+641	350-650	514.5	Beyssac et al. 2002b
b	$737.3+320.9R1-1067R2-80.638R1^2$	100-700	532	Rahl et al. 2005
c	$221R2^2-637.1R2+672.3$	340-655	514.5	Aoya et al. 2010
d	$91.4R2^2-556.3R2+676.3$	340-655	532	Aoya et al. 2010

3.4 Results

3.4.1 Contouring of peak temperatures in different fabric domains

Figure 3.4 shows the contours of peak temperature in the area according to the calibration of Beyssac et al. (2002b), as well as the traces of cross sections for peak temperature that emanate from the core of the ETD (Fig. 3.4). We drew these contours by hand in order to interpolate between points of bracketing peak temperatures as well as to follow the main foliation in the different fabric domains described in section 3.2. Locations with a high sample density are indicated with dark shading in Figure 3.4. The advantage of hand drawing the contours is that we could fit them with the dominant structures in the area, as well as avoid edge effects where the sample density is small and/or points of anomalous peak temperature obviously do not fit the overall pattern. For comparison, the contours of peak temperature from the other three calibrations (Rahl et al. 2005, Aoya et al. 2010 – c, d of Table 3.1) are shown in the Appendix (A-5 to A-7, respectively).

Note that contours of peak temperature are not isotherms! An isotherm represents a temperature attained at a specified time, whereas the contours in Figure 3.4 represent the peak temperatures attained at different times, even for the same thermal event within a given fabric domain. We did not draw any peak-temperature contours in domain 2 (inset to Fig. 3.4) due to the limited number (four) of samples there and the fact that they had almost the same values.

A few measurements (samples AS87, AS-Ka103, AS-Ste135, AS-Zed200, AS-Gm242 and AS-Re292; marked red in Table A-1) yield anomalous peak temperatures which do not fit the overall pattern at all. There are two possible reasons for this: First, graphitization of organic matter in these samples may depend on more than just temperature, as discussed above (section 3.3); Second, the sedimentary protoliths may contain organic detritus eroded from areas that underwent pre-Alpine metamorphism at higher peak temperatures (e.g., Dissel et al. 1978, Itaya 1981) than during the Alpine events discussed here. In addition, we note that sixteen samples (Table A-1) yield more than one peak temperature for a given calibration. These anomalies are discussed below and in section 3.5.1. Most of these samples come from or near the KSZS. In the following, we discuss the pattern of peak-temperature estimates in each of the three fabric domains outlined in Figure 3.2b.

3.4.2 Domain 1

The highest peak temperatures (471 ± 4° to 489 ± 5° C) recorded in the southernmost and structurally lowest part of the Glockner Nappe System north of the KSZS systematically decrease northward without a discernable discontinuity across the contact between Glockner Nappe System and Matrei Zone contact towards the SEMP Fault, as seen in the map (Fig. 3.4) and cross section A-A´ (Fig. 3.5a). The trend and spacing of the contours are rather speculative given the paucity of data in this domain; three points define the 400° C contour which runs parallel to the trace of the main foliation. We have drawn the other contours on the assumption that they trend parallel this foliation. Peak temperatures of less than 350° C are not recorded in this domain because the lithology in the northernmost part of the area is a pure carbonate without CM (Klammkalke). However, we surmise that the peak temperatures there were of the lowermost greenschist-facies as previously mapped (see Oberhänsli et al. 2004). A similar trend of northeast-ward-decreasing peak temperatures is observed further to the east in the Matrei Zone, i.e., north of the northern branch of the KSZS (Fig. 3.5b). This corresponds to a peak temperature field gradient of 8° C/km perpendicular to the main foliation. One sample (sample 190, AS-GrA316; Table A-1 and Fig. 3.3) within the Grauwackenzone north of the SEMP Fault indicates a higher temperature (389 ± 3° C). We attribute this to Late Cretaceous metamorphism ($^{40}Ar/^{39}Ar$ white mica ages of 90-115 Ma, given by of Urbanek et al. 2002), which occurred under greenschist-facies conditions according to previous studies (Schramm 1980).

3.4.3 Domain 2

Peak temperatures of around 500° C were inferred for the four samples within this domain that is characterized by blueschist- to eclogite-facies mineral assemblages (inset to Fig. 3.4). One of the samples has Raman spectra that yield two peak temperature estimates: 503° C and 554° C (sample MH-286b, see Table A-1, discussion in section 3.5.1). Despite the fact that our data are too few to warrant contouring, the similar peak temperatures recorded in both the Glockner- and the Modereck

Nappe Systems (green and blue units in Figs. 3.1-3.5) suggest that these units experienced a common subduction and exhumation history.

3.4.4 Domain 3

The peak-temperature contours within the ETD show a concentric pattern that is very similar to the shape of the isograds around the dome in Figure 3.2. The highest peak temperature (612° C, sample AS-Gös323, sample number 196 in Table A-1 and Fig. 3.3) is located in the Göss Nappe at the core of the ETD as outlined by the main foliation pattern (Fig. 3.2). The contours are poorly constrained due to the predominance of orthogneisses and the corresponding lack of CM measurements in this area. Nevertheless, we feel confident that the contours follow the main foliation around the Hochalm Dome based on our observation that the dome deforms the main foliation which itself is overgrown by amphibolite-facies peak-metamorphic mineral assemblages of the Tauernkristallisation (Scharf et al. submitted a, Chapter 2). The rim of the Hochalm Dome was highly sheared by the KSZS during Miocene time and, hence, the peak-temperature contours must follow the main foliation in this fabric domain. This approach in drawing the contours lies behind the local variations in their trend in Figure 3.3.

Along the perimeter of the ETD, the peak temperature contours generally follow the main foliation of the KSZS. For example, the 500° C contour follows the boundary of the Subpenninic Nappes along the northern dextral branch of the KSZS, then swings around the northeastern corner of the ETD into parallelism with the KNF, before again swinging into concordance with the southern sinistral branch of the KSZS (Fig. 3.4). The peak temperature decreases systematically from the core of the ETD to the KSZS. The peak-temperature field gradient across the steep strike-slip branches of the KSZS is about 30° C/km (cross sections B and H, Figs. 3.5b, h) and reaches as much as 70° C/km across the low-angle normal fault (KNF) at the eastern edge of the ETD (cross sections E and F, Figs. 3.5e, f). This is where the peak-temperature contours are the most closely spaced and where tectonic omission of Penninic- and Subpenninic units in the footwall of the KNF is greatest (Scharf et al. submitted a, Chapter 2).

A subtle but significant feature in Figure 3.4 (see also profile H-H´ of Fig. 3.5h) is that the peak-temperature interval of 500-525° C occurs twice near the southern branch of the KSZS and is separated by a narrow band of 475-500° C (see peak-temperature trough of about 20° C in profile H of Fig. 3.5h). The southern band outlining the 500-525° C interval coincides with the southeastern end of the Sonnblick Gneiss Lamellae (wedge tapering out southeast-ward from the Sonnblick Dome, SB in Fig. 3.2a) whereas the northern band marks the edge of the Hochalm Dome (HA in Fig. 3.2a). As will discussed below, we interpret the Sonnblick- and Hochalm domes as the hot cores of elongate antiforms separated by a relatively cold synform.

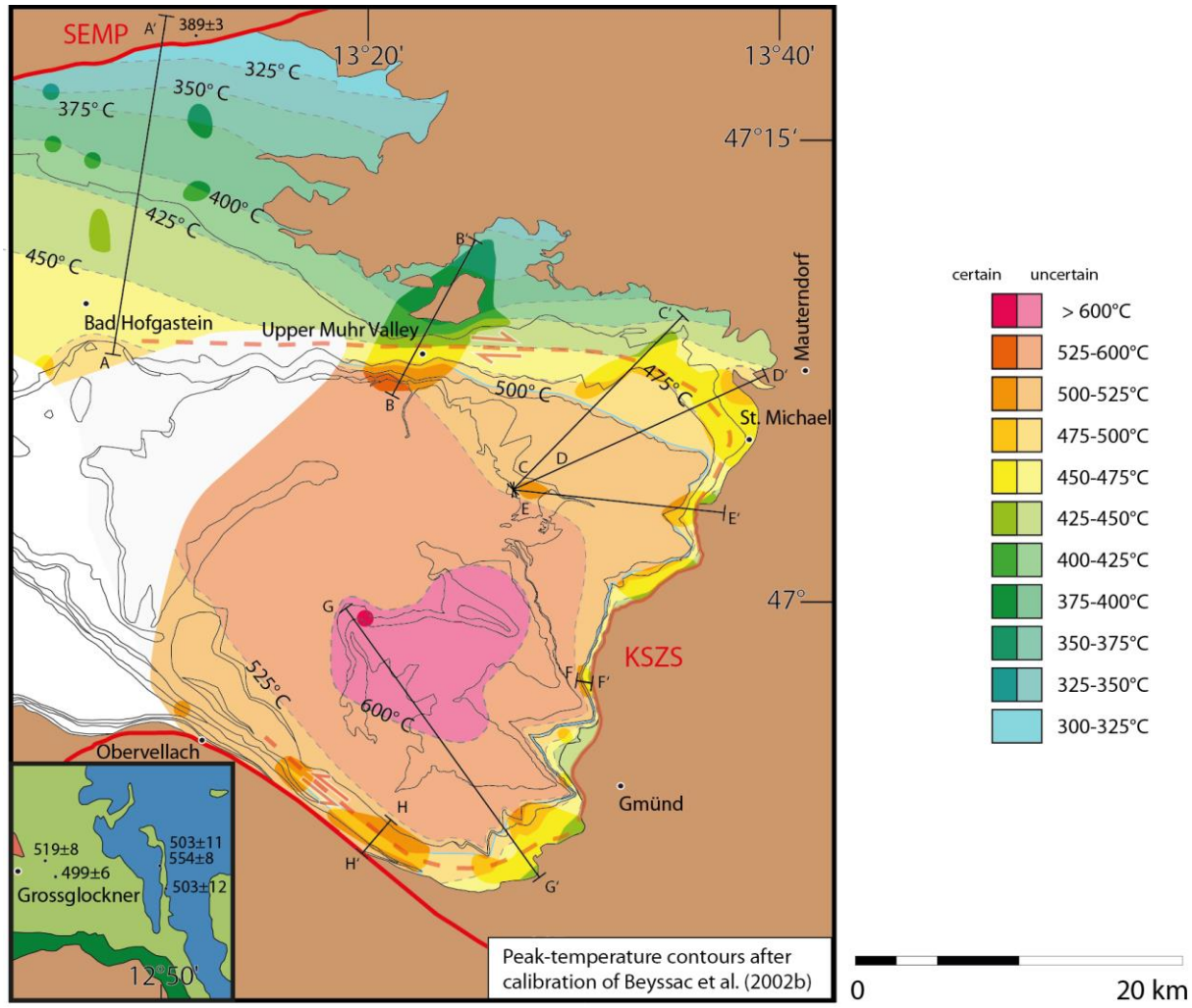

Figure 3.4: Peak-temperature contours in fabric domains 1 and 3 are based on the calibration of Beyssac et al. (2002b). Transparent colours and dashed lines indicate areas and contours where the sample density is low. Brown colours indicate Austroalpine units. Grey lines indicate tectonic contacts separating units of the Tauern Window as taken from Schmid et al. (submitted), Chapter 5. The 500° C peak-temperature contour is marked in blue, as discussed in the text. Inset shows estimated peak temperatures from 4 samples in fabric domain 2. Trace of cross sections shown in Figures 3.3 and 3.4. Sample locations and data in Figure 3.3 and Table A-1.

Figure 3.5: Cross sections (a-h) of peak temperature along traces shown in Figures 3.4 and 3.3. Calibration of Beyssac et al. (2002b) with individual CI (95%) bars. Colours along the horizontal axes indicate the tectonic units in Figures 3.1, 3.2a, 3.3 and 3.4. The boundaries of the KSZS are marked in cross sections b-h by red dotted lines. Note that the horizontal axes in sections f and h are expanded by a factor of 3 for easier viewing. Peak-temperature points are projected into the sections from as much as 2.5 km on either side of the section planes, except in Fig. 3.5a where the projection is up to 5 km from the plane.

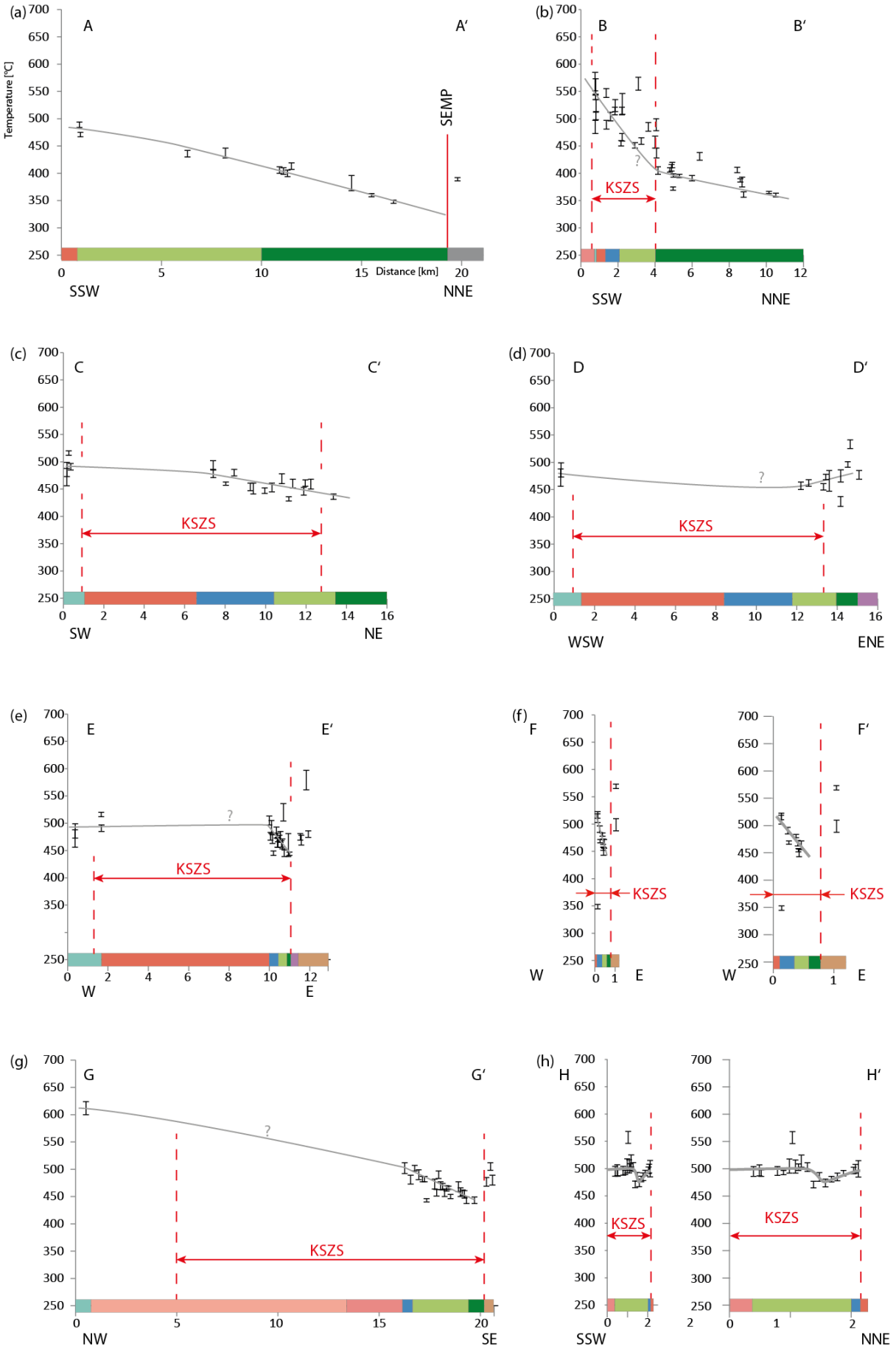
(a)
A
A'
SEMP
Temperature [°C]
Distance [km]
SSW
NNE
(b)
B
B'
KSZS
SSW
NNE
(c)
C
C'
KSZS
SW
NE
(d)
D
D'
KSZS
WSW
ENE
(e)
E
E'
KSZS
W
E
(f)
F
F'
KSZS
KSZS
W
E
W
E
(g)
G
G'
KSZS
NW
SE
(h)
H
H'
KSZS
KSZS
SSW
NNE

Close examination reveals several anomalies: In the Upper Muhr Valley (Figs. 3.2 and 3.4) along the northern branch of the KSZS, peak temperatures significantly scatter in the Modereck and Glockner Nappe Systems (southern part of profile B-B' in Fig. 3.5b) and locally exceed 560° C (e.g., sample AS-Mu125, sample number 43 in Table A-1 and Fig. 3.3). Another positive anomaly in peak temperature occurs at the arcuate, northeastern margin of the KSZS (near Speiereck, west of Mauterndorf and north of St. Michael, Figs. 3.2a and 3.4), where samples (e.g., sample AS-SP160, sample number 69 in Table A-1 and Fig. 3.3) of Penninic- and Lower Austroalpine units yield about 500° C. A low field gradient is recorded across the northeastern part of the ETD, where peak temperatures do not vary significantly across the Subpenninic Storz Nappe (Fig. 3.4 and cross sections C, D and E in Figs. 3.5c-e). This probably reflects the shallow northeastward dip of this nappe.

3.5 Discussion

3.5.1 Multiple peak temperatures in a given sample

Sixteen samples (Table A-1) yield more than one peak temperature per sample as determined from separate clusters of Raman spectra. This is difficult to explain if one assumes that peak temperature is the only factor controlling the maximum degree of order in organic material (section 3.3.1). Most of these samples (14) are located within or close to the KSZS. This is consistent with the idea that shearing locally reduced the ordering of CM in the samples. Alternatively, the multiple peaks can be attributed to a kinetic effect; Katschberg shearing juxtaposed hot and cold rock masses such that cooler rocks just outside of the KSZS experienced an ephemeral heating event. Possibly, the CM in these samples never equilibrated with this short-lived peak temperature. A third possibility is that the separate Raman spectra within one sample result from mixing of detrital sediments with different thermal provinces (Dissel et al. 1987). This may apply to the two samples with multiple Raman spectra that come from fabric domain 2 (sample MH-286b, sample number 200 in Table A-1 and Fig. 3.3) or to the Austroalpine units (sample AS36, sample number 4 in Table A-1 and Fig. 3.3), but in the absence of further information we can only speculate as to the causes.

3.5.2 Age constraints for the inferred peak temperatures

The peak temperatures determined with RSCM can only be interpreted in a geodynamic context if we know the age of metamorphic events in the three fabric domains and in the adjacent Austroalpine units that border the Tauern Window.

The main foliation sampled in fabric domain 1 is deformed by both the SEMP Fault and by the northern branch of the KSZS (Fig. 3.2). Both of these faults are interpreted to have initiated in Late Oligocene to Early Miocene time, certainly no later than 21 Ma, which marks the onset of Adriatic indentation and rapid exhumation in the Tauern Window (Schmid et al. submitted, Scharf et al.

submitted a, Chapter 2, 5). The $^{40}Ar/^{39}Ar$ white mica ages of Liu et al. (2001) for this fabric domain in the South Penninic Matrei Zone range in age from 36.8-28 Ma (excluding one sample with an age of 21.8 Ma) and are interpreted as the age of cooling beneath the closure temperature of 410-350° C (Liu et al. 2001 after von Blanckenburg et al. 1989, Dahl 1996). Regional geologic considerations constrain the onset of accretion in the Matrei Zone, originally located at the southern limit of Alpine Tethys, to have begun no later than 84-94 Ma (e.g., Cenomanian-Santonian flysch ages as discussed in Handy et al. 2010, and references therein). Thus, the available information indicates that the main deformation and peak of metamorphism in fabric domain 1 occurred during Late Cretaceous to Late Paleogene time.

High-pressure metamorphism in fabric domain 2 is constrained to have occurred within a 45-38 Ma time interval based on $^{40}Ar/^{39}Ar$ phengite ages that are interpreted as ages of formation (Kurz et al. 2008). Younger ages for this event have been obtained with the Rb-Sr white mica system (31.5 ± 0.7 Ma; Glodny et al. 2005, 2008) and Lu-Hf garnet chronometry c. 32.7 Ma (Horwartz et al. 2012) but we do not regard them as viable high-pressure ages because they contradict several lines of geological evidence in favor of a pre-Oligocene age (discussion in Schmid et al. submitted, Chapter 5). In any case, the main schistosity in this domain is overgrown by upper greenschist- to amphibolite-facies mineral assemblages of the Oligocene "Tauernkristallisation" (see section 3.2) and is deformed by large Miocene folds (e.g., Sonnblick Dome, Fig. 3.2a). The peak conditions attained in the high-pressure part of the Glockner Nappe System are 1.7 GPa and 570° C (Dachs and Proyer 2001) as documented by pseudomorphs after lawsonite (e.g., Grossglockner area west of the Sonnblick Dome, Fig. 3.2a, Gleissner et al. 2007). The temperatures are roughly compatible with the peak temperatures of about 500° C from Raman microspectroscopy.

The two main foliations in fabric domain 3 (see Fig. 3.2b) are related to different tectonic events, as already outlined above. The first of these under amphibolite-facies conditions is associated with stacking of the Subpenninic nappes in the Venediger Duplex which syn- to post-dates thrusting and exhumation of the overlying high-pressure units in fabric domain 2 (Schmid et al. submitted, Chapter 5). On the other hand, it pre-dates the Tauernkristallisation and subsequent doming, as noted above. The likely age interval for this event is therefore 35-30 Ma. The overprinting retrograde foliation of the KSZS around the perimeter of the ETD is constrained to have formed at 23 to 17 Ma, as discussed in Scharf et al. (submitted a) and Chapter 2. This event was coincident with formation of the Hochalm- and Sonnblick domes (Fig. 3.2a).

3.5.3 Interpretation of peak temperatures in a geodynamic context

Figure 3.6 is a first attempt to depict the different peak temperatures in the three fabric domains (Figs. 3.6a-c) in a tectonic context (Figs. 3.6d-g). The sections in Figs. 3.6d-g show the evolution in a north-south transect of the Tauern Window, and build on previous work (Kurz et al. 2008, Schmid et al.

submitted, Scharf et al. submitted a, Chapter 2 and 5). We distinguish three different thermal regimes associated with different stages of the convergence between Adria and Europe:

(1) The maximum recorded temperature of about 480° C in domain 1 is consistent with the greenschist-facies metamorphism observed in this domain and is interpreted to have resulted from the accretion of oceanic crust of Alpine Tethys in the footwall of the Austroalpine nappes. The units in domain 1 thus represent the leading edge of the advancing Adriatic plate in Paleogene time (Figs. 3.5a, d). Similar peak conditions have been documented from the basal units of exhumed accretionary wedges in other localities (e.g., Taiwan, Suppe 1984) The slight increase in peak temperature going upsection into the Lower Austroalpine units of the northeastern Tauern Window (Figs. 3.4, 3.5d) may reflect the stacking of originally deeper units in the Paleogene Penninic accretionary wedge. We note that the lack of any discernable jump in peak temperatures across the Glockner Nappe System/Matrei Zone thrust contact (Fig. 3.5a, section 3.4.1) indicates that the temperature field was established only after these two units, which derive from different parts of Alpine Tethys, were tectonically juxtaposed. (i.e., after 65Ma and before 42 Ma, see Figs. 3.6d, e).

The post-peak thermal evolution for domain 1 is poorly constrained, but thermochronometric age studies so far indicate that the Matrei Zone as well as parts of the Glockner Nappe System that were unaffected by high-pressure metamorphism (i.e., the Fuscher Nappe; Frasl and Frank 1966) experienced the Tauernkristallisation in Late Oligocene time (labeled TK in Fig. 3.6). Two $^{40}Ar/^{39}Ar$ white mica cooling ages of Liu et al. (2001; their samples YL10, YL12,) show that these units cooled to below 410-350° C some 28 Ma ago. Thus, temperatures during the Tauernkristallisation must have exceeded 410-350° C, but not the previous peak of 480° C (Fig. 3.6a). The single Miocene $^{40}Ar/^{39}Ar$ white mica age in the part of the Matrei Zone immediately adjacent to the northern branch of the KSZS (21.7 Ma, Liu et al. 2001, their sample YL40) is interpreted to reflect advective heating of fabric domain 1 during its juxtaposition with the warm ETD during extensional exhumation along the KSZS.

(2) Three of the samples from this domain 2 are derived from the Glockner Nappe sensu stricto and yield peak temperatures of 500-520° C. None of these samples preserve high-pressure mineral assemblages, but eclogite-facies minerals are present in nearby rocks. One sample (sample MH-286b, sample number 200 in Fig. 3.3 and Table A-1) yields two peak temperatures: 503 ± 11° C and 554 ± 8° C. The sample is a garnetiferous micaschist of probable Early Cretaceous age (Brennkogel Schist) in an imbricate zone that includes slices of both the oceanic Glockner Nappe sensu stricto and the continental Modereck Nappe System (Pestal et al. 2009). Whereas Paleogene eclogite-facies metamorphism is well documented in lenses of the former unit, high-pressure assemblages have not been found in the latter (Pestal et al. 2009; Fig. 3.6e). We are unable to ascertain the causes for two peak temperatures in this sample, but the mineral assemblages in these rocks indicate that similar peak

temperatures prevailed during both the eclogite-facies event (570° C; Dachs and Proyer 2001) and the overprinting Tauernkristallisation (no cooling ages obtained in this area, but Dachs 1990 determines 525° C in the Eclogite Zone, Fig. 3.1). Thus, we are unable to identify which of these two events is recorded by the CM Raman spectra in this domain (Fig. 3.6b).

(3) Our data supports the notion that all rocks of fabric domain 3 (Fig. 3.2) are affected by the Oligocene amphibolite- to greenschist-facies Barrow-type metamorphism (Tauernkristallisation) which resulted from thickening of the European crust (Venediger Duplex formation, Fig. 3.6f). Peak temperatures range from 440° C in the Glockner Nappe System to 612° C in the cover of the Göss Nappe (section 3.4.4). The very steep field gradients in peak temperature along the edges of the ETD (up to 70° C/km) reflect the modifying effects of mylonitic shearing within the KSZS (Figs. 3.4, 3.5, 3.6c, 3.6g). As pointed out above, the steepest gradient in peak temperature occurs in the footwall the KNF and coincides with the site of maximum tectonic thinning of the Subpenninic- and Penninic units (Scharf et al. submitted a, Chapter 2). We estimate the original (pre-Katschberg) peak gradient to have been only about 13° C/km as obtained by dividing the difference between peak temperatures from the bottom (612° C) and top (440° C) of the nappe pile by the estimated 13.5 km of throw along the KNF (Scharf et al. submitted a, Chapter 2). The narrow corridor of lower peak temperatures parallel to the southern branch of the KSZS (Figs. 3.4, 3.5h) may be attributed to isoclinal folding along the eastern prolongation of the Mallnitz Synform (a late-stage synform located between the Hochalm- and Sonnblick domes, see SB and HA Fig. 3.2a, for further details see Scharf et al., submitted a, and Chapter 2) that modified the post-nappe temperature field of the Tauernkristallisation.

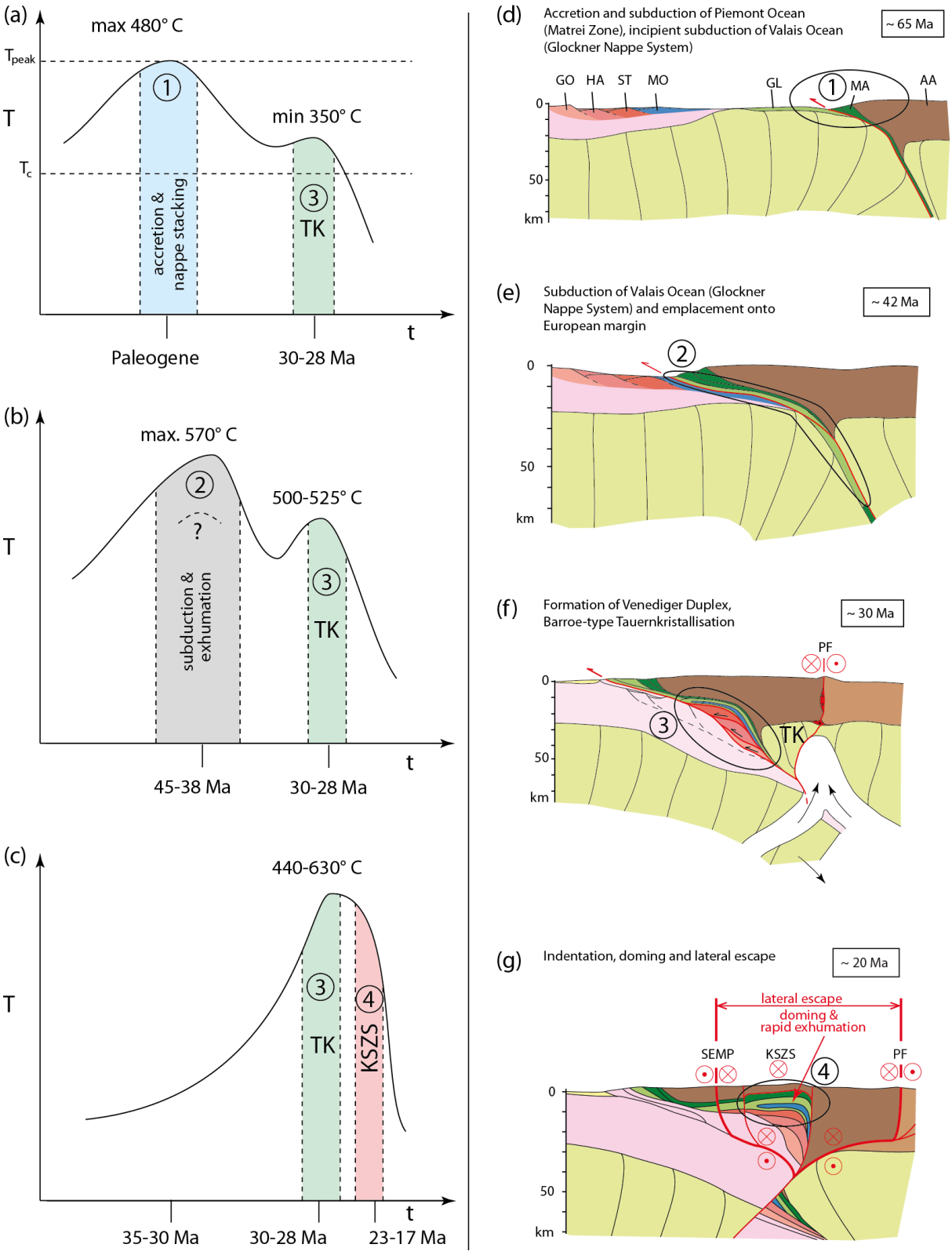

Figure 3.6: Schematic peak temperature versus time curves for the three fabric domains (a-c) and their corresponding tectonic stages (d-g) as discussed in the text. AA – Austroalpine nappes; GL – Glockner Nappe System; GO – Göss Nappe; HA – Hochalm Nappe; KSZS – Katschberg Shear Zone System; Ma – Matrei Zone; MO – Modereck Nappe System; PF – Periadriatic Fault; SEMP – Salzach-Ennstal-Mariazell-Puchberg Fault; ST – Storz Nappe; TK – Tauernkristallisation. Legend as in Figures 3.1 and 3.2. T_c - closure temperature of the $^{40}Ar/^{39}Ar$ System on white mica; T_{peak} - peak temperature obtained in this study.

3.6 Conclusions

By incorporating structural data and geodynamic considerations published elsewhere (e.g. Schmid et al. submitted, Scharf et al. submitted, Chapter 2 and 5) we successfully applied the RSCM method to determine and interpret peak temperature field gradients in three different fabric domains formed in distinct orogenic settings. Fabric domain 1 preserves oceanic units that attained a maximum peak temperature of about 480° C in the upper greenschist-facies just after Late-Cretaceous to Paleogene nappe stacking in an accretionary wedge. Fabric domain 2 experienced peak temperatures of about 500-550° C either during Paleogene burial and exhumation within a subduction/exhumation channel, or during Barrow-type thermal overprinting due to Oligocene nappe-stacking within the Alpine collisional orogen. Fabric domain 3 has a peak-temperature field that resulted from Eo-Oligocene nappe stacking of continental units and that was subsequently modified in Miocene time by post-nappe doming and extensional shearing along the Katschberg Shear Zone System (KSZS). The peak temperatures in the largest dome (Hochalm Dome) range from 612° C in its core to 440° C at its rim. The steepest gradient in peak temperature (up to 70° C/km perpendicular to foliation) occurs along the eastern margin of this dome where mylonitic shearing of the Katschberg Normal Fault (KNF) has significantly reduced the thickness of the Subpenninic- and Penninc nappe pile.

The large number (200) of samples from the study allow us to compare the peak temperatures inferred from four empirical temperature calibrations of Raman spectra for CM (Beyssac et al. 2002b, Rahl et al. 2005, Aoya et al. 2010, with two calibration methods). We found that the calibrations of Beyssac et al. (2002b) and Aoya et al. (2010; $91.4R2^2$-556.3R2+673.3) provide estimates of peak temperatures that are in closest agreement with those based on peak metamorphic mineral assemblages, especially at higher (> 500° C) peak temperatures (calibration methods a and d of Table 3.1). Interestingly, all calibrations yield the same pattern of peak temperatures in each fabric domain and, what is more striking, the differences in these temperature estimates are less than the ± 50° C absolute error of the calibrations (Beyssac et al. 2002b). This is testimony to the robustness of the RSCM method.

Finally, we are confident that the RSCM method can also be used to discern the thermal structure and boundaries of the Cenozoic subduction/exhumation channel preserved in the central part of the Tauern Window. The data available so far indicate that one such boundary occurs within the Glockner Nappe System (black arrow in Fig. 3.1) and may coincide with the transition from fabric domains 1 and 2.

Acknowledgments

We are indebted to many colleagues for discussions, especially Audrey Bertrand, Konrad Hammerschmidt, Susanne Schneider and Claudio L. Rosenberg, all from the Freie Universität Berlin, as well as Ralf Schuster and Gerhard Pestal from the Austrian Geological Survey Vienna, and Bernhard Fügenschuh from the Universität Innsbruck. Special thanks go to Roland Oberhänsli (Universität Potsdam) who kindly supported our work in the Raman lab at the Universität Potsdam. Anna Giribaldi and Sandra Wollnik (both Freie Universität Berlin) are thanked for preparing thin-sections. Martina Grundmann is particularly thanked for drafting the figures. Finally, we acknowledge the support of the National Park Services Hohe Tauern, in particular of Katharina Aichhorn and the staff of the Bios Zentrum in Mallnitz. Our work was financed to a large extent by the German Science Foundation (DFG-project Ha 2403/10). Stefan M. Schmid acknowledges the Alexander-von-Humboldt Foundation for support of his collaborative research in Berlin from 2008-2010.

Chapter 4

Thermal evolution from orogenic doming to extensional exhumation - new perspectives from in-situ $^{40}Ar/^{39}Ar$ Laser-probe ages of white mica (Tauern Window, Eastern Alps)

This chapter will be submitted in Journal of Metamorphic Geology as: Scharf, A., Handy, M.R., Schmid, S.M. & Sudo, M. (in prep.) Thermal evolution from orogenic doming to extensional exhumation - new perspectives from in-situ $^{40}Ar/^{39}Ar$ Laser-probe ages of white mica (Tauern Window, Eastern Alps). The definitive version is available at www.blackwell-synergy.com.

Abstract

$^{40}Ar/^{39}Ar$ Laser ablation on individual white mica grains of Penninic and Subpenninic units from the northeastern margin of the Eastern Tauern Subdome (ETD) reveals ages between 13 and 31 Ma. The scatter of the single grain ages within the nine dated specimens, and in particular their microstructural setting constrains the timing of exhumation along the central part of the ductile Katschberg Shear Zone System (KSZS), particularly along its central segment, the Katschberg Normal Fault, to start at an unknown instant of time before 20 Ma and to end at around 17 Ma. The new data, together with literature data based on other thermochronological methods, indicate that the onset of cooling in the Eastern Tauern Subdome occurred shortly after the thermal peak at around 28-30 Ma and hence, significantly predates the onset of cooling in the Western Tauern Subdome, which occurred at around 20 Ma. The discussion of timing and rates of exhumation in the light of structural evidence reveals that exhumation of the Western Tauern Subdome, linked to the activity of the Brenner Normal Fault, according to the literature data has to be looked for by the differential northward movement (indentation) of the Southern Alps east of the sinistral Giudicarie Belt. It is discussed that the exhumation of the Eastern Tauern Subdome is linked to shearing within the KSZS during its later stages. Cooling and therefor exhumation must have started significantly earlier in the Eastern Tauern Subdome than in the Western Tauern Subdome by a yet unknown alternative mechanism pre-dating indentation of the Southern Alps. Early stages of exhumation are possibly linked to a lateral switch in subduction polarity of the European and Adriatic slabs that occurs beneath the central Tauern Window.

Keywords

Eastern Alps, Katschberg, $^{40}Ar/^{39}Ar$ Laser-ablation, orogen-parallel lateral extrusion,

4.1 Introduction

Determining the exact timing of cooling is crucial for evaluating timing and rates of exhumation in orogens and for discussing mechanisms of exhumation, e.g., discussing the relative importance of tectonic omission and erosional denudation, the latter possibly being climate-driven, in orogens (e.g., Ring et al. 1999, Reiners and Brandon 2006). In the Alps the unique potential of in situ thermochronometry for solving such questions has been exploited since over 40 years ago (e.g., Clark and Jäger 1969, Wagner and Reimer 1972).

This contribution attempts to shed more light on the timing of exhumation in the Tauern Window of the Eastern Alps, whose exhumation is known to be related to orogen-parallel normal faulting that occurred in combination with strike slip faulting and orogen-perpendicular shortening during a late stage in the Alpine history (e.g., Ratschbacher et al. 1991a, Rosenberg et al. 2007) by presenting $^{40}Ar/^{39}Ar$ Laser ablation single grain ages on white micas, combined with careful geochemical and microstructural investigation of the analyzed grains. Existing data of high- and low-temperature geochronometers in the area of the Tauern Window (e.g., Luth and Willingshofer 2008) provide evidence in favor of a different onset of rapid exhumation/cooling in the areas of the Western and Eastern Tauern Window. This is in contrast with the postulate that South-Alpine indentation into the Alps north of the Periadriatic Fault, possibly in combination with Carpathian slab pull, triggered contemporaneous exhumation in the area of the entire Tauern Window (Ratschbacher et al. 1991a, Rosenberg et al. 2007).

While the timing of cooling and exhumation is rather well constrained in the case of the Western Tauern Window from thermochronometry and thermal modeling (e.g., von Blanckenburg et al. 1989, Fügenschuh et al. 1997), the timing constraints available (e.g., Cliff et al. 1985, Dunkl et al. 2003) still remain relatively poor and attempts for modeling exhumation rates are not available. Therefore, in combination with structural and petrological investigations in the Tauern Window in general (Schmid et al. submitted, Chapter 5) and in the eastern Tauern Window in particular (Scharf et al. submitted a,b, Chapter 2 and 3) we present our new $^{40}Ar/^{39}Ar$ Laser ablation single grain ages on white mica in order to reveal the cooling history of the Eastern Tauern Window and to discuss the relevance of these results regarding contemporaneous versus diachronous exhumation in the Tauern Window.

In the following, we first present the geological setting and tectonic frame of the eastern Tauern Subdome. After a description of the methods used we provide the results of dating single

grains of white mica by $^{40}Ar/^{39}Ar$ Laser ablation with particular emphasis on the microstructural setting of the dated grains. Finally we discuss the thermal evolution of the two Tauern subdomes, their exhumation history and the geodynamical frame.

4.2 Geological setting

4.2.1 Tectonic overview

The Tauern Window and adjacent areas in the Eastern Alps expose a nappe stack that formed during the overall convergence between the Adriatic- and European plates in Late Cretaceous to Cenozoic times that characterizes the Alpine orogen (e.g., Trümpy 1960, Frisch 1979, Tricart 1984, Haas et al. 1995, Stampfli et al. 2001a, Schmid et al. 2004). From top to bottom this nappe stack comprises Adria-derived (Austroalpine), oceanic (Penninic) and Europe-derived (Subpenninic) upper crustal slices that became refolded and exhumed in Oligocene to Miocene times (e.g., Schmid et al. submitted, Chapter 5). The Austroalpine units were affected by Late Cretaceous deformation and metamorphism (e.g., Froitzheim et al. 1994, Villa et al. 2000, Schuster 2003). Accretion leading to nappe stacking below the Austroalpine units dominantly occurred in Paleogene to Eocene times when parts of the Subpenninic- and Penninic nappes suffered high-pressure metamorphism. Massive crustal accretion of Europe-derived nappes occurred in Late Eocene to Oligocene times and was followed by Miocene folding and coeval orogen-parallel extrusion (e.g., Schmid et al. submitted, Chapter 5). The Eastern- and Western Tauern subdomes (ETD and WTD, Fig. 4.1) expose Subpenninic basement complexes that experienced upper greenschist- to amphibolite-facies Barrow-type thermal overprint in the Oligocene (the so-called Tauernkristallisation, Sander 1911) that immediately followed duplex formation within the Europe-derived basement rocks (Venediger Duplex; Schmid et al. submitted, Chapter 5). The two Tauern subdomes were highly folded and sheared near their margins and adjacent to the overlying the Austroalpine units during final unroofing and exhumation in the Miocene (e.g., Fügenschuh et al. 1997, Schmid et al. submitted, Scharf et al. submitted a, Chapter 2 and 5).

The eastern margin of the Tauern Window is formed by the so-called Katschberg Shear Zone System (KSZS), an up to 5 km wide belt of mylonites accommodating strike-slip movements and coeval faulting. The KSZS accumulated c. 26 km eastward-directed orogen-parallel stretching in the Miocene (Scharf et al. submitted a, Chapter 2, Fig. 4.1). The central segment of the KSZS, the Katschberg Normal Fault (KNF) represents a shear zone accommodating low-angle normal faulting (Genser and Neubauer 1989). Towards the north and south the orogen-perpendicular KNF bends into two steep dipping orogen-parallel branches of the KSZS accommodating strike-slip motions (Fig. 4.1b). These two branches are interpreted as stretching faults, characterized by decreasing amounts of displacement towards their western ends (Scharf et al. submitted a, Chapter 2).

Within the working area at the eastern rim of the Tauern Window the Penninic nappes (Glockner Nappe System and Matrei Zone) lack evidence for Eocene or older high-pressure metamorphism (Scharf et al. submitted b, Chapter 3). During the Oligocene the formation of the Venediger Duplex leads to the imbrication of a series of horses (Göss-, Hochalm- and Sonnblick-Romate-Storz nappes; Schmid et al. submitted, Chapter 5). This massive accretion of granitoid rocks in the form of the Venediger Duplex probably plays an important role in contributing much to the heat production, similar to the situation in the Lepontine Dome of the Swiss-Italian Alps (Wiederkehr et al. 2008), leading to this Barrow-type thermal event at around 30-28 Ma (Rb/Sr white mica ages of Inger and Cliff 1994, Thöni 1999, Kurz et al. 2008). All the Penninic- and Subpennnic nappes of the Tauern Window were affected by this amphibolite-to-greenschist-facies metamorphic event (e.g., Oberhänsli et al. 2004, Schuster et al. 2004, Schmid et al. submitted, Scharf et al. 2012, submitted a, Chapter 2 and 5). Alpine-age peak temperature estimates using Raman microspectroscopy on carbonaceous material (RSCM, Scharf et al. 2012, submitted b, Chapter 3) reveals that the Tertiary Alpine peak temperatures in our sampling area (Fig. 4.1b) were between 450° C and 525° C, in the core of the Hochalm Dome peak temperatures were above 600° C. According to the mineral assemblages the peak temperature and pressure estimates in the Hochalm Dome are 630° ± 30° C and 0.8 GPa, respectively, during this metamorphic event (e.g., Droop 1985).

The indentation of the Southern Alps east of the Giudicarie Belt as a part of the Adriatic microplate into the northward adjacent Venediger Duplex and overlying nappes leads to north-south shortening by post-nappe folding and contemporaneous orogen-parallel extension by lateral extrusion towards the east within the units north of the Periadriatic Fault (Ratschbacher et al. 1991a, Rosenberg et al. 2007, Scharf et al. submitted a, Chapter 2). This led to rapid cooling and exhumation rates in the Subpenninic- and Penninic units in the Tauern Window (e.g., Fügenschuh et al. 1997, Schmid et al. submitted, Scharf et al. submitted a, Chapter 2 and 5). Orogen-parallel extension was assisted by the opening of the Pannonian Basin (Scharf et al. submitted a, Chapter 2) at c. 20 Ma (e.g., Fodor et al. 1999).

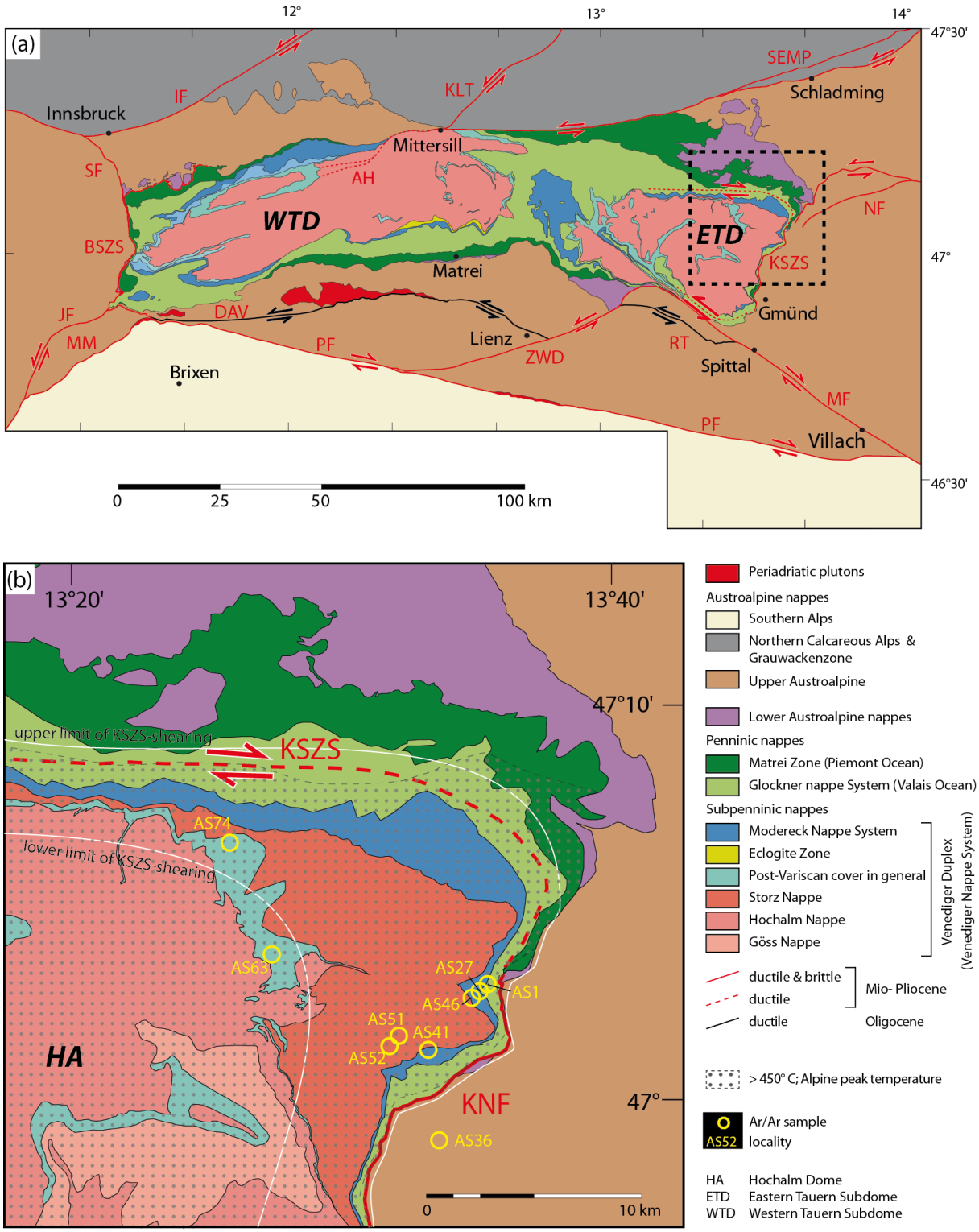

Figure 4.1: (a) Tectonic map of the Tauern Window; dotted box outlines the investigated area. AH – Ahorn Shear Zone; BSZS – Brenner Shear Zone System; DAV – Defereggen-Antholz-Vals Fault; IF – Inntal Fault; JF – Jaufen Fault; KLT – Königsee-Lammertal-Traunsee Fault; KNF – Katschberg Normal Fault; KSZS – Katschberg Shear Zone System; MF – Mölltal Fault; MM - Meran-Mauls Fault; NF – Niedere Tauern Southern Fault; PF – Pustertal Fault; RT – Ragga-Teuchl Fault; SEMP – Salzach-Ennstal-Mariazell-Puchberg Fault; ZWD – Zwischenbergen-Wöllatratten-Drau Fault; (b) Tectonic map at the northeastern end of the Tauern Window indicating the location of the nine samples collected for $^{40}Ar/^{39}Ar$ Laser ablation on white mica (Table 4.1) and Alpine peak temperature above 450° C (Scharf et al. submitted b, Chapter 3). White lines delimit the upper and lower limit of Katschberg-related shearing. Maps modified from Schmid et al. (submitted), Chapter 5.

4.2.2 Sample locations

The sampling area is located in the northeastern corner of the Tauern Window (Fig. 4.1) the exact location is given in Table 4.1. Eight samples were taken from the Penninic- and Subpenninic units in the footwall of the KSZS, one sample from the Austroalpine units in the hangingwall of the KSZS (Fig. 4.1b). The tectonic units and their evolution are presented and discussed in Schmid et al. (submitted), Scharf et al. (submitted a) and in Chapters 2 and 5.

Two samples (AS63, AS74) are metapelites from the Permo-Mesozoic cover of the Subpenninic units. Such post-Variscan metasediments, mostly marbles and mica-schists (e.g. Silbereck Unit, Exner 1939) only suffered Alpine-age metamorphism and are sandwiched between the Hochalm- and Storz nappes of the Venediger Duplex (Fig. 4.1b). Two samples (AS51, AS52) are pre-Variscan paragneisses (Storz Complex of Exner 1971) that are part of the Storz Nappe (Fig. 4.1b). This nappe represents the structurally unit of the Venediger Duplex (Schmid et al. submitted, Chapter 5). Another three samples (AS27, AS41 and AS46 all from the Brennkogel Formation) are metapelites taken from the Modereck Nappe System (Fig. 4.1b) located above the roof-thrust of the Venediger Duplex and detached from the distal-most European continental margin (Schmid et al. submitted, Chapter 5). Sample AS1 is a metapelites from the Glockner Nappe System, derived from the Valais branch of the Alpine Tethys (Fig. 4.1b). Sample AS36, is a paragneiss belonging to the Austroalpine units (Koralpe-Wölz Nappe System) in the hangingwall of the KSZS (Fig. 4.1b).

4.2.3 Previous $^{40}Ar/^{39}Ar$ dating

Previous age estimates based on the $^{40}Ar/^{39}Ar$ white mica technique in the area of the eastern Tauern Window were presented by Liu et al. (2001) who published plateau ages from Penninic and surrounding Austroalpine nappes from the area of the northeastern margin of the Tauern Window. Late Eocene to Oligocene ages (37-25 Ma) are reported from the Penninic units with a general trend towards younger ages towards the core of the ETD. A second and younger age group (c. 22 Ma) was found for the low temperature release steps in samples from the contact zone with the Ausroalpine units. Cretaceous (c. 80 Ma) and Paleogene (55-50 Ma) age groups were obtained for the Lower Austroalpine units.

Liu et al. (2001) interpreted the 37-25 Ma age group in terms of continuous cooling of the Penninic nappe stack through the $^{40}Ar/^{39}Ar$ retention temperature of white mica, post-dating a Paleogene (pre-37 Ma) metamorphic overprint related to nappe stacking. The Miocene ages around 22 Ma were interpreted as dating retrogression during the activity of the Katschberg Normal Fault (KNF). The disadvantage of this technique is that bulk ages or plateaus representing all the white mica in a given sample are obtained, rendering the interpretation of the ages rather difficult. By applying the laser ablation method we hope to discriminate between different and microstructurally controlled generations of white mica.

4.3 The Method

Nine samples using the $^{40}Ar/^{39}Ar$ situ laser-ablation (LA) technique (e.g., Merihue and Turner 1966, Maluski and Monié 1988, Kelley et al. 1994, McDougall and Harrison 1999) combined with micro-structural investigations were analyzed in this study. 1 mm thick micro-probe quality samples with 7 mm in diameter were drilled out from the oriented samples (parallel to the stretching lineation and perpendicular to the main foliation, if a main foliation is exists). The careful research on this section with the electron microprobe JEOL JXA-8200 at the Freie Universität Berlin has been conducted in light of geochemistry and structural relationship of white micas. After the carbon coating on the sample surface the coating was removed. The nine section samples were wrapped in commercial grade Al foil, loaded into the 99.999% pure Al container, then sent to the NRG reactor for the neutron activation located at Petten, Netherlands. Additionally, the Al container was finally wrapped by a Cd foil at the reactor. The irradiation with fast neutrons (neutron flux of $1.1x10^{13}$ n/cm^2-s) was performed (or conducted) for 10 h. The Fish Canyon Tuff sanidine (27.5 Ma; Uto et al. 1997, Ishizuka 1998) was used as the neutron flux-monitoring mineral during irradiation for estimating J-values.

Two months later, the samples were returned to the University of Potsdam and then analyzed at the $^{40}Ar/^{39}Ar$ laboratory of the university. The analysis was done with the same analytic system and conditions as in Schneider et al. (submitted) were adopted. For extracting Argon gas from the samples, the Nd-YAG UV pulse laser, New Wave © Gantry Dual Wave laser ablation systems, whose possible maximal energy was 6 mJ with a wavelength of 266 nm was used. Cleaning of the sample gas was done with SAES © getters and cold trap (≤ -114° C) in the ultrahigh-vacuum purification line. After 10 min of purification by those getters and trap the sample gas was sent to the noble gas mass spectrometer, Micromass © 5400. The calculation of ages and errors was performed according to Uto et al. (1997).

In total, 87 measurements on white micas of nine samples were done. Every third or fourth analysis was the analysis of blank. The used laser-beam size was 75 µm, and the typical length for laser ablation on the sample surface was 1000-1500 µm along one big grain or split into several pieces (up to six), depending on grain size and orientation (parallel to main foliation, perpendicular to main foliation, shear bands). The results are listed in Table 4.1.

4.4 Results

4.4.1 Sample Strategy

Our method allows for analyzing single grains or pairs of white mica that are classified with respect to their deformational history. Eight samples are located within the European basement rocks or nearby within the Glockner Nappe System (< 1 km away from the contact in map view, Fig. 4.1b).

Table 4.1: Results of isotopic analyses for $^{40}Ar/^{39}Ar$ dating and alignment of the white mica grains with respect to microstructural elements (< sm – foliation predating the foliation related to the activity of the KSZS; sm – foliation oriented parallel and formed during the activity of the KSZS; C' – Shear bands formed during KSZS shearing; > sm – grains overgrowing the KSZS-related foliation; no sm – no preferred orientation of the mica grains). Sample numbers, J-values, lithologies, tectonic nappes and GPS-coordinates with elevation are listed.

Age (Ma)	±1σ	$^{40}Ar^*/^{39}ArK$	±1σ	$^{40}Ar/^{39}Ar$	±1σ	$^{38}Ar/^{39}Ar$	±1σ	$^{37}Ar/^{39}Ar$	±1σ	$^{36}Ar/^{39}Ar$	±1σ	$\%40Ar_{atm}$	Microstructure
Sample AS1; J = 0.002393; metapelite; Glockner Nappe System; N 47°03'14.2'' E 13°35'11.6'', 1965 m													
no isochrone age													
16.71	0.83	3.888	0.194	4.727	0.037	0.012	<0.001	<0.001	<0.001	0.003	0.001	17.7	< sm
17.23	0.47	4.011	0.110	4.463	0.011	0.013	<0.001	<0.001	<0.001	0.002	<0.001	10.1	sm
16.34	0.76	3.802	0.178	5.187	0.033	0.015	<0.001	<0.001	<0.001	0.005	0.001	26.7	sm
18.49	0.59	4.305	0.136	4.869	0.022	0.013	<0.001	<0.001	<0.001	0.002	<0.001	11.6	< sm
17.61	0.76	4.099	0.177	4.641	0.020	0.015	<0.001	<0.001	<0.001	0.002	0.001	11.7	< sm
16.17	0.60	3.761	0.140	5.421	0.039	0.013	<0.001	<0.001	<0.001	0.006	<0.001	30.6	sm
15.52	0.51	3.610	0.118	4.757	0.037	0.014	<0.001	<0.001	<0.001	0.004	<0.001	24.1	sm
18.25	0.30	4.248	0.068	4.592	0.030	0.012	<0.001	<0.001	<0.001	0.001	<0.001	07.1	< sm
18.37	0.49	4.278	0.114	4.466	0.017	0.012	<0.001	<0.001	<0.001	0.001	<0.001	04.2	< sm
18.04	0.63	4.199	0.146	4.786	0.027	0.011	<0.001	<0.001	<0.001	0.002	<0.001	12.3	sm
Sample AS27; J = 0.002391; metapelite; Modereck Nappe System; N 47°03'07'' E 13°34'50.2'' 2059 m													
no isochrone age													
23.08	1.55	5.385	0.362	14.596	0.128	2.823	0.041	<0.001	<0.001	0.015	0.020	44.8	sm
17.53	1.59	4.084	0.372	14.448	0.061	18.212	1.393	<0.001	<0.001	0.365	0.002	03.6	sm
23.42	0.56	5.465	0.129	8.832	0.063	2.911	0.039	<0.001	<0.001	0.004	0.010	18.2	sm
23.48	0.61	5.478	0.142	5.958	0.038	2.466	0.031	<0.001	<0.001	0.003	0.013	15.7	sm
24.57	0.56	5.734	0.129	8.037	0.054	2.451	0.030	<0.001	<0.001	0.006	0.006	23.2	sm
22.86	0.69	5.334	0.161	9.353	0.051	3.782	0.048	<0.001	<0.001	0.005	0.017	22.6	sm
24.75	0.69	5.777	0.160	7.895	0.030	3.949	0.040	<0.001	<0.001	0.003	0.033	14.9	sm
19.00	0.74	4.427	0.173	7.307	0.045	3.470	0.069	<0.001	<0.001	0.035	0.002	70.3	sm
Sample AS 36; J = 0.002388; paragneiss; Upper Austroalpine, Koralpe-Wölz Nappe System; N 46° 59'23.8'' E 13°33'20.1'' 2162 m													
no isochrone age													
78.11	0.50	18.530	0.096	19.578	0.069	0.014	<0.001	<0.001	<0.001	0.004	<0.001	05.4	no sm
78.68	0.47	18.667	0.086	19.487	0.054	0.012	<0.001	<0.001	<0.001	0.003	<0.001	04.2	no sm
77.73	0.60	18.436	0.126	20.157	0.072	0.015	<0.001	<0.001	<0.001	0.006	<0.001	08.5	no sm
79.47	0.49	18.860	0.093	20.190	0.044	0.013	<0.001	<0.001	<0.001	0.005	<0.001	06.6	no sm
72.63	0.62	17.203	0.134	18.963	0.081	0.014	<0.001	<0.001	<0.001	0.006	<0.001	09.3	no sm
75.20	0.61	17.825	0.131	18.953	0.091	0.013	<0.001	<0.001	<0.001	0.004	<0.001	06.0	no sm
76.32	0.63	18.096	0.134	19.489	0.124	0.013	<0.001	<0.001	<0.001	0.005	<0.001	07.1	no sm
75.07	0.66	17.793	0.144	19.271	0.093	0.012	<0.001	<0.001	<0.001	0.005	<0.001	07.7	no sm
75.31	0.53	17.851	0.108	19.549	0.080	0.013	<0.001	<0.001	<0.001	0.006	<0.001	08.7	no sm
75.72	0.64	17.949	0.136	18.718	0.077	0.014	<0.001	<0.001	<0.001	0.003	<0.001	04.1	no sm
Sample AS41; J = 0.002385; metapelite; Modereck Nappe System; N 47°01'29.8 E 13°32'49.4 2148 m													
Isochrone: Age = 17.5 ± 1.5 Ma; Initial 40Ar/36Ar = 310 ± 95 Ma; MSWD = 1.3													
17.76	0.49	4.148	0.114	6.025	0.023	0.013	<0.001	<0.001	<0.001	0.006	<0.001	31.2	C'
19.30	0.40	4.510	0.092	4.790	0.025	0.012	<0.001	<0.001	<0.001	0.001	<0.001	05.8	sm
18.33	0.49	4.281	0.114	5.220	0.023	0.015	<0.001	<0.001	<0.001	0.003	<0.001	18.0	sm
17.74	0.51	4.142	0.117	5.170	0.024	0.014	<0.001	<0.001	<0.001	0.003	<0.001	19.9	sm
18.92	0.28	4.421	0.063	5.079	0.024	0.013	<0.001	<0.001	<0.001	0.002	<0.001	13.0	sm
15.81	0.24	3.690	0.055	4.284	0.019	0.013	<0.001	<0.001	<0.001	0.002	<0.001	13.9	sm
18.24	0.45	4.261	0.104	5.125	0.030	0.014	<0.001	<0.001	<0.001	0.003	<0.001	16.9	C'
17.35	0.34	4.051	0.078	4.242	0.008	0.013	<0.001	<0.001	<0.001	0.001	<0.001	04.5	sm
18.50	0.32	4.321	0.073	4.949	0.026	0.014	<0.001	<0.001	<0.001	0.002	<0.001	12.7	sm
18.62	0.51	4.349	0.118	4.705	0.029	0.012	<0.001	<0.001	<0.001	0.001	<0.001	07.6	sm

Age (Ma)	±1σ	$^{40}Ar^*/^{39}ArK$	±1σ	$^{40}Ar/^{39}Ar$	±1σ	$^{38}Ar/^{39}Ar$	±1σ	$^{37}Ar/^{39}Ar$	±1σ	$^{36}Ar/^{39}Ar$	±1σ	$\%40Ar_{atm}$	Microstructure
Sample AS46; J = 0.002383; metapelite; Modereck Nappe System; N 47°02‘55.1‘‘ E 13°34‘44.2‘‘ 2018 m													
no isochrone age													
17.87	0.50	4.177	0.116	4.924	0.011	0.013	<0.001	<0.001	<0.001	0.003	<0.001	15.2	sm
18.92	0.75	4.424	0.175	5.110	0.045	0.014	<0.001	<0.001	<0.001	0.002	0.001	13.4	sm
19.08	0.32	4.463	0.072	5.462	0.040	0.012	<0.001	<0.001	<0.001	0.003	<0.001	18.3	sm
20.00	0.62	4.679	0.145	5.539	0.036	0.012	<0.001	<0.001	<0.001	0.003	<0.001	15.5	sm
19.74	0.47	4.618	0.109	5.003	0.029	0.013	<0.001	<0.001	<0.001	0.001	<0.001	07.7	sm
Sample AS51; J = 0.00238; paragneiss; Storz Nappe; 47°01‘54.1‘‘ E 13°31‘45.4‘‘ 1757													
no isochrone age													
12.33	5.17	2.883	1.213	8.696	0.440	0.018	<0.001	<0.001	<0.001	0.020	0.004	66.9	sm
21.68	1.67	5.081	0.393	11.331	0.204	0.013	<0.001	<0.001	<0.001	0.021	0.001	55.2	sm
14.66	2.14	3.428	0.503	8.675	0.221	0.017	<0.001	<0.001	<0.001	0.018	0.002	60.5	sm
21.47	2.07	5.031	0.488	9.613	0.308	0.017	<0.001	<0.001	<0.001	0.016	0.001	47.7	sm
18.78	1.53	4.396	0.359	14.017	0.221	0.015	<0.001	<0.001	<0.001	0.033	0.001	68.6	sm
24.56	2.97	5.760	0.700	10.862	0.218	0.012	<0.001	<0.001	<0.001	0.017	0.002	47.0	sm
20.05	0.29	4.695	0.065	5.707	0.016	0.012	<0.001	<0.001	<0.001	0.003	<0.001	17.7	sm
21.39	0.76	5.012	0.178	7.350	0.033	0.014	<0.001	<0.001	<0.001	0.008	0.001	31.8	sm
19.81	0.42	4.640	0.097	7.265	0.050	0.016	<0.001	<0.001	<0.001	0.009	<0.001	36.1	sm
21.92	1.58	5.136	0.373	11.185	0.091	0.018	<0.001	<0.001	<0.001	0.020	0.001	54.1	sm
22.90	1.23	5.367	0.290	10.641	0.092	0.017	<0.001	<0.001	<0.001	0.018	0.001	49.6	C'
19.28	0.63	4.515	0.148	6.424	0.044	0.011	<0.001	<0.001	<0.001	0.006	<0.001	29.7	C'
30.75	2.96	7.223	0.701	16.115	0.198	0.012	<0.001	<0.001	<0.001	0.030	0.002	55.2	sm
Sample AS52; J = 0.002377; paragneiss; Storz Nappe; N 47°01‘47.9‘‘ E 13°31‘35.3‘‘ 1815 m													
no isochrone age													
16.26	1.12	3.808	0.264	8.492	0.041	0.012	<0.001	<0.001	<0.001	0.016	0.001	55.2	sm
13.54	1.40	3.170	0.328	5.352	0.067	0.015	<0.001	<0.001	<0.001	0.007	0.001	40.8	sm
19.53	0.59	4.578	0.137	6.417	0.032	0.012	<0.001	<0.001	<0.001	0.006	<0.001	28.7	sm
21.20	0.23	4.973	0.051	5.929	0.011	0.012	<0.001	<0.001	<0.001	0.003	<0.001	16.1	sm
21.71	0.83	5.092	0.195	5.457	0.022	0.013	<0.001	<0.001	<0.001	0.001	0.001	06.7	sm
14.89	0.83	3.487	0.194	5.096	0.023	0.015	<0.001	<0.001	<0.001	0.005	0.001	31.6	sm
19.56	0.75	4.587	0.175	5.488	0.024	0.014	<0.001	<0.001	<0.001	0.003	0.001	16.4	sm
19.62	0.57	4.601	0.133	5.728	0.016	0.013	<0.001	<0.001	<0.001	0.004	<0.001	19.7	sm
19.69	0.77	4.617	0.181	6.131	0.026	0.012	<0.001	<0.001	<0.001	0.005	0.001	24.7	sm
22.09	0.55	5.184	0.129	6.699	0.014	0.015	<0.001	<0.001	<0.001	0.005	<0.001	22.6	sm
20.39	0.99	4.782	0.232	11.247	0.049	0.018	<0.001	<0.001	<0.001	0.022	0.001	57.5	sm
Sample AS63; J = 0.002374; metapelite; Permo-mesozoic cover of Hochalm Nappe; N 47° 04‘04.5‘‘ E 13°27‘21.7‘‘ 1905 m													
no isochrone age													
17.94	0.50	4.210	0.117	4.955	0.025	0.011	<0.001	<0.001	<0.001	0.003	<0.001	15.0	no sm
16.48	0.73	3.864	0.171	5.781	0.027	0.014	<0.001	<0.001	<0.001	0.006	0.001	33.2	no sm
19.08	0.40	4.477	0.093	5.510	0.028	0.013	<0.001	<0.001	<0.001	0.003	<0.001	18.7	no sm
17.93	0.46	4.207	0.106	5.063	0.011	0.013	<0.001	<0.001	<0.001	0.003	<0.001	16.9	no sm
18.82	0.77	4.418	0.180	4.817	0.016	0.013	<0.001	<0.001	<0.001	0.001	0.001	08.3	no sm
17.22	0.56	4.040	0.130	4.695	0.020	0.012	<0.001	<0.001	<0.001	0.002	<0.001	13.9	no sm
17.62	0.42	4.134	0.097	4.975	0.019	0.014	<0.001	<0.001	<0.001	0.003	<0.001	16.9	no sm
19.84	0.79	4.657	0.185	6.246	0.013	0.014	<0.001	<0.001	<0.001	0.005	0.001	25.4	no sm
18.40	0.23	4.319	0.052	5.486	0.031	0.014	<0.001	<0.001	<0.001	0.004	<0.001	21.3	no sm
19.50	0.48	4.578	0.113	5.096	0.014	0.016	<0.001	<0.001	<0.001	0.002	<0.001	10.2	no sm
Sample AS74; J = 0.00237; metapelite; Permo-mesozoic cover of Hochalm Nappe; N 47°06‘51.2‘‘ E 13°25‘42.8‘‘ 1363 m													
no isochrone age													
20.62	0.36	4.849	0.083	5.236	0.018	0.013	<0.001	<0.001	<0.001	0.001	<0.001	07.4	> sm
19.47	0.41	4.578	0.094	4.908	0.009	0.012	<0.001	<0.001	<0.001	0.001	<0.001	06.7	sm
19.48	0.43	4.580	0.100	5.255	0.021	0.014	<0.001	<0.001	<0.001	0.002	<0.001	12,8	> sm
20.39	0.31	4.796	0.072	5.224	0.029	0.013	<0.001	<0.001	<0.001	0.001	<0.001	08.2	sm
19.73	0.65	4.641	0.152	5.316	0.015	0.014	<0.001	<0.001	<0.001	0.002	0.001	12.7	> sm
20.77	0.41	4.886	0.096	4.984	0.017	0.012	<0.001	<0.001	<0.001	<0.001	<0.001	02.0	> sm
19.82	0.36	4.661	0.082	5.508	0.020	0.013	<0.001	<0.001	<0.001	0.003	<0.001	15.4	sm
18.78	0.51	4.416	0.119	4.909	0.019	0.014	<0.001	<0.001	<0.001	0.002	<0.001	10.1	sm
19.13	0.42	4.498	0.098	4.723	0.016	0.011	<0.001	<0.001	<0.001	0.001	<0.001	04.8	sm
20.19	0.45	4.748	0.105	5.030	0.016	0.012	<0.001	<0.001	<0.001	0.001	<0.001	06.6	> sm

Peak temperatures in the Subpenninic- and immediately adjacent Penninic units were reached during a Barrow-type thermal event referred to as "Tauernkristallisation" of ill-constrained age estimated at around 30-28 Ma (Scharf et al. submitted b, Chapter 3). The eight samples suffered Alpine peak temperatures of 450° C to 525° C (Scharf et al. submitted b, Chapter 3). For fine-grained white mica this is well above the expected closure temperature of the $^{40}Ar/^{39}Ar$ on white mica when assuming that the results of the diffusion experiments of Harrison et al. (2009) are applicable in nature. Assuming a cooling rate of around 10-30° C/Ma during the Miocene (Scharf et al. submitted a, Chapter 2) and taking a grain size of white mica of 100 µm in diameter (we measured a range of grain sizes between 10-1000 µm) the cooling rate would be below 400° C, raising to > 450° C only once the grain size approaches 500 µm.

Sample AS36 is derived from the Upper Austroalpine (Koralpe-Wölz Nappe System) in the hangingwall of the KSZS (Fig. 4.1b), a unit that was primarily involved during the Cretaceous-age orogenic cycle (e.g., Schmid et al. 2004, Handy and Oberhänsli 2004). The amphibolite-facies mineral assemblage of this sample indicates pre-Cenozoic peak temperatures in excess of 450° C as indicated by the peak temperature estimates of Scharf et al. (submitted b, Chapter 3, sample 4 in Table A-1).

All the samples except for AS36 (Upper Austroalpine) and AS63 (one of the two samples from the Silbereck Unit) were collected within a fabric domain that is strongly affected by deformation during the activity of the KSZS (see Fig. 4.1b and Scharf et al. submitted b, Chapter 3, Fig 3.2b). Therefore the ages of at least some of the individual mica grains within these seven samples are expected to indicate the timing of cooling below a grain-size dependent closing temperature after the Tauernkristallisation, or alternatively, formation ages not necessarily reflecting a cooling temperature (see review of Villa 2010).

4.4.2 Geochemistry of white micas

The chemistry of white mica was measured for 258 single spots on nine samples with the microprobe. The variations in chemistry are shown in Figure 4.2 and listed in Table A-2. The samples from the Tauern Window reveals similar chemistry (Fig. 4.2a), ignoring their micro-fabric. Only sample AS27, however, shows a slightly higher Al-ce and Fe-Al-ce components with respect to the other data from the field area. Nevertheless, sample AS36 (from the Upper Austroalpine nappes) has a significant different geochemistry. In addition, the Al (p.f.u.) versus Si (p.f.u.) and Mg+Fe (p.f.u.) versus Si (p.f.u.) content of the different white micas and their relative microstructure are presented in Figs. 4.2b, c. There no significant differences between the samples and their microstructure can be observed. The detailed geochemical analyses of the white micas with respect to their microfabrics are listed in the Appendix in Table A-2.

Additional, SEM pictures were developed to detect fabric domains of the white micas and moreover, for orientation within the sample during laser ablation studies in the $^{40}Ar/^{39}Ar$ Laboratory of the University of Potsdam.

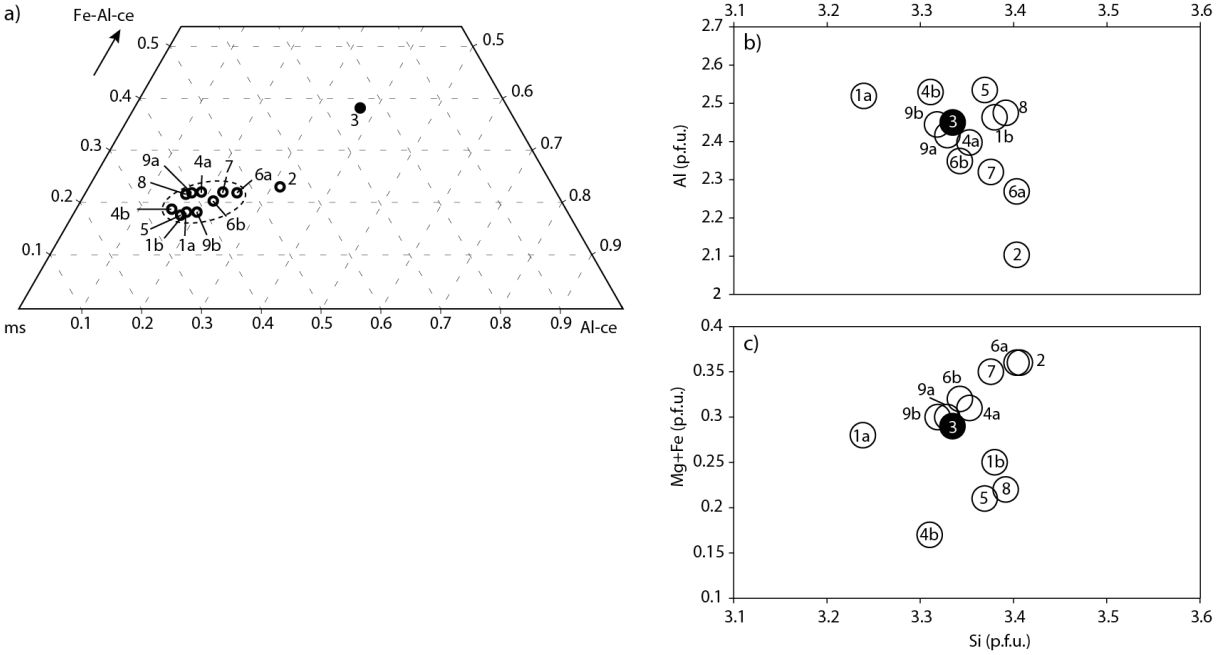

Figure 4.2: Compositional range of white micas depending on their microstructure from all nine samples (Table 4.1). (a) Fe-Al-ce (Celadonit), ms (Muscovite) and Al-ce (Celadonite); (b) Al (p.f.u.) versus Si (p.f.u.); (c) Fe+Mg (p.f.u.) versus Si (p.f.u.). The numbers refer to the nine samples listed in Table 4.1 and Table A-2. 1a – sample AS1, sm; 1b – sample AS1, > sm; 2 – sample AS27, sm; 3 –sample AS36, no sm; 4a – sample AS41, sm; 4b – sample AS41, C'; 5 – sample AS46, sm; 6a – sample AS51, sm; 6b – sample AS51, C'; 7 – sample AS52, sm; 8 – sample AS63, no sm; 9a – sample AS74, sm; 9b – sample AS74, < sm. Abbreviations: < sm – white mica in foliation predating the foliation related to the activity of the KSZS; sm – white mica in foliation oriented parallel and formed during the activity of the KSZS; C' – white mica aligned with shear bands formed during KSZS shearing; > sm – white mica overgrowing the KSZS-related foliation; no sm – no preferred orientation of the mica grains). Black circle: white mica from the hangingwall of the KSZS; open circles: white mica from the footwall of the KSZS.

4.4.3 $^{40}Ar/^{39}Ar$ age data

The age data are listed in Table 4.1, which also indicates sample names and localities, J-values, rock type, tectonic units, GPS-coordinates, elevations and microstructures of white micas with respect to the foliation formed during the activity of the KSZS. The $^{40}Ar/^{39}Ar$ Laser ablation technique produces high spatial resolution data (e.g., Kelley et al. 1994), which makes in-situ measurements of single grains or grain aggregates with respect to their microstructure possible (Figs. 4.3 and 4.4). Figures 4.5 and 4.6, together with Table 4.1 show the age results obtained with $^{40}Ar/^{39}Ar$ Laser-ablation on white mica. The measurement procedure was performed in microstructurally controlled individual grains. The following five different types of white mica grains were categorized:

(1) Older white micas in folded domains that pre-date the foliation formed during the activity of the KSZS (sample AS1, grains labeled "< sm" in Table 4.1.; see central parts of Figs. 4.3.a and 4.4.a).

(2) White mica oriented parallel to, but not necessarily formed during younger straining leading to the formation of the KSZS (grains labeled "sm" in Table 4.1.; some grains in samples AS1, AS41,

AS51 and AS74, all measured grains in samples AS27, AS46 and AS52; see parts of Figs. 4.3a and 4.4a).

(3) White mica locally defining shear bands that are co-genetic with the foliation related to the KSZS (some grains found in AS41 and AS51 labeled "C' " in Table 4.1.; see Figs. 4.3b and 4.4b).

(4) White mica overgrowing the foliation formed during the activity of the KSZS (five grains in sample AS74 labeled "> sm" in Table 4.1.; see Figs. 4.3c and 4.4c).

(5) Samples, which do not preserve a preferred orientation of the white mica grains, which, together with the quartz microstructures containing 120° grain-boundaries, indicates annealing (all grains in samples AS36 and AS63; see Figs. 4.3d and 4.4d).

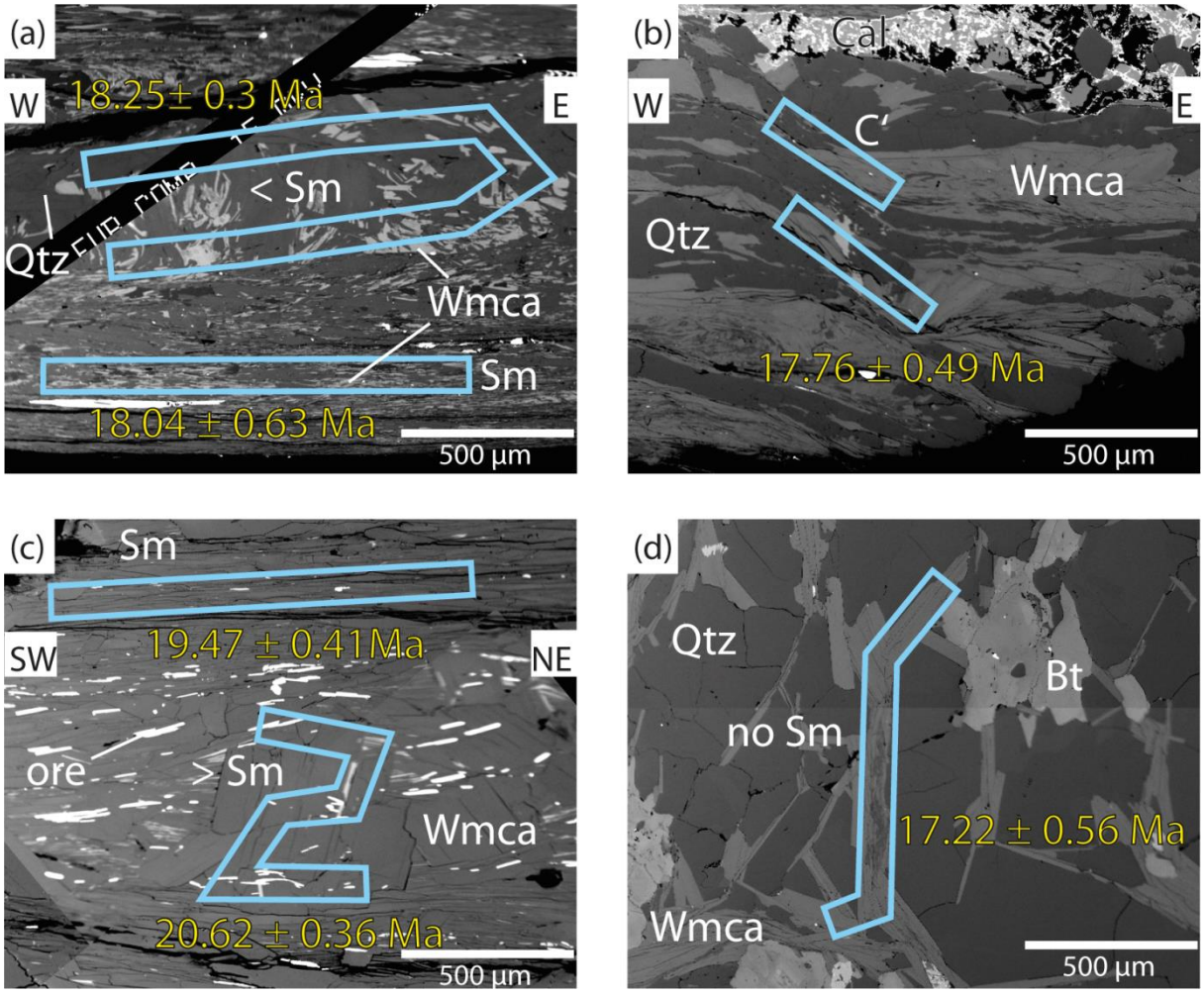

Figure 4.3: Scanning electron microscope (SEM) back scatter photomicrographs showing microstructural features of white micas analyses. The laser-ablated areas are marked in blue with the corresponding ages. Errors are σ-1. Note that in parts (e.g., sample AS1 of Fig. 4.3.a) the ages are not those of a single white mica grain since the mica grains are < 75 µm and hence, the age represents an integral over several white micas within a given microstructural domain. (a) Sample AS1; note that near the upper and lower margin all minerals are oriented parallel to the main foliation formed during shearing within the KSZS (sm) while the minerals in the central part became folded and reoriented during the formation of the KSZS (< sm). (b) White mica oriented parallel to shear bands in sample AS41 indicating top-E shearing during the formation of the KSZS (C'). (c) Post-kinematically growing white mica (> sm) in respect to the foliation formed during the activity of the KSZS in sample AS74. (d) Annealed white mica and quartz microfabrics in sample AS63 lacking a foliation (no sm).

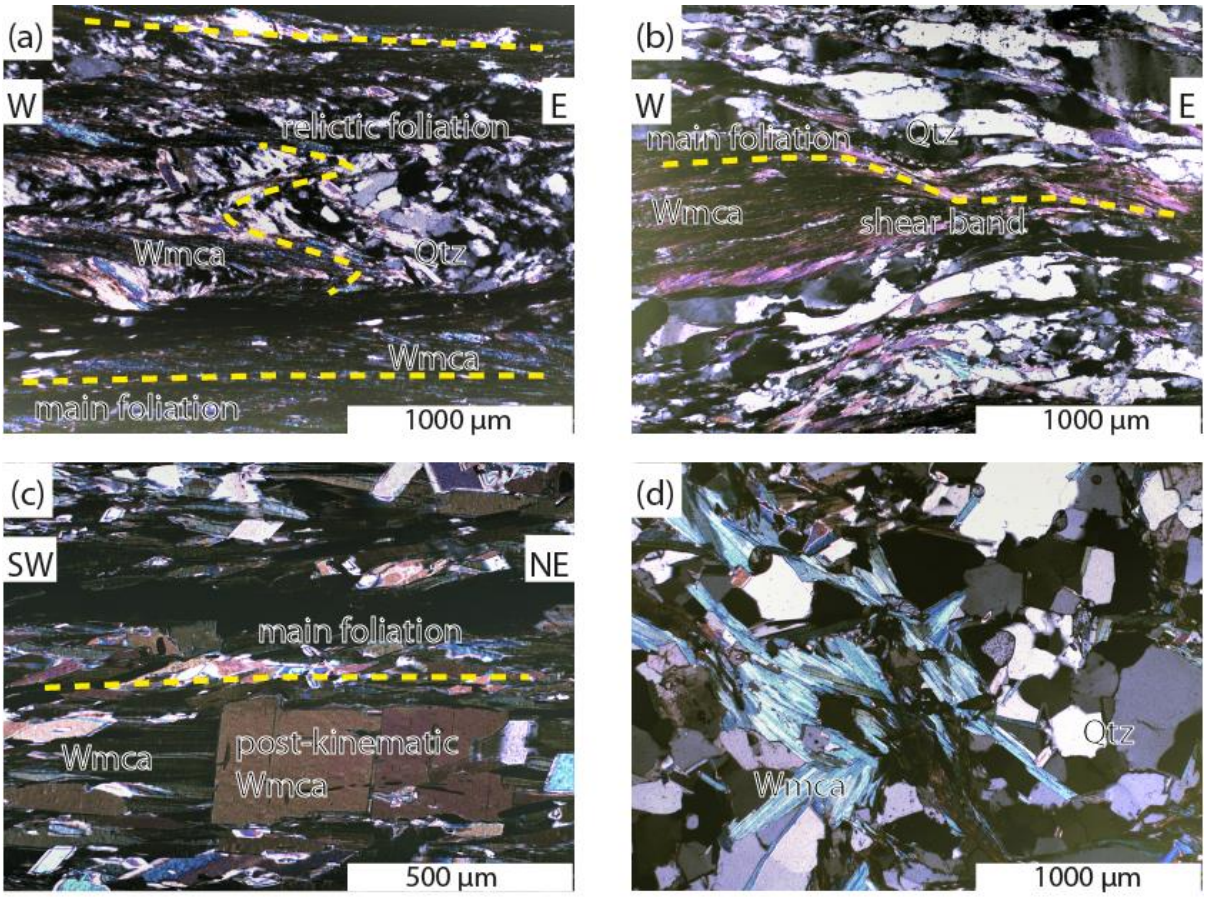

Figure 4.4: Typical microstructures of white mica under the optical microscope. All photos were taken under crossed nichols. (a) Sample AS1; mica grains are preferentially oriented parallel to the Katschberg-related main foliation (sm) in the upper and lower parts of the micrograph while a folded domains (< sm) are preferentially seen in the central part of the micrograph; the formation of the latter mica aggregates appears to be relatively older. (b) Shear bands (C') affecting white mica in sample AS41. (c) Post-kinematic white micas overgrowing (> sm) the main foliation formed during shearing related to the KSZS in sample AS74. (d) Post-kinematically growing white mica lacking a preferred orientation (no sm) in sample AS63 taken from a fabric domain unaffected by shearing during the formation of the KSZS.

Parallel to their longest axes, measured white micas are at least 10-500 µm long. Individual single grains below a length of 75 µm could not be measured. In such cases the in-situ $^{40}Ar/^{39}Ar$ ages were estimated from white mica aggregates contained within a given fabric domain. Thereby it could not be excluded that other minerals were ablated during gas extraction (e.g., quartz and chlorite).

Before explicitly discussing relationships between age and microstructural setting of the white mica grains we discuss the single grain ages and their scatter for all the samples analyzed. Thereby we calculate the arithmetic mean of the single grain ages obtained for all the measured grains within a given sample (briefly referred to as "mean age"), and we list the scatter of these grain ages without considering the σ-1 errors of the single grain ages (Table 4.1). Additionally, we also calculate the weighted average age of all grains, or certain groups of grains, within a given sample (see Figs. 4.5 and 4.6).

The smallest scatter in the grain ages is found in sample AS74, yielding a mean age of 19.84 Ma +0.93–1.06 Ma while the weighted average age for all grains is 19.74 ± 0.13 Ma, Fig. 4.5h).

AS74 is from the northern dextral strike-slip branch of the KSZS (Fig. 4.1) and contains two categories of mica grains (sm and > sm). The weighted average ages only insignificantly differ from each other (Fig. 4.5h). A small scatter is also found in the annealed sample AS63 giving a mean age of 18.28 Ma +1.8–1.22 Ma (weighted average age: 18.19 ± 0.14 Ma, see Fig. 4.5.g). The scatter in Sample AS46 with a mean age of 19.12 Ma +0.88 –1.25 Ma (weighted average age: 18.9 ± 0.21 Ma, Fig. 4.5d) is also small, but the number of grains measured (N = 5) is also very little. A somewhat greater scatter is seen in specimen AS41 with a mean age of 18.06 +1.24–2.25 Ma (weighted average age: 17.63 ± 0.11 Ma, see Fig. 4.5c). In view of their small to moderate scatter the four samples mentioned so far did not warrant the calculation of weighted average ages for subpopulations within the specimens (see Fig. 4.5). The weighted average ages for these four samples only vary little and are between 17.63 Ma (AS41) and 19.74 Ma (AS74) in spite of the fact that the four samples substantially vary in terms of location (AS63 is outside the area affected by the shearing within the KSZS, while AS41 and AS46 are within an intensely sheared part of the KSZS near the margin of the ETD (Fig. 4.1).

Sample AS1 with a mean age of 17.27 Ma +1.22–1.75 Ma (weighted average age: 17.34 ± 0.16 Ma, see Fig. 4.5a) has a small scatter although it contains two categories of grains (< sm and sm) whose weighted average means do not significantly differ. The scatter of grain ages is significantly greater in the following three samples (Table 4.1): AS27 (22.34 Ma +2.41–4.81 Ma; weighted average age: 22.87 ± 0.7 Ma, Fig. 4.5b); AS51 (20.74 Ma +10.01–8.41 Ma; weighted average age: 19.94 ± 0.72 Ma, Fig. 4.5e); AS52 (18.95 Ma +3.14–5.41 Ma; weighted average age: 20.29 ± 0.16 Ma, see Fig. 4.5f). Sub-populations in these three samples exhibit rather old weighted average ages (23.57 ± 0.27 Ma in the case of specimen AS27, see Fig. 4.5b) or rather young weighted average ages (15.27 ± 0.6 Ma and 14.18 ± 1.96 Ma) for sample AS52 and AS51 (see Figs. 4.5f and 4.5e), respectively.

Sample AS36 (Table 4.1), originating from the Upper Austroalpine units in the hangingwall of the KSZS, reveals a mean age of 76.42 Ma +2.26–3.79 Ma (weighted average age: 76.92 ± 0.56 Ma, Fig. 4.6). This is expected since the degree of Tertiary-age metamorphism in the Austroalpine units above the KSZS did not allow for resetting the $^{40}Ar/^{39}Ar$-System that hence reflects Cretaceous-age metamorphism.

4.4.4 Relationships between ages and microstructural setting of the analyzed grains

Sample AS1, which clearly contains two categories of mica grains (< sm and sm, see Figs. 4.3a and 4.4a) exhibits a small scatter in ages, and the weighted average ages of the sub-populations do significantly but not substantially differ (17.96 ± 0.22 Ma for < sm grains aligned in an older foliation and 16.48 ± 0.25 Ma for sm grains aligned in the foliation related to the KSZS). The small difference in the weighted average ages of the two populations of grains agrees with the microstructural analysis suggesting that < sm grains are relatively older.

Sample AS74 is the only other sample that contains strictly separate generations of grains (see Figs. 4.3c and 4.4c): white mica grains oriented parallel to the foliation related to the KSZS (sm) and post-kinematic white mica (> sm). The ages of the two populations only differ insignificantly, the supposedly younger grain population (> sm) even yielding a slightly older weighted average age (20.05 ± 0.19 Ma) in respect to the grains related to KSZS shearing (19.5 ± 0.17 Ma). Hence, while the correlation of grain ages with their microstructural setting was weak in the case of sample AS1, any such correlation is inexistent in this sample AS74. Moreover, even though it contains post-kinematic grains, the weighted average mean of the entire population (19.74 ± 0.13 Ma) is one of the oldest amongst the samples analyzed.

Two specimens are characterized by a main foliation related to the KSZS (sm) and co-genetic shear bands (C'): AS41 and AS51 (Table 4.1). Hence, both of them underwent shearing during top east orogen-parallel extension. In the case of sample AS41 the two white mica grains contained in shear bands (C') yield 18.24 ± 0.45 Ma and 17.76 ± 0.49 Ma and are, therefore, close to the age-range of the grains oriented parallel to the foliation (sm) of the KSZS that vary between 19.3 ± 0.4 Ma and 15.81 ± 0.24 Ma (see Table 4.1). Paradoxically, the youngest grain age is part of the sm population, although the mica aligned in shear would be expected to be younger. In sample AS51 the grain ages for micas aligned in shear bands (C') are 22.9 ± 1.23 Ma and 19.28 ± 0.63 Ma while the distribution of grain ages of mica aligned within the main foliation scatters substantially and varies between 30.75 ± 2.96 Ma and 12.33 ± 5.17 Ma (Table 4.1). It is remarkable that two of the grains aligned with sm even define the youngest weighted average mean of all the sub-populations (Fig. 4.5e; 14.18 ± 1.96 Ma).

Specimens AS27, AS46 and AS52 only contain white mica grains aligned parallel to the foliation formed during the activity of the KSZS. The scatter of single gain ages is considerable in two of this group of specimens where two sub-populations of grains can be discerned (see Figs. 4.5b and 4.5f).

The specimen within the Tauern Window that only contains annealed white mica (AS63) and which is the only one outside the area affected by the shearing within the KSZS does not reveal a weighted average age (18.19 ± 0.14 Ma) that would greatly differ from those of the specimens from within the KSZS.

In summary, there appears to be no clear relationship between grain ages and microstructural setting of the mica grains: in one case (sample AS41) the differences in grain ages even contradict microstructural evidences. No systematic age variations can be discerned with respect to the microstructural setting of the grains (< sm, sm, C' or > sm).

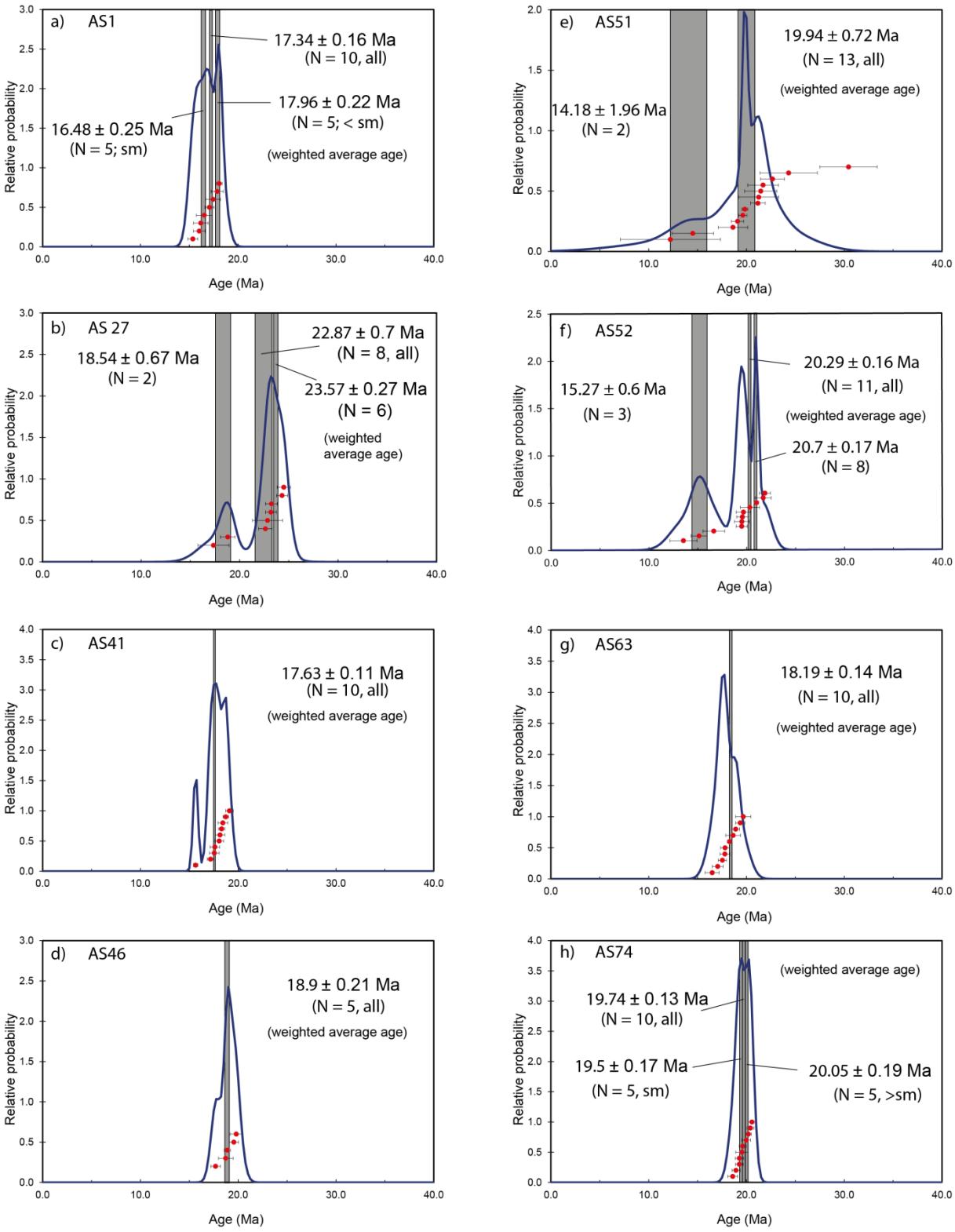

Figure 4.5: Summary of probability versus age distribution of samples in the footwall of the KSZS: (a) sample AS1; (b) sample AS29; (c) sample AS41; (d) sample AS46; (e) sample AS51; (f) sample AS52; (g) sample AS63; (h) sample AS74. Note that ages given in numbers within this figure are weighted average grain ages while N represents the number of grain ages used for calculating such weighted average grain ages. Blue lines indicate the relative probability for finding a given single grain age; red dots with σ-1 error bar are the single grain data listed in Table 4.1; grey stripes visualize the weighted average grain ages including their σ-1 error of all grain ages, or of certain groups of grain ages, respectively. Note that specimens AS27 (b), AS51 (e) and AS52 (f) preserve two clearly distinct age populations. sm – KSZS foliation; < sm – older than KSZS foliation; > sm – younger than KSZS foliation.

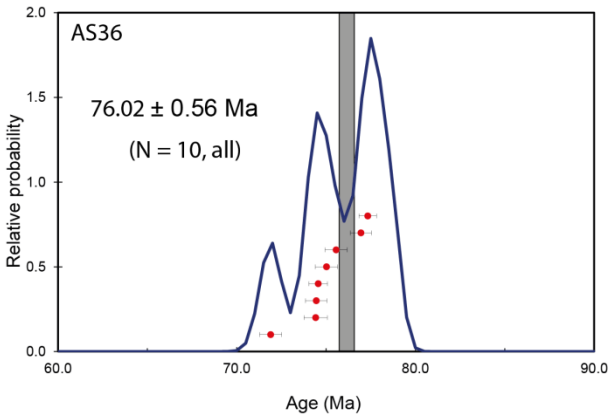

Figure 4.6: Probability versus age distribution of sample AS36 from the Austroalpine in the hangingwall of the KSZS. Note that age given in numbers is the weighted average grain age while N represents the number of grain ages used for calculating this weighted average grain age. Blue line indicates the relative probability for finding a given single grain age; red dots with σ-1 error bar are the single grain data listed in Table 4.1; grey stripe visualizes the weighted average grain age including the σ-1 error.

4.5 Discussion

4.5.1 Errors

The absolute errors (given in σ-1) of single grain ages are mostly less than 1 Ma, which is less than 5% absolute error. Only nine of 87 data have an error larger than 1 Ma (Table 4.1). In the case of sample AS36 the errors are less than 0.7 Ma. The absolute ages being around 76 Ma, the absolute errors are less than 1%.

4.5.2 Interpretation of age data presented in this study

In the following we first discuss the age data obtained on the two samples that contain a mixture of synkinematic white mica grains and white mica grains that are either pre-kinematic (sample AS1) or post-kinematic (sample AS74). These two samples are good examples for arguing in favor of an interpretation of the $^{40}Ar/^{39}Ar$ data in terms of cooling ages.

In specimen AS1 the age difference between the two microstructurally distinct grain populations (< sm and sm) is very small and hence, it is unlikely that two distinct formation ages of mica can be postulated or that strain-induced Ar-loss producing younger ages in some of the grains did occur. At the site of specimen AS1 cooling below the closing temperature would have occurred at around 17 Ma ago (17.34 ± 0.16 Ma is the weighted average age of all grains). Given the small grain size within this specimen (< 100 µm) and assuming a cooling rate of 20° C/Ma the closing temperature for this specimen is expected to lie at around 400° C, provided the diffusion experiments of Harrison et al. (2009) are applicable to nature. If KSZS-related shearing is interpreted to predate cooling across some 400° C such shearing would have occurred before some 17 Ma ago at the site of sample AS1, namely fairly close to the top of the KSZS and within the Glockner Nappe System (Fig.

4.1). The fact that the maximum metamorphic temperature in this area was around 475° C according to Scharf et al. (submitted b, Chapter 3), i.e. above the expected closing temperature, makes an interpretation in terms of cooling ages likely.

In the case of sample AS74, the second sample with two microstructurally distinct grain populations (sm and > sm), no significant difference in ages is preserved either, the younger and post-kinematic grain population even yielding slightly older ages. Since sample AS74 contains post-kinematic white mica and since all grain ages in this specimen are also best interpreted in terms of cooling ages, such cooling below the closure temperature is likely to have occurred after the shearing within this part of the KSZS. Hence, motion along the site of AS74, near the structural base of the KSZS, i.e. at a relatively deeper structural level relative to that of sample AS1 (Fig. 4.1), is expected to be older than about 20 Ma (19.74 ± 0.13 Ma is the weighted average age of all grains). Assuming a cooling rate of 20° C/Ma and considering the large (500 µm, Figs. 4.3c and 4.4c) size of post-kinematic white mica in this specimen the closure temperature would be expected to be at around 470° C (again according to Harrison et al. 2009), i.e. only slightly below the maximum temperatures reached at this locality (between 500° and 525° C according to Scharf et al. submitted b, Chapter 3). This, in turn, would indicate that KSZS-related shearing at this locality is likely to have occurred under temperatures that were near the peak-metamorphic temperatures. The slightly older age of the post-kinematic grain population could reflect the larger grain size observed in this younger mica generation (see Fig. 4.4c).

In combination, the above presented interpretations would suggest the onset of shearing along the KSZS before some 20 Ma near the structural base of this shear zone and in the interior of the ETD (location of sample AS74). Shearing towards the top of the KSZS (location of sample AS1) probably occurred later but ended before 17 Ma and at lower temperatures.

The totally annealed sample AS63 is structurally below the KSZS. The weighted average mean of the grain ages is around 18 Ma (Fig. 4.5g), indicating that exhumation by KSZS related shearing must have started before some 18 Ma ago, regardless as to whether the ages are interpreted as formation or cooling ages. This is consistent with the onset of shearing before some 20 Ma ago based on the interpretation of nearby sample AS74.

The oldest weighted average age is found in specimen AS27 (23.57 ± 0.27 Ma for six out of a total of 8 grains measured, see Fig. 4.5b). Since AS27 is located close to the top of the KSZS and close to AS1 one would in fact expect a relatively young cooling age for this sample. However, as mentioned earlier, mica in this sample shows higher Al-ce and FE-Al-ce components with respect to the other data from the field area. Since the peak-Alpine metamorphic temperature of this sample (475-450° C, Scharf et al. submitted b, Chapter 3, Fig. 4.1b) might be close to the cooling temperature expected at the grain size of this specimen (elongated white micas up to 1000 x 100 µm) the isotopic signature of the $^{40}Ar/^{39}Ar$ system might only have been partly reset in which case an interpretation in terms of cooling ages would not be appropriate.

The rest of the measured samples (AS41, AS46, AS 51and AS52) are at least not incompatible with the interpretation based on samples AS1 and AS74 that shearing within the KSZS might have occurred within the > 20 to > 17 Ma age interval, shearing and cooling migrating from the base towards the top of the KSZS.

Sample AS41 also close to the top of the KSZS yields a weighted average age of 17.63 ± 0.11 Ma (Fig. 4.5c). One grain age is significantly younger (15.8 ± 0.24 Ma) suggesting that local shearing after 17 Ma or even later might have led to local Ar-loss. Sample AS46, again close to the top of the KSZS, has a weighted average age of 18.9 Ma ± 0.21 Ma (Fig. 4.5d). Sample AS51 from a paragneisses of the Storz Nappe, and therefore structurally deeper, shows widely scattering ages: ten out of thirteen ages have a mean age of 21.2 +3.4–2.4 Ma (eight from the main foliation and two from shear bands), one is significantly older (30.75 ± 2.96 Ma) and two yield a weighted average mean of 15.27 ± 0.6 Ma (Fig. 4.5e). This sample does not allow for a simple interpretation in terms of cooling ages. The oldest grain possibly yields an isotopic signature related to the Tauernkristallisation at 30-28 Ma. The two younger ages (12.33 ± 5.17 Ma and 14.66 ± 2.14 Ma) are probably affected by locally ongoing late-stage shearing after 17 Ma ago that led to Ar-loss. Alternatively subgrain-size reduction during shearing along the KNF might have reduced the closure temperature in the white mica system of less than 400° C (Harrison et al. 2009). Sample AS52, also from the Storz Nappe, provides two distinct groups of ages of white mica, both being microstructurally undistinguishable (all grains are oriented parallel to the foliation related to KSZS shearing): a first group with a weighted average age of 20.7 ± 0.17 Ma and a second one with 15.27 ± 0.6 Ma (Fig. 4.5f). Again a simple interpretation in terms of cooling ages is not possible. The younger age group may again indicate locally ongoing shearing and Ar-loss until some 15 Ma ago.

Although the complexity of the data makes an interpretation difficult we conclude that shearing along the KSZS probably commenced at an unknown instant of time before some 20 Ma ago at the base of the KSZS under high temperatures (about 470° C). It is suggested that shearing subsequently migrated towards the top of the KSZS, where deformation continued until > 17 Ma under lower temperature conditions around 400° C. Everywhere within the KSZS the cooling ages did not significantly post-date the end of deformation since the peak temperatures never were largely in excess of the closing temperatures for the $^{40}Ar/^{39}Ar$ system (Scharf et al. submitted b, Chapter 3). Substantially younger grain ages found in parts of the grains within some of the specimens may indicate loss of Ar during locally ongoing shearing until 17 Ma or even later. Mylonitic shearing within the KSZS until 15 Ma ago, however, is unlikely for other reasons. As discussed in Scharf et al. (submitted a, Chapter 2) the intramontane Miocene sedimentary basins that formed in the hangingwall of the KSZS started to open at around 17 Ma. This, together with the cooling curve of the area discussed later, suggests a transition towards from viscous to frictional (cataclastic) flow at the top of the KSZS at around 17 Ma ago.

4.5.3 Comparison with other radiometric age data from the eastern end of the Tauern Window

Liu et al. (2001) provided Ar-Ar plateau-ages on white mica from an area 5 to 10 km further northeast of our study area indicating a general trend towards younger ages going towards the KSZS and the core of the ETD. Mean ages are between 21.7 Ma and 28.4 Ma in three samples from the Glockner Nappe System and the Matrei Zone closest to the KSZS and to our area. Liu et al. (2001) interpreted these ages to be related to cooling postdating the Tauernkristallisation, which would suggest substantially earlier cooling immediately northeast of our study area. This study indicates the possibility that cooling may have started substantially before some 20 Ma ago and perhaps before the activity of the KSZS but they do not allow bracketing the ending of the shearing along the KSZS.

Rb/Sr ages on white mica ages from the Hochalm Dome provided by Cliff et al. (1985) and Favaro and Schuster et al. (in prep.) are in the range of 27-19.6 Ma and 24.4-21.1 Ma, respectively. Note that these data were collected from rocks that are structurally below the KSZS. When interpreted as ages dating cooling below a closure temperature of 500 ± 50° C (Purdy and Jäger 1976) such cooling would have initiated substantially earlier than 20 Ma ago. Yet unpublished Rb/Sr biotite ages by Favaro and Schuster (in prep.) from the same area of investigation are around 18.6-17.3 Ma indicating cooling below 300 ± 50° C (Jäger et al. 1967, von Blanckenburg et al. 1989) which is compatible with the interpretation of our data presented above suggesting activity of the exhuming KSZS between > 20 Ma and 17 Ma ago.

Figure 4.7 presents a cooling curve (red curve) showing that our $^{40}Ar/^{39}Ar$ on white mica ages, which we place at a temperature interval 400-470° C (depending on grain size; see discussion above and Harrison et al. 2009), are in line with the cooling trend of the ETD after the Oligocene Barrow-type thermal overprint (Tauernkristallisation) indicated by all other data available. Rapid cooling would start in Late Oligocene/Early Miocene. The cooling rate probably accelerated before 20 Ma. The zircon fission track ages of Dunkl et al. (2003) of 17.5-16.7 Ma with a closure temperature: 260 ± 20° C (Foster et al. 1996, Fügenschuh et al. 1997) confirm the inference made by Scharf et al. (submitted a, Chapter 2) that the transition to cataclastic deformation at the top of the KSZS occurred at or shortly before 17 Ma ago. Figure 4.7 also summarizes geochronological data from the Western Tauern Subdome (blue curve and boxes) that cooled earlier; this will be further discussed below.

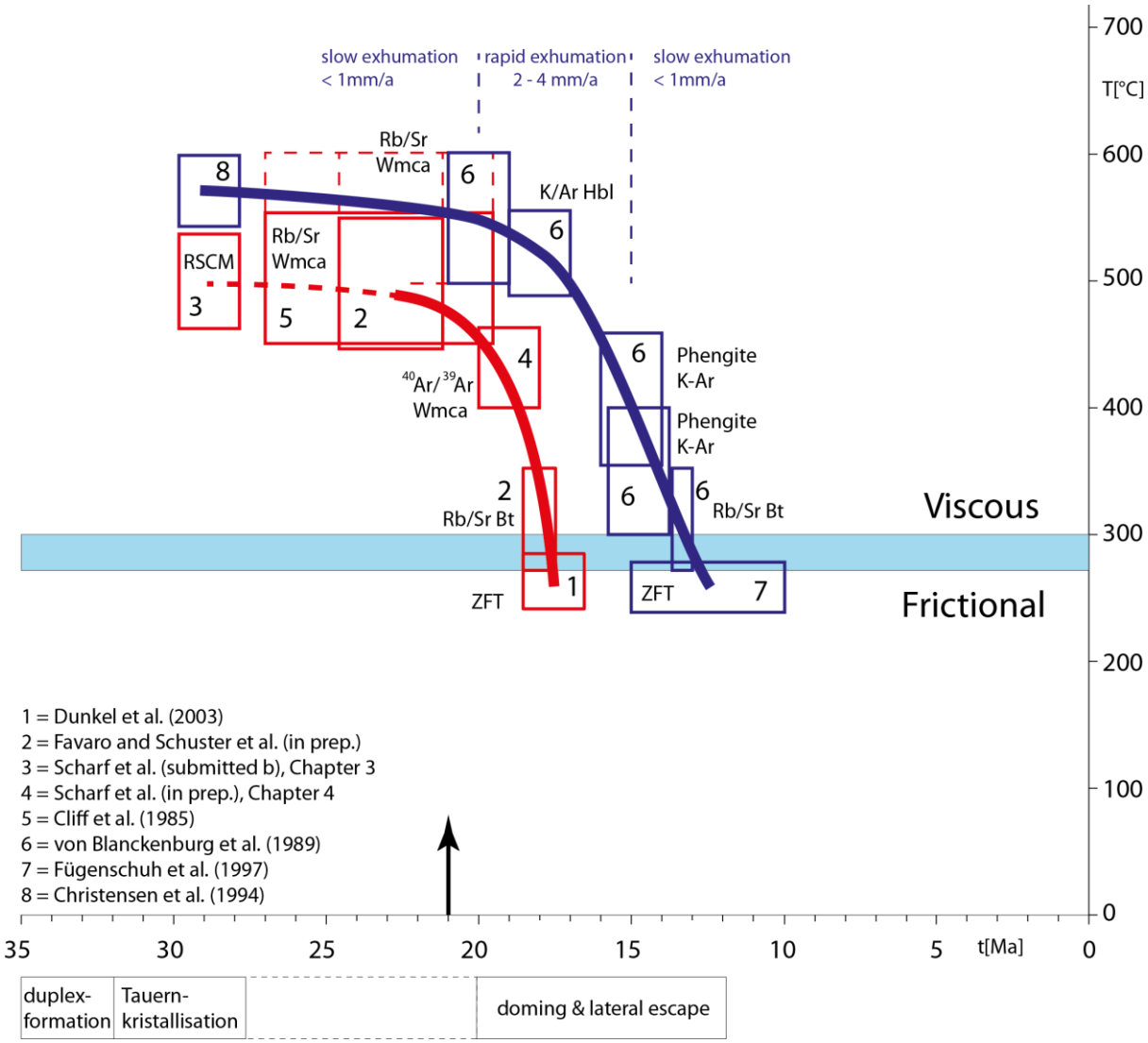

Figure 4.7: Temperature-time evolution of the Eastern- and Western Tauern subdomes. Blue curve, boxes and letters: Cooling curve based on thermal modeling for a point in the WTD located near the BNF (from Fügenschuh et al. 1997 after data of von Blanckenburg et al. 1989). Red curve, boxes and letters: cooling curves for the northeastern margin of the ETD. Boxes indicate range of conditions assuming closure temperatures listed below. Red dotted boxes using the same closure temperatures as in Fügenschuh et al. (1997) see also von Blanckenburg et al. (1989) for discussion. Temperature interval of frictional-viscous transition in quartz-rich rocks taken from Handy et al. (1999) and Stipp et al. (2002). Lower left boxes indicate peak temperature (in east, from Raman microspectroscopy on carbonaceous material of 450-525° C – RSCM, Scharf et al. 2012, submitted b, Chapter 3, assuming an age at 30-28 Ma of Christensen et al. 1994); in west from von Blanckenburg et al. (1989) at 30-28 Ma (Christensen et al. 1994). Sample localities and acronyms listed in Chapter 2 (Fig. 2.5). Closure temperatures used for red curve: Rb/Sr white mica 500 ± 50° C (Purdy and Jäger 1976); 400-470° C (depending on grain size; Harrison et al. 2009); Rb/Sr biotite 300 ± 50° C (Jäger et al. 1967; used in Favaro and Schuster et al. in prep.); 260 ± 20° C (Foster et al. 1996, used in Dunkel et al. 2003). Arrow at 21 Ma indicates the start of the indentation of the Southern Alps east of the Giudicarie Belt (Scharf et al. submitted b, Chapter 2), see discussion in the text. Note that the samples uses for the Rb/Sr on white mica ages estimates in the ETD are from the Hochalm Dome where the Alpine peak temperatures > 600° C (Droop et al. 1985, Scharf et al. submitted b, Chapter 3)

4.5.4 Exhumation rates

In the WTD, thermobarometric data combined with thermal modeling valid for a point at some 5 km horizontal distance from the Brenner Normal Fault (BNF, Fügenschuh et al. 1997) indicate that exhumation was slow (< 1 mm/a) until about 20 Ma (Fig. 4.7, blue curve). Thereafter, the exhumation rate of this point near the base of the BNF increased rapidly to about 4 mm/a and remained high (2-4 mm/a) until about 15 Ma, when it decreased to 1 mm/a. Rapid cooling, however, did not start before some 18 Ma ago lasting long beyond 15 Ma (Fügenschuh et al. 1997). The proposed onset of rapid exhumation at 20 Ma fits well with stratigraphic evidence. Indentation of the Eastern Alps near the western Tauern Window began at 21 Ma, as discussed in Schmid et al. (submitted) and Scharf et al. (submitted a), Chapter 2 and 5. Cooling and exhumation to conditions below the viscous-frictional transition in quartz-rich rocks of the BNF occurred at 15-12.5 Ma (Fig. 4.7, blue curve).

No thermal modeling is available yet for the eastern margin of the ETD and hence, statements concerning exhumation rates are rather speculative. The other difference to keep in mind is that the cooling curve for the ETD presented in Figure 4.7 is valid for a larger area rather than for a single point in space. The interpretation of our own data only allow for determining the onset of shearing within the KSZS to predate 20 Ma. The exact timing of the acceleration of shearing causing accelerated cooling is unknown and we speculate that it occurred at around 21 Ma (Fig. 4.7, red curve). However, as shown by Figure 4.7 (red curve) cooling, and therefore exhumation, must have started relatively earlier compared to the WTD. For obvious reasons it is suggested that the cooling rate accelerated during the activity of the KSZS, possibly commencing at around 21 Ma and lasting until 17 Ma ago according to the interpretation of our own data. In that case, the earlier stages of exhumation would be unrelated to movements along the KNF. Given the total amount of exhumation across the KSZS of 13.5 km (Scharf et al. submitted a, Chapter 2) and assuming an onset of rapid cooling and exhumation at around 21 Ma, coincident with the indentation of the eastern part of the Southern Alps along the Giudicarie Belt (Scharf et al. submitted a, Chapter 2), an exhumation rate of 3.4 mm/a would be calculated. Of course this represents an upper bound for the exhumation rate during the activity of the KSZS. Moreover, a late start of rapid exhumation around 21 Ma would require that the timing of the onset of rapid exhumation almost coincides with the onset of rapid cooling, with a very short delay time. This would be unlike the situation at the western margin of the Tauern Window where the delay time is substantial (Fügenschuh et al. 1997). A relatively shorter delay time between cooling and exhumation across the KNF is manifested, when compared to that noted cooling and exhumation across the Brenner Normal Fault. However this is plausible in view of the inference that exhumation across the KNF is predominantly by normal faulting, with a very minor role of erosion (Scharf et al. submitted a, Chapter 2), in view of the certainly more substantial, but in its exact magnitude still disputed amount of contemporaneous north-south shortening during normal faulting across the Brenner Fault (Rosenberg and Garcia 2011, 2012, Fügenschuh et al. 2012). Erosion

certainly plays a more important role in the exhumation of the WTD (Schmid et al. submitted, Chapter 5), increasing delay time between exhumation and cooling.

4.5.5 Did indentation of the Southern Alps east of the Giudicarie Belt also trigger the exhumation of the Eastern Tauern Window?

The onset of Miocene northward indentation of the Southern Alps into the western Tauern Window east of the Giudicarie Belt is post-dates 21.5 Ma, i.e. the age of deposition of the youngest sediments affected by transpression across the Giudicarie Belt (Luciani and Silvestrini 1996, Schmid et al. submitted, Scharf et al. submitted a, Chapter 2 and 5). This event is held responsible for the onset of rapid exhumation at about 20 Ma of the WTD east of the Brenner Normal Fault (Fig. 4.7, blue curve; Fügenschuh et al. 1997). This same mechanism can only trigger rapid exhumation of the ETD across the KSZS as well, provided that the lag time between rapid exhumation and cooling is considerably shorter in the case of the ETD. As discussed above, this is feasible but by no means certain. What is certain, assuming that the cooling curves presented in Figure 4.7 are approximately correct, is that cooling must have started earlier in the ETD compared to the WTD, a fact that has also been noted by previous workers (e.g., Luth and Willingshofer 2008). The cause for earlier onset of cooling and exhumation in the ETD is yet unknown and is unlikely to be directly related indentation by transpression across the Giudicarie Belt. Hence, the working hypothesis proposed by Schmid et al. (submitted, Chapter 5) and Scharf et al. (submitted a, Chapter 2), that transpression across the Giudicarie Belt and indentation of the Eastern Southern Alps triggered contemporaneous rapid exhumation of the entire Tauern Window after 21.5 Ma, remains to be tested and/or modified. If this working hypothesis is not correct, an alternative mechanism has to be proposed for the earlier onset of exhumation in the ETD, documented by the Rb/Sr data on white mica and biotite (Cliff et al. 1985, Favaro and Schuster et al. in prep.). Alternatively, indentation may have migrated from east to west, for which there is no structural evidence.

Lippitsch et al. (2003) documented a lateral switch in subduction polarity of the European- and Adriatic slabs that occurs beneath the Tauern Window and adjacent units based of mantle tomographic imaging. West of the Giudicarie Belt and the Tauern Window the European slab dips towards the south while east of the western Tauern Window it is the Adriatic slab that dips towards the northeast below the European mantle. The changeover occurs in the area of the central Tauern Window (Schmid et al. submitted, their Fig. 5, Chapter 5). Also, the style of folding due to north-south shortening that is contemporaneous with orogen-parallel extension differs rather markedly when comparing cross sections across the western to the eastern Tauern Window (Schmid et al. submitted, their Fig. 3, Chapter 5). Although exact timing and causes of this lateral change on a lithospheric scale are still poorly understood, these changes could be possibly be related to the differences observed in the cooling curves depicted in Figure 4.7.

4.6 Conclusions

The single grain age data obtained by $^{40}Ar/^{39}Ar$ laser ablation on white mica, together with geochemical and microstructural investigations indicate that most ages can be interpreted as dating cooling below a closing temperature (400-470° C, depending on cooling rate and grain size). These data indicate that cooling of the Eastern Tauern Subdome (ETD) caused by shearing within the KSZS started before 20 Ma, possibly at around 21 Ma. Taking also into account the cooling curve derived from literature data, exhumation must started very substantially before 20 Ma (Fig. 4.7), and hence, significantly earlier than reported for the Western Tauern Subdome (WTD; around 20 Ma ago; Fügenschuh et al. 1997). Our interpretation of the data, partly based on structural and geodynamical considerations (Schmid et al. submitted, Scharf et al. submitted a, Chapter 2 and 5) proposes that cooling possibly accelerated at around 21 Ma ago, i.e. coincident with the onset of the activity of the KSZS. The cooling curve suggests that the transition from viscous to cataclastic flow at the top of the KSZS occurred at around 17 Ma. This is compatible with the onset of sedimentation in the Miocene intramontane basins immediately east and in the hangingwall of the KSZS (Scharf et al. submitted a, Chapter 2).

The causes for the significant differences in the timing for the onset of cooling after the 30-28 Ma Barrow-type metamorphic event ("Tauernkristallisation") between the WTD and ETD remain to be investigated further. In the case of the WTD whose exhumation is linked to the activity of the Brenner Normal Fault the trigger for rapid exhumation (onset at 20 Ma, Fügenschuh et al 1997) has to be looked for by the differential northward movement (indentation) of the Southern Alps east of the sinistral Giudicarie Belt that cannot started before 21.5 Ma (Schmid et al. submitted, Chapter 5, Scharf et al. submitted a, Chapter 2). In the case of the exhumation of ETD whose late (post-21Ma) stages of exhumation are proposed to be linked to the exhumation by normal faulting and strike slip shearing across the KSZS, an alternative mechanism for cooling and exhumation pre-dating indentation of the Southern Alps and shearing along the KSZS has yet to be looked for.

Acknowledgment

We are indebted to many colleagues for discussions, especially Audrey Bertrand, Konrad Hammerschmidt, Silvia Favaro, Ralf Mielke, Claudio L. Rosenberg and Susanne Schneider, all from the Freie Universität Berlin, as well as Ralf Schuster and Gerhard Pestal from the Austrian Geological Survey, Vienna and Bernhard Fügenschuh from the Universität Innsbruck. Roland Oberhänsli and Martin J. Timmermann (all from the Universität Potsdam) are thanked in a very special way for taking care and supports in the $^{40}Ar/^{39}Ar$ lab at the Universität Potsdam. Anna Giribaldi, Sandra Wollnik (both Freie Universität Berlin) and Christine Fischer (Universität Potsdam) are thanked for preparing

thin-sections and helping drilling the nuggets for the $^{40}Ar/^{39}Ar$ dating. Martina Grundmann is explicit thanked for drafting figures. Our work was financed in part by the German Science Foundation (DFG-project Ha 2403/10). Stefan M. Schmid acknowledges the Alexander-von-Humboldt Foundation for support of his collaborative research in Berlin from 2008-2010.

Chapter 5

The Tauern Window (Eastern Alps, Austria) – A new tectonic map, cross sections and tectonometamorphic synthesis

This chapter is submitted in Swiss Journal of Geosciences as: Schmid, S.M., Scharf, A., Handy, M.R. & Rosenberg, C.L. (submitted), The Tauern Window (Eastern Alps, Austria) – A new tectonic map, cross sections and tectonometamorphic synthesis. The original publication is available at www.springerlink.com.

Abstract

We present a tectonic map of the Tauern Window and surrounding units, combined with a series of crustal-scale cross sections parallel and perpendicular to the Alpine orogen. This compilation, largely based on literature data and completed by own investigations, reveals that the present-day structure of the Tauern Window is primarily characterized by a crustal-scale duplex, the Venediger Duplex (Venediger Nappe System), formed during the Oligocene, and overprinted by doming and lateral extrusion during the Miocene. This severe Miocene overprint was most probably triggered by the indentation of the Southalpine units east of the Giudicarie Belt initiating at around 20 Ma and linked to a lithosphere-scale reorganization of the geometry of mantle slabs. A kinematic reconstruction shows that accretion of European Lithosphere and oceanic domains to the Adriatic (Austroalpine) upper plate, accompanied by high-pressure overprint of some of the units of the Tauern Window has a long history, starting in Turonian times (around 90 Ma) and culminating in Lutetian to Bartonian times (45-37 Ma).

Keywords

Tauern Window, Eastern Alps, tectono-metamorphic evolution, geodynamic

5.1 Introduction

The Tauern Window of the Eastern Alps exposes exhumed parts of Europe-derived crust that were accreted to the base of an Adria-derived upper plate, represented today by the Austroalpine nappes (e.g., Schmid et al. 2004). Spectacular surface geology (e.g., Lammerer et al. 2008), together with the results of deep seismic reflection measurements (e.g., Lüschen et al. 2006) offer a unique opportunity to understand crustal-scale collisional accretion in the Alps followed by late-Alpine indentation, crustal-scale folding, orogen-parallel extension and lateral extrusion that led to the final exhumation of a high-grade metamorphic Cenozoic nappe stack that pierced the Austroalpine orogenic lid by a combination of tectonic and erosional unroofing (e.g., Ratschbacher et al. 1991, Rosenberg et al. 2007).

We present a newly compiled tectonic map of the Tauern Window and surrounding units with the aim of replacing the still widely used nomenclature based on traditional terms such as "Zentralgneise", "Altes Dach", "untere Schieferhülle", "obere Schieferhülle" and "Nordrahmenzone" (e.g., Thiele 1980). This better reflects the progress made in geology over the past 100 years and allows for better understanding orogenic processes in a modern geodynamical framework. To our knowledge, Kurz et al. (1996, 1998a) were the first to introduce a modern nomenclature for the tectonic units of the Tauern Window and their work was influential in our own compilation. We make use of the tectonic map for constructing new cross sections that help visualize the complex three-dimensional geometry of tectonic units, including important along-strike changes in the structure of the Tauern Window. Finally we discuss the kinematics and dynamics of deformation, as well as the metamorphic evolution of this area, which represents a first-class natural laboratory for studying orogenic processes.

Most of the published articles and maps used will be cited below in their proper context. At this stage, we only mention the most important references: Pestal and Hejl (2005) was used for a large part of the map. Also important were Exner (1962a), van Bemmelen and Meulenkamp (1965), Becker (1993), Egger et al. (1999), Frisch (1980a), Häusler (1988), Kurz et al. (1998a), Lammerer and Weger (1998), Schmid et al. (2004), Pestal et al. (2009), Veselá and Lammerer (2008), Veselá et al. (2008) and Töchterle (2011). Numerous regular 1:50.000 map sheets available from the Geologische Bundesanstalt Wien (*http://www.geologie.ac.at/de/GEOMARKT/karten.html*) were also extremely helpful.

5.2 Major tectonic units of the Tauern Window and its surroundings

We now characterize the major tectonic units shown in Plate 1. Table 5.1 facilitates the correlation of tectonic units from west to east.

5.2.1 Subpenninic nappes of the Venediger Duplex (or Venediger Nappe System)

We refer to these nappes as Subpenninic based on their interpretation as deriving paleogeographically from the European margin (Milnes 1974, Schmid et al. 2004). In the classical nomenclature (e.g., Thiele 1980), these units were referred to as (1) "Altes Dach" (***Variscan basement*** of Plate 1), (2) the "Zentralgneise" (***Permo-Carboniferous intrusions*** of Plate 1), and (3) the ***post-Variscan cover*** (Plate 1), partly corresponding to what is often referred to as the "Untere Schieferhülle". In our compilation, the post-Variscan cover comprises not only the Mesozoic cover of units 1 and/or 2, but also continental, volcanodetrital and volcanic rocks of Late Carboniferous to Triassic age. These include Late Carboniferous (post-310 Ma) to Permo-Triassic clastic continental sediments intercalated with meta-volcanic layers, often referred to as the Wustkogel Formation (Frasl 1958; note that throughout the text we use the term formation in an informal way), that were deposited in small basins (Veselá and Lammerer 2008, Veselá et al. 2011), as well as a series that is generally referred to as "Jungpaläozoikum" (Pestal et al. 2009, see section 5.2.3. for details). Although the age of the latter is poorly constrained we suspect that the "Jungpaläozoikum" experienced only one phase of (Alpine) metamorphism and deformation. Hence it is of great importance for tracing nappe boundaries, as discussed below in more detail.

What is traditionally referred to as Venediger "Nappe" or "Complex" (Frisch 1976, 1977, Kurz et al. 1998a) is a duplex structure that consists of a folded stack of nappes arranged in a horse-like manner between a roof thrust and a floor thrust, as first recognized by Lammerer and Weger (1998, see also Lammerer et al. 2008, their Fig. 8). The floor thrust is not exposed at the earth's surface, whereas the roof thrust is found at the base of rather thin continental basement slices (gneiss lamellae) and/or their former post-Variscan cover, including an eclogitic sliver of sedimentary and magmatic (mafic) origin ("Units in the hangingwall of the Venediger Duplex" of Plate 1), also derived from the distal European margin. In many places the tectonic contacts between individual nappes of the Venediger Duplex are clearly seen to abut against this roof thrust.

The ***Ahorn and Göss Nappes (26)*** of the western and eastern Tauern Window, respectively, are the structurally lowest nappes of the Venediger Duplex. In view of very substantial along-strike changes in structure, however, it is unlikely that they represent lateral equivalents that connect via the subsurface in a cylindrical fashion. The Ahorn Nappe can easily be separated from the overlying Tux-Granatspitz Nappe based on post-Variscan cover sequences that include continental deposits of the Late Carboniferous-Permian Riffler-Schönach Basin (Veselá et al. 2008). The contact of the Göss

Nappe from the overlying Hochalm Nappe is more difficult to trace because of the frequent absence of an intervening post-Variscan cover. We follow Exner (1980) who emphasised that a clear separation between the gneissic core of the Göss dome and the overlying Permo-Carboniferous gneisses is locally provided by the Draxel Complex (part of the "Jungpaläozoikum" of Schuster et al. 2006). Where this "Jungpaläozoikum" is missing, the nappe contact is defined by migmatitic gneisses that include amphibolites formed during Variscan metamorphism, separating post-Variscan gneiss cores.

The ***Tux-Granatspitz and Hochalm Nappes (25)*** occupy an intermediate structural position within the Venediger Duplex. However, their lateral continuity across the central Tauern Window is also questionable. The highest nappes within the duplex are the ***Zillertal-Riffl Nappe (24)*** of the western Tauern Window, the ***Sonnblick-Romate Nappe (24)*** of the eastern-central area and the ***Mureck-Storz Nappe (24)*** of the easternmost Tauern Window. These nappes are all directly overlain by the roof thrust and must, hence, be considered as structural equivalents even though they are separated from each other in map view. The Mureck-Storz Nappe has a separate mylonitic orthogneiss slice at its base (Mureck-Gneis or -Decke of Exner 1982).

The rocks of the Venediger Duplex reached temperatures of 500 to 600° C during Alpine Barrow-type metamorphism (Oberhänsli et al. 2004, Schuster et al. 2004 and references therein). In the case of the southwestern Tauern Window (Selverstone et al. 1984, Selverstone 1985, 1988, 1993) the pressure maximum of 1.0-1.1 GPa predated the attainment of peak temperature conditions of 550° C and 0.7 GPa at 30 Ma (Christensen et al. 1994). Garnet growth under decreasing pressures (Selverstone 1993, Christensen et al. 1994) was pulse-like during the interval of 30-20 Ma (Pollington and Baxter 2010). The ***Eclogite Zone (21)*** of the Central Tauern was thrust onto the Venediger Duplex after the end of a first phase of decompression ending at about 32 Ma, and then was re-heated at around 30 Ma (Kurz et al. 2008, their Fig. 4). Hence, equilibration of the Venediger Duplex under Barrow-type conditions ("Tauernkristallisation" of Sander 1911) probably occurred at 30-28 Ma in the Tauern Window (see also Inger and Cliff 1994, Cliff et al. 1998). Rapid cooling during contemporaneous orogen-parallel stretching and orogen-perpendicular shortening started around 20 Ma (von Blanckenburg et al. 1989, Fügenschuh et al. 1997, Luth and Willingshofer 2008, Scharf et al. 2011, submitted a, Chapter 2).

5.2.1.1 Variscan basement

We restrict the term "Variscan" to metamorphic formations that are intruded by, and hence, predate, most of the typically 310 to 270 Ma plutonic rocks referred to as "Zentralgneise" (Finger et al. 1993, 1997, Eichhorn et al. 2000, Veselá et al. 2011). Only the 335 Ma Ahorn Gneiss is known to be older (Veselá et al. 2011), but outcrops that would expose its contact with the country rocks are missing. Shortening related to Variscan Orogeny probably ended by Early Westphalian time (about 310 Ma ago) and was followed by a period of high heat flow related to extensional collapse and/or magmatic underplating associated with widespread magmatic activity (Finger et al. 1997, Schuster and Stüwe

2008) typical for Late Carboniferous and Permian times all over Central Europe (e.g., Burg et al. 1994, Ziegler 1992). In the traditional literature, the term "Altes Dach" denotes those parts of the pre-Mesozoic metamorphic basement that show clear intrusive contacts with the Zentralgneis whereas "Altkristallin" denotes pre-Late Carboniferous basement in general (Pestal et al. 2009). The pre-Alpine metamorphic grade of this Altkristallin ranges from greenschist facies (i.e., Habachphyllite of the northernmost central Tauern Window, Frasl 1958) to amphibolite facies including migmatites (Komplex der Alten Gneise of the Riffl Nappe further south; Frasl and Frank 1966).

Radiometric dating has also revealed pre-Variscan tectono-metamorphic events. A reworked block of meta-gabbro found within the Mesozoic Kaserer Series (see section 5.2.3.) from the western Tauern Window yielded zircon with ages of 534 ± 9.4 Ma (Veselá et al. 2008). Pre-Variscan ages (Eichhorn et al. 2001, Kebede et al. 2005) were also found for a part of the so-called and poorly defined "Habach Series" of the central part of the Tauern Window (Frasl 1958, Höck 1993), specifically for the Lower Habach Formation or Lower Magmatic Sequence as defined by Kebede et al. (2005). This is a meta-ophiolitic association that comprises mafic and ultramafic series belonging to the Tux-Granatspitz Nappe of the central Tauern Window (Plate 1).

Another large pre-Variscan basement complex in the central part of the Tauern Window (see Kebede et al. 2005 for a compilation of radiometric ages) is the "Old Gneiss Series" (= "Komplex der Alten Gneise" of Frasl and Frank 1966). This series consists of Pre-Cambrian to Ordovician amphibolite, biotite gneisses and micaschists. These contain younger migmatitic layers and anatectic granites that formed during the Variscan event, i.e., in Early Carboniferous time (Eichhorn et al. 1999, 2000, Schermaier 1991). Elongate layers of strongly deformed Early Carboniferous granitoids (e.g., the Felbertauern Gneiss Lamellae, Eichhorn et al. 2000) form the base of a thrust sheet of this "Serie der Alten Gneise" that was also described as Riffl Nappe in the literature (Frisch 1980a). However, in contrast to Frisch (1980a), we suspect that this Riffl Nappe (Zillertaler-Riffl Nappe of Plate 1) is of Alpine age (see below). Where post-Variscan series are only locally preserved or missing, we mapped the boundary between Tux-Granatspitz Nappe and Zillertaler-Riffl Nappe in the central Tauern Window on the basis of distinctions in basement lithology. The basement complex of the Zillertaler-Riffl Nappe (mostly "Serie der Alten Gneise") is lithologically very distinct from the tectonically underlying series of the Tux-Granatspitz Nappe (pre-Variscan Lower Magmatic Sequence and Variscan-age Basisamphibolit, Kebede et al. 2005). The "Storz Komplex" (Exner 1971a), also part of the Zillertaler-Riffl Nappe, makes up much of the Mureck-Storz Nappe of the easternmost Tauern Window (Table 5.1 and Plate 1) and is a pre-Variscan basement complex lithologically similar to the "Komplex der Alten Gneise". A part of the Greiner Group (Lammerer 1986) intruded by the Zillertaler Zentralgneis in the western Tauern Window is probably also of pre-Variscan age.

Pre-Mesozoic series overlying the Lower Habach Formation of the Tux-Granatspitz Nappe of the central Tauern Window (Obere Magmatitabfolge and Habach Phyllites) correspond to the Habach Group as defined and mapped by Pestal et al. (2005). These series are typical for the structurally

higher parts of the Tux-Granatspitz Nappe preserved in synclines that also include series that lack a pre-Variscan overprint, amongst them calc-alkaline volcanites often interpreted in terms of an island-arc environment (e.g., Vavra and Frisch 1989) and related sediments, the Habach Phyllites (Pestal et al. 2009 and references therein). Some of these volcanites yield Early Carboniferous to Permian ages (Kebede et al. 2005 and references therein) whereas the age of sedimentation of the Habach Phyllites remains unknown. In the absence of clear age criteria we group these series of the Habach Group with the Variscan basement although some these volcanites probably have a Late Carboniferous to Permian (i.e., post-Variscan) age.

5.2.1.2 Permo-Carboniferous intrusions

We regard the Zentralgneise of the Göss-, Tux-Granatspitz-, Hochalm-, Zillertal-Riffl-, Sonnblick-Romate- and Mureck-Storz Nappes whose ages typically vary between 310 and 270 Ma (Finger et al. 1993, 1997, Eichhorn et al. 2000, Veselá et al. 2011), to be post-Variscan (i.e., to have intruded after the Variscan Orogeny) because they discordantly intrude Variscan and/or older metamorphic fabrics, and hence, are only affected by Alpine-age deformation. For simplicity, we also put the Zentralgneis of the Ahorn Nappe in the same category although its Early Carboniferous age (Veselá et al. 2011) indicates that it must have intruded during rather than after Variscan orogeny.

5.2.1.3 Post-Variscan cover

The cover of suspected Late Carboniferous to Permian age that post-dates Variscan metamorphism, i.e., the ***Post-Variscan cover (23)***, plays a particularly important role in tracing nappe boundaries where Mesozoic strata are missing. Pestal et al. (2005, 2009) mapped such metasedimentary formations (e.g., Murtörl Formation and Draxel Complex, interpreted as "Jungpaläozoikum") at several locations with the same signature. Despite remaining uncertainties regarding their exact age, we interpreted these occurrences to represent cover in the sense that their age of deposition most probably post-dates Variscan tectono-metamorphism.

The Murtörl Formation (Murtörlserie of Exner 1971a) was originally defined within a tectonic slice of the eastern Tauern Window that structurally overlies the Venediger Duplex (so-called Murtörl-Schrovin-Schuppe discussed later), but the term was also used for other occurrences of the same formation by Pestal et al. (2005, 2009), e.g., for the so-called "Woiskenschiefer" (Exner 1956, 1957) that separate the Sonnblick-Romate Nappe (uppermost structural level within the Venediger Duplex) from the underlying Hochalm Nappe (see Table 5.1 for correlations of structural units). The rocks of the Draxel Complex (Exner 1971b, 1980, 1982) define the thrust contact between the Göss- and overlying Hochalm Nappe. Unfortunately, both Murtörl Formation and Draxel Complex remain undated. Some workers have resorted to using the character of their contacts with magmatic bodies, including dykes that are considered part of the "Zentralgneis", as a criterion for determining the age of the sediments of the "Jungpaläozoikum"; meta-sediments injected by dykes (Schuster et al. 2006)

were interpreted to also have experienced Variscan tectono-metamorphism. Unfortunately, this criterion would only pertain if the "Zentralgneise" were indeed Variscan. In our view, however, the Zentralgneise should be regarded post-Variscan; recent studies have shown that sedimentation and magmatic activity were contemporaneous in Late Carboniferous to Permian times (Veselà et al. 2008, 2011).

Following Pestal et al. (2005, 2009) we also considered the so-called Zwischenelendschiefer (Lerchbaumer et al. 2010) of the cover of the Hochalm Nappe, the "Schiefer mit Biotitporphyroblasten" (Cornelius and Clar 1939) of the Granatspitz area (Tux-Granatspitz Nappe of the central Tauern Window) and the Furtschaglschiefer (Lammerer 1986) of the cover of the Zillertal-Riffl Nappe in the western Tauern Window as parts of this post-Variscan cover. Radiometric dating has so far only yielded "maximum ages" inferred from detrital zircons: 356 ± 2 Ma for the Furtschaglschiefer (Klötzli unpublished as quoted in Lerchbaumer et al. 2010); 362 ± 6 Ma and 368 ± 17 Ma for the Biotitporphyroblastenschiefer (Kebede et al. 2005) and 360 ± 13 Ma for the Zwischenelendschiefer (Lerchbaumer et al. 2010). These data merely indicate that the Variscan-age rocks must have contained Latest Devonian to Earliest Carboniferous detrital zircons. The data set is remarkable for its lack of detrital zircons shed from the Zentralgneise. Moreover, the Biotitporphyroblastenschiefer of the Felbertal and Amertal transgress directly onto the so-called "Basisamphibolit" (an amphibolite horizon forming the base of the Obere Magmatitabfolge and the frame of the Zentralgneis Intrusion in the Granatspitz area, Kebede et al. 2005 and references therein). The protolith-age of the Basisamphibolit is 343 ± 1 Ma (Early Carboniferous) based on U-Pb zircon data (Kebede et al. 2005). The overlying Biotitporphyroblastenschiefer yields detrital zircons with 362 ± 6 Ma (Kebede et al. 2005), i.e., zircons that are older than the underlying Basisamphibolit. In summary, all these data suggest that the above-discussed series are post-Variscan in age.

The following formations certainly fall into the post-Variscan and Pre-Mesozoic age range: (1) the Mauerertal-Formation overlying the Altkristallin of the Zillertal-Riffl Nappe dated with fossils as Westphalian to Stephanian (312-299 Ma; Franz et al. 1991, Pestal et al. 1999) and (2) the so-called Porphyrmaterialschiefer comprising volcanites dated at around 283 Ma based on U-Pb zircon ages (Söllner et al. 1991, Loth et al. 1997). The latter are widespread in higher tectonic units (Wolfendorn Nappe; Frisch 1973/74) but also occur, together with Triassic marbles, in the Late Paleozoic cover of the Tux-Granatspitz Nappe near the contact to the Glockner Nappe System (Frank et al. 1987).

Summarizing, there are good reasons to group the post-Variscan Permo-Carboniferous cover with the Mesozoic cover in order to provide an effective means of separating Alpine tectonic units within the Venediger Duplex. The Mesozoic strata will be discussed in a separate section that also considers the paleogeographic position of the Subpenninic units, including those in the hangingwall of the Venediger Duplex (section 5.2.3). Where present, these lithologies provide unambiguous lithostratigraphic criteria for tracing nappe contacts.

5.2.2 Subpenninic nappes in the hangingwall of the Venediger Duplex

Two observations provide a key for distinguishing between units of the Venediger Duplex and the overlying Subpenninic nappes: Firstly, Frank (1969) recognized a large isoclinal fold (his Seidlwinkl Fold Nappe) that is neither part of the Venediger Duplex nor of the Glockner Nappe System. Instead, it is part of what we call Modereck Nappe System, described below (section 5.2.2.3). Together with thin basement slices this fold roots south of, and in, the hangingwall of the Venediger Duplex. Secondly, it was found that the Eclogite Zone in the central southern part of the Tauern Window occupies a structural position above the Venediger Duplex but below a lateral equivalent of the Seidlwinkl Nappe. The envelope of the Seidlwinkl Nappe that is in contact with the Glockner Nappe System is also locally overprinted by high-pressure metamorphism (Kurz et al. 1996, 1998a, 2008). Taken together, these facts point to a tectonic and metamorphic evolution of the Eclogite Zone and parts of the Seidlwinkl Nappe (Modereck Nappe System), which is distinct from that of the underlying Venediger Duplex. The northwestern part of the Tauern Window exposes a third Subpenninic slice that lacks high-pressure overprint: the Wolfendorn Nappe (Frisch 1973/74). Weakly metamorphosed units such as the Eisbrugg Slice and Geroldstein Mesozoic in the southwestern Tauern Window are also part of the Modereck Nappe System (Oehlke et al. 1993, Rockenschaub et al. 2003), as well as the Murtörl-Schrovin Unit of the northeastern Tauern Window (see Table 5.1).

5.2.2.1 Wolfendorn Nappe

The **Wolfendorn Nappe** ***(22)*** of the northwestern Tauern Window thrusts two imbricates of the Venediger Duplex: the Tux-Granatspitz Nappe and Ahorn Nappe. This thin nappe or slice was defined by Frisch (1973/74) who realized that it has a pre-Triassic substratum (the Late Palaeozoic Porphyrmaterialschiefer, see Fig. 5.1) that substantially differs from the basement of the underlying Venediger Duplex. However, at the type locality of the Wolfendorn Nappe (a mountain peak of the same name) the Porphyrmaterialschiefer (see section 5.2.1) is missing, and the base of the Wolfendorn Nappe contains only a thin band of Triassic strata separating the Late Jurassic Hochstegenkalk of the Venediger Duplex (cover of the Tux-Granatspitz Nappe) from the Hochstegenkalk of the Wolfendorn Nappe (Frisch (1973/74). The latter is stratigraphically overlain by the Kaserer Series of suspected Cretaceous age (Frisch 1973/74, 1980b, Lammerer 1986, Rockenschaub et al. 2003, Rockenschaub et al. 2007), a formation that is typical for the Wolfendorn Nappe (Fig. 5.1). In our compilation, we share the view of Frisch (1973/74) and Rockenschaub et al. (2003), being aware that the structure of the Wolfendorn area and the age of the Kaserer Series is still highly controversial (see Veselá and Lammerer 2008, Lammerer et al. 2008, 2011, Töchterle 2011 for differing views).

5.2.2.2 Eclogite Zone

The ***Eclogite Zone*** (Plate 1) occupies a tectonic position above the Venediger Duplex and below the Modereck Nappe System (section 5.2.2.3). Eclogite-facies conditions of 1.9-2.2 GPa and 600-630° C (Hoschek 2001) were reached at 45-42 Ma (Zimmermann et al. 1994, Ratschbacher et al. 2004, Kurz et al. 2008), followed by a first stage of decompression lasting to 32 Ma. Later, reheating to amphibolite-facies conditions (Tauernkristallisation) affected the entire nappe stack including the Venediger Duplex (see Glodny et al. 2008 for a differing view regarding timing). The onset of subduction is poorly constrained, but available radiometric data suggest an age between 55 and 45 Ma ago (Berger and Bousquet 2008).

The eclogite-facies metamorphism during Early Cenozoic time indicates subduction of the most distal European passive continental margin to a depth of at least 80 km (Ratschbacher et al. 2004, Schuster et al. 2004, Thöni 2006, Kurz et al. 2008). The Eclogite Zone comprises felsic and carbonatic rocks (quartzites, paragneisses, garnet-micaschists, calcites, marbles, and siliceous dolomites, Franz and Spear 1983) and also contains small lenses of mafic eclogites. These lithologies are part of a volcano-sedimentary sequence of the distal continental slope (Miller et al. 1980, 2007); the mafic material represent intrusions into the most distal European margin close to the continent-ocean transition, in parts the Eclogite Zone may also represent a tectonic mélange (Miller et al. 1980). Either way, it is unlikely that the Eclogite Zone is part of the oceanic Glockner Nappe System. In summary, the Eclogite Zone is derived from the most distal European margin, analogous to the Adula Nappe of the Central Alps in Switzerland (Schmid et al. 2004).

5.2.2.3 Modereck Nappe System

The term "Modereck Nappe" was coined by Kober (1922) and Hottinger (1935) to denote the structurally highest basement slice in the Sonnblick area that is occasionally also referred to as the Rote Wand Nappe or Rote Wand – Modereck Nappe (e.g., Kurz et al. 2008). We use the term ***Modereck Nappe System (20)*** to denote all the units in a similar structural position immediately below the Glockner Nappe System. The Seidlwinkl Nappe, an isoclinal fold nappe whose extent is limited to the central Tauern Window (Frank 1969) finds its root at the Rote Wand and Stanziwurten peaks on the southwestern flank of the Sonnblick Dome. It has a gneissic core ("Gneislamelle 4" of Exner 1962a, Alber 1976) that comprises mostly the Permo-Triassic Wustkogel Formation. Parts of the Modereck Nappe System located in the Grossglockner area are, together with the adjacent Eclogite Zone, affected by eclogite-facies metamorphism (Plate 1).

Following Kurz (1996), we also consider the Murtörl-Schrovin Schuppe (Schuppe = thin nappe slice) in the eastern Tauern Window (Schuster et al. 2006) as a part of the Modereck Nappe System. This slice consists essentially of the Late Paleozoic Murtörl Formation (Exner 1971a) overlain by the Wustkogel and Seidlwinkl Formations (Schrovin-Gruppe of Exner 1971a). Slivers attributed to the Modereck Nappe System are also found in the Matrei area of the southern central Tauern Window where they occur as basement lamellae (so-called "Glimmerschieferlamelle" consisting of quartz-rich

muscovite bearing mica-schists) that are associated with Triassic marbles and Cretaceous Brennkogel Formation. These slivers separate the underlying Eclogite Zone from the tectonically higher Glockner Nappe System (Spear and Franz 1986, Kurz et al. 1998a).

Gneiss and amphibolite slivers, accompanied by Mesozoic marble and Kaserer Series, a lateral equivalent of the Brennkogel Formation (Fig. 5.1), are also found south of and around the southwestern tip of the basement of the Zillertal-Riffl Nappe (Lower and Upper Eisbrugg Lamellae of Oehlke et al. 1993). They tectonically overlie a thin veneer of Hochstegen Marble belonging to the Venediger Duplex. Thin Mesozoic slivers of the Modereck Nappe System are also exposed around the southern, western and northwestern margins of Ahorn and Tux-Granatspitz Nappes (Modereck Nappe of Rockenschaub et al. 2003, 2011, Decker et al. 2009). These slivers lie above the Wolfendorn Nappe and consist predominantly of Permo-Skythian clastics, evaporite-bearing Triassic carbonates and Keuper quartzites in the Seidlwinkl Facies (Rockenschaub et al. 2003; "Triassic base of the Upper Schieferhülle" of Töchterle et al. 2011). It is possible that some of the overlying metasediments ("Bündnerschiefer") that we group with the Glockner Nappe System in fact represent the stratigraphic cover of Permo-Triassic strata belonging to the Modereck Nappe System (Decker et al. 2009, Rockenschaub et al. 2011, Töchterle 2011, Töchterle et al. 2011). However, we regard the majority of the calcschists of the northwestern Tauern Window to be in tectonic contact with the Seidlwinkl-Rote Wand Nappe and we therefore group them with the Glockner Nappe System.

5.2.3 Stratigraphical and paleogeographical considerations regarding the Mesozoic cover of the Subpenninic nappes

The Mesozoic sediments of the Subpenninic nappes remain undated due to their strong metamorphic overprint. An exception is the Hochstegen Marble, an outer shelf deposit whose Late Jurassic age is documented by fossils (Klebelsberg 1940, Kiessling 1992, Höfer and Tichy 2005). Hence, dating these metasediments relies almost entirely on lithostratigraphical comparisons with well-dated series elsewhere in the Alps and its foreland. The facies of the Hochstegen Marble was taken either as typical for the Briançonnais paleogeographical domain (e.g., Frisch 1979, Tollmann 1987), or alternatively, for the European (Helvetic) Margin (e.g., Lammerer 1986, Trümpy 1992, Froitzheim et al. 1996). The answer to this dilemma has profound implications for the eastward lateral extent of the Briançonnais continental fragment separating the Piemont-Liguria and Valais oceanic domains, the origin of the Rhenodanubian Flysch (north or south of the Subpenninic Units), and thirdly and most importantly, the amount of Cenozoic north-south shortening (see discussion by Kurz 2006).

Figure 5.1 shows lithostratigraphic sections compiled for the Venediger Duplex, the Wolfendorn Nappe and parts of the Modereck Nappe System in the western and eastern parts of the Tauern Window (see figure legend for references), arranged from northwest to southeast according to paleogeographical position. Occurrences of the Late Jurassic Hochstegen Marble are restricted to the Venediger Duplex and parts of the Wolfendorn Nappe. We explain its absence in the Modereck Nappe

System as due to erosion below an unconformity at the base of the Brennkogel Formation and its lateral equivalent, the Kaserer Series. As proposed by Lemoine (2003), the dark calcschists and black shales of the Brennkogel Formation, with intercalations of quartzite beds and carbonatic breccias, is an association that is typical for the so-called "Gault-type" black shales found elsewhere in Mid-Cretaceous deposits of the Alps. These rocks were deposited in an oxygen-starved environment during one of the several Cretaceous global anoxic events (probably OAE1a, Takashima et al. 2006). Such lithologies are widespread in the Subbriançonnais Units of eastern Switzerland (Schams-, Tasna- and Falknis Nappes, e.g., Rück and Schreurs 1995), the Rhenodanubian Flysch Zone (e.g., Mattern and Wang 2008) and the Valaisan Units of Switzerland and Savoie (e.g., Bertle 2004, Loprieno et al. 2011). The similarity of the sequences of the Seidlwinkl Fold Nappe exposed along the Grossglockner Road (Frasl and Frank 1966) and the External Valais Units of the Versoyen (Loprieno et al. 2011) is striking: a Cretaceous-age post-rift sequence directly transgresses a Germanic-type Triassic pre-rift sequence, the previously deposited Late Jurassic limestone having been eroded during rifting associated with the opening of the Valais Ocean.

An older angular unconformity of Lower Jurassic age (Frisch 1975) is responsible for the direct transgression of Lower Jurassic quartzites and black shales onto the basement of the northwestern tip of Tux-Granatspitz Nappe in the western Tauern Window. It indicates local erosion of previously deposited Triassic strata. This same graphite-rich formation, known as the Schwarzkopf Formation in the central and eastern Tauern Window (Pestal et al. 2009), was probably deposited during the Toarcian global anoxic event (Takashima et al. 2006) and overlays Late Triassic Keuper beds. Frisch (1975) recognized the strong similarity of this formation with the so-called Gresten Facies found in the Ultrahelvetic Grestener Klippenzone at the northern border of the Alps, a facies that extends into the Moravian Zone of the Bohemian Massif (Faupl 1975). This same Gresten Facies is widespread all over the Europe-derived Tisza- and Dacia Mega-Units of the circum-Pannonian area (Schmid et al. 2008). In our view, the presence of the Lower Jurassic Gresten Facies, together with the Germanic character of the Triassic deposits, strongly supports a European origin of the Subpenninic Units and virtually excludes their provenance within an eastern extension of the Briançonnais continental fragment. The latter ends eastward somewhere between the Engadine and Tauern windows (Schmid et al. 2004).

Interestingly, the Brennkogel Formation is very similar to many of the meta-sediments of the Glockner Nappe System. This is particularly true for the profile across the Mesozoic cover of the Hochalm Nappe (Silbereckserie of Exner 1982, 1983) where the Brennkogel Formation, mapped as "Bündnerschiefer" (Häusler 1995), stratigraphically overlies marbles (Silbereckmarmor) recently dated as Late Jurassic (Höfer and Tichy 2005). This indicates that there must be a continuous transition from the Subpenninic units that represent the distal European margin to the sediments of the Glockner Nappe System that were deposited largely on oceanic lithosphere (Valais Ocean, see below). In conclusion, the Subpenninic nappes appear to be relics of the distal European margin that faced the

Valais Oceanic domain. This precludes a paleogeographic origin of the Rhenodanubian Flysch from north of the Tauern Window and points to an amount of Cenozoic north-south shortening across the Eastern Alps that is of the same order of magnitude as that reported for an Alpine transect across eastern Switzerland (e.g., some 500 km, Schmid et al. 1996).

5.2.4 Ophiolitic units

The paleogeographic position of the most voluminous part of the ophiolite-bearing units of the Tauern Window, referred to as Glockner Nappe System, is controversial. While some authors (e.g., Frisch 1980b, Kurz 2006) attribute the Glockner Nappe System to the Piemont-Liguria Ocean (PLO), others parallelize it with the calcschists and ophiolites of the Valais Ocean (VO) exposed in the Lower Engadine Window west of the Ötztal Nappe (e.g., Trümpy 1992, Schmid et al. 2004). At first sight, grouping it with one of the two oceans of Alpine Tethys (PLO or VO) would seem to be a semantic exercise considering that the intervening Briançonnais continental sliver wedges out between the Engadine and Tauern windows (Schmid et al. 2005, discussion above and in Kurz 2005). However, the following criteria allowed us to assign ophiolite-bearing units east of the Engadine Window to one or the other of these oceanic domains: (1) age of rifting and passive margin formation regarding these two oceanic domains (Mid-Jurassic vsersus Early Cretaceous, Frisch 1979), (2) presence (PLO) or absence (VO) of radiolarites and aptychus limestones deposited on exhumed mantle rocks, (3) presence of rock assemblages that are characteristic for an ocean-continent transition along either the Adriatic (PLO) or the European (VO) margins, (4) evidence for early accretion to either the Adriatic margin (PLO) during Cretaceous top-west nappe stacking in the Eastern Alps or Cenozoic accretion to the European margin (VO).

5.2.4.1 Glockner Nappe System

The term ***Glockner Nappe System (19)*** denotes a nappe pile with calcareous micaschists and subordinate metapelites (Glockner Nappe of Staub 1924) of probable Cretaceous age, often intercalated with prasinites or amphibolites, depending on grade of metamorphism (Pestal et al. 2009). In the northern central part of the Tauern Window, the metasediments of the Glockner Nappe System are often purely siliciclastic or carbonate-poor and phyllitic (so-called Fuscher Phyllit, Pestal et al. 2009). The lithological association of the Glockner Nappe System is very similar to the Valais-derived calcschists of the Engadine Window and the Valais units of Savoie (Jeanbourquin and Burri 1991, Steinmann 1994, Loprieno et al. 2011). This series is distinguished from the Piemont-Liguria Ocean derived associations based on the criteria discussed above. The Cenozoic age of high-pressure metamorphism in the Glockner Nappe System (Plate 1) indicates that parts of the Glockner Nappe System were subducted and exhumed during the Cenozoic Alpine orogeny, together with the most distal part of the European margin (Eclogite Zone). In summary, all this indicates that the Glockner

Nappe System comprises relics of the Valais Ocean, together with the Rhenodanubian Flysch along the northern margin of the Eastern Alps (Schmid et al. 2004).

The Glockner Nappe System remains to be subdivided, for two main reasons. First, parts of the metasediments attributed to the Glockner Nappe System, particularly those in the northern parts of the Tauern Window, may have been deposited on continental rather than oceanic lithosphere, lenses of serpentinites, occasionally associated with metagabbros (Pestal et al. 2009 and references therein) are rather rare. Secondly, metamorphic grade varies from eclogite-facies (southern central part of the Tauern Window in vicinity to the Seidlwinkl Fold Nappe and the Eclogite Zone, Sturm et al. 1997, Dachs and Proyer 2001) to uppermost greenschist- or lower blueschist-facies conditions elsewhere (Schuster et al. 2004 in Oberhänsli et al. 2004). The maximum pressure and temperature determined for the Glockner Nappe System in the southern part of the central Tauern Window (Dachs and Proyer 2001) are only slightly less than those obtained for the adjacent Eclogite Zone.

5.2.4.2 Reckner Ophiolitic Complex

The ***Reckner Ophiolitic Complex (18)*** is a piece of exhumed subcontinental mantle with occurrences of ophicalcites, stratigraphically overlain by Jurassic radiolarites and younger pelagic sediments (Enzenberg-Praehauser 1967, 1976, Koller and Pestal 2003). This is typical for ophiolitic sequences derived from the Piemont-Liguria Ocean (Froitzheim and Manatschal 1996). Strangely enough, this ophiolitic complex overlies the Upper Austroalpine Innsbruck Quartzphyllite Unit and forms a klippe on top of the Lower Austroalpine Hippold and Reckner Nappes, Reckner Ophiolitic Complex, Hippold and Reckner nappes were deformed under blueschist-facies conditions in Early Cenozoic time, as indicated by $^{40}Ar/^{39}Ar$ white mica ages of 50-57 Ma for the Reckner Ophiolitic Complex (Dingeldey et al. 1997, Ratschbacher et al. 2004). Pressures obtained for Matrei Zone and Innsbruck Quartzphyllite Unit in the footwall of these three blueschist-facies units are distinctly lower (Dingeldey et al. 1997). This suggests younger, out-of-sequence thrusting of the Reckner Ophiolitic Complex and underlying Hippold and Reckner Nappes onto the Innsbruck Quartzphyllite Unit.

5.2.4.3 Matrei Zone

The interpretation of mélange in the Matrei Zone as relics of the Piemont-Liguria Ocean is undisputed. The Matrei Zone formed near the overriding Adriatic (Austroalpine) margin (Frisch et al. 1987).

The type locality of the ***Matrei Zone (17)*** is at the southern margin of the Tauern Window. Following Koller and Pestal (2003) and Pestal et al. (2009) we also include the so-called "Nordrahmenzone", defining the northern contact zone of the Tauern Window to the Austroalpine units, into this same tectonic unit. The Matrei Zone is lithologically very heterogeneous and represents an imbricate zone or mélange zone with huge blocks, up to several km wide. "Bündnerschiefer"-type sediments and subordinate ophiolitic lithologies (mafic-ultramafic rocks and/or their pelagic cover) are mixed with sediments of Permian to Jurassic age that are clearly derived from the Adriatic margin

(Austroalpine). Some authors (e.g., Frisch et al. 1987) prefer to interpret the Austroalpine blocks as olistoliths; others consider the Matrei Zone and lateral equivalents elsewhere as a tectonic mélange or imbricate zone (Arosa Zone, Valsertal Zone, Winkler and Bernoulli 1986). In any case, the setting of the Matrei Zone is that of an accretionary prism that formed during the subduction of the Piemont-Liguria Ocean in front and below the Austroalpine as a part of the Adria upper plate during Late Cretaceous times (Handy et al. 2010).

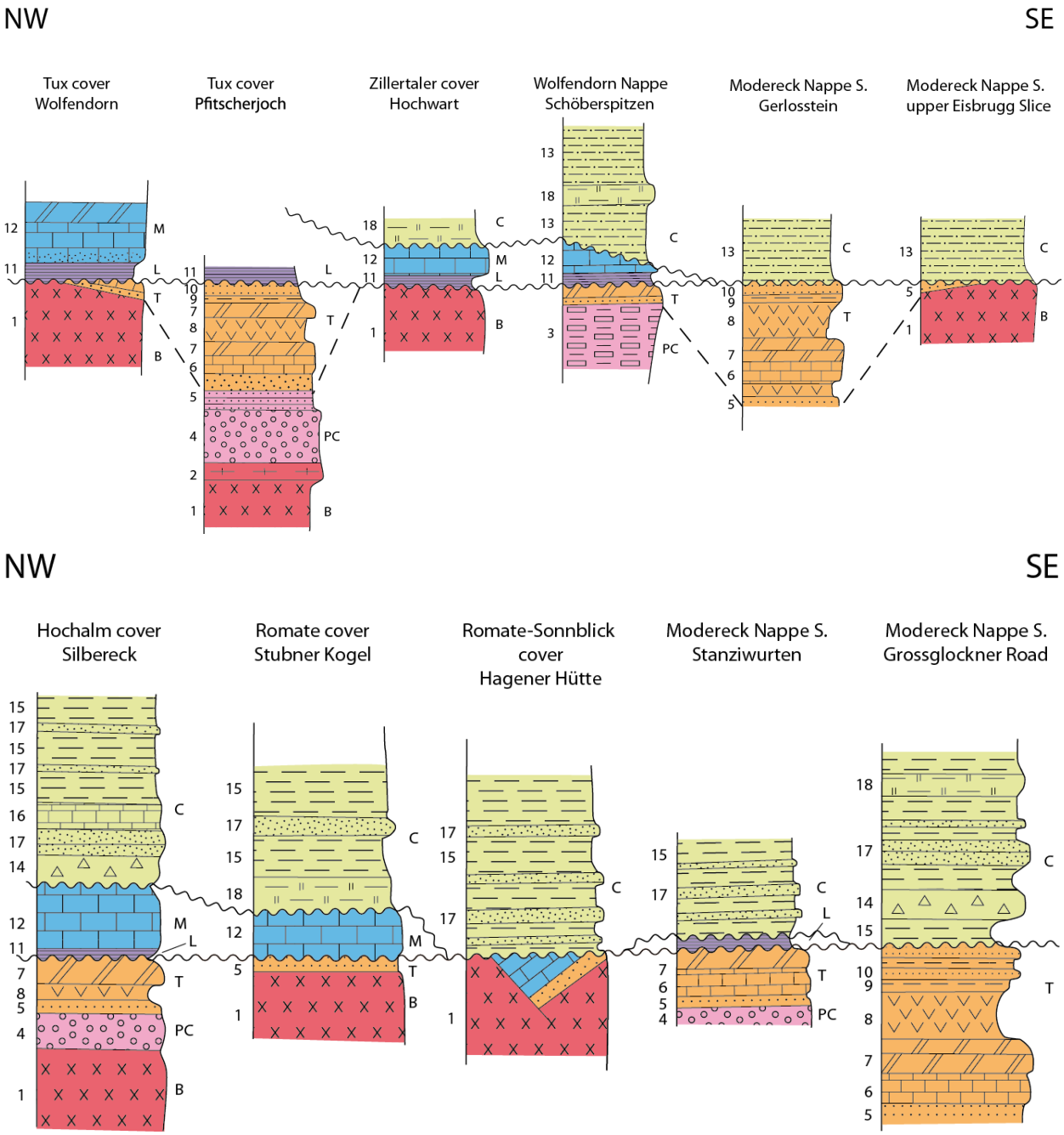

Figure 5.1: Stratigraphic columns complied after: Alber (1976), Brandner et al. (2008), Exner (1982), Frisch (1975, 1980b), Frasl and Frank (1966), Höfer and Tichy (2005), Klebelsberg (1940), Kurz (2006), Kurz et al. (1998a), Lammerer (1986), Lemoine 2003, Rockenschaub et al. (2003), Thiele 1970, Veselá and Lammerer (2008), Veselá et al. (2008). The lithologies are 1 - granite gneiss; 2 - Variscan basement; 3 - Porphyrmaterialschiefer; 4 - conglomerates; 5 - Permo-Skythian quartzites; 6 - limestones; 7 - dolomites; 8 - evaporites; 9 - chloritoid schists; 10 - Keuper quartzites; 11 - Liassic black schists and sandstones; 12 -

Hochstegen limestones; 13 - Kaserer Series in general; 14 - dolomite breccias; 15 - black phyllites; 16 - slaty limestones; 17 - Brennkogel quartzites; 18 – calcschists. The capital letters stand for: B - basement; PC - Late Carboniferous to Permian; T - Triassic; L – Lower and Middle Jurassic; M - Upper Jurassic; C - Cretaceous (Brennkogel Formation and Kaserer Series).

Little is known about grade and age of metamorphism in the Matrei Zone. Dingeldey et al. (1997) report 0.6-0.7 GPa and 400° C for the Matrei Zone at the northwestern margin of the Tauern Window while Koller and Pestal (2003) report blueschist-facies overprint for the Matrei Zone at the southern rim of the Tauern Window. Dingelday et al. (1997) report Eocene ages of metamorphism, indicating that the Matrei Zone was re-worked during Cenozoic orogeny, when the Glockner Nappe System was accreted to an upper plate that, apart from the Austroalpine, also included the previously accreted Matrei Zone.

5.2.5 Lower Austroalpine nappes

The Lower Austroalpine Nappes comprise tectonic units originally located at the most distal passive margin of Adria (Froitzheim and Eberli 1990, Schmid et al. 2004). Drawing a clear boundary with the Upper Austroalpine units is difficult, particularly in the northeastern and eastern corners of the Tauern Window. For example, we do not regard the Katschberg Zone Quartzphyllites, running parallel to the central part of the Katschberg Shear Zone System (Scharf et al. 2011, submitted a, Chapter 2), as part of the lower Austroalpine Nappe System for reasons discussed below. Mesozoic series with spectacular rift-related breccias that are typical for the Lower Austroalpine Nappes appear at the northern margin of the Tauern Window in the Tarntal area south of Innsbruck, and in the Radstätter Tauern units at the northeastern edge of the Tauern Window (Häusler 1988). Lower Austroalpine series have also been described from small areas south of the Tauern Window (Fuchs et al. 1996, Pestal and Hejl 2005, Fuchs and Linner 2005).

The Lower Austroalpine nappes around the Tauern Window suffered intense deformation and greenschist- or blueschist-facies overprinting, from the onset of subduction of the Piemont-Liguria Ocean in Late Cretaceous time to final closure of the Valais Ocean in Eocene time. The $^{40}Ar/^{39}Ar$ white mica ages obtained for metamorphism in the Radstätter Tauern range between 80 and 50 Ma (Liu et al. 2001) but are younger in the Tarntal area (44 to 37 Ma, Dingeldey et al. 1997).

5.2.5.1 Hippold Nappe and Hochfeind Nappe

The breccious sediments of the ***Hippold Nappe (16)*** near the northwestern corner of the Tauern Window are interpreted as base of fault scarp breccias, shed from the south in lower and mid-Jurassic times (Häusler 1988). These breccias are overlain by Late Jurassic radiolarites (Enzenberg-Praehauser 1976). Representatives of the most distal part of the Austroalpine passive margin are also found in the form of breccias in the ***Hochfeind Nappe (16)*** of the Radstätter Tauern near the northeastern margin of the Tauern Window (Häusler 1988, Becker 1993). While the Hochfeind Nappe, as expected, immediately overlies the mélange of the Matrei Zone the structural position of the Hippold Nappe on top of the Upper Austroalpine Innsbruck Quarzphyllite Unit is due to late-stage folding and thrusting.

5.2.5.2 Reckner Nappe and Main Nappe Group

Reckner Nappe (15) is the traditional name (Häusler 1988) for the tectonically higher of the two Lower Austroalpine thrust sheets that tectonically overlie the Innsbruck Quartzphyllite Unit near the northwestern corner of the Tauern Window ("Kalkwand Deckscholle" of Enzenberg-Praehauser 1976, "Tarntal Nappe" of Decker et al. 2009). The sediments of the Reckner Nappe are relatively poor in breccias, their facies being nearer to that of the Upper Austroalpine units. In terms of facies they can be compared to the Pleisling Nappe of the Radstätter Tauern (Häusler 1988). The Pleisling Nappe forms a large part of a pile of imbricates referred to as ***Main Nappe Group (15)*** in the Radstätter Tauern by Becker (1993).

5.2.5.3 Lower Austroalpine south of the Tauern Window

The ***Lower Austroalpine south of the Tauern Window (14)*** consists of Variscan basement and predominantly Permo-Skythian clastics (Pestal and Hejl 2005). A distinction of these units from Lower Austroalpine slivers, incorporated in the Matrei Zone, is often difficult (Fuchs and Linner 2005).

5.2.6 Upper Austroalpine basement-cover nappes

These nappes referred to as Central Austroalpine nappes (Froitzheim et al. 2008) occupy the central part of the Alpine orogen presently located south of the detached Grauwackenzone and Northern Calcareous Alps cover units and north of the Southern Alps. Most, but not all of these nappes are affected by Alpine (Cretaceous-age = Eoalpine) metamorphism (Schuster et al. 2004, Oberhänsli et al. 2004, Schmid et al. 2004). Formerly they were subdivided into Middle and Upper Austroalpine units, a subdivision now abandoned for various reasons (see discussions in Schuster and Frank 1999, Schmid et al. 2004). Their paleogeographic relationship with the detached units of the Grauwackenzone and Northern Calcareous Alps is only partly understood. Nagel (2006) clearly showed that the so-called Phyllitgneiszone, regarded as the basement of the Lechtal Nappe (a part of the Bavarian Nappes of the Northern Calcareous Alps), is an integral part of the Silvretta Nappe. Hence, a part of the Bajuvaric Nappes represents the cover of one of these Central Austroalpine Nappes. This is definitely not the case for Grauwackenzone and the Tirolian and Juvavic Nappes of the Northern Calcareous Alps that were detached from their substratum during the very early stages of Eoalpine orogeny (Schuster 2003, Schmid et al. 2004, Handy et al. 2010).

5.2.6.1 Silvretta-Seckau Nappe System

The Silvretta Nappe, including its Mesozoic cover, was thrust towards WNW and over the Lower Austroalpine units of eastern Switzerland during Eoalpine (Cretaceous) orogeny (Froitzheim et al.

1994) and is located west of the area covered by Plate 1. The Seckau Crystalline Complex is located east of our tectonic map (Schmid et al. 2004). The largest area attributed to this nappe system within the area of Plate 1 is taken up by the Innsbruck Quartzphyllite Unit and the Schladming Nappe.

In view of the important role for better understanding the transition zone between Lower and Upper Austroalpine units we mapped the ***overturned Permo-Mesozoic cover of the Schladming Nappe (13)*** separately from the overlying crystalline basement of the Schladming Nappe. This flat lying cover, mostly consisting of phyllites and sericitic quartzites of Permian to Lower Triassic age, was recognized as representing the overturned stratigraphic cover of the Variscan basement of the Upper Austroalpine Schladming Nappe by Slapansky and Frank (1987) and Becker (1993). Similar overturned cover is seen southeast of the locality Obertauern (NNW of Mauterndorf, see Plate 1), but here in stratigraphic cover with Paleozoic quartzphyllites (Fanning Phyllites of Exner 1989) rather than with the typical Schladming Orthogneisses forming the basement of the Schladming Nappe northeast of Obertauern. Exner (1989) parallelized the Fanning Phyllites with the Katschberg Quartzphyllites (quartzphyllites and phyllonites, Schuster et al. 2006). The latter is, however, commonly attributed the Lower Austroalpine Nappe System (e.g., Schuster et al. 2006). Since the overturned Mesozoic cover of the Schladming orthogneisses series can be traced along strike into the overturned cover of the Fanning Phyllites and the Katschberg Quartzphyllites (Pestal and Hejl 2005) we prefer to attribute Fanning Phyllites and Katschberg Quartzphyllites to the Silvretta-Seckau Nappe System, together with other quartzphyllites or phyllonite series such as the Innsbruck Quartzphyllites Unit.

The ***high-grade Variscan basement of Schladming and Campo Nappes (12)*** is mapped separately from the various phyllitic units of the Silvretta-Seckau Nappe System, although the separation between, for example, Schladming high-grade orthogneisses and amphibolites from Fanning Phyllites, represents a lithological rather than an Alpine-age tectonic boundary. Only a thin and westernmost band of the Campo high-grade Variscan basement reaches our map in the Meran area (Plate 1). There it is separated from the Texel Unit of the Koralpe-Wölz Nappe System by the Thurnstein Mylonite Zone to the north (Viola et al. 2001), and it borders the Drauzug-Gurktal Nappe System (Tonale Nappe, Viola et al. 2003) to the south.

Amongst the ***Innsbruck-Wagrain-Katschberg Quartzphyllite Units (11)*** the Innsbruck Quartzphyllite Unit that, besides quartzphyllites, also includes phyllonites (Patscherkofel Crystalline), schists (Steinkogel Schists) and orthogneiss (Kellerjochgneis) lenses (Piber and Tropper 2003, Pestal et al. 2009), is the most voluminous part. It was formerly considered as Lower Austroalpine. However, as discussed above, this Palaeozoic (Silurian to Devonian) sedimentary series do not form the stratigraphic substratum of the Lower Austroalpine Mesozoic sediments exposed in the overlying Hippold Nappe. Moreover, the Alpine grade of metamorphism is much lower (lower greenschist-facies, Piber and Tropper 2003) than that of the Hippold Nappe (Dingeldey et al. 1997). Therefore we consider the Innsbruck Quartzphyllite Unit as part of the Silvretta-Seckau Nappe System. Following

Pestal et al. (2009), we parallelize the Innsbruck Quartzphyllite Unit with the Wagrein Phyllite located south of the Salzach-Ennstal-Mariazell-Puchberg (SEMP) Fault. This parallelization indicates a sinistral dislocation of the Wagrein Phyllit with respect to the Innsbruck Quartzphyllite Unit along the SEMP Fault by some 60 km (see Plate 1). As already discussed, we also included the Katschberg Quartzphyllites into the same group of phyllites. On the other hand we linked the Ennstal Phyllite Unit (Pestal et al. 2009), located north of the high-grade basement of the Schladming Nappe with the Wölz Micaschists of the Koraple-Wölz Nappe System, both being connected around an east-plunging antiform with the Schladming Nappe in its core (Plate 1).

5.2.6.2 Koralpe-Wölz Nappe System

The Koralpe-Wölz high-pressure Nappe System comprises a series of basement units characterized by significant, often pressure dominated, Eoalpine metamorphic overprint (Schuster et al. 2001, Schuster 2003). It includes eclogitic MORB-type gabbros yielding Permian protolith ages (Miller and Thöni 1997) but lacks Mesozoic cover, detached early on now located in the Northern Calcareous Alps (Froitzheim et al. 2008).

The Texel Unit of the ***Texel-Millstadt-Wölz Unit (10)***, located southwest of the Tauern Window, is known for its Cretaceous-age (c. 90 Ma) eclogitic parageneses (Hoinkes and Thöni 1987, Habler et al. 2006, Thöni 2006). It is southerly adjacent to the Schneeberg Unit that forms the part of the ***Schneeberg-Radentheim Unit (9)*** located west of the Tauern Window, a unit consisting of amphibolite-grade sequences of meta-pelitic metasediments of Late Palaeozoic age that only suffered Alpine-age metamorphism (Krenn et al. 2011). The Schneeberg Unit, sandwiched between the northerly adjacent and structurally higher Ötztal Nappe and the southerly adjacent Texel Unit, was formerly interpreted as north-dipping normal fault zone (Sölva et al. 2005). Recently, Pomella (2011) and Floess et al. (in press) interpreted this north-dipping fault zone at the base of the Ötztal Nappe as an originally south-dipping nappe boundary that became overturned during Cenozoic times.

East of the Brenner and Jaufen faults, units of the Koralpe-Wölz Nappe System are extremely thinned out near Sterzing and can be followed further east into the northern Deferegger Alps and the Schober and Polinik-Prijakt crystalline units (Schuster et al. 2001, Schuster 2003, Schmid et al. 2004). There they are in a sub-vertical orientation and juxtaposed with the southerly adjacent and structurally higher Drauzug-Gurktal Nappe System along steeply inclined Late Alpine faults, such as the sinistral Defereggen-Antholz-Vals (DAV) Fault (Borsi et al. 1973, Mancktelow et al. 2001).

The Mölltal Fault dextrally offsets the eclogitic Polinik-Prijakt Crystalline Unit against its lateral equivalent to the east, the Millstatt Unit. The Millstatt eclogitic Unit is overlain by the amphibolite-grade Radentheim Unit of the Koralpe-Wölz Nappe System (Krenn et al. 2011). This configuration is analogous to that found west of the Tauern Window, which suggests that these configurations were adjacent to each other before orogen-parallel extension during the formation of the Tauern Window torn them apart (Frisch et al. 1998). East of the Tauern Window the amphibolite-

grade Wölz Unit forms the northern part of the Texel-Millstadt-Wölz Unit, separated from the southern part by the klippe of the overlying Ötztal-Bundschuh Nappe System. This upper greenschist- to amphibolite-grade Wölz Unit tectonically underlies the eclogite-facies equivalents of the Millstatt Unit. The Saualpe-Koralpe Unit is only found east of the area of the tectonic map of Plate 1. The greenschist-facies Ennstal Phyllite Unit adjacent to the SEMP Fault forms the structurally lowermost part of the Koralpe-Wölz Nappe System (see Schuster et al. 2001, Schuster 2003, Schmid et al. 2004, Froitzheim et al. 2008 for more details).

5.2.6.3 Ötztal-Bundschuh Nappe System

The Ötztal-Bundschuh Nappe System occupies an intermediate tectonic position between, in terms of the Cretaceous nappe stack, the non- or weakly metamorphosed Drauzug-Gurktal Nappe System in its hangingwall, and the Koralpe-Wölz high-pressure Nappe System in its footwall (Schmid et al. 2004). Ötztal- and Bundschuh nappes, located immediately west and east of the Tauern Window, respectively, are characterised by a strong field metamorphic gradient regarding Eoalpine metamorphism: grade of metamorphism rapidly increases downwards and towards the contact with the higher grade Koralpe-Wölz Nappe System (Schuster et al. 2001, Schuster 2003). The effects of Miocene-age orogen-parallel stretching during east-directed lateral extrusion of the Austroalpine nappes towards the east (Ratschbacher et al. 1991) separated Ötztal- and Bundschuh nappes that originally were fairly close to each other.

The ***Variscan basement (8)*** of this nappe system is typically polymetamorphic (Thöni 1999). Its ***Mesozoic cover (7)***, preserved in the form of the Brenner Mesozoic (west of the Tauern Window) and the Stangalm Mesozoic (east of the Tauern Window) defines the nappe boundary in respect to the tectonically higher Drauzug-Gurktal Nappe System. The Stangalm Mesozoic formerly served as a proof for the "Middle Austroalpine" position of the Central Austroalpine nappe stack below the Drauzug-Gurktal Nappe System (Tollmann 1977).

5.2.6.4 Drauzug-Gurktal Nappe System

The highest nappe system, the Drauzug-Gurktal Nappe System was formerly located in a more southerly paleogeographic position in respect to the Northern Calcareous Alps and has close paleogeographical affinities to the adjacent Southern Alps, the Transdanubian Range in Hungary and the Dinarides (Schmid et al. 2004, 2008). Large parts of this nappe system were not metamorphosed at all; others at most reached lower greenschist-facies during the Alpine cycle (Schuster et al. 2004, Oberhänsli et al. 2004). At present most of this nappe system is restricted to an area south of the **s**outhern border of **A**lpine **m**etamorphism, referred to as SAM by Hoinkes et al. (1999), and immediately north of the Periadriatic Fault.

The following pre-Mesozoic ***basement complexes (6)*** belonging to this nappe system follow the Periadriatic Fault, from west to east: Tonale Nappe, Meran-Mauls Basement, Gailtal Basement, South

Deferegger Alps and Strieden Complex (Schuster et al. 2001). At the western margin of the tectonic map (Plate 1) the Palezoic of the flat-lying Steinach Nappe thrusts the Mesozoic cover of the Ötztal Nappe (Brenner Mesozoic). This is analogous to the situation at the eastern margin of the map were the flat-lying Gurktal Nappe thrusts the Mesozoic cover of the Bundschuh Nappe. The Graz Paleozoic also belongs to this group of nappes but is restricted to an area east of the area covered by Plate 1. Some of these basement complexes (Gurktal Nappe and Graz Paleozoic) are un-conformably covered by Gosau Beds. Others (Strieden Complex) are covered by non-metamorphic Mesozoic sediments, often in direct stratigraphic contact (Drauzug Mesozoic).

Mesozoic cover (5) of this nappe system is principally preserved in the east-west elongated strip, the so-called Drauzug (van Bemmelen and Meulenkamp 1965). A thin isolated sliver of this Drauzug near Sterzing is referred to as Mauls Mesozoic. This cover was formerly deposited onto the northerly and southerly adjacent basement complexes, some of the stratigraphic contacts still being locally preserved. Small klippen (Blaser Nappe) represent the detached Mesozoic cover of the Steinach Nappe (Fügenschuh et al. 2000).

5.2.7 Upper Austroalpine: far travelled cover nappes

These nappes consist of Paleozoic and Mesozoic cover units that started to detach from their crystalline substrate very early on, i.e. since the Valanginian (Faupl and Wagreich 2000). They reached the foreland of the Cretaceous-age Eastern Alpine orogen before their crystalline underpinnings left behind became involved in Cretaceous-age (Eoalpine) metamorphism.

5.2.7.1 Grauwackenzone

The detached Ordovician to Permian series of the ***Grauwackenzone (4)*** within the area of Plate 1 belongs to the Norian Nappe that forms the stratigraphic base of the southern edge of the Tirolian Nappe System of the Northern Calcareous Alps. These Palaeozoic sediments were metamorphosed under lower greenschist-facies conditions during Cretaceous times. The Grauwackenzone is bordered to the south either by the sinistral SEMP Strike-Slip Fault Zone (central and eastern part of Plate 1) or by the thrust contact with the structurally lower Innsbruck Quartzphyllite Unit (western part of Plate 1).

5.2.7.2 Northern Calcareous Alps

Within Plate 1 most of the area mapped as ***Northern Calcareous Alps (3)*** is part of the Tirolian Nappe System. This Tirolian Nappe System is underlain by the Bajuvaric Nappe System and overlain by the Juvavic Nappe System (Schmid et al. 2004), exposed in the northwestern-most and northeasten-most parts of Plate 1, respectively.

5.2.7.3 Southern Alps and Periadriatic plutons

No geological or tectonic details have been mapped regarding the ***Southern Alps (2)***. East of the Giudicarie Fault, they act as an indenter related to the uplift and exhumation of the Tauern Window (Ratschbacher et al. 1991, Rosenberg et al. 2004). Note, however, that the Southern Alps were internally deformed during the Miocene (e.g. Castellarin et al. 2006). Hence they represent a deformable indenter. The mostly Oligocene-age ***Periadriatic Plutons (1)*** align along the Periadriatic Fault and their emplacement is related to Oligocene-age transpression along the Periadriatic Fault System (Rosenberg 2004), transpression that pre-dates dextral movements during Miocene-age lateral extrusion of the Eastern Alps.

Table 5.1: Correlation of tectonic nappes in and arround the Tauern Window (Eastern Alps)

General Tectonic setting	Tectonic Nappe Systems		Nr.	West	Central	East
Periadriatic plutons			1	Rensen Pluton	Rieserferner Pluton	-
Southern Alps			2	Southern Alps (Adriatic Indenter)	Southern Alps (Adriatic Indenter)	Southern Alps (Adriatic Indenter)
Upper Austroalpine:			3	Northern Calcareous Alps	Northern Calcareous Alps	Northern Calcareous Alps
far travelled cover nappes			4	Grauwackenzone	Grauwackenzone	Grauwackenzone
Upper Austroalpine:	Drauzug-Gurktal	Permo-Mesozoic cover	5	Blaser Nappe, Mauls Triassic	Drauzug	Drauzug
basement-cover nappes	Nappe System	basement	6	Steinach Nappe, Mauls-Meran basement	South Deferegg Units, Strieden Complex	Gurktal Nappe
	Ötztal-Bundschuh	Permo-Mesozoic cover	7	Brenner Mesozoic	-	Stangalm Mesozoic
	Nappe System	basement	8	Ötztal Nappe	-	Bundschuh Nappe
	Koralpe-Wölz	monometamorphic basement	9	Schneeberg Unit	-	Radentheim Unit
	Nappe System	polymetamorphic basement	10	Texel Nappe	North Defregg Unit, Schober Unit, Polinik-Prijakt Unit	Millstatt Nappe, Wölz Nappe
	Silvretta-Seckau	Variscan low-grade basement	11	Innsbruck Quarztphyllite	-	Wagrain & Katschberg Quartzphyllite Units
	Nappe System	Variscan high-grade basement	12	Campo Unit	-	Schladming Nappe
		Permo-Mesozoic cover Schladming Nappe	13	-	-	overturned Permo-Mesozoic cover
Lower Austroalpine nappes		south of Tauern Window	14	-	Sadnig-Group	-
		north of Tauern Window	15	Tarntal Nappe	-	Main Nappe Group/ Lantschfeld Nappe/ Pleisling Nappe
		north of Tauern Window: distal-most facies	16	Hippold Nappe	-	Hochfeind Nappe
Ophiolite-bearing units	Upper Penninic	Piemont-Liguria Ocean & L. Austroalpine	17	Nordrahmen Zone north of Tauern Window	Matrei Zone south of Tauern Window	Nordrahmen Zone north of Tauern Window
	Upper Penninic	Piemont-Liguria Ocean	18	Reckner Ophiolitic Complex	-	-
	Lower Penninic	Valais Ocean	19	Glockner Nappe System	Glockner Nappe System	Glockner Nappe System
Units derived from the distal	Units in the hangingwall	Modereck Nappe System	20	Eisbrugg-Slice, Geroldstein Mesozoic	"Glimmerscheiferlamelle", Seidlwinkl-Rote Wand Nappe	Murtörl-Schrovin Unit
European margin	of the		21	-	Eclogite Zone	-
(Subpenninic nappes)	Venediger Duplex		22	Wolfendorn Nappe	-	-
		post-Variscan cover in general	23	Hochstegenkalk, Kaserer Serie	Maurertal Unit, Murtörl- Fm	Angertal/ Silbereck Unit/ Draxel Unit
	Venediger	uppermost structural level	24	Zillertal Nappe	Riffl Nappe, Sonnblick-Romate Nappe	Mureck Gneissic Slice & Storz Nappe
	Duplex	intermediate structural level	25	Tux Nappe	Granatspitze Nappe	Hochalm Nappe
		lowermost structural level	26	Ahorn Nappe	-	Göss Nappe

5.3 Major Late Alpine fault zones

In the following discussion of major Late Alpine fault zones (Plate 1) we use the term "fault" for simplicity and describe their nature briefly. Most of these faults accommodated substantial displacements that post-date nappe stacking. We now describe them, proceeding from south to north.

Segments of the Periadriatic Fault define the northern edge of the South Alpine indenter (Ratschbacher et al. 1991, Rosenberg et al. 2007). The ***North Giudicarie Fault*** is a Miocene-age sinistral strike slip zone that overprints Oligocene-age dextral strike slip associated with a formerly straight Periadriatic Fault (Stipp et al. 2004, Pomella et al. 2011). It forms the westernmost branch of a set of sinisitrally transpressive thrusts defining a broader Giudicarie Belt located outside Plate 1. At the southwestern edge of the map (Plate 1) it bends into the southwest to northeast striking ***Meran-Mauls Fault*** (Viola et al. 2001), an Oligocene-age ductile zone of dextral strike slip, changing to Miocene-age brittle top-to-the-southeast thrusting (Pomella et al. 2011). In the area north of the Meran-Mauls Fault kinematic interpretations are contradictory. According to Stöckli (1995, version depicted in Plate 1 with a question mark) a dextral mylonitic zone of Miocene-age, that we term the ***Sterzing-Mauls Fault,*** kinematically links the southern end of the mylonites of the Brenner Normal Fault with the long WNW-ESE-trending ***Pustertal-*** and ***Gailtal Faults.*** The latter faults are parts of the Periadriatic Fault System and accommodated, after an Oligocene sinistral precursor, Miocene-age brittle dextral strike slip (Mancktelow et al. 2001). According to others (Schneider and Rosenberg in prep.), however, the area west of Mauls is instead characterized by sinistral mylonites, an observation that severely challenges a kinematic link between the Brenner Mylonites and the Periadriatic Fault.

These segments of the Periadriatic Fault spatially and kinematically interact with a series of faults located north of, and branching off the Periadriatic Fault System. In the west the Miocene-age ***Passeier Fault*** branches off the North Giudicarie Fault and accommodates some 15 km of sinistral strike slip motion under ductile to brittle conditions (Müller et al. 2001, Viola et al. 2001). At its northern tip it kinematically interacts with the ***Jaufen Fault,*** a complex fault zone that was repeatedly active (Viola et al. 2001, Floess et al. in press). In Cretaceous times it acted as a thrust that brought the Mauls-Meran basement complex on top of the eclogitic Texel Unit. In Miocene times this old tectonic contact became overturned due to tight folding of the Mauls-Meran basement complex during late Alpine, north-directed indentation of the Southern Alps Pomella et al. 2011, Floess et al. in press). Finally, it acted as a steeply north-dipping sinistrally transtensive fault zone, kinematically linked with the southern end of the Brenner Normal Fault (Selverstone 1988, Fügenschuh et al. 1997, Rosenberg and Garcia 2011). The western end of an Oligocene-age mylonite zone, the sinistral ***DAV Defereggen-Antholz-Vals (DAV) Fault*** **(**Borsi et al. 1973, Kleinschrodt 1987), is overprinted by younger dextral mylonites of the previously described Sterzing-Mauls Fault (Stöckli 1995, Mancktelow et al. 2001). Since the DAV Fault follows the boundary between the Koralpe-Wölz and the Drauzug-Gurktal Nappe Systems it very likely has a long history going back into Cretaceous times (see discussion in

Mancktelow et al. 2001). Much of its activity is, however, temporarily linked to the emplacement of the Rieserferner Pluton and, hence, of Oligocene age (Wagner et al. 2006). The ***Drautal Fault*** is a brittle sinistral transpressive strike slip fault of Miocene age (Heinisch and Schmidt 1984) that spatially and kinematically interferes with the Pustertal dextral strike slip fault. We propose that the Drautal Fault represents a conjugate fault in respect to the Pustertal Fault, delimiting, together with its northeastern continuation, referred as ***Zwischenbergen-Wöllatratten Fault*** (Exner 1962b), the western edge of a triangular block whose tip indents the Tauern Window during the Miocene, squeezing the western termination of the Sonnblick Dome (Scharf et al. submitted a, Chapter 2). The dextral and brittle Micoene ***Mölltal Fault*** (Kurz and Neubauer 1996) delimits the eastern end of this triangular block, offsetting the southern margin of the Tauern Window by some 20 km and slightly offsetting the Gailtal Fault. We propose that the eastern termination of the sinistral DAV Fault near Lienz was sinistrally offset by the Miocene-age Drautal and Zwischenbergen-Wöllatratten faults. Thereby the ***Ragga-Teuchl Fault*** (Hoke 1990), defining the boundary between the Koralpe-Wölz and the Drauzug-Gurktal Nappe Systems, would represent the easternmost continuation of the Oligocene-age DAV Fault, cut by the younger Mölltal Fault in the east.

Two Miocene-age normal fault zones that accommodate orogen-parallel extension are characterized by a broad mylonitic zone with a brittle lid and delimit the western and eastern termination of the Tauern Window. The ***Brenner Normal Fault*** in the west represents a normal fault with a substantial amount (at least some 44 km) of orogen-parallel extension according to some authors (Axen et al. 1995, Fügenschuh et al. 1997, 2012). Others, emphasising the effects of substantial amounts of north-south compression only observed east of the Brenner Normal Fault, propose much smaller (2-14 km) estimates (Rosenberg and Garcia 2011, 2012). In any case, all authors agree that north-south-compression by folding of the Subpenninic nappe stack and east-west extension is contemporaneous. The southern termination of the ductile mylonite belt that accompanies the Brenner Normal Fault is also a matter of debate. Some authors (Stöckli 1995, Fügenschuh et al. 2012) propose that the Brenner Mylonites find their continuation in the dextral ***Sterzing-Mauls Fault*** while the brittle late-stage parts of the Brenner Normal Fault join the Jaufen Fault. Others (Rosenberg and Garcia 2012) propose that the extensional displacements of the Brenner Normal Fault reduce to zero south of Sterzing and, hence, that this fault does not have a southern continuation. Similarly, there is a controversy about the existence or non-existence of the ***Tauern Northern Boundary Fault***, proposed to represent the transformation of the displacements across the Brenner ductile normal fault mylonites into sinistral strike slip motion by Töchterle et al. (2011) and Fügenschuh et al. (2012). Thereby the ***Silltal Fault*** would split off the ductile Brenner Mylonites and only represent the northern continuation of late-stage and brittle normal faulting across the Brenner Normal Fault. Rosenberg and Garcia (2012), on the other hand, reject this interpretation, based on the lack of structural and petrological evidence; they suggest that both the ductile and brittle components of extensional displacement continue northward into the Silltal Fault.

The ***Katschberg Normal Fault*** (Genser and Neubauer 1989) represents a ductile normal fault at the eastern termination of the Tauern Window that formed contemporaneously with north-south shortening that started in Early Miocene times; its lateral ends swing around the northeastern and southeastern edges of the Tauern Window as part of the Late-Alpine Katschberg Shear Zone System (Scharf et al. 2011,submitted a, Chapter 2) which results in ductile dextral and sinistral strike slip shearing in the calcschists of the Glockner Nappe System at the northern and southern terminations of the Katschberg Normal Fault. While some authors regard the sinistrally transtensive ***Niedere Tauern Southern Fault*** (Zeilinger 1997, Wölfler et al. 2011) as the direct northeastern continuation of the Katschberg Normal Fault, our map compilation excludes such a direct link (see Plate 1). Analogous to the brittle Mölltal Fault, the brittle Niedere Tauern Southern Fault developed during a later stage of lateral extrusion, i.e. after ductile deformation ceased due to falling temperatures. The age of the basin fill (Tamsweg Neogene) located between the two branches of the Niedere Tauern Southern Fault and its relationships with faulting indicate that this brittle phase initiated at around 17 Ma ago (Zeilinger 1997, Strauss et al. 2001) while the cooling history in the area of the Katschberg Normal Fault indicates activity of this essentially ductile normal fault long before 17 Ma (Scharf et al. 2011, submitted a, Chapter 2 and 4).

The ***Salzach-Ennstal-Mariazell-Puchberg (SEMP) Fault*** represents, after the dextral Periadriatic Fault, the second-most important Miocene-age Alpine strike slip fault zone. Sinistral offset of the Innsbruck-Wagrein-Katschberg Quartzphyllite Unit amounts to some 60 km. Additional, the northeast to southwest striking sinistral ***Königsee-Lammertal-Traunsee (KLT) Fault*** flows into the SEMP. A c. 10 km offset of the Grauwackenzone was estimated by (Decker et al. 1994a, b). Both these strike slip zones are conjugate and active coevally during the Miocene, producing substantial east-west extension (Ratschbacher et al. 1991). Rosenberg and Schneider (2008) convincingly demonstrated that the western termination of the SEMP Fault has to be looked for along the ***Ahorn Fault,*** a broad deformation belt within the Ahorn Nappe, where deformation along the SEMP Fault becomes increasingly transpressive and entirely ductile. Westward, sinistral strike slip is gradually transformed into late stage north-south shortening by upright folding (Rosenberg and Schneider 2008, Töchterle et al. 2011). The ***Inntal Fault*** is another sinistral strike slip zone located further north, additionally accommodating some 20-40 km (Ortner et al. 2006) or 50 km (Linzer et al. 2002) sinistral strike slip offset.

5.4 Large scale structure of the Tauern Window

The cross sections of Plate 2 illustrate the large-scale architecture of the Tauern Window. All orogen-perpendicular sections (sections 2–8) show a re-folded duplex structure. In profiles 2 to 4, located in vicinity to the TRANSALP seismic section (Lüschen et al. 2006) the amount of post-duplex north-

south shortening (referred to as D5 later on) can only roughly be assessed since exact initial geometry of the roof thrust and exact mechanism of folding are unknown. Assuming conservation of line length of an originally horizontal roof thrust, located at some 12 km depth before D5 folding (depth of the Sub-Tauern Ramp at the northern margin if the Venediger Duplex (see Lammerer et al. 2008), a surprisingly consistent value varying between 31 and 32 km is obtained for post-duplex shortening in all the three western profiles. The deep structure of profiles 5 to 8 is unconstrained and we can only guess that the amount of post-duplex north-south-shortening roughly remains the same further east.

The lateral changes in style and geometry of post-duplex folding are very marked. However, cross section 2 exhibits an overturned roof thrust at the southern margin of the duplex structure while the northern parts of the roof thrust exhibit a moderate dip of around 45°; cross sections 3 and 4 show a rather symmetrical post-duplex dome. A drastic change in geometry occurs further east (sections 5 to 8). In sections 6 to 8 post-duplex doming is rather broad, the hinge of this dome being located much nearer to the southern margin of the Venediger Duplex in profiles 2 to 4. This difference is even more salient from inspection of Fig. 5.2. In the western Tauern Window the traces of the hinges of the post-duplex antiforms (labelled D5, see Chapter 5.5 for the discussion of the phases of deformation) run WSW-ENE and gradually approach the SEMP Fault at the northern margin of the Venediger Duplex. Those in the eastern Tauern Window, however, strike WNW-ESE and disappear westward. The Granatspitz Dome is confined to the central Tauern Window and disappears in both directions. We conclude that these post-duplex (D5) structures are significantly non-cylindrical.

Figure 5.2 additionally shows the three branch lines related to duplex formation that can be extracted from the tectonic map of Plate 1. Two WSW-ENE-oriented ones are from the western Tauern Window and a WNW-ESE oriented one from the eastern Tauern Window. Originally, these branch lines possibly were sub-parallel to each other, and became reoriented during D5 post-duplex folding. This again underlines important differences between western and eastern Tauern Window due to post-duplex overprint.

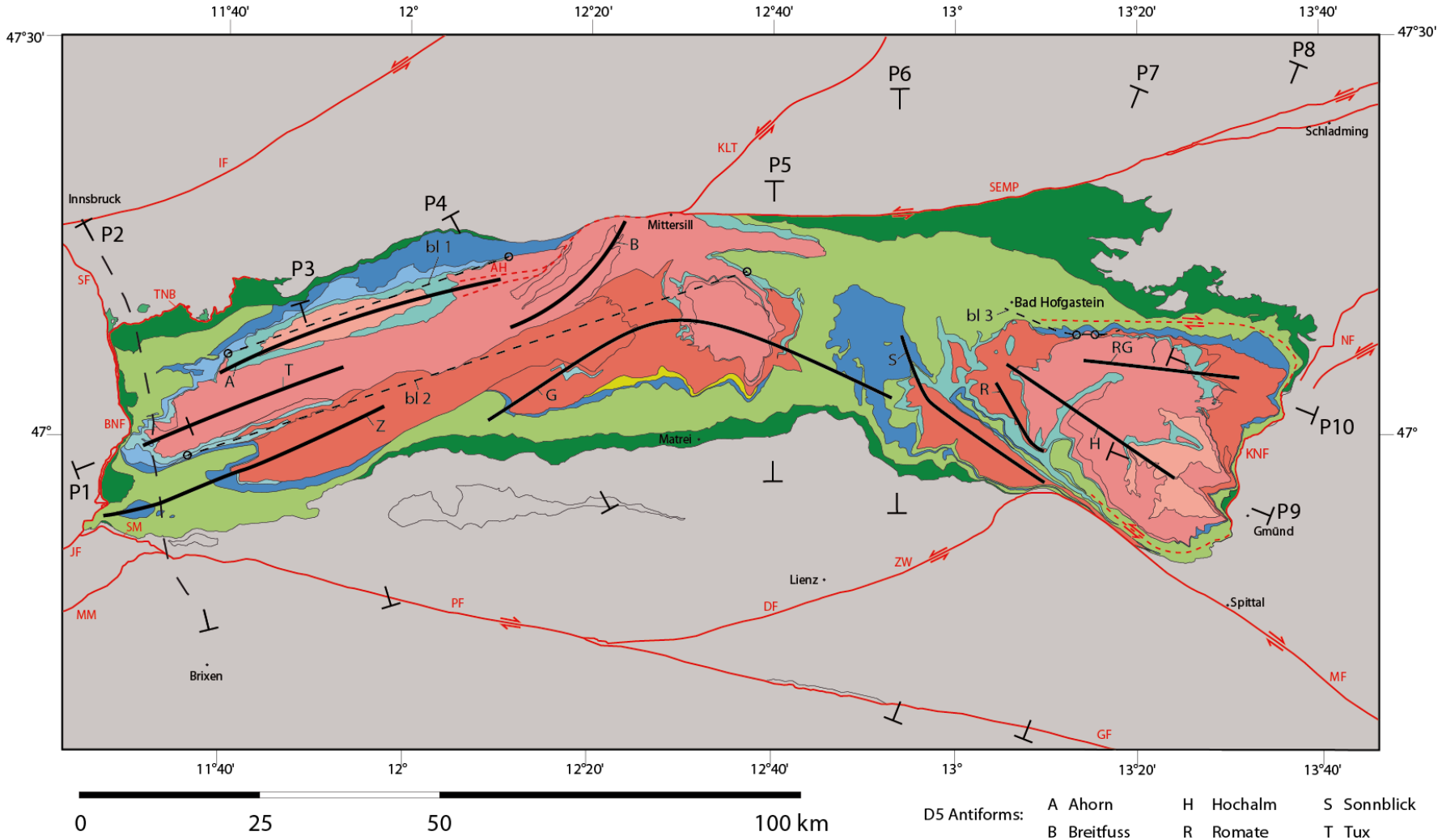

D5 Antiforms: A Ahorn; B Breitfuss; G Granatspitz; H Hochalm; R Romate; RG Rotgülden; S Sonnblick; T Tux; Z Zillertal

D4 branch lines: bl 1 front of Tux Nappe; bl 2 front of Zillertal-Riffl Nappe; bl 3 front of Romate-Storz Nappe

Figure 5.2: Tectonic map showing the hinge lines of post-duplex (D5) antiforms and selected branch lines with cut-off points (circles), related to duplex-formation (D4) that could be extracted from the tectonic map of Plate 1. Also superimposed are the traces of the cross sections (P1 – P10) presented in Plate 2 and major faults that affect the Austroalpine and South-Alpine frame around the Tauern Window. Legend for tectonic map and abbreviation as in Plate 1.

The late-stage antiforms cannot be traced across the Brenner- and Katschberg normal faults, which, amongst other arguments, leads to the conclusion that north-south shortening is coeval with orogen-parallel extension achieved by these normal faults at the western (cross section 1 and 1bis) and eastern (cross sections 9 and 10) margin of the Tauern Window. While all authors agree about the contemporaneity of late stage north-south shortening and orogen-parallel extension there is an on-going debate about the amount of orogen-parallel extension across the Brenner Normal Fault (see e.g., Fügenschuh et al. 1997, Rosenberg and Garcia 2011, Fügenschuh et al. 2012, Rosenberg and Garcia 2012). The construction of the parts of profiles 1 and 2 that lie above the earth's surface is made by projecting structures from the unfolded hangingwall west of the Brenner Normal Fault on top of the folded area, east of the Brenner Normal Fault. These constructions result in a dramatic attenuation of the thickness of the Glockner Nappe System and result in estimating a minimum amount of east-west stretching across the central part of the Brenner Normal Fault of around 44 km (Fügenschuh et al. 2012). Note, however, that, as clearly pointed out by Rosenberg and Garcia (2012), the amount of tectonic omission gradually decreases to the north and south. Hence, the estimate of a stretch of 44 km (Fügenschuh at al 2012), and the geometry shown in profile 1, can only be valid for the area around the Brennerbad locality (near the intersection point between profiles 1 and 2 in Plate 2).

In contrast, the construction of profiles 1bis and 2bis is made by projecting the folded structures east of the Brenner Normal Fault above the surface. A control on the nappe thicknesses of profiles 1bis and 2b is obtained by projecting the top of the Glockner Nappe System upward, which dips with 40° westward underneath a half-klippe of Matrei Zone immediately NNE of Sterzing (Plate 1). This results in a thickness of the Glockner Nappe System of less than 3 km in the profiles, corresponding to an attenuation of approximately 20% with respect to its thickness in the footwall. This geometry reflects the idea of older mylonites having been folded in the core of the Tauern Antiform and then cut by younger ones at lower structural levels, a process that causes tectonic omission in the absence of significant extension (see Rosenberg and Garcia 2012 for more details). These authors estimated the amount of east-west extension to be between 2 and 14 km only.

Orogen parallel extension estimated across the Katschberg Normal Fault is around 26 km (Scharf et al. submitted a, Chapter 2), valid at the locus of maximum tectonic omission, i.e. near the trace of cross section 9 in Plate 2, constructed sub-parallel to the hinge line of the Hochalm Dome (see Figure 5.2). According to Lammerer and Weger (1998) there is, additionally, an unknown amount of post-duplex homogeneous stretching parallel to the D5 folds (their Fig. 10) in the western Tauern Window. Adding some tens of kilometres of such homogeneous WSW-ENE-oriented stretch to the orogen-parallel extension achieved by offset across the Brenner- and Katschberg normal faults, the total orogen-parallel stretch may amount to as much as 100 km across the entire Tauern Window when using the estimate of Fügenschuh et al. (2012) regarding orogen-parallel extension across the Brenner Normal Fault. Of course, it is considerably less when using the estimate of Rosenberg and Garcia (2011, 2012) for the amount of extension across the Brenner Normal Fault. In any case, the estimate of

160 km orogen-parallel extension across the Tauern Window obtained by Frisch et al. (1998, 2000), is unrealistically high since it entirely neglects denudation by erosion induced by contemporaneous north-south-shortening, as pointed out by Rosenberg et al. (2007).

On a lithospheric scale the Tauern Window is located in a transition zone between a western part of the Alpine orogen, presently characterized by a southeast-dipping European slab descending beneath the Alps and the easternmost part of the Alps characterized by a northeast-dipping Adriatic slab beneath the Alpine edifice (Lippitsch et al. 2003, Kissling et al. 2006). Figure 5.3 clearly shows that the western part of the Tauern Window, together with the area around the northern part of the Giudicarie Fault offsetting the Periadriatic Fault (Stipp et al. 2004, Pomella et al. 2011) are located in an intermediate location where present-day slab polarity is undetermined while the eastern part of the Tauern Window is located in the area characterized by an Adriatic slab presently descending northeastward below the Alps. Given the unchanged architecture of the nappes that characterize the crustal geometry of the Alpine edifice this change in polarity primarily affected a decoupled mantle configuration and was induced at a late stage during Alpine orogeny, i.e., at around 20 Ma (Ustaszewski et al. 2008). Possibly the non-cylindricity of the structures shown in Figure 5.2, as well as the relative anticlockwise and clockwise rotations of the branch lines related to duplex formation in the western and eastern Tauern Window, respectively, from an unknown intermediate (east-west?) strike is the result of this post-20 Ma reorganization of the geometry of the mantle slabs. Alternatively, this non-cylindricity only concerns the crust and simply resulted from the indentation of the South-Alpine Block east of the Giudicarie Fault as illustrated by analogue modelling (Rosenberg et al. 2004) aimed to simulate the Tauern Window. According to this modelling the different orientation of the D5 upright folds formed as a consequence of conjugate transpressional faults, with differences in fold amplification leading to a more localized deformation in the western Tauern Window.

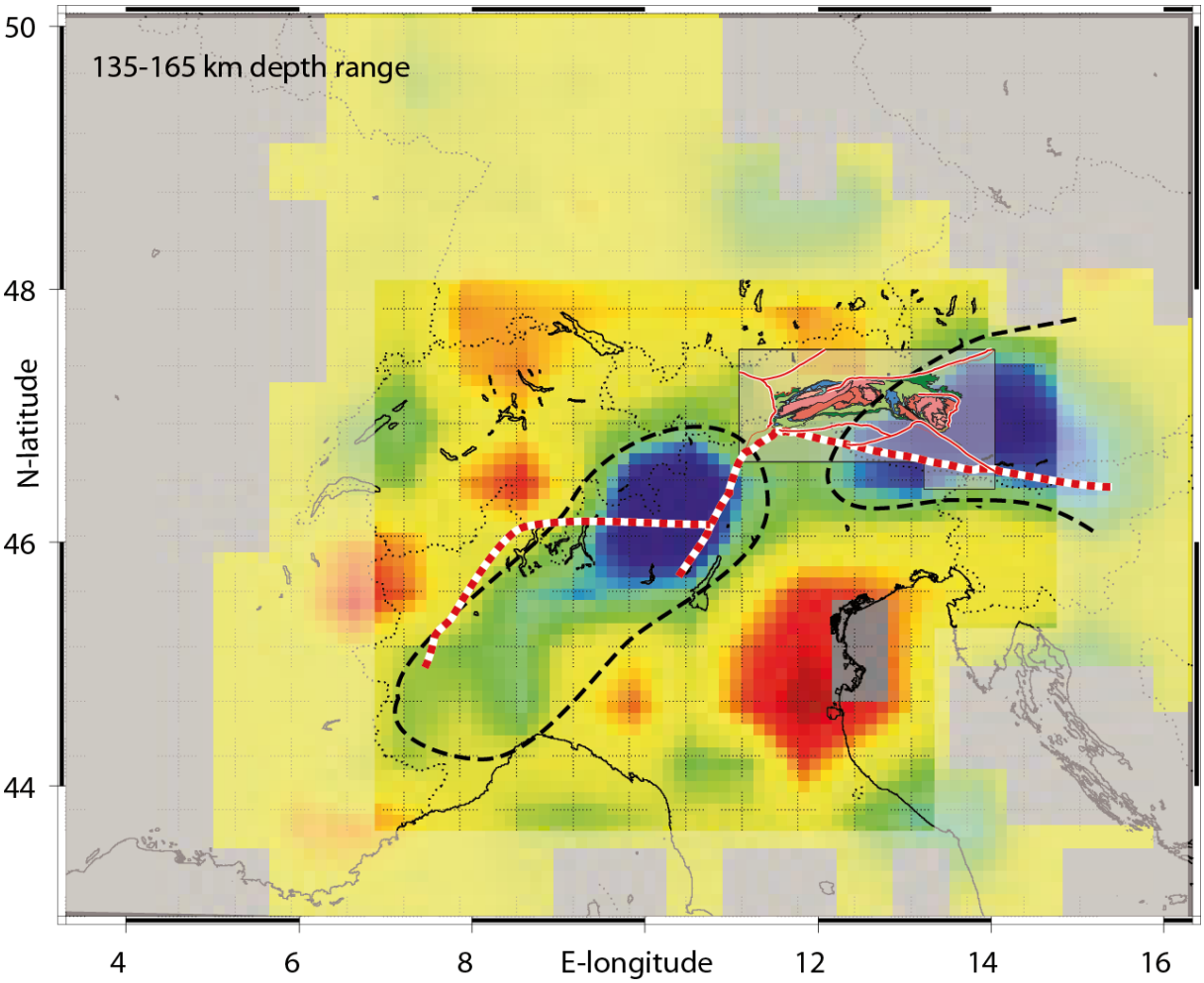

Figure 5.3: Horizontal depth section at 150 km depth through the 3-D Vp model from Lippitsch et al. (2003; their Fig. 13) illustrating the variations in Vp within the upper mantle at that depth relative to the chosen 1D initial model, superimposed with the outlines of the Tauern Window (see Plate 1) and the trace of the Periadriatic Fault, offset by the Giudicarie Fault (red stippled line). The positive velocity anomalies of > 4% Vp (dark blue) in the Western and Eastern Alps are associated with a southeast-dipping European lithosphere in the Western Alps and a northeast-dipping Adriatic lithosphere in the Eastern Alps, respectively (see Lippitsch et al. 2003, Kissling et al. 2006 for further details). Note that the transition zone between the two regimes is located along the Giudicarie Fault and the western part of the Tauern Window.

5.5 Discussion: Kinematic evolution of the Tauern Window in the framework of the Alps

On the basis of map pattern (Plate 1) and cross-sections (Plate 2), combined with paleogeographical arguments based on a re-assessment of the Mesozoic cover of the Subpenninic nappes (Figs. 5.1a, b) we now discuss the kinematic evolution of the Tauern Window. The exact timing of the five steps or phases shown in Figures 5.4a-f is notoriously difficult because of the difficulties in interpreting radiometric ages in terms of tectono-metamorphic events, particularly in case of the high-pressure events (e.g., Berger and Bousquet 2008).

5.5.1 Subduction of the Piemont-Liguria Ocean and accretion of oceanic relics in front of the Austroalpine nappe stack

There are only a few reliable age data from the Tauern Window and immediate surroundings concerning the first deformational stage (D1) illustrated in Figure 5.4a. Matrei Zone and Reckner Ophiolitic Complex accreted to the Austroalpine nappe stack since Turonian times (about 90 Ma). Firstly, this interpretation is based on the attribution of Matrei Zone and Reckner Ophiolitic Complex to the Piemont-Liguria Ocean; secondly it is based on paleontological and radiometric age data from the western margin of the Austroalpine nappe stack in eastern Switzerland (e.g., Ring et al. 1988, Handy et al. 1993, 1996, Froitzheim et al. 1994, Schmid et al. 1996) that demonstrate the involvement of units of the Piemont-Liguria Ocean (Platta Nappe and Arosa Mélange) in west to WNW-directed nappe stacking during Late Cretaceous (post-Cenomanian) orogeny. The timing constraints are summarized in Handy et al. (2010, their Table 6).

It is very likely that the southernmost parts of the Valais Ocean, i.e. parts of the Glockner Nappe System, also reached the subduction zone at the active margin in front of the by now pre-structured Austroalpine nappe pile by the end of the Cretaceous (scenario depicted in Fig. 5.4a). The radiometric ages obtained for metamorphism in the Lower Austroalpine Radstätter Tauern, ranging between 80 and 50 Ma (Liu et al. 2001) document that the northern margin of the Austroalpine nappe pile continues to represent an active margin until Eocene times. This is also supported by age data of Dingelday et al. (1997) that indicate Eocene metamorphism from the Matrei Zone and thereby demonstrate re-working of Matrei Zone and Lower Austroalpine during the Cenozoic.

5.5.2 Subduction of the Valais Ocean and parts of the distal-most European margin

Figure 5.4b depicts Cenozoic subduction of the Glockner Nappe System and parts of the most distal parts of the European margin (Eclogite Zone and parts of the Modereck Nappe System) below an essentially rigid upper plate consisting of the Austroalpine nappe stack, including the previously accreted Matrei Zone, at about 41 Ma ago. After the closing of the Valais Ocean the most distal parts of the European continental margin also became part of the high-pressure belt.

We are well aware of the problems that arise when interpreting radiometric data in terms of the timing of eclogite-facies metamorphism in parts of the Glockner Nappe System and in the Eclogite Zone, respectively (Thöni 2006). Although no direct radiometric data are available for the age of eclogite-facies overprint of the Glockner Nappe System, this overprint is likely to immediately pre-date the 36-32 Ma age range obtained by Zimmermann et al. (1994) for blueschist-facies metamorphism related to subsequent exhumation. Also, it is likely that high-pressure overprint in the Glockner Nappe System occurred more or less contemporaneously with that of the Bündnerschiefer of the Engadine Window, also attributed to the Valais Ocean and reported to have occurred at 42-40 Ma ago (Wiederkehr et al. 2009). The ages proposed for high-pressure metamorphism in the Eclogite Zone are between 45-42 Ma (Ratschbacher et al. 2004) and around 39 Ma for parts of the Modereck

Nappe System (Kurz et al. 2008b). Herwartz et al. (2011) obtained an age of around 37 Ma for Alpine-age eclogite-facies overprint of the Adula Nappe that represents a lateral equivalent of the Eclogite Zone in Eastern Switzerland (Schmid et al. 2004). In conclusion, there is strong evidence that parts of the Glockner Nappe System and the Modereck Nappe System, as well as the Eclogite Zone, underwent eclogite-facies overprint within the 45-37 Ma age range.

Glodny et al. (2005, 2008), on the other hand, propose an Oligocene age (31.5 ± 0.7 Ma) for eclogite-facies overprint of the Eclogite Zone, an age that is not only in conflict with all the above cited data but also with a multitude of geological constraints regarding the evolution of the greater Alpine area during the Oligocene (Handy et al. 2010) that, for example, suggest substantial exhumation of high-pressure units before the intrusion of the Periadriatic Plutons and the onset of movements along the Periadriatic Fault System (Rosenberg 2004). Rb/Sr multimineral isochrons of pristine eclogites and related eclogitic veins (Glodny et al. 2005, 2008) can only be interpreted as a pressure peak age if one accepts post-pressure-peak closed system behavior with respect to Rb and Sr in a strict sense (Thöni 1996). This is a questionable assumption in view of the subsequent re-heating during a Barrow-type event ("Tauernkristallisation") and after decompression (Kurz et al. 2008).

5.5.3 Exhumation of the high-pressure units and incipient accretion of the European crust

The spectacular large-scale isoclinal fold that folds the D2 thrust between Glockner and the Modereck Nappe Systems (Fig. 5.4c), the Seidlwinkl Fold Nappe first described by Frank (1969), is only preserved in the central part of the Tauern Window (cross section 6 of Plate 2). The effect of D3 folding is partial exhumation of eclogitic rocks found in the Eclogite Zone and in parts of the Modereck- and Glockner nappe systems (see area of eclogite-facies overprint in Plate 1), juxtaposing eclogites with non-eclogitic parts of the Glockner Nappe System. The fact that this fold nappe is limited to the central Tauern Window, i.e., the part of the Tauern Window where eclogite-facies became exhumed to the earth's surface, supports the view that D3 isoclinal folding represents a first stage of exhumation of the high-pressure units. We envisage incipient accretion of the mostly non-eclogitic part of the Subpenninic nappes to have occurred contemporaneously with this first stage of exhumation of high-pressure rocks in the same still-active subduction channel (e.g., Gerya et al. 2002). Decompression of the Eclogite Zone to some 1.0 GPa or less took place during the 38-32 Ma time interval (Kurz et al. 2008b). Hence, we attribute D3 deformation depicted in Figure 5.4c to this same time interval.

5.5.4 Formation of the Venediger Duplex and Tauern "Kristallisation"

The formation of the Venediger Duplex depicted in Figure 5.4d (D4) predates final equilibration of all eclogitic and non-eclogitic units in all the Subpenninic nappes and the Glockner Nappe System under the p-T conditions that locally reached amphibolite-facies conditions during the Barrow-type event known as the "Tauernkristallisation". This overprint was prograde in the case of the newly accreted

Venediger Duplex but probably associated with re-heating of the high-pressure units that cooled during D3 decompression according to the p-T path compiled by Kurz et al. (2008, their Fig. 4), also taking into account previously published literature data (Spear and Franz 1986, Inger and Cliff 1994, Zimmermann et al. 1994, Stöckhert et al. 1997, Kurz et al. 1998b, 2001, Dachs and Proyer 2001).

The duration of D4 duplex formation that immediately predates Barrow-type "Tauernkristallisation" is unknown. According to Christensen et al. (1994) final equilibration of garnet under peak conditions of 550° C and 0.7 GPa in the western Tauern Window took place at 30 Ma. Rb/Sr whole-rock and white mica ages from the central Tauern Window cluster around 30-28 Ma and may approximately date the "Tauernkristallisation", since this same range of ages is found in the Eclogite Zone and in the adjacent Glockner Nappe System (Inger and Cliff 1994). This interpretation is supported by the Th-Pb allanite ages of Cliff et al. (1998) from the Mallnitz Synform north of the Sonnblick Dome, which clusters around 28 Ma. In summary, D4 deformation terminated at around 28 Ma ago.

The D4 duplex formation scenario (Fig. 5.4d) is contemporaneous with the intrusion of the Periadriatic Plutons (in this case the Rieserferner, see cross-section 4 of Plate 2) that also took place at around 32 Ma (Rosenberg 2004), probably related to slab break-off due to decreasing rates of subduction (von Blanckenburg and Davies 1995).

5.5.5 Indentation, doming and lateral extrusion

The configuration of mantle slabs beneath the Eastern Alps changed fundamentally in the Early Miocene (Ustaszewski et al. 2008). After the European slab broke off (Fig. 5.4d), the Adriatic slab started to subduct northeastwards beneath the Alpine edifice, as depicted in Figure 5.4e (mantle configuration only valid for the eastern half of the Tauern Window, see Fig. 5.3). At about the same time the Southern Alpine crust east of the Giudicarie Belt started to indent while their lithospheric underpinnings started to subduct beneath the Eastern Alps (Lippitsch et al. 2003). This led to doming in the Tauern Window and lateral extrusion of the Eastern Alps (Ratschbacher et al. 1991, Rosenberg et al. 2007, Scharf et al. submitted a, Chapter 2). Also Carpathian slab-rollback and extension of the Pannonian Basin also started at about the same time (Horváth et al. 2006).

Determining exactly when the doming and lateral extrusion began, including initial activity of the Brenner- and Katschberg normal faults, is crucial for deciding if rapid exhumation and orogen-parallel extension were triggered by indentation of the Southern Alps east of the Giudicarie Belt, or alternatively, by Pannonian extension, or by both. It is widely accepted that both processes had to interact in order to allow for the observed phenomena of coeval doming and lateral extrusion, as first proposed by Ratschbacher et al. (1991). However, different authors place different emphasis on the relative importance of these two processes and/or invoke alternative processes such as gravitational collapse of an over thickened crust (see Rosenberg et al. 2007, Scharf et al. submitted a, Chapter 2 for a discussion on this topic).

The timing constraints regarding the exhumation history of the Tauern Window may either be based on radiometric dating of syn-kinematic shearing post-dating "Tauernkristallisation" suspected to be related to exhumation (e.g., Schneider et al. submitted) or, alternatively, on interpreting data on the cooling history. Schneider et al. (submitted) derived an age range for syn-kinematic sinistral shearing along several shear zones kinematically linked to the SEMP Fault by $^{40}Ar/^{39}Ar$ in situ analyses. According to them the onset of this sinistral deformation cannot be older than the oldest age of 32 Ma obtained for syn-kinematic phengite in the northernmost (Ahorn) shear zone and not older than 24-20 Ma for other sinistral shear zones located further south.

Dating the onset of exhumation based on cooling ages is problematic since the onset of rapid cooling lags behind the onset of rapid exhumation. Hence, we need additional information, including better temporal constraints on the p-T path of the exhumed rocks and thermo-mechanical modelling of the exhumation history. So far, the onset of rapid exhumation has only been determined for an area in the footwall of the Brenner Normal Fault to be around 20 Ma (Fügenschuh et al. 1997).

The exhumation history of the Katschberg Normal Fault is more difficult to ascertain and discussed in more detail in Scharf et al. (submitted a) and in Chapter 2. At first sight, available thermochronological data indicate that rapid cooling of the eastern Tauern Window started earlier, i.e., before 20 Ma (see compilation of data by Luth and Willingshofer 2008). If exhumation by normal faulting indeed started earlier in the east, this extension cannot have been triggered by extension in the Pannonian Basin and subduction rollback in the Carpathians, which started no earlier than 20 Ma (e.g., with the onset of rifting in the Pannonian Basin, Horváth et al. 2006). Extension related to strike-slip and oblique-slip faulting in the Eastern Alps started even later: at 18 Ma in the Styrian Basin (e.g., Hohenegger et al. 2009), at about 17 Ma in various intramontane basins such as the Fohnsdorf Basin (e.g., Strauss et al. 2001) and at 16 Ma in the Vienna Basin (e.g., Hölzel et al. 2008).

On the other hand, triggering of rapid exhumation by the indentation of the Southern Alps along the Giudicarie Belt, including the Giudicarie Fault and an eastward adjacent sinisitrally transpressive fault system (Massironi et al. 2006) is possible provided that doming and lateral extrusion in the western Tauern Window did not start before some 21 Ma, the stratigraphically constrained onset of sinistral motion along the Giudicarie Belt. This constraint comes from the age of the youngest pelagic sediments affected by activity of the frontal parts of the Giudicarie Belt, extending from Meran (Plate 1) southwards to Lake Garda, a belt that is linked to thrusting along the Milano Belt in front of the Lombardian Alps (Schönborn 1992). At Monte Brione on the northern end of Lake Garda, the base of this pelagic sediment includes a part of the planktonic foraminiferal zone 5 (Luciani and Silvestrini 1996), which starts at 21.5 Ma (Berggren et al. 1995). Hence, activity along the Giudicarie Belt sets in after 21.5 Ma, which is consistent with the onset of rapid exhumation along the Brenner Normal Fault (20 Ma, Fügenschuh et al. 1997).

While these stratigraphic data constrain the maximal age for the onset of indentation and related D5 deformation within the Tauern Window it should be noted that parts of the Tauern Window

may well have undergone earlier (i.e., pre-D5) periods of exhumation, as suggested by some Rb/Sr white mica ages (e.g., Cliff et al. 1985) when interpreted as cooling ages, as well as by the formation ages obtained for sinistral shear zones in the western Tauern Window by Schneider et al. (submitted), discussed above. The period between 29 and 21 Ma ago is characterized by on-going shortening across the Alpine Chain, concentrated in the northern foreland of the Alps and along the Southern steep belt of the Alps in the vicinity of the Periadriatic Fault (Schmid et al. 1996), as well as by conjugate sinistral and dextral shearing along the Engadine Fault and the Tonale Fault, respectively (Schmid and Froitzheim 1993, Ciancaleoni and Marquer 2008) leading to a pre-21 Ma period of lateral extrusion pre-dating our D5. Hence, a general uplift in the vicinity of the present Tauern Window could easily have led to an earlier, i.e., Late Oligocene to Early Miocene, period of exhumation by erosion.

Miocene-age (D5) and possibly older lateral extrusion is inadequately depicted in profile view (Fig. 5.4e) since it involves three-dimensional strain partitioning between north-south shortening and east-west extension, the latter again partitioned into strike-slip motion along sinistral (e.g., SEMP Fault) and dextral (e.g., Periadriatic Fault) shear zones, as well as normal faulting along the Brenner- and Katschberg normal faults. The interaction of the SEMP Fault with folding has been worked out in detail (Rosenberg and Schneider 2008), and also that between north-south compression and orogen-parallel extension in the area of the Katschberg Normal Fault (Scharf et al. submitted a, Chapter 2). However, determining the relative and absolute amounts of north-south shortening and east-west-extension in the area of the Brenner Normal Fault (Rosenberg and Garcia 2012, Fügenschuh et al. 2012) and on the scale of the entire Tauern Window requires further investigations. There are indications that a scenario of indentation, exhumation, doming and lateral extrusion very probably continues to the present day (e.g., Massironi et al. 2006) although the velocities at which these processes occur have probably decreased from their values at the onset of rapid exhumation some 20 Ma ago (Fügenschuh et al. 1997).

Figure 5.4f depicts a schematic cross section through the central Tauern Window at is present stage, e.g., parallel to cross section 6 of Plate 2. Most active tectonic is reduced south of the Tauern Window. The Tauern Window is yield minor seismically activities along its western and eastern border (Reinecker and Leonhard 1999, Reiter et al. 2005).

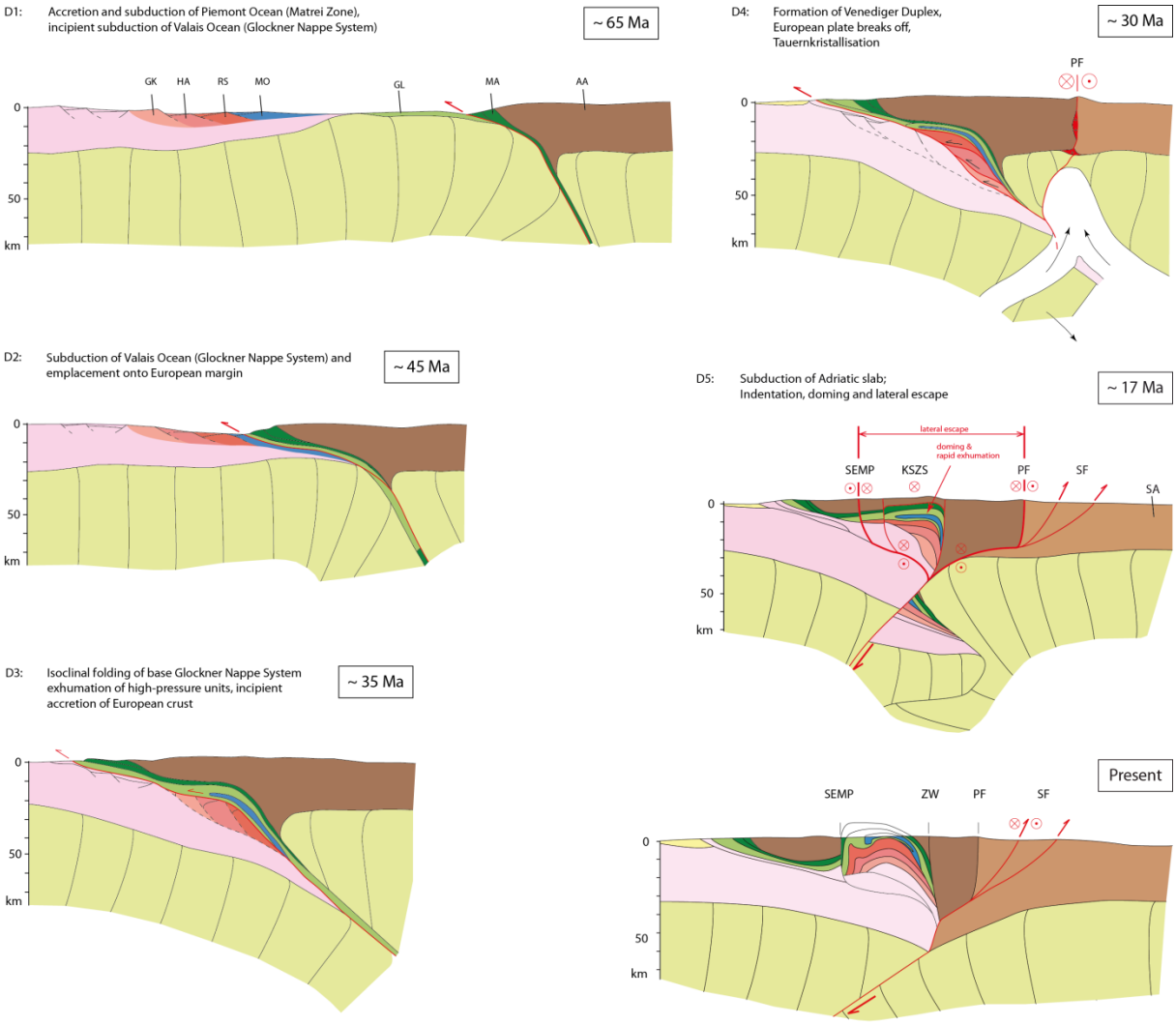

Figure 5.4: Sketches illustrating the kinematic evolution of the Tauern Window. (a) D1 subduction of the Piemont-Liguria Ocean and accretion of oceanic relics in front of the Austroalpine Nappe Stack (~ 65 Ma). (b) D2 subduction of the Valais Ocean and parts of the distal European Margin (~ 45 Ma). (c) D3 exhumation of the high-pressure units and incipient accretion of the European Crust (~ 35 Ma). (d) D4 formation of the Venediger Duplex and Tauern "Kristallisation" (~ 30 Ma). (e) D5 Indentation, doming and lateral extrusion (~ 17 Ma). (f) Schematic present-day lithosphere-scale section across the eastern part of the Tauern Window. Tectonic nappes: AA – Austroalpin units; GK – Göss Nappe; GL – Glockner Nappe System; HA – Hochalm Nappe; MA – Matrei Zone. MO – Modereck Nappe System; RS – Romate-Storz Nappe; SA – Southern Alps. Major Faults: KSZS – Katschberg Shear Zone System; PF – Periadriatic Fault; SEMP – Salzach-Ennstal-Mariazell-Puchberg Fault; SF – Sava Fault; ZW – Zwischenbergen-Wöllatratten Fault. Note that active faults are red and inactive faults are black.

5.6 Conclusions and unanswered questions

The Tauern Window exposes a Cenozoic-age nappe pile consisting of crustal slices derived from the distal continental margin of Europe (Subpenninic units) and the Valais Ocean (Glockner Nappe System), accreted to an upper plate already formed during the Cretaceous and consisting of the Austroalpine nappe pile and previously accreted ophiolites derived from the Piemont-Liguria Ocean. The present-day architecture of the Tauern Window is primarily characterized by a crustal scale Late

Alpine duplex, the Venediger Duplex, which formed during the Late Eocene to Early Oligocene. This duplex structure was severely overprinted by doming and lateral extrusion, most probably triggered by the indentation of the South Alpine units east of the Giudicarie Belt beginning at around 20 Ma ago and linked to a lithosphere-scale reorganization of the geometry of the mantle slabs.

While this work hopefully contributes to a better understanding of the three-dimensional structure of the Tauern Window, two important problems remain: What was the relative contribution of orogen-parallel extension by normal faulting, escape-type strike-slip faulting and orogen-normal compression, all of which acted contemporaneously during the Miocene? The answer to this question has a strong bearing on the relative importance of tectonic versus erosional denudation. A second unsolved problem concerns the quantification of kinematic and dynamic interactions between crustal (Adria indentation, Carpathian roll-back and Pannonian extension) and mantle structures (reorganization of the mantle slabs beneath the Eastern Alps) that fundamentally and abruptly changed the lithosphere-scale geometry of the Alps-Carpathians-Dinarides system during a very severe Miocene-age overprint initiating at around 20 Ma ago.

Acknowledgements

We greatly benefitted from advice and scientific interactions with R Schuster, M. Rockenschaub and G. Pestal from the Geologische Bundesanstalt in Wien, as well as with R. Brandner, A. Töchterle and B. Fügenschuh from Universität Innsbruck, B. Lammerer from Universität München, W. Kurz from Universität Graz and E. Kissling from ETH Zürich. The contributions of our colleagues at the Freie Universität are also highly appreciated, especially A. Bertrand, S. Favaro, S. Garcia, P. Gipper, K. Hammerschmidt, F. Hawemann and S. Schneider. We thank M. Grundmann for her assistance in drawing. We were supported in part by grants from the German Science Foundation (DFG grants Ha 2403/10 and RO 2177/5) and the Alexander-von-Humboldt Foundation (to S.M. Schmid).

Chapter 6

Outlook and future work

Based on my Ph.D. thesis five possible feature research projects would be useful. These future projects are circling around the problem of the different exhumation/cooling histories of both Tauern subdomes and about processes in subduction/exhumation channels.

6.1 Projects related to different exhumation/cooling history of the Tauern subdomes

(1) First, my Ph.D. study reveals regionally different rapid exhumation histories and, hence, rapid cooling development between the Western and Eastern Tauern subdome, an Oligocene/Miocene to Miocene exhumation history, respectively (Scharf et al. in prep., Chapter 4). This raises the fundamental question what the reasons are and the driving forces behind it.

A possible answer might be that the collision between Adria and Europe is not coevally along strike of the orogen. Thus, the collision south of the Eastern Tauern Subdome starts earlier with respect to the Western Tauern Subdome. If this assumption is right, motion direction of the Adriatic microplate with respect to stable Europe was probably not perpendicular to the southern European margin. Therefore, a collision between both continents with an associated rapid exhumation starts earlier in an area south of the Eastern Tauern Subdome than south of the Western Tauern Subdome (marked by the onset of differential motion along the Giudicarie Belt at c. 21 Ma). Consequently, a kinematic divide between both Tauern subdomes must exist.

Previous geophysical investigations clearly identify a switch in dip direction and length of the European slab beneath the Tauern Window (e.g., Lippitsch et al. 2003, Kissling et al. 2006, Handy et al. 2010, in prep., Schmid et al. submitted, Chapter 5). The different slab polarity remarkably coincides with a change in structure and style of European basement rocks in the Tauern Window. Therefore, the questions arise: How is the connection and relationship between mantle and surfaces structures, in general? Where is the kinematic-divide between both exhumation structures in the Tauern Window?

This new project will handle in detail the proposed kinematic-divide with respect to structural, mineralogical/petrological, geochronological and geophysical aspects. Subsequent research can involve analog and/or numeric modeling and comparison with similar structures in other orogens. Finally, a new proposal for geophysical research and tectonics (AlpArray) through the Eastern Alps, Dinarides and Southern Alps has been requested, which would help to envisage the structures beneath the Tauern Window in detail.

(2) The second project could be related to tectonic processes at the eastern end of the Tauern Window and to associated units to the south. During the Oligocene to Miocene northward indentation of the Adriatic microplate into stable Europe, a triangle zone between the Periadriatic Fault and the Tauern Window was formed. This triangle zone were bisects along the sinistral Zwischenbergen-Wöllatratten-Drau (ZWD) Fault. This leads to a different amount of exhumation in the Eastern Tauern Subdome (Scharf et al. submitted a, Chapter 2). Hence, exhumation structures in the Tauern Window and the age of sinistral motion along the ZWD must be in line with existing geochronological data in the Tauern Window. No satisfying geochronological and structural research in shear/fault zones south of the Tauern Window has been carried out so far, especially in the light of the exhumation history in the Eastern Tauern Subdome.

(3) The third project could start in the eastern Tauern Window. During my Ph.D. thesis I investigated the shear zone system at the eastern end of the Tauern Window (Katschberg Shear Zone System – KSZS; Scharf et al. submitted a, Chapter 2), a combination of strike-slip and low-angle normal shear zones with a lateral motion of 26 km towards the east. This, indirectly, implies that part of this Miocene fault system are stretching faults (sensu Means 1989, 1990). The mission of this future project is to clarify the geochronological history of this area. Therefore, a systematic younging from west to east of all cooling systems (Rb/Sr on mica, $^{40}Ar/^{39}Ar$ on mica, and fission tracks methods) should be corroborated parallel to the stretching shear zones, partly already confirmed by Rb/Sr on biotite cooling ages (Favaro and Schuster et al. in prep.). This project calls for comparisons with other large scale stretching faults in different orogens and will help to understand the kinematics and timing of such impressive processes of orogen-parallel extension during convergent.

(4) The fourth project could be concerned in more detail about the $^{40}Ar/^{39}Ar$ Laser ablation research on white micas I have done so far (Scharf et al. in prep., Chapter 4). Clear time constraints for the ending of the KSZS activity could be evaluated. A more comprehensive work across the whole KSZS would help to define the end of ductile shearing along the KSZS. An associated research on grain sizes of the white mica with respect to the closure temperature would essentially contribute to the interpretation of the $^{40}Ar/^{39}Ar$ Laser ablation ages on white micas.

6.2 Project related to processes in a subduction/exhumation channel

The fifth possible project could start in the central part of the Tauern Window. My peak-temperature estimates based on Raman microspectroscopy on carbonaceous material (RSCM) and petrology shows that possibly no high-pressure-dominated Penninic units at the eastern end of the Tauern Window occur. The high-pressure-related peak temperatures are at c. 520° C, whereas the non-high-pressure

units suffer a maximum of 480° C (Scharf et al. submitted b, Chapter 3). Moreover, no relicts of any high-pressure mineral assemblages or pseudomorphoses after them could be identified. The high-pressure unit was isoclinally folded (Seidlwinkl Fold) during exhumation in the vicinity of the Grossglockner, whereas no comparable structures are found in the non-high-pressure Penninic unit (Schmid et al. submitted, Chapter 5). A clear structural jump between the high-pressure (Glockner Nappe sensu stricto, Frasl and Frank 1966) and non-high-pressure nappe (Fuscher Nappe, Pestal et al. 2009) of the Glockner Nappe System can be observed. Therefore, I assume that this high-pressure Glockner Nappe was a subduction and/or exhumation channel during Eocene times. Another undefined aspect are the metamorphic conditions of the core of the Seidlwinkl Fold. These folds consist of units of the European distal continental margin (Modereck Nappe System) in their core, surrounded by the high-pressure mineral-assemblages-bearing Glockner Nappe. The contact of the Modereck- to the Glockner Nappe System is characterized by a tectonic mélange which contains eclogite-facies rocks. A non-high-pressure-related Modereck Nappe System (core of the Seidlwinkl Fold) would clearly demonstrate that isoclinal folding is restricted to exhumation.

This future work will use the RSCM technique with sampling across the structural boundary of the Penninic nappes and the Seidlwinkl Fold to hopefully reveal the shape of the subduction/exhumation channel. In total, a better understanding of processes in a subduction- or exhumation channel (Shreve and Cloos 1986, Cloos and Shreve 1988) should be the overall goal of this project.

Chapter 7

Summary and conclusions

This chapter describes the main structural, mineralogical/petrological, geochronological and kinematic results of this thesis and their interpretations.

7.1 Structural and petrological evolution of the Tauern Window

The Tauern Window exposes European and Penninic units. These units were partly accreted, subducted, exhumed, folded and highly sheared during the Cenozoic. All these processes can be studied along-strike of the whole window, but no place reveals all features. Hence, lateral changes in style of metamorphism and deformation are common. Penninic units at the northeastern part of the Tauern Window preserves evidence for Paleogene accretion and nappe stacking (D1), as manifested by a WNW-dipping stretching direction and no indications for any high-pressure related mineral association (typical mineral assemblages of this part of the Penninic nappes are calcite + quartz + chlorite + white mica ± albite in the calc-schists and chlorite + plagioclase + epidote in the mafic rocks). Some remnants of subduction-related tectonic are found in the European- and Penninic units (D2). In the Eclogite Zone, at the southern central Tauern Window and parts of the Glockner Nappe System near the Grossglockner preserve eclogite- and high-pressure-facies mineral assemblages (garnet + omphacite, lawsonite or pseudomorphoses after it). During exhumation of parts of the Penninic units during Late Eocene times (D3) the spectacularly Seidlwinkl Fold was generated. Formation of the Venediger Duplex (D4) before c. 32 Ma and an afterwards Barrow-type thermal overprint (Tauernkristallisation at 30-28 Ma) is indicated by duplex formation within the European units and amphibolite-facies mineral assemblages (biotite + staurolite + amphibole). The roofthrust of the duplex is clearly visible by the contact of the European margin (Modereck Nappe System) and partly by the Glockner Nappe System with European basement units. The floorthrust of the duplex is not exposed in the Tauern Window. The final shape of the Tauern Window was established during the Oligocene to Miocene continuous northward indentation of the Adriatic microplate. In the Tauern Window coeval folding and orogen-parallel lateral extrusion significantly redeformed the previous thickened edifice (D5). The style of D5-folds between the Western and Eastern Tauern subdomes is different. The Western Tauern Subdome is tightly folded with upright fold axes plains striking WSW-ENE, but the Eastern Tauern Subdome is openly folded with much smaller amplitudes. The fold axes strike WNE-ESE. The Tauern Window is bounded at the western and eastern ends by low-angle extensional normal faults, the Brenner- and Katschberg normal faults, respectively. These are kinematically linked to conjugate strike-slip shear zones to form the Brenner- and Katschberg shear zone systems (BSZS and KSZS). A later orogen-parallel motion under frictional conditions (D6) is

manifested by strike-slip faults at the northern and southern rim of the eastern Tauern Window, the Salzach-Ennstal-Mariazell-Puchberg (SEMP) Fault and Mölltal (MF) Fault, respectively.

7.2 The Katschberg Shear Zone System (KSZS)

The central part of the KSZS is marked by a low-angle normal shear zone – the Katschberg Normal Fault (KNF). The dip angle of the KNF is 20-30°. This shear zone bends towards the north into a steep, dextral east-west trending strike-slip shear zone. The southern end of the KNF bends into a sub-vertical sinistral strike-slip shear zone. The foliation in the KSZS is parallel to the shear zone system and carries a consequently east to southeast dipping stretching lineation. Furthermore, the host of sense-of-shear indicators denotes motion of the whole KSZS towards the E to-SE. The Katschberg-related structures are preserved up to the lowermost rocks of the Austroalpine units along of the KNF. Hence, the structural boundary between the footwall and the hangingwall of the KNF is not obligatory parallel to the Austroalpine/Penninic contact. It excises this contact into the Austroalpine units for maximum 100 m. The northern and southern branches of the KSZS become stretching faults whose displacements decrease 26 km farther west to zero. The KSZS comprises a $\leq$ 5 km wide belt of retrograde amphibolite- to greenschist-facies mylonites that accommodated Neogene exhumation and orogen-parallel stretching of the underlying nappe complex. The kinematic continuity of top to the E to -SE ductile shearing along the KNF with strike-slip shearing along its steep ends, combined with maximum tectonic omission of nappes in the Eastern Tauern Subdome in the footwall of the KNF, indicate that north-south shortening, orogen-parallel stretching and normal faulting were coeval. Also, the field gradient in the place of greatest tectonic omission along the KNF is 70° C/km, in contrast to areas where no Katschberg-related shearing occurs (7-8° C/km). Evidence for brittle faulting that capped the mylonite are found only at the KNF, the northern and southern strike-slip branches of the KSZS do not show any cataclasites. The brittle structures of the KNF are not connected with any other surrounded fault zones (e.g., Niedere Tauern Southern Fault, Hochstuhl Fault, Mölltal Fault).

7.3 Timing of exhumation and orogen-parallel stretching at the KSZS

My investigation using $^{40}Ar/^{39}Ar$ Laser ablation on white micas, combined with structural and other geochronological research (Rb/Sr on white mica and biotite, zircon fission track) yield evidence for the onset of rapid cooling of the Eastern Tauern Subdome between the end of the Tauernkristallisation (28 Ma) and a certain time before the $^{40}Ar/^{39}Ar$ Laser ablation on white micas mean ages interpreted as cooling ages (20 Ma). The Alpine peak temperatures in the Eastern Tauern Subdome are around 630° C. This is confirmed by my peak temperature estimates using the Raman microspectroscopy on

carbonaceous material. Rapid cooling certainly continued to c. 17 Ma, when the rocks pass the viscous-to-frictional transition at c. 300-270° C. The onset of rapid exhumation ensued after the Tauernkristallisation at 28 Ma and a certain time before the onset of rapid cooling. Most motion along the KSZS predates 20-17 Ma. This is proven by the $^{40}Ar/^{39}Ar$ Laser ablation ages on white micas with considering of their microstructures.

It is not clear when exactly the rapid exhumation at the eastern end of the Tauern Window starts. For geodynamics reasons the onset of rapid exhumation should be the same as for the Western Tauern Subdome (21 Ma). Alternatively, when rapid exhumation predates 21 Ma, another unknown mechanism must be responsible for the different rapid exhumation/cooling history in the entire Tauern Window. Thus, rapid exhumation migrates in time and space from east (e.g., south of the eastern Tauern Window) towards west (e.g., south of the western Tauern Window). A geodynamic consequence of this new interpretation of the onset of rapid exhumation in the Tauern Window is a kinematic decoupling between the Eastern- and Western Tauern subdoms.

7.4 Kinematics and driving forces for the evolution of the KSZS

In my work I could show that large amplitude double-plunging folding and normal faulting, associated with east-directed stretching within the eastern Tauern Window were coeval. These exhumation structures are the direct result of the overall northward motion of the Adriatic microplate with respect to stable Europe. South of the Tauern Window and north of the Periadriatic Fault a triangular zone with low internal Oligocene to Miocene deformation is fragmented into two blocks (the Rieserferner Block, west of the Zwischenbergen-Wöllatratten-Drau (ZWD) Fault and the Drau-Möll Block east of this fault). The Drau-Möll Block indented c. 12 km further to the north, than the Rieserferner Block and is, thus, responsible for the distinct appearance of the KSZS. In total c. 32 km of Oligocene to Miocene orogen-perpendicular shorting is accumulated within the Tauern Window. The amount of orogen-parallel east-west extension measured approximately 100 km within the Tauern Window. The western Tauern Window records an east-west extension of 70-80 km, whereas the eastern Tauern Windows records 26 km. Adriatic indentation began at c. 25 Ma south of the Eastern Tauern Subdome and started at 21 Ma south of the Western Tauern Subdome, which is manifested in the west by the first strike-slip motion along the Giudicarie Belt.

Most eastward-directed motion at the eastern end of the Tauern Window was active up to c. 17 Ma ago. On the other hand, east-west directed strike-slip was triggered by the extension of the Pannonian Basin reaching the study area at 17 Ma. Extension and strike-slip in the Eastern Alps resulted from roll-back subduction beneath the Carpathians. On this ground, rollback cannot account as trigger for the eastward directed orogen-parallel extrusion of the Tauern Window. Nevertheless, the later may facilitate the lateral extension in the Tauern Window. Therefore, the northward directed

indentation of the Adriatic microplate into stable Europe was and still is the primary force driving the tectonics of the Eastern Alps and adjacent areas.

References

Alber, J. (1976) Seriengliederung, Metamorphose und Tektonik des Hocharngebietes (Rauristal, Salzburg). Unpublished PhD thesis Universität Wien, 229pp.

Angel, F. & Staber, R. (1950) Geologische Karte des Ankogel-Hochalm-Gebietes 1:50.000. In. Angel, F. & Staber, R. 1952, Wien (Freytag & Berndt).

Aoya, M., Kouketsu, Y., Endo, S., Shimizu, H., Mizukami, T., Nakamura, D. & Wallis, S. (2010) Extending the applicability of the Raman carbonaceous-material geothermometer using data from contact metamorphic rocks. Journal of Metamorphic Geology, 28, 895-914, doi:10.1111/j.1525-1314.2010.00896.x.

Axen, G.J., Bartley, J.M. & Selverstone, J. (1995) Structural expression of a rolling hinge in the footwall of the Brenner Line normal fault, eastern Alps. Tectonics, 14, 1380-1392.

Bada, G., Grenerczy, G., Tóth, L., Horváth, F., Stein, S., Cloetingh, S., Windhoffer, G., Fodor, L., Pinter, N. & Fejes, I. (2007) Motion of Adria and ongoing inversion of the Pannonian Basin:seismicity,gps velocitys and stress transfer. In: Stein S, Mazzotti S (Eds.). Continental Intraplate Earthquakes: Science, Hazard, and Policy Issus. Geological Society of America, Special Paper 425.

Beaumont, C., Jamiesont, R.A., Nguyen, M.H. & Lee, B. (2001) Himalayan tectonicsexplained by extrusion of a low-viscosity crustal channel coupled to focused surface denudation. Nature, 414, 738-742.

Becker, B. (1993) The Structural Evolution of the Radstadt Thrust System, Eastern Alps, Austria – Kinematics, Thrust Geometries, Strain Analysis. Tübinger Geowissenschaftliche Arbeiten, 14, 92pp.

Behrmann, J.H. (1990) Zur Kinematik der Kontinentkollision in den Ostalpen. Geotektonische Forschung, 76, 1-180.

Berger, A. & Bousquet, R. (2008) Subduction-related metamorphism in the Alps: Review of isotopic ages based on petrology and their geodynamic consequences. In S. Siegesmund, S., B. Fügenschuh & N. Froitzheim (Eds.). Tectonic Aspects of the Alpine-Dinaride-Carpathian System. Geological Society, London, Special Publications 298, 117-144.

Berggren, W.A., Kent, D.V., Swisher, C.C. & Aubry, M.-P. (1995) A revised Cenozoic geochronology and chronostratigraphy. In: W.A Berggren, D.V.Kent, M.-P. Aubry & J. Hardenbol (Eds.). Geochronology, Time Scales and stratigraphic correlation. SEPM special publication, 54, 129-212.

Bertle, R.J. (2004) The sedimentary record of North Penninic Schistes Lustrés of the Lower Engadine Window and its correlation to the Tauern Window (Eastern Alps). Jahrbuch der Geologischen Bundesanstalt Wien, 144, 165-171.

Beyssac, O., Rouzaud, J.N., Goffé, B., Brunet, F. & Chopin, C. (2002a) Graphitization in a high pressure, low-temperature metamorphic gradient: a Raman microspectroscopy and HRTEM study. Contributions to Mineralogy and Petrology, 143, 19-31.

Beyssac, O., Goffé, B., Chopin, C. & Rouzaud, J.N. (2002b) Raman spectra of carbonaceous material in metasediments: a new geothermometer. Journal of Metamorphic Geology, 20, 859-871.

Beyssac, O., Brunet, F., Petitet, J.P., Goffé, B. & Rouzaud, J.N. (2003a) Experimental study of the microtextural and structural transformations of carbonaceous material under pressure and temperature. European Journal of Mineralogy, 15, 937-951.

Beyssac, O., Goffé, B., Petitet, J.P., Froigneux, E., Moreau, M. & Rouzaud, J.N. (2003b) On the characterization of disordered and heterogeneous carbonaceous materials by Raman spectroscopy. Spectrochimica Acta Part A – Molecular and Biomolecular Spectroscopy, 59, 2267-2276.

Beyssac, O., Bollinger, L., Avouac, J.P. & Goffé, B. (2004) Thermal metamorphism in the lesser Himalaya of Nepal determined from Raman spectroscopy of carbonaceous material. Earth and Planetary Science Letters, 225, 233-241.

Bigi, G., Castellarin, A., Catalano, R., Coli, M., Cosentino, D., Dal Piaz, G.V., Lentini, F., Parotto, M., Patacca, E., Praturlon, A., Salvini, F., Sartori, R., Scandone, P. & Vai, G. (1989) Synthetic structural kinematic map of Italy, Sheets 1 and 2, C.N.R. Progetto Finalizzato Geodinamica, SELCA Firenze.

Bonijoly, M., Oberlin, M. & Oberlin, A. (1982) A possible mechanism for natural graphite formation. Inernational Journal of Coal Geology, 1, 238-312.

Borsi, S., Del Moro, A., Sassi, F.P. & Zirpoli, G. (1973) Metamorphic evolution of the Austridic rocks to the south of the Tauern window (Eastern Alps): radiometric and geopetrological data. Memorie della Societa Geologica Italiana, 12, 549-571.

Bousquet, R., Oberhänsli, R., Goffé, B., Wiederkehr, M., Koller, F., Schmid, S.M., Schuster, R., Engi, M., Berger, A. & Martinotti, G. (2008) Metamorphism of metasediments at the scale of an orogen: a key to the Tertiary geodynamic evolution of the Alps. Geological Society, London, Special Publications, 298, 393-411, doi:10.1144/SP298.18.

Brandner, R. Reiter, F. & Töchterle, A. (2008) Überblick zu den Ergebnissen der geologischen Vorerkundung für den Brenner-Basistunnel. GeoAlp, 5, 165–174.

Burbank, D.W. (2002) Rates of erosion and their implications for exhumation. Mineralogical Magazine, 66 (1), 25-52, doi:10.1180/0026461026610014.

Burg, J.-P., Vandendriessche, J. & Brun, J.P. (1994) Syn- to post-thickening extension in the Variscan belt of Western Europe: Modes and structural consequences. Géologie de la France, 3, 33-51.

Buseck, P.R. & Bo-Jun, H. (1985) Conversion of carbonaceous material to graphite during metamorphism. Geochimica et Cosmochimica Acta, 49, 2003-2016.

Bustin, R.M., Ross, J.V. & Moffat, I. (1986) Vitrinite anisotropy under differential stress and high confining pressure and temperature: preliminary observations. International Journal of Coal Geology, 6, 343-351.

Bustin, R.M., Ross, J.V. & Rouzaud, J.N. (1995) Mechanism of graphite formation from kerogen: experimental evidence. International Journal of Coal Geology, 28, 1-36.

Castellarin, A., Nicolich R., Fantoni, R., Cantelli, L., Sella, M. & Selli, L. (2006) Structure of the lithosphere beneath the Eastern Alps (southern sector of the TRANSALP transect). Tectonophysics, 414, 259-282.

Castellarin, A., Vai, G.B. & Cantelli, L. (2006) The Alpine evolution of the Southern Alps around the Giudicarie faults: a late cretaceous to early Eocene transfer zone. Tectonophysics, 414, 2-3.

Christensen, J.N., Selverstone, J.,Rosenfeld, J. L. & DePaolo, D. J. (1994) Correlation by Rb-Sr geochronology of garnet growth histories from different structural levels within the Tauern Window, Eastern Alps. Contributions to Mineralogy and Petrology, 118, 1–12.

Ciancaleoni, L. & Marquer, D. (2008) Late Oligocene to early Miocene lateral extrusion at the eastern border of the Lepontine dome of the central Alps (Bergell and Insubric areas, eastern central Alps). Tectonics, 27, TC4008, doi: 10.1029/2007TC002196.

Clark, S.P. & Jäger, E. (1969) Denudation rate in the Alps from geochronologic and heat flow data. American Journal of Sciences, 267(10), 1143-1160.

Cliff, R.A., Norris, R.J., Oxburgh, E.R. & Wright, R.J. (1971) Structural, metamorphic and geochronological studies in the Reisseck and southern Ankogel Groups, the EasternAlps. (ed. Oxburgh ER.). Jahrbuch der Geologischen Bundesanstalt Wien, 114, 121-272.

Cliff, R.A., Norris, R.J., Oxburgh, E.R. & Wright, R.J. (1981) Structural, metamorphic and geochronical studies in the Reisseck and southern Ankogel Groups. Jahrbuch der Geologischen Bundesanstalt, 114, 121-272.

Cliff, R.A., Droop, G.T.R. & Rex, D.C. (1985) Alpine metamorphism in the south-east Tauern Window, Austria: 2. Rates of heating, cooling and uplift. Journal of Metamorphic Petrology, 3, 403-415.

Cliff, R.A., Oberli, F., Meier, M. & Droop G.T.R. (1998) Achieving geological precision in metamorphic geochronology: A Th-Pb age for the syn-metamorphic formation of the Mallnitzermulde synform, Tauern Window, from individual allanite porphyroblasts. Mineralogical Magazine, 62A, 337 – 338.

Cloos, M. & Shreve, R.L. (1988) Subduction-Channel Model of Prism Accretion, Melange Formation, Sediment Subduction, and Subduction Erosion at Convergent Plate Margins: 1. Background and Description. Pageophysics, 128 (3/4), 455-502.

Cornelius, H.P. & Clar, E. (1939) Geologie des Grossglocknergebietes (1. Teil). Abhandlungen der Zweigstelle Wien der Reichsstelle für Bodenforschung, 25, 1-305.

Cuesta, A., Dhamelincourt, P., Laureyns, J., Martinez-Alonso, A. & Tascon, J.M.D. (1994) Raman microprobe studies on carbon materials. Carbon, 32, 1523-1532.

Dachs, E. (1986) High-pressure mineral assemblages and their breakdown products in metasediments south of the Grossvenediger, Tauern Window, Austria. Schweizerische Mineralogische und Petrographische Mitteilungen, 66, 145-161.

Dachs, E. (1990) Geothermobarometry in metasediments of the southern Grossvenediger area (Tauern Window, Austria). Journal of metamorphic Geology, 8, 217-230.

Dachs, E. & Proyer, A. (2001) Relics of high-pressure metamorphism from the Grossglockner region, Hohe Tauern, Austria: Paragenetic evolution and PT-paths of retrogressed eclogites. European Journal of Mineralogy, 13, 67–86.

Dahl, P.S. (1996) The crystal-chemical basis for Ar retention in micas: Inferences from interlayer partitioning and implications for geochronology. Contributions to Mineralogy and Petrology, 123, 22-39.

Decker, K., Dell'mour, R., Linzer, H.-G. & Peresson, H. (1994a) Exploration in polyphase orogens-brittle deformations oft he Calcareous Alps deciphered. European Association of Petroleum Geoscientists and Engineers: 6th Conference Vienna, Austria, 572.

Decker, K., Peresson, H. & Faupel, P. (1994b) Die miozäne Tektonik der östlichen Kalkalpen: Kinematik, Paleospannungen und Deformationsabteilung während der „lateralen Extrusion" der Zentralalpen. Jahrbuch der Geologischen Bundesanstalt, 137/1, 5-18.

Decker, K., Feijth, J., Frieling, D. Frisch, W., Gruber, A., Kolenprat, B., Magiera, J., Nowotny, A., Poscher, G., Reiter, F., Riedl, F., Rockenschaub, M., Scheibner, T. & Zasadny, J. (2009) Geological map sheet 148 Brenner 1:50.000. Geologische Bundesanstalt Wien.

Deutsch, A. (1984) Young Alpine dykes south of the Tauern Window (Austria): A K-Ar and Sr isotopestudy. Contributions to Mineralogy and Petrology, 85, 45-57.

Dewey, J.F., Shackleton, R.M., Chengfa, C. & Yiyin, S. (1988) The Tectonic Evolution of the Tibetan Plateau. Philosophical Transactions of the Royal Society of London, 327, 379-413.

Dingeldey, C., Dallmeyer, R.D., Koller, F. & Massone, H.J. (1997) P-T-t history of the Lower Austroalpine Nappe Complex in the „Tarntaler Berge" NW of the Tauern Window: implications for the geotectonic evolution of the central Eastern Alps. Contributions to Mineralogy and Petrology, 129, 1-19.

Dippel, B. & Heintzenberg, J. (1999) Soot characterisation in atmospheric particals from dources by NIR FT Raman spectroscopy. Journal of Aerosol Sciences, 30 (Suppl. 1), 908-908.

Dissel, C.F.K., Brothers, R.N. & Black, P.M. (1978) Coalification and graphitization in high-pressure schists in New Caledonia. Contributions to Mineralogy and Petrology, 68, 63-78.

Doglioni, C. & Bosellini, A. (1987) Eoalpine and mesoalpine tectonics in the Southern Alps. Geologische Rundschau, 76, 735-754.

Droop, G.T.R. (1981) Alpine metamorphism of politic schists in the south-east Tauern Window, Austria. Schweizerische Mineralogische und Petrographische Mitteilungen, 61, 237-273.

Droop, G.T.R (1985) Alpine metamorphism in the south-east Tauern Window, Austria: 1. P-T variations in space and time. Journal of metamorphic Geology, 3, 371-402.

Dunkl, I., Frisch, W. & Grundmann, G. (2003) Zircon fission track thermochronolgy of the southeastern part of the Tauern Window and adjacent Austroalpine margin, Eastern Alps. Eclogae geologae Helvetica, 96, 209-217.

Eder, N. & Neubauer, N. (2000) On the edge of the extruding wedge: Neogene kinematics and geomorphology along the southern Niedere Tauern, Eastern Alps. Eclogae geologae Helvetica, 93, 81-92.

Egger, H. Krenmayr, H.G., Mandl, G.W., Matura, A., Nowotny, A., Pascher, G., Pestal G., Pistonik, J., Rockenschaub, M. & Schnabel, W. (1999) Geologische Übersichtskarte der Republik Österreich 1 1'000'000. Geologische Bundesanstalt Wien.

Eichhorn, R., Höll, R., Loth, G. & Kennedy, A. (1999) Implications of U-Pb SHRIMP zircon data on the age and evolution of the Felbertal tungsten deposit (Tauern Window, Austria). International Journal of Petrology, 88, 469-512.

Eichhorn, R., Loth, G., Höll, R., Finger, F., Schermaier, A. & Kennedy, A. (2000) Multistage Variscan magmatism in the central Tauern Window (Austria) unveiled by U/Pb SHRIMP zircon data. Contributions to Mineralogy and Petrology, 139, 418-435.

Eichhorn, R., Loth, G. & Kennedy, A. (2001). Unravelling the pre-Variscan evolution of the Habach terrane (Tauern Window, Austria) by U-Pb SHRIMP zircon data. Contributions to Mineralogy and Petrology, 142, 147-162.

England, P.C. & Thompson, A.B. (1984) Pressure-Temperature-Time Paths of Regional Metamorphism I. Heat Transfer during the Evolution of Regions of Thickened Continental Crust. Journal of Petrology, 25(4), 894-928, doi:10.1093/petrology/ 25.4.894.

Enzenberg-Praehauser, M. (1967) Die Geologie der Tarntaler Berge (Wattener Lizum), Tirol. Mitteilungen der Gesellschaft Geologischer Bergbaustudenten, 17, 5-50.

Enzenberg-Praehauser, M. (1976) Zur Geologie der Tarntaler Breccie und ihrer Umgebung im Raum Hippold-Kalkwand (Tuxer Voralpen, Tirol). Mitteilungen der Gesellschaft Geologischer Bergbaustudenten, 23, 163-180.

Exner, C. (1939) Das Ostende der Hohen Tauern zwischen Mur- und Maltatal (I. Teil). - Jahrbuch Zweigstelle, Wien, Reichsstation der Bodenforschung. Jahrbuch der Geologischen Bundesanstalt, 89, 285- 314.

Exner, C. (1956) Geologische Karte der Umgebung von Gastein 1:50.000. Geologische Bundesanstalt Wien.

Exner, C. (1957) Erläuterungen zur Geologischen Karte von Gastein. Geologische Bundesanstalt Wien, 168pp.

Exner, C. (1962a) Geologische Karte der Sonnblickgruppe. Geologische Bundesanstalt Wien.

Exner, C. (1962b) Die Perm-Trias-Mulde des Gödnachgrabens an der Störungslinie von Zwischenbergen (Kreuzeckgruppe, östlich Lienz). Verhandlungen der Geologischen Bundesanstalt, 1962, 24–27.

Exner, C. (1962c) Sonnblicklammele und Mölltalline. Jahrbuch der Geologischen Bundesanstalt, 105, 273-256.

Exner, C. (1964) Erläuterungen zur Geologischen Karte der Sonnblickgruppe. Geologische Bundesanstalt, Wien.

Exner, C. (1971a) Geologie der peripheren Hafnergruppe (Hohe Tauern). Jahrbuch der Geologischen Bundesanstalt, 114, 1-119.

Exner, C. (1971b) Aufnahmen 1970 auf Blatt Muhr (156) und Vergleichsbegehungen auf Blatt Spittal a.d.Drau (182). Verhandlungen der Geologischen Bundesanstalt Wien, 1971/4, 28-30.

Exner, C. (1980) Geologie der Hohen Tauern bei Gmünd in Kärnten. Jahrbuch der Geologischen Bundesanstalt, 123, 343-410.

Exner, C. (1982) Geologie der zentralen Hafnergruppe (Hohe Tauern). Jahrbuch der Geologischen Bundesanstalt, 125, 51-154.

Exner, C. (1983) Erläuterungen zur Geologischen Karte der Hafnergruppe (with attached Geological Map 1:25'000). Mitteilungen der Gesellschaft der Geologie und Bergbaustudenten Österreichs, 29, 41-74.

Exner, C. (1989) Geologie des mittleren Lungaus. Jahrbuch der Geologischen Bundesanstalt Wien, 132, 7–103.

Faupl, P. (1975) Kristallinvorkommen und terrigene Sedimentgesteine in der Grestener Klippenzone (Lias-Neokom) von Ober- und Niederösterreich. Jahrbuch der geologischen Bundesanstalt Wien, 118, 1-74.

Faupl, P. & Wagreich, M. (2000) Late Jurassic to Eocene Paleeogeography and geodynamic evolution of the Eastern Alps. Mitteilungen der Österreichischen Geologischen Gesellschaft, 92, 79–94.

Favaro, S., Schuster, R., Handy, M.R., Scharf, A. & Pestal, G. (2012) The Mallnitz synform and its relation to the Mölltal fault (Tauern Window, Eastern Alps, Austria). Geophy R Abstracts 14:EGU2012-10371, EGU 9th General Assembly 22-27April 2012, Vienna.

Favaro, S. et al. (in prep.) Ductile to brittle structures along the Mölltal Fault (Eastern Alps, Austria).

Favaro, S. & Schuster et al. (in prep.) Rb-Sr on biotite and white mica ages at the Hochalm- and Sonnblick domes.

Ferreiro Mählmann, R., Petrova, T.V., Pironon, J., Stern, W.B., Ghanbaja, J., Dubessy, J. & Frey, M. (2002) Transmission electron microscopy study of carbonaceous material in a metamorphic profile from diagenesis to amphibolite facies (Bündnerschiefer, Eastern Switzerland). Schweizerische Mineralogische und Petrographische Mitteilungen, 82, 253-272.

Finger, F., Frasl, G., Haunschmid, B., Lettner, H., von Quadt, A., Schermaier, A., Schindlmayr, A.O. & Steyrer, H.P. (1993) The Zentralgneise of the Tauern Window (Eastern Alps): insight into an intra-alpine Variscan Batholith. In: J.F. von Raumer & F. Neubauer (Eds.). Pre-Mesozoic Geology in the Alps. Springer Verlag, 375-391.

Finger, F., Roberts, M.P., Haunschmid, B., Schermaier, A. & Steyrer, H.P. (1997) Variscan granitoids of central Europe: their typology, potential sources and tectonothermal relations. Mineralogy and Petrology, 61, 67-96.

Floess, D., Pomella, H., Speckbacher, R., Fügenschuh, B. & Tropper, P. (in press). Geometry and kinematics of the Eoalpine collision in the western Austroalpine basement units. International Journal of Earth Sciences.

Florineth, D. & Froitzheim, N. (1994) Transition from continental to oceanic basement in the Tasna nappe (Engadine window, Graubünden, Switzerland): evidence for Early Cretaceous opening

of the Valais ocean. Schweizerische Mineralogische und Petrographische Mitteilungen, 74, 437-448.

Fodor, L., Csontos, L., Bada, G., Györfi, I. & Benkovics, L. (1999) Tertiary evolution of the Pannonian Basinsystem and neighbouring orogens: a new synthesis of palaostress data. In: Durand B, Jolivet L, Horvath F, Seranne M. (Eds.). The Mediterranean Basins: Tertiary Extension within the Alpine Orogen. Geological Society Special Publication, 156, 295-334.

Foeken, J.P.T., Persano, C., Stuart, F.M. & ter Voorde, M. (2007) Role of topography in isotherm perturbation: Apatite (U-Th)/He and fission track results from the Malta tunnel, Tauern Window, Austria. Tectonics, 26, doi:10.10129/2006TC002049.

Foster, D.A., Gleadow, A.J.W. & Noble, W.P. (1996) Sphene and zircon fission track closure temperaturerevisted: Empirical calibration from 40Ar/39Ar diffusion studies of K-feldspar and biotite. International Workshop on Fission-Track Dating, Gent, Abstracts 37.

Frank, W. (1965) Tektonische Gliederung der Glockner und Granatspitzgruppe. Ph.D. thesis, Wien.

Frank, W. (1969) Geologie der Glocknergruppe. In: Neue Forschungen im Umkreis der Glocknergruppe. Wissenschaftliche Alpenvereinshefte des Deutschen Alpenvereins, 21, 95-111.

Frank, W., Miller, C. & Pestal, G. (1987) Map sheet 152, Matrei in Osttirol 1:50.000. Geologische Bundesanstalt Wien.

Franz, G. & Spear, F.S. (1983) High pressure metamorphism of siliceous dolomites from the Central Tauern Window, Austria. American Journal of Science, 283, 396-413.

Franz, G., Mosbrugger, V. & Menge, R. (1991) Carbo-Permian pterophyll leaf fragments from an amphibolite facies basement, Tauern Window, Austria. Terra Nova, 3, 137-141.

Frasl, G. & Frank, W. (1966) Einführung in die Geologie und Petrographie des Penninikums im Tauernfenster mit besonderer Berücksichtigung des Mittelabschnittes im Oberpinzgau, Land Salzburg. Der Aufschluss, Sonderheft, 15, 30-58, Heidelberg.

French, B.M. (1964) Graphitization of organic material in a progressively metamorphosed Precambrian iron formation. Science, 146, 917-918.

Frisch, W. (1973/74) Die stratigraphisch-tektonische Gliederung der Schieferhülle und die Entwicklung des penninischen Raumes im westlichen Tauernfenster (Gebiet Brenner – Gerlospass). Mitteilungen der Geologischen Gesellschaft, Wien, 66-67, 9-20.

Frisch, W. (1975) Hochstegen-Fazies und Grestener Fazies – ein Vergleich des Jura. Neues Jahrbuch Geologische Paläontologische Monatshefte, 1975/2, 82-90.

Frisch, W. (1976) Ein Modell zur alpidischen Evolution und Orogenese des Tauernfensters. Geologische Rundschau, 65, 375-393.

Frisch, W. (1979) Tectonic progradation and plate tectonic evolution of the Alps. Tectonophysics, 60, 121–139.

Frisch, W. (1980a) Tectonics of the Western Tauern Window. Mitteilungen der österreichischen Geologischen Gesellschaft, 71/72, 65-71.

Frisch, W. (1980b) Post-Hercynian formations of the western Tauern Window: sedimentological features, depositional environment, and age. Mitteilungen der österreichischen Geologischen Gesellschaft, 71/72, 49-63.

Frisch, W., Gommeringer. K., Kelm. U. & Popp. F. (1987) The Upper Bündner Schiefer of the Tauern Window - A Key to Understanding Eoalpine Orogenic Processes in the Eastern Alps. In: H.W. Flügel & P. Faupl (Eds.). Geodynamics of the Eastern Alps. Deuticke Vienna, 55-69.

Frisch, W., Kuhlemann, J., Dunkl, I. & Brügel, A. (1998) Palinspastic reconstruction and topographic evolution of the Eastern Alps during late Cenozoic tectonic extrusion. Tectonophysics, 297, 1–15.

Frisch, W., Dunkl., I. & Kuhlemann, J. (2000) Post-collisional orgogen-parallel large-scale extension in the Eastern Alps. Tectonophysics, 327, 239-265.

Froitzheim, N. & Eberli, G.P. (1990) Extensional detachment faulting in the evolution of a Tethys passive continental margin, eastern Alps, Switzerland. Geological Society of America Bulletin, 102, 1297–1308.

Froitzheim, N., Schmid, S.M. & Conti, P. (1994) Repeated change from crustal shortening to orogen-parallel extension in the Austroalpine units of Graubünden. Eclogae geologicae Helvetiae, 87, 559-612.

Froitzheim, N., Schmid, S.M. & Frey, M. (1996) Mesozoic paleogeography and the timing of eclogite-facies metamorphism in the Alps: A working hypothesis. Eclogae geologicae Helvetiae, 89, 81-110.

Froitzheim, N. & Manatschal, G. (1996) Kinematics of Jurassic rifting, mantle exhumation, and passive margin formation in the Austroalpine and Penninic nappes (eastern Switzerland). Bulletin of the Geological Society of America, 108, 1120-1133.

Froitzheim, N., Plasienka, D. & Schuster, R. (2008) Alpine tectonics of the Alps and Western Carapathians. In: T. McCann, T. (Ed.). The geology of Central Europe. Geological Society London, 1141-1232.

Fuchs, G. & Linner, M. (2005) Die geologische Karte der Sadnig-Gruppe: Ostalpines Kristallin in Beziehung zur Matreier Zone. Jahrbuch der Geologischen Bundesanstalt, 145, 293-301.

Fuchs, G., Linner, M. & Heinisch, H. (1996) Geologische Karte der Sadnig-Gruppe. Jahrbuch der Geologischen Bundesanstalt, 145/3&4. Geologische Bundesanstalt Wien.

Fügenschuh, B., Seward, D. & Mantckelow, N.S. (1997) Exhumation in a convergent orogen: the western Tauern Window. Terra Nova, 9, 213–217.

Fügenschuh, B., Mancktelow, N.S. & Seward, D. (2000) Cretaceous to Neogene cooling and exhumation history of the Oetztal-Stubai basement complex, eastern Alps: A structural and fission track study. Tectonics, 19, 905-918.

Fügenschuh, B., Mancktelow, N.S. & Schmid, S.M. (2012) Comment on Rosenberg and Garcia: Estimating displacement along the Brenner Fault and orogen-parallel extension in the Eastern Alps. International Journal of Earth Sciences, 101, 1451-1455.

Genser, J. & Neubauer, F. (1989) Low angle normal faults at the eastern margin of the Tauern Window (Eastern Alps). Mitteilungen der österreichischen Geologischen Gesellschaft, 81, 233–243.

Gerya, T.V., Stöckhert, B. & Perchuk, A.L. (2002) Exhumation of high-pressure metamorphic rocks in a subduction channel: A numerical simulation. Tectonics, 21/6, 1056, doi:10.1029/ 2002TC001406.

Gleissner, P., Glodny, J. & Franz, G. (2007) Rb-Sr isotopic dating of pseudomorphs after lwasoniteinmetabasalts from the –glockner nappe, Tauern Window, Eastern Alps. European Journal of Mineralogy, 19, 723-734.

Glodny, J., Ring, U., Kühn, A., Gleissner, P. & Franz, G. (2005) Crystallization and very rapid exhumation of the youngest Alpine eclogites (Tauern Window, Eastern Alps) from Rb/Sr mineral assemblage analysis. Contributions to Mineralogy and Petrology, 149, 699-712.

Glodny, J., Ring, U. & Kühn, A. (2008) Coeval high-pressure metamorphism, thrusting, strike-slip, and extensional shearing in the Tauern Window, Eastern Alps. Tectonics, 27, TC4004, doi:10.1029/2007TC002193.

Gradstein, F., Ogg, J. & Smith, A.G. (2004) A Geologic Time Scale. Cambridge University Press Cambridge 589 pp.

Grasemann, B. & Mancktelow, N.S. (1993) Two-dimensional thermal modeling of normal faulting: the Simplon Fault Zone, Central Alps, Switzerland. Tectonophysics, 225, 155-165.

Grenerczy, G., Sella, G., Stein, S. & Kenyeres, A. (2005) Tectonic implications of the GPS velocity field in the northern Adriatic region. Geophysical Research Letters, 32, doi:10.1029/ 2005GL022947.

Grew, E.S. (1974) Carbonaceous material in some metamorphic rocks of New England and other areas. Journal of Geology, 82, 50-73.

Gruber, T., Waldeck-Zerda, T. & Gerspacher, M. (1994) Raman studies of heat-treated carbon blacks. Carbon, 32, 1377-1382.

Grundmann, G. & Morteani, M. (1985) The young uplift and the thermal history of the central Eastern Alps (Austria, Italy). Evidence from Apatite Fission Track Ages. Jahrbuch der Geologischen Bundesanstalt, 128, 197-216.

Guedes, A. ,Noronha, F. & Prieto, A.C. (2005) Characterisation of dispersed organic matter from lower Palaeozoic metasedimentary rocks by organic petrography, X-ray diffraction and micro-Raman spectroscopy analyses. Inernational Journal of Coal Geology, 62, 237-249.

Haas, J., Kovacs, S., Krystin, L. & Lein, R. (1995) Significance of Late Permian-Triassic facies zones in terrane reconstructions in the Alpine-North Pannonic domain. Tectonophysics, 242, 19-40.

Habler, G., Thöni, M. & Sölva, H. (2006) Tracing the high pressure stage in the polymetamorphic Texel Complex (Austroalpine basement unit, Eastern Alps): P–T–t–d constraints. Mineralogy and Petrology, 88, 269–296.

Handy, M.R. & Oberhänsli, R. (2004) Metamorphic structure of the Alps, age map of the metamorphicstructure of the Alps – tectonic interpretation and outstanding problems, in

Explanatory Notes to the map: Metamorphic Structure of the Alps, (Eds.). Oberhänsli, R. Mitteilungen der Österreichischen Mineralogischen Gesellschaft, 149, 201-226.

Handy, M.R., Herwegh, M. & Regli, C. (1993) Die Tektonische Entwicklung der westlichen Zone von Samedan (Oberhalbstein, Graubünden). Eclogae Geologicae Helvetiae, 86, 785–817.

Handy, M.R., Herwegh, M., Kamber, B., Tietz, R. & Villa, I. (1996) Geochronologic, petrologic and kinematic constraints on the evolution of the Err-Platta boundary, part of a fossil continent–ocean suture in the Alps (eastern Switzerland). Schweizerische Mineralogische und Petrographische Mitteilungen, 76, 453–474.

Handy, M.R., Franz, L., Heller, F., Janott, B. & Zurbriggen, R. (1999) Multistage accretion and exhumation of the continental crust (Ivrea crustal section, Italy and Switzerland). Tectonics, 18(6), 1154-1177.

Handy, M.R., Babist, J., Rosenberg, C.L., Wagner, R. & Konrad, M. (2005) Decoupling and is relation to strain partitioning in continental lithosphere – Insight from the Periadriatic fault system (European Alps). In: Deformation Mechanism, Rheology and Tectonics, edited by Gapais, D., Brun, J.P. & Cobbold, P.R. Geological Society of London Special Publication, 243, 249-276.

Handy, M. R., Schmid, S.M., Bousquet, R., Kissling, E. & Bernoulli, D. (2010) Reconciling plate-tectonic reconstructions of Alpine Tethys with the geological–geophysical record of spreading and subduction in the Alps. Earth-Science Reviews, 102, 121–158.

Harris, T.M. (1981) Diffusion of 40Ar in hornblende. Contributions to Mineralogy and Petrology, 78, 324-331.

Harrison, M.T., Célérier, J., Aikman, A.B., Hermann, J. & Heizler, M.T. (2009) Diffusion of 40Ar in muscovite. Geochemica et Cosmochimica Acta, 73, 1039-1051.

Häusler, H. (1988) Unterostalpine Jurabreccien in Österreich. Versuch einer sedimentologischen und paläogeographischen Analyse nachtriadischer Breeccienserien im unterostalpinen Rahmen des Tauernfensters (Salzburg.Tirol). Jahrbuch der Geologischen Bundesanstalt, 131, 21-125.

Häusler, H. (1995) Map sheet Muhr (Blatt 156) 1:50.000, edited by H. Häusler and mapped by W. Demmer, C. Exner, H. Häusler und A. Tollmann. Geologische Bundesanstalt Wien.

Heinisch, H. & Schmidt, K. (1984) Zur Geologie des Thurntaler Quarzphyllits und des Altkristallins südlich des Tauernfensters (Ostalpen, Südtirol). Geologische Rundschau, 73, 113-129.

Hejl, E. (1997) “Cold spots” during the Cenozoic evolution of the Eastern Alps: thermochronological interpretation of apatite fission-track data. Tectonophysics, 272, 159-172.

Herwartz, D., Nagel, T.J., Münker, C., Scherer, E.E. & Froitzheim, N. (2011) Tracing two orogenic cycles in one eclogite sample by Lu–Hf garnet chronometry. Nature Geoscience, 4/3, 178-183.

Herwartz, D., Nagej. T.J., Sandmann, S., Brovarone, A.V., Rexroth, S., Rojas-Agramonte, Y., Froitzheim, N., Kröner, A., Skublov, S.G. & Münker, C. (2012) Traditional applications and novel approaches in Lu-Hf geochronology. Geophysical Research Abstract, 14, EGU2012-9123, Vienna.

Höck, V. (1980) Distribution maps of inerals of the Alpine metamorphism in the Penninic Tauern window, Austria. Mitteilungen österreichischer geologische Gesellschaft, 71/72, 119-127.

Höck, V. (1993) The Habach-Formation and the Zentralgneis - a key in understanding the Palaeozoic evolution of the Tauern Window (Eastern Alps). In: von Raumer, J., Neubauer, F. (Eds.). Pre-Mesozoic Geology in the Alps. Springer, Berlin, 361-374.

Hohenegger, J., Rögl, F., Coric, S., Pervesler P., Lirer, F., Roetzel, R., Scholger, R. & Stingl, K. (2009) The Styrian Basin: A key to the Middle Miocene (Badenian/Langhian) Central Paratethys transgressions. Austrian Journal of Earth Sciences, 102, 102-132.

Hoinkes, G. & Thöni, M. (1987) New findings of eclogites within the eoalpine amphibolite grade area of the Ötztal basement. Terra Cognita, 7, 96.

Hoinkes, G., Koller, F., Rantitsch, G., Dachs, E., Höck, V., Neubauer, F. & Schuster, R. (1999) Alpine metamorphism of the Eastern Alps. Schweizerische Mineralogische und Petrographische Mitteilungen, 79, 1155-181.

Hoke, L. (1990) The Altkristallin of the Kreuzeck Mountains, SE Tauern Window, Eastern Alps - Basement Crust in a Convergent Plate Boundary Zone. Jahrbuch der Geologischen Bundesanstalt Wien, 133, 5-87.

Holtz, F., Johannes, W., Tamic, N. & Behrens, H. (2001) Maximum and minimum water contents of granitic melts generated in the crust: a reevaluation and implications. Lithos, 56, 1-14.

Hölzel, M., Wagreich, M., Faber, R. & Strauss, P. (2008) Regional subsidence analysis in the Vienna Basin (Austria). Austrian Journal of Geosciences, 101, 88-98.

Horváth, F. (1993) Towards a mechanical model for the formation of the Pannonian basin. Tectonophysics, 226, 333-357.

Horváth, F., Dövényi, P., Szalay, Á. & Royden, L.H. (1988) Subsidence, thermal and maturation history of the Great Hungarian Plain. In: Royden, L.H. & Horváth, F. (Eds.). The Pannonian Basin: a Case Study in Basin Evolution. American Association Petroleum Geology Memoirs, 45, 355-372.

Horváth, F., Bada, G., Szafián, P., Tari, G., Ádám, A. & Cloetingh, S. (2006) Formation and deformation of the Pannonian Basin: constraints from observational data. In: D.G. Gee & R. Stephenson (Eds.). European Lithosphere dynamics. Geological Society London Memoirs, 32, 191–206.

Hoschek, G. (2001) Thermobarometry of metasediments and metabasites from the Eclogite zone of the Hohe Tauern, Eastern Alps, Austria. Lithos, 59, 127-150.

Hottinger, A. (1935) Geologie der Gebirge zwischen der Sonnblick-Hocharn-Gruppe und dem Dalzachtal in den östlichen Hohen Tauern. Eclogae geologicae Helvetiae, 28, 249-268.

Inger, S. & Cliff, R.A. (1994) Timing of metamorphism in the Tauern Window, Eastern Alps: Rb-Sr ages and fabric formation. Journal of Metamorphic Geology, 12, 695–707.

Ishizuka, O. (1998) Vertical and horizontal variations of the fast neutron flux in a single irradiation capsule and their significance in the laser-heating 40Ar/39Ar analysis: Case study for the hydraulic rabbit facility of the JMTR reactor, Japan. Geochemical Journal, 32, 243-252.

Ishizuka, O., Yuasa, M. & Uto, K. (2002) Evidence of porphyry copper-type hydrothermal activity from a submerged remnant back-arc volcano of the Izu-Bonin arc: implication for the volcanotectonic history of back-arc seamounts. Earth and Planetary Science Letters, 198, 381-99.

Itaya, T. (1981) Carbonaceous material in politic schists of the Sanbagawa metamorphic belt in central –shikoku, Japan. Lithos, 14, 215-224.

Jäger, E., Niggli, E. & Wenk, E. (1967) Rb-Sr Altersbestimmungen an Glimmern der Zentralalpen. Beitrag zur Geologischen Karte der Schweiz, 134, 67.

Jawhari, T., Roid, A. & Casado, J. (1995) Raman spectroscopy characterization of some commercially available carbon black materials. Carbon, 33, 1561-1565.

Johnson, M.R.W. (2002) Shortening budgets and the role of continental subduction during the India-Asia collision. Earth Sciences Reviews, 59, 101-123.

Jeanbourquin, P. & Burri, M. (1991) Les metasediments du Pennique inférieur dans la région de Brigue-Simplon–Lithostratigraphie, structure et contexte geodynamique dans le basin Valaisan. Eclogae Geologicae Helvetiae, 84, 463–481.

Kebede, T., Klötzli, U.S. & Pestal, G. (2003) Single zircon U-Pb geochronology of pre-variscan and variscan basement units of the central Tauern window, Eastern Alps (Austria). Mitteilungen der Österreichischen Mineralogischen Gesellschaft, 148, 182-184.

Kebede, T., Klötzli, U., Koster, J. & Skiöld, T. (2005) Understanding the pre-Variscan and Variscan basement components of the central Tauern Window, Eastern Alps (Austria): constraints from single zircon U-Pb geochronology. International Journal of Earth Sciences, 94, 336-353.

Kelley, S.P., Arnaud, N.O. & Turner, S.P. (1994) High spatial resolution $^{40}Ar/^{39}Ar$ investigations using an ultra-violet laser probe extraction technique. Geochemica et Cosmochimica Acta, 58, 3519-3525.

Kiessling, W. (1992) Paleontological and facial features of the Upper Jurassic Hochstegen Marble (Tauern Window, eastern Alps). Terra Nova, 4, 184–197.

Kissling, E., Schmid, S.M., Lippitsch, R., Ansorge, J. & Fügenschuh, B. (2006) Lithosphere structure and tectonic evolution of the Alpine arc: new evidence from high-resolution teleseismic tomography. In: D.G. Gee & R.A. Stephenson (Eds.). European Lithosphere dynamics. European Lithosphere Dynamics Geological Society of London Memoirs, 32, 129-145.

Klebelsberg, R. (1940) Ein Ammonit aus dem Hochstegenkalk des Zillertals (Tirol). Zeitschrift der Deutschen Geologischen Gesellschaft, 92, 582-586.

Kleinschrodt, R. (1987) Quarzkorngefügeanalyse im Altkristallin südlich des westlichen Tauernfensters (Südtirol/Italien). Erlanger geologische Abhandlungen, 114, 1–82.

Kober, L. (1922) Das östliche Tauernfenster. Denkschrift der Akademie der Wissenschaften Wien, Mathematisch-Naturwissenschaftliche Klasse Kl. 98.

Koller, F. & Pestal, G. (2003) Die ligurischen Ophiolite der Tarntaler Berge und der Matreier Schuppenzone. In: M. Rockenschaub (Ed.). Arbeitstagung 2003 der Geologischen Bundesanstalt Trins im Gschnitztal. Geologische Bundesanstalt Wien, 65-76.

Krenn, K., Kurz, W., Fritz, H. & Hoinkes, G. (2011) Eoalpine tectonics oft he Eastern Alps: implications from the evolution of monometamorphic Austroalpine units (Schneeberg and Radenthein Complex). Swiss Journal of Earth Sciences, 104, 471-491, doi:10.1007/s00015-011-0087-8.

Kribek, B., Hrabal, J., Landais, P. & Hladikova, J. (1994) The association of poorly ordered graphite, coke and bitumens in greenschist facies rocks of the Ponikla Group, Lugicum, Czech Republic: the results of graphitization on various types of carbonaceous matter. Journal of Metamorphic Geology, 12, 493-503.

Kurz, W. (2005) Comment on „Tectonic map and overall architecture of the Alpine orogen“ by S.M. Schmid, B. Fügenschuh, E. Kissling & R. Schuster. Eclogae geologicae Helvetiae, 97, 93–117. Eclogae geologicae Helvetiae, 98, 97-98.

Kurz, W. (2006) Penninic Paleogeography from the Western toward the Eastern Alps—still open questions? International Geology Review, 48, 996–1022.

Kurz, W. & Neubauer, F. (1996) Deformation partitioning during updoming of the Sonnblick area in the Tauern Window (Eastern Alps, Austria). Journal of Structural Geology, 18, 1327-1343.

Kurz, W., Neubauer, F. & Genser, J. (1996) Kinematics of Penninic nappes (Glockner nappe and basement-cover nappes) in the Tauern Window (Eastern Alps) during subduction and Penninic-Austroalpine collision. Eclogae geologicae Helvetiae, 89, 573-605.

Kurz, W., Neubauer, F., Genser, J. & Dachs, E. (1998a) Alpine geodynamic evolution of passive and active continental margin sequences in the Tauern Window (eastern Alps, Austria, Italy): a review. Geologische Rundschau, 87, 225-242.

Kurz, W., Neubauer, F. & Dachs, E. (1998b) Eclogite meso- and microfabrics: implications for the burial and exhumation history of eclogites in the Tauern Window (Eastern Alps) from P-T-d paths. Tectonophysics, 285, 183–209.

Kurz, W., Neubauer, F., Genser, J., Unzog, W. & Dachs, E. (2001) Tectonic Evolution of Penninic Units in the Tauern Window during the Palaeogene: Constraints from Structural and Metamorphic Geology. In: W.E. Piller & M. Rasser (Eds.). Paleogene of the Eastern Alps: Österreichische Akademisch wissenschaftliche, Schriftenreihe der erdwissenschaftlichen Kommission, 14, 11–56.

Kurz, W., Handler, R. & Bertoldi, C. (2008) Tracing the exhumation of the Eclogite Zone (Tauern Window, Eastern Alps) by 40Ar/39Ar dating of white mica in eclogites. Swiss Journal of Geosciences, 101, Supplement 1, S191-S206.

Kurz, W., Wölfler, A., Rabitsch, R. & Genser, J. (2011) Polyphase movement on the Lavanttal Fault Zone (Eastern Alps): reconciling the evidence from different geochronological indicators. Swiss Journal of Geosciences, 104, 323-343.

Lahfid, A., Beyssac, O., Deville, E., Negro, F., Chopin, C. & Goffé, B. (2010) Evolution of Raman spectrum of carbonaceous material in low-grade metasediments of the Glarus Alps (Switzerland). Terra Nova, 22, 354-360, doi:10.1111/j.1365-3121.2010.00956.x.

Lammerer, B. (1986) Das Autochthon im westlichen Tauernfenster. Jahrbuch der Geologischen Bundesanstalt, 129, 51-67.

Lammerer, B. & Weger, M. (1998) Footwall uplift in an orogenic wedge: the Tauern Window in the Eastern Alps of Europe. Tectonophysics, 285, 213-230.

Lammerer, B., Gebrande, H., Lüschen, E. & Vesela, P. (2008) A crustal-scale cross-section through the Tauern Window (eastern Alps) from geophysical and geological data. In: S. Siegesmund, B. Fügenschuh & N. Froitzheim (Eds.). Tectonic Aspects of the Alpine-Dinaride-Carpathian System. Geological Society London Special Publications, 298, 219-229.

Lammerer, B., Selverstone, J. & Franz, G. (2011) Field trip to the Tauern Window region along the TRANSALP seismic profile, Eastern Alps, Austria. In: S. Carena & A.M. Friedrich (Eds.). Geological Society of America Field Guide, 22, 1–20.

Landis, C.A. (1971) Graphitization of dispersed carbonaceous material in metamorphic rocks. Contributions to Mineralogy and Petrology, 30, 34-45.

Large, D.J., Christy, A.G. & Fallick, A.E. (1994) Poorly crystalline carbonaceous matter in high grade metasediments: implications for graphitization and metamorphic fluid composition. Contributions to Mineralogy and Petrology, 116, 108-116.

Laubscher, H.P.V. (1971) Das Alpen-Dinariden-Problem und die Palinspastik der südlichen Tethy. International Journal of Earth Sciences, 40, 813-833.

Laubscher, H.P.V. (1988) The arcs of the Western Alps and the North Apennines: an updated view. Tectonophysics, 146(10), 67-78.

Lemoine, M., Bailot, G & Tricart, P. (1987) Ultramafic and gabbroic ocean floor of the Ligurian Tethys (Alps, Corsica, Apennines): in search of a genetic model. Geology, 15, 622-625.

Lemoine, M. (2003) Schistes lustrés from Corsica to Hungary: back to the original sediments and tentative dating of partly azoic metasediments. Bulletin de la Société géologique de France, 174/3, 197-209.

Lenkey, L. (1999) Geothermics of the Pannonian Basis and its bearing on the tectonics of Basin volution. PhD thesis, Vrije Universiteit, Amsterdam

Lerchbauer, L. (2008) Petrographical, geochemical and geochronological investigations on the Variscan basement in the Kleinelendtal/Hohe Tauern (eastern Tauern Window, Austria). Diploma-thesis, Universität Wien, 117pp.

Lerchbaumer, L., Kloetzli, U. & Pestal, G. (2010) Schists and amphibolites of the Kleinelendtal (Ankogel-Hochalm-Gruppe / Hohe Tauern, Austria) / New insights on the Variscan basement in the Eastern Tauern Window. Austrian Journal of Earth Scineces, 103/2, 138-152.

Lespade, P., Marchand, A., Couzi, M. & Cruege, F. (1984) Charactérisation de matéeriaux carbonés par microspectrométrie Raman. Carbon, 22, 375-85.

Linzer, H.-G., Decker, K., Peresson H., Dell'Mour, R. & Frisch, W. (2002) Balancing lateral orogenic float of the Eastern Alps. Tectonophysics, 354, 211 –237.

Lippitsch, R., Kissling, E. & Ansorge, J. (2003) Upper mantle structure beneath the Alpine orogen from high-resolution teleseismic tomography. Journal of Geophysical Research, 108, B8, 2376, doi:10.1029/2002JB002016.

Liu, Y., Genser, J., Handler, R., Friedl, G. & Neubauer F. (2001) 40Ar/39Ar muscovite ages from the Penninic-Austroalpine plate boundary, Eastern Alps. Tectonics, 20, 526-547.

Loprieno, A., Bousquet, R., Bucher, S., Ceriani, S., Dalla Torre, F.H., Fügenschuh, B. & Schmid, S.M. (2011) The Valais units in Savoy (France): a key area for understanding the palaeogeography and the tectonic evolution of the Western Alps. International Journal of Earth Sciences, 100, 963–992.

Loth, G., Eichhorn, R., Höll, R. & Kennedy, A. (1997) Age and evolution of the Stubach Group (Tauern Window, Eastern Alps): U-Pb-SHRIMP results of zircons from several gneiss types. Berichte der Deutschen Mineralogischen Gesellschaft, 9, 230.

Luciani, V. & Silvestrini, A. (1996) Planktonic foraminiferal biostratigraphy and paleoclimatology of the Oligocene/Miocene transition from the Monte Brione Formation (Northern Italy, Lake Garda). Memorie di Scienze Geologiche, 48, 155-169.

Lüschen, E., Borrini, D., Gebrande, H., Lammerer, B., Millahn, K., Neubauer, F., Nicolich, R. & TRANSALP Working Group (2006). TRANSALP—deep crustal Vibroseis and explosive seismic profiling in the Eastern Alps. Tectonophysics, 414, 9 –38.

Luth, S.W. & Willingshofer, E. (2008). Mapping of the post-collisional cooling history of the Eastern Alps. Swiss Journal of Geosciences, 101, Supplement 1, 207-223.

Maluski, H. & Monié, P. (1988) $^{40}Ar/^{39}Ar$ laser-probe multidating inside single biotites of a Variscan orthogneiss (Pinet Massif Central, France). Chemical Geology, 73, 245-263.

Mancktelow, N.S., Stöckli, D.F., Grollimund, B., Müller, W., Fügenschuh, B., Viola, G., Seward, D. & Villa, I.M. (2001). The DAV and Periadriatic fault system in the Eastern Alps south of the Tauern Window. International Journal of Earth Sciences, 90, 593-622.

Márton, E., Drobne, K., Ćosović, V. & Moro, A. (2003) Palaeomagnetic evidence for Tertiary counterclockwise rotation of Adria. Tectonophysics, 377, 143-156.

Márton, E., Zampien, D., Kázmér, M., Dunkl, I. & Frisch, W. (2011) New Paleocene-Eocene paleomagnetic results from the foreland of the Southern Alps confirm decoupling of stable Adria from the African plate. Tectonophysics, 504, 89-99.

Massironi, M., Zampieri, D. & Caporali, A. (2006) Miocene to present major fault linkages through the Adriatic indenter and the Austroalpine-Penninic collisional wedge (Alps of NE Italy). In: G. Moratti, A. Chalouan (Eds.).Tectonics of the Western Mediterranean and North Africa. Geological Society of London Special Publications, 262, 245-258.

Mattern, F. & Wang, P. (2008) Out-of-sequence thrusts and paleogeography of the Rhenodanubian Flysch Belt (Eastern Alps) revisited. International Journal of Earth Sciences, 97, 821-833.

McDougall, I. & Harrison, M.T. (1999) Geochronology and Thermochronology by the $^{40}Ar/^{39}Ar$ Method. Oxford University Press, Oxford, 269 pp.

Means, W.D. (1989) Stretching faults. Geology, 17, 893-896.

Means, W.D. (1990) One-dimensional kinematics of stretching faults. Journal of Structural Geology, 12(2), 267-272.

Merihue, C. & Turner, G. (1966) Potassium-Argon Dating by Activation with Fast Neutrons. Journal of Geophysical Research, 71, 2852-2857.

Miller, C. & Thöni, M. (1997) Eo-Alpine eclogitisation of Permian MORB-type gabbros in the Koralpe (Eastern Alps, Austria): New geochronological, geochemical and petrological data. Chemical Geology, 137, 283–310.

Miller, C., Satir, M. & Frank, W. (1980) High-pressure metamorphism in the Tauern Window. Mitteilungen der österreichischen Geologischen Gesellschaft, 71/72, 89– 97.

Miller, C., Konzett, J., Tiepolo, M., Armstrong, R.A. & Thöni, M. (2007) Jadeite-gneiss from the Eclogite Zone, Tauern Window, Eastern Alps, Austria: Metamorphic, geochemical and zircon record of a sedimentary protolith. Lithos, 93, 68-88.

Milnes, A.G. (1974) Structure of the Pennine zone (Central Alps): a new working hypothesis. Bulletin of the Geological Society of America, 85, 1727–1732.

Müller, W., Prosser, G., Mancktelow, N., Villa, I., Kelley, S., Viola, G. & Oberli, F. (2001) Geochronological constraints on the evolution of the Periadriatic Fault System (Alps). International Journal of Earth Sciences, 90, 623–653.

Nagel, T. (2006) Structure of Austroalpine and Penninic units in the Tilisuna area (Eastern Rätikon, Austria): Implications for the paleogeographic position of the Allgäu and Lechtal nappes. Eclogae geologicae Helvetiae, 99, 223–235.

Nakamura, K., Fujitsuka, M. & Kitajima, M. (1990) Disorder.induced line broadening in first-order Raman scattering from graphite. Physical Review, 41, 12260-12263.

Nasdala, L., Smith, D.C., Kaindl, R. & Ziemann, M.A. (2004) Raman spectroscopy: analytical perspectives in mineralogical research. In: A. Beran and E. Libowitzky (Eds.). Spectroscopic Methods in Mineralogy. EMU Notes in Mineralogy, 6, European Mineralogical Union, Eötvös University Press, Budapest, 281-343.

Nemanich, R.J. & Solin, S.A. (1979) First- and second-order Raman scattering from finite-size crystals of graphite. Physical Review, B 20, 392-401.

Nemes, F., Neubauer, F., Cloetingh, S. & Genser, J. (1997) The Klagenfurth Basin in the EasternAlps: an intra-orogenic decoupled flexural basin. Tectonophysics, 282, 189-203.

Neubauer, F., Genser, J., Kurz, W. & Wang, X. (1999) Exhumation of the Tauern Window. Eastern Alps. Physics and Chemistry of the Earth, 24, 675-680.

Nover, G., Stoll, J.B. & von der Gönna, J. (2005) Promotion of graphite formation by tectonic stress – a laboratory experiment. Geophysical Journal International, 160, 1059-1067.

Nussbaum, C. (2000) Neogene tectonics and thermal maturity of sediments of the easternmost southern Alps (Friuli area, Italy). Ph.D. thesis, Universsité de Neuchâtel, Neuchâtel, Switzerland, 2000.

Oberhänsli, R. & Goffé, B. (2004) Explanatory notes to the map: metamorphic structure of Alps, introduction. Mitteilungen der österreichischen Mineralogischen Gesellschaft, 149, 115-123.

Oberhänsli, R., Bousquet, R., Engi, M., Goffé, B., Gosso, G., Handy, M., Höck, V., Koller, F., Lardeaux, J.-M., Polino, R., Rossi, P., Schuster, R., Schwartz, S. & Spalla I. (2004) Metamorphic structure of the Alps 1: 1'000'000. Commission for the Geological Map of the World, Paris.

Oehlke, M., Weger, M. & Lammerer, B. (1993). The "Hochfeiler Duplex" - Imbrication Tectonics in the SW Tauern Window. Abhandlungen der Geologischen Bundesanstalt Wien, 49, 107-124.

Okuyama-Kusunose, Y. & Itaya, T. (1987) Metamorphism of carbonaceous material in the Tono contact aureole, Kitakami Mountains, Japan. Journal of Metamorphic Geology, 5, 121-139.

Ortner, H. & Stingl, V. (2003) 5th Workshop of Alpine Geological Studies Field Trip Guide E1: Lower Inn valley (southern margin of the Northern Calcareous Alps, Transalp traverse). Geologische Paläontologische Mitteilungen Innsbruck, 26, 1-20.

Ortner, H., Reiter, F. & Brandner, R. (2006) Kinematics of the Inntal shear zone – sub-Tauern ramp fault system and the interpretation of the TRANSALP seismic section, Eastern Alps, Austria. Tectonophysics, 414, 241-258.

Pasteris, J.F. (1989) In situ analysis in geological thin-sections by Laser Raman microprobe microspectroscopy: a cautionary note. Applied Spectroscopy, 43, 567-570.

Paulissen, W.E., Luth, S.M., Grunert, P., Coric, S. & Harzhauser, M. (2011). Integrated high-resolution stratigraphy of a Middle to Late Miocene sedimentary sequence in the central part of the Vienna Basin. Geologica Carpathica, 62/2, 155-169.

Pestal, G., Brüggemann-Ledolter, M., Draxler, I., Eibinger, D., Eichenberger, H., Reiter, C. & Svecik, F. (1999) Ein Vorkommen von Oberkarbon in den mittleren Hohen Tauern. Jahrbuch der Geologischen Bundesanstalt, 141, 491-502.

Pestal, G., Hejl, E., E., Egger, H., van Husen, D., Linner, M., Mandl, G.W., Moser, M., Reitner, J. Rupp, C. & Schuster, R. (2005) Geologische Karte von Salzburg 1:200.000. Geologische Bundesanstalt Wien, 2005.

Pestal, G., Hejl, E., Braunstingl, R. & Schuster, R. (2009) Erläuterungen Geologische Karte von Salzburg 1 : 200.000. Land Salzburg und Geologische Bundesanstalt Wien, 1-162.

Piber, A. & Tropper, P. (2003) Preliminary Eo-Alpine thermobarometric results of the Austroalpine crystalline basement nappes in the northwest of the Tauern Window between the Zillertal and the Wipptal (Eastern Alps, Tyrol). In: M. Rockenschaub (Ed.), Arbeitstagung 2003 der Geologischen Bundesanstalt Trins im Gschnitztal. Geologische Bundesanstalt Wien, 59-64.

Pieri, M. & Groppi, G. (1981) Subsurface geological structure of the Po Plain, Italy. Program Final Geodinamics Pubblications, 414, 1-13.

Piller, W.E., Harzhauser, M. & Mandic, O. (2007) Miocene Central Paratethys stratigraphy – current status and future directions. Stratigraphy, 4, 151-168.

Poirier, J.P. (1985) Creep of Crystals – High-Temperature Deformation Processes in Metals, Ceramicsand Minerals. Cambridge University Press, Cambridge.

Pollington, A.D. & Baxter, E.F. (2010) High resolution Sm-Nd garnet geochronology reveals the uneven pace of tectonometamorphic processes. Earth and Planetary Science Letters, 293, 63-71.

Pomella, H. (2011) The Cenozoic evolution of the Giudicarie fault system (Eastern/Southern Alps, northern Italy). A geochronological, structural and paleomagnetic study. Unpublished Ph.D. thesis Universität Innsbruck, 150pp.

Pomella, H., Klötzli, U., Scholger, R., Stipp, M. & Fügenschuh, B. (2011) The Northern Giudicarie and the Meran-Mauls fault (Alps, Northern Italy) in the light of new paleomagnetic and geochronological data from boudinaged Eo-/Oligocene tonalites. International Journal of Earth Sciences, 100, 1827–1850.

Polinski, R.K. & Eisbacher, G.H. (1991) Deformation partitioning during polyphase oblique convergence in the Karawanken Mountains, southeastern Alps. Journal of Structural Geology, 14(10), 1203-1213.

Praus, O., Pecova, J., Petr, V., Babuska, V. & Plomerova, J. (1990) Magnetotelluric and seismological determination of lithosphere-asthenosphere transition in Central Europe. Physics of the Earth and Planetary Interiors, 60, 212-218.

Purdy, J.W. & Jäger, E. (1976) K-Ar ages on rock-forming minerals from the Central Alps. Memorie degli Istituti di Geolgia e Mineralogia dell'Università de Padova, 30, 33pp.

Quinn, A.W. & Glass, H.D. (1958) Rank of coal and metamorphic grade rocks of Narragansett basin of Rhode Island. Economic Geology, 53, 563-576.

Rahl, J.M., Anderson, K.M., Brandon, M.T. & Fassoulas, C. (2005) Raman spectroscopic carbonaceous material thermometry of low-grade metamorphic rocks: Calibration and application to tectonic exhumation in Crete, Greece. Earth and Planetary Science Letters, 240, 339-354.

Rantisch, G., Grogger, W., Teichert, C., Ebner, F., Hofer, C., Maurer, E.M., Schaffer, B. & Toth, M. (2004) Conversion of carbonaceous material to graphite within the Graywacke Zone of the Eastern Alps. International Journal of Earth Sciences, 93, 959, 973.

Ratschbacher, L., Neubauer, F., Schmid, S.M. & Neugebauer, J. (1989) Extension in compressional orogenic belts: the Eastern Alps. Geology, 17, 404-407.

Ratschbacher, L., Merle, O., Davy, P. & Cobbold P (1991a) Lateral extrusion in the eastern Alps, Part 1: Boundary conditions and experiments scaled for gravity. Tectonics, 10, 245-256.

Ratschbacher, L., Frisch, W., Linzer, H.-G. & Merle, O. (1991b) Lateral extrusion in the Eastern Alps, part 2: Structural analysis. Tectonics, 10, 257-271.

Ratschbacher, L., Dingeldey, Ch., Miller Ch., Hacker, B.R. & McWilliams, M.O. (2004) Formation, subduction, and exhumation of Penninic oceanic crust in the Eastern Alps: time constraints from $^{40}Ar/^{39}Ar$ geochronology. Tectonophysics, 394, 155-170.

Reinecker, J. (2000) Stress and deformation: Miocene to present-day tectonics in the Eastern Alps. Tübinger Geowissenschaftliche Arbeiten Serie A, 55, 128.

Reinecker, J. & Lenhardt, W.A. (1999) Present-day stress field and deformation in eastern Austria. International Journal of Earth Sciences, 88, 532-550.

Reiners, P.W. & Brandon, M.T. (2006) Using Thermochronology to Understand Orogenic Erosion. Annual Review of Earth Planet Sciences, 34, 419-466.

Reischenbacher, D., Rifelj, H., Sachsenhofer, R.F., Jelen, M., Ćorić, S., Gross, M. & Teichenbacher, B. (2007) Early Badenian paleoenvironment in the Lavanttal Basin (Mühldorf Formation; Austria): evidence from geochemistry and paleontology. Austrian Journal of Earth Sciences, 100, 202-229.

Reiter, F., Lenhardt, W.A. & Brandner, R. (2005) Indications for activity of the Brenner Normal Fault Zone (Tyrol, Austria) from seismological and GPS data. Austrian Journal of Earth Sciences, 97, 16-23.

Ring, U., Ratschbacher, L. & Frisch, W. (1988) Plate-boundary kinematics in the Alps: Motion in the Arosa suture zone. Geology, 16, 696-698.

Ring, U., Brandon, M., Willet, S. & Lister, G. (1999) Exhumation processes. Geological Society, London, Spcial Publication, 154(1), 1-27.

Robbins, G.A. (1972) Radiogenic argon diffusion in muscovite under hydrothermal conditions. M.Sc. Thesis, Brown University, Rhode Island.

Rockenschaub, M., Kolenprat, B. & Nowotny, A. (2003) Das westliche Tauernfenster. In: M. Rockenschaub (Ed.), Arbeitstagung 2003 der Geologischen Bundesanstalt Trins im Gschnitztal. Geologische Bundesanstalt Wien, 7-38.

Rockenschaub, M., Feijth, J. & Janda, C. (2007) Sedimentological results requiring a new tectonic framework for the NW Tauern Window. Geophysical Research Abstracts, Vol. 9, 11151. SRef-ID: 1607-7962/gra/EGU2007-A-11151.

Rockenschaub, M., Nowotny, A., Brandner, R., Fenti, V., Frisch, W., Friz, C., Frizzo, P., Kolenprat, B., Magiera, J., Prager, C., Reiser, M., Scheiber, T., Bistacchi, A., Dal Piaz, G.V., Dal Piaz, G., Massironi, M., Monoppoli, B., Schiavo, A. & Toffolon, G. (2011) Geological map sheet 175 Sterzing 1:50.000. Geologische Bundesanstalt Wien.

Rosenberg, C.L. (2004) Shear zones and magma ascent: A model based on a review of the Tertiary magmatism in the Alps. Tectonics, 23, TC3002, doi:10.1029/2003TC001526.

Rosenberg, C.L. & Schneider, S. (2008) The western termination of the SEMP Fault (eastern Alps) and its bearing on the exhumation of the Tauern Window. In: S. Siegesmund, B. Fügenschuh & N. Froitzheim (Eds.). Tectonic Aspects of the Alpine-Dinaride-Carpathian System. Geological Society London Special Publications, 298, 197-21.

Rosenberg, C.L. & Berger, A. (2009) On the causes and modes of exhumation and lateral growth of the Alps. Tectonics, 28, doi:10.1029/2008TC002442.

Rosenberg, C.L. & Garcia, S. (2011). Estimating displacement along the Brenner Fault and orogen-parallel extension in the Eastern Alps. International Journal of Earth Sciences, 100, 1129–1145.

Rosenberg, C.L. & Garcia, S. (2012) Reply to the comment of Fügenschuh et al. on the paper „Estimating displacement along the Brenner Fault and orogen-parallel extension in the Eastern Alps“ by Rosenberg & Garcia, International Journal of Earth Sciences (Geologische Rundschau), 100, 1129–1145. International Journal of Earth Sciences, 101, 1457-1464.

Rosenberg, C. L., Brun, J.-P. & Gapais, D. (2004) An indentation model of the Eastern Alps and the origin of the Tauern Window. Geology, 32, 997-1000.

Rosenberg, C.L., Brun, J.P., Cagnard, F. & Gapais, D. (2007) Oblique indentation in the Eastern Alps: Insights from laboratory experiments. Tectonics, 26, TC2003. doi:10.1029/2006TC 001960.

Royden, L.H. & Burchfield, B.C. (1989) Are systematic variations in thrust belt style related to plate boundary processes? (The western Alps versus the Carpathians). Tectonics, 8, 51-61.

Royden, L.H., Horváth, F. & Burchfield, B.C. (1982) Transform faulting, extension and subsidence in the Carpathian Pannonian region. Geological Society of America Bulletin, 73, 717-725.

Royden, L.H., Burchfield, B.C., King, R.W. & Wang, E. (1997) Surface Deformation and Lower Crustal Flow in Eastern Tibet. Science, 276, 788-790 doi:10.1126/science.276.5313.

Rück, P. & Schreurs, G. (1995) Die Schamser Decken - The Schams nappes. Teil I: Stratigraphisch-sedimentologische Untersuchungen der Schamser Decken. Part II: Geometry and Kinematics of the Schams nappes and adjacent tectonic units in the Penninic zone. Beiträge zur Geologischen Karte der Schweiz Neue Folge, 167, 199pp.

Ruppel, C., Royden, L. & Hodges, K.V. (1988) Thermal modeling of extensional tectonics: application to pressure-temperature-time histories of metamorphic rocks. Tectonics, 7(5), 947-957.

Sachsenhofer, R.F., Lankreijer, A., Cloetingh, S. & Ebner, F. (1997) Subsidence analysis and quantitative basin modeling in the Styrian Basin (Pannonian Basin System, Austria). Tectonophysics, 272, 175-196.

Sachsenhofer, R.F., Kogler, A., Polesny, H., Strauss, P. & Wagreich, M. (2000) The Neogene Fohnsdorf Basin: Basin formation and basin inversion during lateral extrusion in the Eastern Alps (Austria). Geologische Rundschau, 89, 415-430.

Sadezky A., Muckenhuber, H., Grothe, H., Niessner, R. & Pöschl, U. (2005) Raman microspectroscopy of soot and related carbonaceous materials: Spectral analysis and structural informations. Carbon, 43, 1731-1742.

Sander, B. (1911) Geologische Studien am Westende der hohen Tauern. Bericht –Denkschrift der kaiserlichen Akademie der Wissenschaften Wien, 83, 257-319.

Scharf, A., Favaro, S., Handy, M. & Schmid, S.M.: (2011) Exhumation-related structures at the eastern margin of the Tauern Window (Eastern Alps). Abstract in Volume International Conference Fragile Earth: Geological Processes from Global to Local Scales and Associated Hazards Munich, paper No. 27-6.

Scharf, A., Ziemann, M. & Handy, M.R. (2012) Peak-Temperature (Tp) estimations with Raman micro spectroscopy on carbonaceous material (RSCM) as a tool for distinguishing tectometamorphic regimes in the Tauern Window (Eastern Alps, Austria). Abstract EGU 2012-5259.

Scharf, A., Handy, M.R., Favaro, S. & Schmid, S.M. (submitted, a). Modes of orogen-parallel stretching and extensional exhumation of thickening orogenic crust in response to microplate indentation and slab roll-back (Tauern Window, Eastern Alps). International Journal of Earth Sciences.

Scharf, A., Handy, M.R. Ziemann, M.A. & Schmid, S.M. (submitted, b) Peak temperature patterns of accretion, subduction and collision preserved in the eastern subdome of the Tauern Window (Eastern European Alps) – A study with Raman microspectroscopy on carbonaceous material (RSCM).

Scharf, A., Handy, M.R., Schmid, S.M. & Sudo, M. (in prep.) Thermal evolution from orogenic doming to extensional exhumation - new perspectives from in-situ $^{40}Ar/^{39}Ar$ laser-probe ages of white mica (Tauern Window, Eastern Alps).

Schermaier, A. (1991) Geologische und Petrographische Untersuchungen zur präalpidischen Entwicklung des Tauernfensters am Ostrand des Venedigermassivs (Hohe Tauern). Jahrbuch der Geologischen Bundsanstalt Wien, 134, 345-367.

Schmid, S.M., Aebli, H.R., Heller, F. & Zingg, A. (1989) The role of the Periadriatic Line in the tectonic evolution of the Alps. Geological Society of London, Special Publication, 45, 153-171.

Schmid, S.M. & Froitzheim N. (1993) Oblique slip and block rotation along the Engadine line. Eclogae geolicae Helvetiae, 86/2, 569-593.

Schmid, S.M., Pfiffner, O.A., Froitzheim, N., Schönborn, G. & Kissling, E. (1996) Geophysical-geological transect and tectonic evolution of the Swiss-Italian Alps. Tectonics, 15, 1036-1064.

Schmid, S.M., Fügenschuh, B., Kissling, E. & Schuster, R. (2004) Tectonic map and overall architecture of the Alpine orogen. Eclogae geologicae Helvetiae, 97, 93-117.

Schmid, S.M., Fügenschuh, B., Kissling, E. & Schuster, R. (2005) Reply to Comment by W. Kurz on "Tectonic map and overall architecture of the Alpine orogen". Eclogae geologicae Helvetiae, 98, 99–101.

Schmid, S.M., Bernoulli, D., Fügenschuh, B., Matenco, L., Schefer, S., Schuster, R., Tischler, M. & Ustaszewski, K. (2008) The Alpine-Carpathian-Dinaridic orogenic system: correlation and evolution of tectonic units. Swiss Journal of Geosciences, 101(1), 139-183.

Schmid, S.M., Scharf, A., Handy, M.R. & Rosenberg, C.L. (submitted) The Tauern Window (Eastern Alps, Austria) – A new tectonic map, cross-sections and tectonometamorphic synthesis. Swiss Journal of Geosciences.

Schneider, S., Hammerschmidt, K. & Rosenberg, C.L. (submitted) Dating the life time of ductile shear zones: age constraints from $^{40}Ar/^{39}Ar$ in situ analyses. Earth and Planetary Science Letters.

Schönborn, G. (1992) Alpine tectonics and kinematic models of the central Southern Alps. Memorie di Scienze Geologiche, Istituti di Geologia e Mineralogia dell' Universita di Padova, 44, 229–393.

Schönborn, G. (1999) Balancing cross sections with kinematics constraints: The Dolomites (northern Italy). Tectonics, 18, 527-545.

Schönlaub, H.P., Exner, C. & Nowotny, A. (1976) Das Altpaläozoikum des Katschberges und seiner Umgebung (Österreich). Verhandlungen der Geologischen Bundesanstalt, 1976, 115-146

Schramm, J.M. (1980) Bemerkungen zum Metamprphosegeschehen in klastischen Sedimentgesteinen im Salzburger Abschnitt der Grauwackenzone und der Nördlichen Kalkalpen. Mitteilungen Österreichische Geologische Gesellschafft, 71/72, 379-384.

Schumacher, M.E., Schönborn, G., Bernoulli, D. & Laubscher, H.P. (1997) Rifting and collision in the Southern Alps. In: Deep Structure of the Alps: Results of NFP20. Pfiffner, O.A., Lehner, P., Heitzmann, P., Müller, S. & Steck, A. (Eds.). – Birkhäuserverlag Basel Switzerland, 380 pp.

Schuster, R. (2003) Das eo-Alpidische Ereignis in den Ostalpen: Plattentektonische Situation und interne Struktur des Ostalpinen Kristallins. In: M. Rockenschaub (Ed.), Arbeitstagung 2003 der Geologischen Bundesanstalt Trins im Gschnitztal. Geologische Bundesanstalt Wien, 141-159.

Schuster, R. & Frank W. (1999) Metamorphic evolution of the Austroalpine units east of the Tauern Window: indications for Jurassic strike slip tectonics. Mitteilungen der Gesellschaft der Geologie- und Bergbaustudenten Österreichs, 42, 37-58.

Schuster, R. & Stüwe, K. (2008) Permian metamorphic event in the Alps. Geology, 36/8, 603–606.

Schuster, R., Scharbert, S., Abart, R. & Frank W. (2001) Permo-Triassic extension and related HT/LP metamorphism in the Austroalpine – Southalpine realm. Mitteilungen der Gesellschaft der Geologie- und Bergbaustudenten Österreichs, 45, 111-141.

Schuster, R., Koller, F., Hoeck, V., Hoinkes, G. & Bousquet, R. (2004) Explanatory notes to the map Metamorphic Structure of the Alps. Mitteilungen der österreichischen Mineralogischen Gesellschaft, 149, 175-199.

Schuster, R., Pestal, G. & Reitner, J.M. (2006) Eräuterungen zu Blatt 182 Spittal an der Drau. Geologische Karte der Republik Österreich. Geologische Bundesanstalt Wien, 115pp.

Sciunnach, D., Scardia, G., Tremolada, F. & Silva, I.P. (2010) The Monte Orfano Conglomerate revisited: stratigrphic constraints on Cenozoic tectonic uplift of the Southern Alps (Lombardy, northern Italy). International Journal of Earth Sciences, 99, 1335-1355, doi10.1007/s00531-009-0452-2.

Selverstone, J. (1985) Petrological constraints on imbrication, metamorphism, and uplift in the SW Tauern Window. Tectonics, 4, 687-704.

Selverstone, J. (1988) Evidence for east–west crustal extension in the Eastern Alps: implications for the unroofing history of the Tauern Window. Tectonics, 7, 87–105.

Selverstone, J. (1993) Micro- to macroscale interactions between deformational and metamorphic processes, Tauern Window, Eastern Alps. Schweizerische Mineralogische und Petrographische Mitteilungen, 73, 229-239.

Selverstone, J. (2005) Are the Alps Collapsing? Annual Review of Earth and Planet Sciences, 33, 113-132.

Selverstone, J., Spear, F.S., Franz, G. & Morteani, G. (1984) High-pressure metamorphism in the SW Tauern Window, Austria: P-T paths from hornblende – kyanite –staurolite schists. Journal of Petrology, 25, 501-531.

Selverstone, J., Axen, G.J. & Bartley, J.M. (1995) Fluid inclusion constraints on the kinematics of footwall uplift beneath the Brenner Line normal fault, eastern Alps. Tectonics, 14, 264-278.

Senftl, E. & Exner, C. (1973) Rezente Hebung der Hohen Tauern und geologische Interpretation. Verhandlungen der Geologischen Bundesanstalt, 2, 209-234.

Shreve, R.L. & Cloos, M. (1986) Dynamics of Sediment Subduction, Melange Formation, and Prism Accretion. Journal of Geology, 35, 65-82.

Siivola, J. & Schmid, R (2007) Recommendations by the IUGS Subcommission on the Systematics of Metamorphic Rocks: List of mineral abbreviations. Web version 01.02.07. IUGS Commission on the Systematics in Petrology.

Slapansky, P. & Frank, W. (1987) Structural evolution and geochronology of the northern margin of the Austroalpine in the Northwestern Schladming Crystalline (NE Radstädter Tauern). In: Flügel, W.H. & Faupl, P. (Eds.). Geodynamics of the Eastern Alps. Deuticke Wien, 244-262.

Slejko, D., Carulli, G.B., Nicolich, R., Rebez, A., Zanferrari, A., Cavallin, A., Doglioni, C., Carraro, F., Castaldini, D., Illiceto, V., Semenza, E. & Zanolla, C. (1989) Seismotectonics of the Eastern Southern-Alps: a review. Bollettino di Geofisica Teorica ed Applicata, 31, 122, 109-136.

Söllner, F., Höll, R. & Miller, H. (1991) U-Pb-Systematik der Zirkone in Metasedimenten ("Porphyroiden") aus der Nördlichen Grauhwackenzone und dem Tauernfenster (Ostalpen, Österreich). Zeitschrift der Deutschen Geologischen Gesellschaft, 142, 285-299.

Sölva, H., Grasemann, B., Thöni, M., Thiede, R.C. & Habler, G. (2005) The Schneeberg Normal Fault Zone: Normal faulting associated with Cretaceous SE-directed extrusion in the Eastern Alps (Italy/Austria). Tectonophysics, 401, 143–166.

Spear, F.S. & Franz, G. (1986) P-T evolution of metasediments from the Eclogite Zone, south-central Tauern Window, Austria. Lithos, 19, 219-234.

Stampfli, G. (1993) Le Briançonnais: Terrain exotique dasn les Alpes? Eclogae Geologica Helvetica, 86, 1-45.

Stampfli, G., Mosar, J., Favre, P., Pillevuit, A. & Vannay, J.-C. (2001) Permo-Mesozoic evolution of the western Tethys realm: the Neo-Tethys East Mediterranean Basin connection. In: Ziegler, P.A., et al. (Eds.). Peri-Tethys Memoir 6: Peri-Tethyan Rift/Wrench Basins and Passive Margins. Mémoires du Muséum Natnional d'histoire Naturelle Paris, 186, 51-108.

Staub, R. (1924) Der Bau der Alpen. Beiträge zur Geologischen Karte der Schweiz, NF82, 272pp.

Steininger, F.F. & Wessely, G. (2000) From the Tethyan Ocean to the Paratethys Sea: Oligocene to Neogene Stratigraphy, Paleogeography and Paleobiography of the circum-Mediterranean region and the Oligocene to Neogene Basin evolution in Austria. Mitteilungen Österreichischen Geologischen Gesellschaft, 92, 95-116.

Steinmann, M. (1994) Ein Beckenmodell für das Nordpenninikum der Ostschweiz. Jahrbuch der Geologischen Bundesanstalt, 137 (4), 675-721.

Stipp, M., Stünitz, H., Heilbronner, R. & Schmid, S.M. (2002) The eastern Tonale fault zone: a natural laboratory for crystal plastic deformation of quartz over a temperature range from 250 to 700° C. Journal of Structural Geology, 24, 1861-1884.

Stipp, M., Fügenschuh B., Gromet, L. P., Stünitz H. & Schmid S. M. (2004) Contemporaneous plutonism and strike-slip faulting: A case study from the Tonale fault zone north of the Adamello pluton (Italian Alps). Tectonics, 23, TC3004, doi:10.1029/2003TC001515.

Stöckhert, B., Massonne, H-J. & Nowlan, E.U. (1997) Low differential stress during high-pressure metamorphism: The microstructural record of a metapelite from the Eclogite Zone, Tauern Window, Eastern Alps. Lithos, 41, 103–118.

Stöckli, D.F. (1995) Tectonics SW of the Tauern Window (Mauls area, Südtirol). Unpublished diploma thesis ETH Zürich, 270pp.

Strauss, P., Wagreich, M., Decker, K. & Sachsenhofer, R.F. (2001) Tectonics and sedimentation in the Fohnsdorf-Seckau Basin (Miocene, Austria): From a pull-apart basin to a half-graben. International Journal of Earth Sciences, 90, 549-559.

Sturm, R., Dachs, E. & Kurz, W. (1997) Untersuchung von Hochdruckrelikten in Grüngesteinen des Grossglocknergebietes (zentrales Tauernfenster, Österreich): Erste Ergebnisse. Zentralblatt für Geologie und Paläontologie, 3/4, 345–363.

Suchy, V., Frey, M. & Wolf, M. (1997) Vitrinite reflectance and shear-induced graphitization in orogenic belts: A case study from the Kandersteg area, Helvetic Alps, Switzerland. International Journal of Coal Geology, 34, 1-20.

Suppe, J. (1984) Kinematics of arc-continent collision, flipping of subduction, and back-arc spreading near Taiwan. Memoir of the Geological Society of China, 6, 21-33.

Sze, S.K., Siddique, N., Sloan, J.J. & Escribano, R. (2001) Raman spectroscopic characterization of carbonaceous aerosol. Atmospheric Environment, 35, 561-568.

Tapponnier, P., Peltzer, G. & Armijo, R. (1986) On the mechanics of the collision between India and Asia. Geological Society of London, Special Publication, 19, 113-157.

Takashima. R., Nishi, H., Huber, B.T. & Leckie, R.M. (2006) Greenhouse world and the Mesozoic Ocean. Oceanography, 19/4, 82-92.

Teichmüller, M. (1987) Organic material and very low-grade metamorphism. In M. Frey (Ed): Low temperature metamorphism. Black, Glasgow and London, 114-161.

Termier, P. (1903) Les nappes des Alpes Orientales et la synthèse des Alpes. Bulletin de la Societe Géologique de France, 4(3), 711-765.

Thiele, O. (1970) Zur Stratigraphie und Tektonik der Schieferhülle der westlichen Hohen Tauern. Verhandlungen der geologischen Bundesanstalt Wien, 1970, 230-244.

Thiele O. (1980) Das Tauernfenster. In: R. Oberhauser (Ed.): Der Geologische Aufbau Österreichs, 300-314, Springer Wien.

Thöni, M. (1999) A review of geochronological data from the Eastern Alps. Schweizerische Mineralogische und Petrographische Mitteilungen, 79, 209-230.

Thöni, M. (2006) Dating eclogite facies metamorphism in the Eastern Alps – approaches, results, interpretations: a review. Mineralogy and Petrology, 88, 123-148.

Töchterle, A. (2011) Aspects of the geological evolution of the northwestern Tauern Window - Insights from the geological investigations for the planned Brenner base tunnel. Unpublished PhD thesis University Innsbruck, 100pp (includes a geological-tectonic map of the westernmost Tauern Window at the scale 1:50'000).

Töchterle, A., Brandner, R. & Reiter, F. (2011) Strain partitioning on major fault zones in the northwestern Tauern Window - insights from the investigations of the Brenner base tunnel. Austrian Journal of Earth Sciences, 104, 15-35.

Tollmann, A. (1977) Geologie von Österreich. Band 1. Die Zentralalpen. Deuticke Wien, 766pp.

Tollmann, A. (1987) The alpidic evolution of the Eastern Alps. In: Flügel, H. W. & Faupl, P. (Eds.). Geodynamics of the Eastern Alps. Vienna, Austria, Deuticke Wien, 361–378.

Tomljenovic, B. & Csontos, L. (2001) Neogene-Quaternary structures in the border zone between Alps, Dinarides and Pannonian Basin (Hrvatsko zagorje and Karlovac Basins, Croatia). International Journal of Earth Sciences, 90, 560-578.

Tricart, P. (1984) From passive margin to continental collision: a tectonic scenario for the Western Alps. American Journal of Science, 284, 97-120.

Trümpy, R. (1960) Paleotectonic evolution of the Central and Western Alps. Geological Society of America Bulletin, 71, 843-908.

Trümpy, R. (1992) Ostalpen und Westalpen – Verbindendes und Trennendes. Jahrbuch der geologischen Bundesanstalt Wien, 135/4, 875-882.

Tuinstra, F. & Koenig, J.L. (1970) Raman spectrum of graphite. Journal of Chemical Physics, 53, 1126-1130.

Urbanek, C., Frank. W., Grasemann, B. & Decker, K. (2002) Eoalpine versus Tertiary deformation: Dating of heterogeneously partitoned strain (Tauern Window, Austria). Pangeo Austria: Erdwissenschaften in Österreich 28.-30.6.2002 (Program and abstract). Institute for geology and paleontology, Universität Salzburg.

Ustaszewski, K., Schmid, S.M., Fügenschuh, B., Tischler, M., Kissling, E. & Spakman, W. (2008) A map-view restoration of the Alpine-Carpathian-Dinaridic system for the Early Miocene. In: N. Froitzheim & S.M. Schmid (Eds.). Orogenic processes in the Alpine collision zone. Swiss Journal of Geosciences, 101/Supplement 1, 273–294.

Uto, K., Ishizuka, O., Matsumoto, A., Kamioka, H. & Togashi, S. (1997) Laser-heating 40Ar/39Ar dating system of the Geological Survey of Japan: system outlines and preliminary results. Bulletin of the Geological Survey of Japan, 48, 23-48.

van Bemmelen, R.W. & Meulenkamp, J.E. (1965) Beiträge zur Geologie des Drauzugs (Kärnten, Österreich). Jahrbuch der Geologischen Bundesanstalt, 108, 213-268.

Vavra, G. & Frisch, W. (1989) Pre-Variscan back-arc and island-arc magmatism in the Tauern Window (Eastern Alps). Tectonophysics, 169, 271-280.

Venzo, S. (1939) Nuovo lembo tortoniano strizzato tra le filladi ed il permiano a Stringo di Valsugana (Trentino meridionale orientale). Bulletin Society Geological Italia, 58, 175-185.

Veselá, P. & Lammerer, B. (2008) The Pfitsch-Mörchner basin, an example of the post Variscan sedimentary evolution in the Tauern Window (Eastern Alps). In: N. Froitzheim & S.M. Schmid (Eds.). Orogenic processes in the Alpine collision zone. Swiss Journal of Geosciences, 101/Supplement 1, 73–88.

Veselá, P., Lammerer, B. Wetzel, A. Söllner, F. & Gerdes, A. (2008) Post-Variscan to Early Alpine sedimentary basins in the Tauern Window (eastern Alps). In: S. Siegesmund, B. Fügenschuh & N. Froitzheim (Eds.). Tectonic Aspects of the Alpine-Dinaride-Carpathian System. Geological Society of London, Special Publications, 298, 83-100.

Veselá, P., Söllner, F., Finger, F. & Gerdes, A. (2011) Magmato-sedimentary Carboniferous to Jurassic evolution of the western Tauern Window, Eastern Alps (constraints from U-Pb zircon dating and geochemistry). International Journal of Earth Sciences, 100, 993–1027.

Villa, I.M. (1998) Isotopic closure. Terra Nova, 10, 42-47.

Villa, I.M. (2010) Disequilibrium Textures vs Equilibriúm Modelling: Geochronology at the Crossroads. In: Spalla, M.I., Marotta, A.M. & Gosso, G. (Eds.). Advances in interpretation of geological processes. Geological Society, London, Special Publications, 332, 1-15.

Villa, I.M., Hermann, J., Münthener, O. & Trommsdorff, V. (2000) $^{39}Ar/^{40}Ar$ dating of multiply zoned amphibole generations (Malenco, Italian Alps). Contribution to Mineralogy and Petrology, 140, 363-381.

Viola, G., Mancktelow, N. & Seward, D. (2001) Late Oligocene-Neogene evolution of Europe-Adria collision - New structural and geochronological evidence from the Giudicarie fault system (Italian Eastern Alps). Tectonics, 20, 999-1020.

Viola, G., Mancktelow, N., Seward, D., Meier A. & Martin, S. (2003) The Pejo fault system: An example of multiple tectonic activity in the Italian Eastern Alps. Geological Society of America Bulletin, 115, 515-532.

von Blanckenburg, F., Villa, I.M., Baur, H., Morteani, G. & Steiger, R.H. (1989) Time calibration of a PT-path from the Western Tauern Window, Eastern Alps: the problem of closure temperatures. Contributions Mineralogy and Petrology, 101, 1-11.

von Blanckenburg, F. & J. H. Davies (1995) Slab breakoff: A model for syncollisional magmatism and tectonics in the Alps. Tectonics, 14, 120–131.

Vrabec, M. & Fodor, L. (2006) Late Cenozoic tectonics of Slovenia: structural styles at the Northeastern corner of the Adriatic microplate. in Pinter, N., Grenerczy, G., Weber, J., Stein, S. & Medak, D. (Eds.). The Adria microplate: GPS geodesy, tectonics and hazards. Volume 61: Nato Scie Series, IV, Earth and Environmental Sciences Dordrecht Springer, 151-168.

Vrabec, M., Preseren, P.P. & Stopar, B. (2006) GPS study (1996-2002) of active deformation along the Periadriatic fault system in northeastern Slovenia: tectonic model. Geologica Carpathica, 57, 57-65.

Wada, H., Tomita, T., Matsuura, K., Iuchi, K., Ito, M. & Morikiyo, T. (1994) Graphitization of carbonaceous matter during metamorphism with references to carbonate and politic rocks of contact and regional metamorphism, Japan. Contributions to Mineralogy and Petrology, 118, 217-228.

Wagner, G.A. & Reimer, G.M. (1972) Fission track tectonics: the tectonic interpretation of fission track apatite ages. Earth and Planetary Science Letters, 14(2), 263-268.

Wagner, R., Rosenberg, C.L., Handy, M.R., Möbus, C. & Albertz, A. (2006) Fracture-driven intrusion and upwelling of a mid-crustal pluton fed from a transpressive shear zone −The Rieserferner Pluton (Eastern Alps). Geological Society of America Bulletin, 118, 219-237.

Waldhauser, F., Lippitsch, R., Kissling, E. & Ansorge, J. (2002) High-resolution teleseismic tomographyof upper mantle structure using an a priori three-dimensional crustal model. Geophysical Journal International, 150, 403-414.

Wang, Y., Alsmeyer, D.C. & McCreery, R.L. (1990) Raman spectroscopy of carbon materials: structural basis of observed spectra. Chemistry of Materials, 2, 557-563.

Wiederkehr, M., Bousquet, R., Schmid, S.M. & Berger, A. (2008) From subduction to collision:Thermal overprint of HP/LT ,eta-sediments in the north-eastern Lepontine Dome (Swiss Alps) and consequences regarding the tectono.metamorphic evolution ot the Alpine orogenic wedge. In: Froitzheim, N. & Schmid, S.M. (Eds.). Orogenic processes in the Alpine collision zone. Swiss Journal of Geosciences, 101, 127-155.

Wiederkehr, M., Sudo, M., Bousquet, R., Berger, A. & Schmid, S.M. (2009) Alpine orogenic evolution from subduction to collisional thermal overprint: The 40Ar/39Ar age constraints from the Valaisan Ocean, Central Alps. Tectonics, 28, TC6009:1-28, doi:10.1029/2009TC00 2496.

Wiederkehr. M., Bousquet, R., Ziemann, M.A., Berger, A. & Schmid, S.M. (2011) 3-D assessment of peak-metamorphic conditions by Raman spectroscopy of carbonaceous material: an example from the margin of the Lepontine dome (Swiss Central Alps). International Journal of Earth Sciences, 100, 1029-1063.

Winkler, W. & Bernoulli D. (1986) Detrital high-pressure/low-temperature minerals in a late Turonian flysch sequence of the eastern Alps (western Austria): Implications for early Alpine tectonics. Geology, 14, 598-601.

Wölfler, A., Dekant, C., Danisik, M., Kurz, W., Dunkl, I., Putis, M. & Frisch, W. (2008) Late stage differential exhumation of crustal blocks in the central Eastern Alps: evidence from fission track and (U-Th)/He thermochronology. Terra Nova, 20, 378-384.

Wölfler, A., Kurz, W., Danisik, M. & Rabitsch, R. (2010) Dating of fault zone activity by apatite fission track and apatite (U-Th)/He thermochronometry: A case study from the Lavanttal fault system (Eastern Alps). Terra Nova, 22, 274-282.

Wölfler, A., Kurz, W., Fritz, H. & Stüwe, K. (2011) Lateral extrusion in the Eastern Alps revisited: Refining the model by thermochronological, sedimentary, and seismic data. Tectonics, 30, TC4006, doi:10.1029/2010TC002782.

Wopenka, B. (1991) Raman-spectra of graphite as indicators of degree of metamorphism. Canadian Mineralogist, 29, 1-9.

Wopenka, B. & Pasteris, J.D. (1993) Structural characterization of kerogens to granulite-facies graphite – Applicability of Raman microprobe spectroscopy. American Mineralogist, 78, 533-447.

Yui, T.F., Huang, E. & Xu, J. (1996) Raman spectrum of carbonaceous material: A possible metamorphic grade indicator for low-grade metamorphic rocks. Journal of Metamorphic Geology, 14, 115-124.

Zanchi, A., D'Adda, P., Zanchetta, S. & Berra, F. (2012) Syn-thrust deformation across a transverse zone (central Southern Alps, N. Italy). Swiss Journal of Geosciences, 105, 19-38.

Zeilinger, G. (1997) Das Tamsweger Tertiär: Fazies und Deformation eines intramontanen Beckens und seine regionale geodynamische Bedeutung. Unpublished Diplomas Thesis, Universität Tübingen, 69pp.

Ziegler, P. (1992) Plate tectonics, plate moving mechanisms and rifting. Tectonophysics, 215, 9-34.

Zimmermann, R., Hammerschmidt, K. & Franz, G. (1994) Eocene High Pressure Metamorphism in the Penninic Units of the Tauern Window (Eastern Alps) - Evidence from Ar40-Ar39 Dating and Petrological Investigations. Contributions to Mineralogy and Petrology, 117, 175–186.

Appendix

A-1 Additional information to Chapter 3

A-1.1 Samples used in the RSCM study

Table A-1 listed all 200 samples, including locations, tectonic units, mineral assemblages, Raman spectra ratios (R1 and R2, see discussion in section 3.3) and peak temperatures with their confidence intervals used in the RSCM study.

Table A-1: List of all RSCM samples analyzed and discussed in section 3.2.1., shown in Figure 3.3. Numbers for tectonic units (#) are taken from Schmid et al. (submitted), Chapter 5: Si(23) - post-Variscan cover; Mo(20) - Modereck Nappe System; Gl(19) - Glockner Nappe System; Ma(17) - Matrei Zone; HN(16) - Hochfeind Nappe (Lower Austroalpine); KQ(11) - Katschberg Quartzphyllite Unit (Upper Austroalpine); KWN(10) - Koralpe-Wölz Nappe System (Upper Austroalpine); GW(4) - Grauwackenzone (Upper Austroalpine). Minerals found in a given sample are listed in order of decreasing modal abundance. Number of recorded Raman spectra (# spec.) R1 and R2 ratios (mean value and standard deviation SD), are RSCM-inferred mean temperature and uncertainty given for the 95% confidence interval (CI). Temperature uncertainty was determined by dividing the standard deviation of the measurement by the square root of the number of measurements, multiplied by a parameter whose value depends on the number of measurements as well as on the chosen confidence interval. Samples highlighted in red letters are not used to define the iso-temperature contours (see section 3.4.1 for discussion). Last four columns show peak temperatures and CI values for calibrations a – Beyssac et al. 2002b; b – Aoya et al. 2010; c – Aoya et al. 2010; and d – Rahl et al. 2005; as listed in Table 3.1.

Table A-1: List of allRSCM samples

#	Sample	GPS coordinates		elev.	Tectonic		#	R1		#	R2		a		b		c		d	
	name	N	E	[m]	unit	Mineral assemblage	spec. R1	Mean	SD	spec. R2	Mean	SD	T(°C)	CI	T(°C)	CI	T(°C)	CI	T(°C)	CI
1	AS1	47°03'14,2"	13°35'11,6"	1965	Gl(19)	Qtz, Cal, Wmca, Grt	9	0.41	0.1	9	0.37	0.05	475	9.8	456	10.5	481	10.0	465	8.06
2	AS30ab	47°03'13,3"	13°34'19,0"	2194	Mo(20)	Ab, Wmca, Qtz	18	0.40	0.07	18	0.38	0.03	471	6.4	444	9.4	477	7.1	461	6.88
2	AS30noab	47°03'13,3"	13°34'19,0"	2194	Mo(20)	Ab, Wmca, Qtz	16	0.31	0.06	16	0.36	0.04	483	9.1	450	14.4	479	10.2	463	9.75
3	AS32	47°03'15,8"	13°34'02,6"	2233	Mo(20)	Qtz, Ab, Wm	17	0.27	0.06	17	0.31	0.03	505	7.7	491	12.3	497	12.4	479	10.9
4	AS36	46°59'23,8"	13°33'20,1"	2162	GN (19)	Qtz, Wmca, Grt, Bt, Chl	5	0.30	0.07	5	0.37	0.05	478		435		477		461	
4	AS36	46°59'23,8"	13°33'20,1"	2162	GN (19)	Qtz, Wmca, Grt, Bt, Chl	13	0.12	0.04	13	0.20	0.03	551	7.9	561	14.6	564	8.0	549	8.45
4	AS36	46°59'23,8"	13°33'20,1"	2162	GN (19)	Qtz, Wmca, Grt, Bt, Chl	6	0.05	0.03	6	0.10	0.01	597		646		614		603	
5	AS38	47°00'58,5"	13°32'36,9"	2219	Gl(19)	Cal, Qtz, Wmca, Ab	19	0.46	0.09	19	0.41	0.03	458	6.3	428	6.3	463	6.9	448	6.55
6	AS39	47°01'09,2"	13°32'27,0"	2500	Gl(19)	Cal, Qtz, Wmca, Ab	20	0.43	0.07	20	0.37	0.03	475	6.5	462	14.0	482	7.4	466	7.12
7	AS43	47°02'13,9"	13°35'54,5"	1491	KQ(11)	Qtz, Wmca, Ab, Czo, Pl	2	0.05	0.01	2	0.10	0.03	598		650		623		612	
8	AS46	47°02'55,1"	13°34'44,2"	2018	Mo(20)	Ab, Wmca, Qtz, Czo, Grt	16	0.29	0.08	16	0.33	0.05	493	11.7	468	16.6	502	12.8	486	12.6
9	AS55	47°04'26,7"	13°36'20,4"	1734	Gl(19)	Qtz, Wmca, Cal, Ab	18	0.49	0.07	18	0.44	0.03	445	5.9	405	12.3	441	7.0	428	6.43
10	AS60	47°03'55,0"	13°36'07,6"	1805	Ma(17)	Cal, Qtz, Wmca, Ab	13	0.53	0.2	13	0.41	0.08	460	20.7	447	28.6	470	21.4	455	20.4
11	AS63	47°04'04,5"	13°27'21,6"	1905	Si(23)	Qtz, Wmca, Cal, Czo	15	0.32	0.11	15	0.38	0.07	472	15.8	424	25.8	485	15.2	469	15.6
12	AS64	47°04'04,5"	13°27'21,6"	1905	Si(23)	Cal, Qtz, Wmca, Ab, Czo	19	0.30	0.09	19	0.35	0.06	486	12.5	451	19.8	494	14.0	478	13.7
13	AS66	47°04'10,9"	13°36'11,0"	1701	Gl(19)	Cal, Wmca, Qtz	14	0.45	0.08	14	0.40	0.04	462	9.2	434	10.9	470	11.0	454	10.5
13	AS66	47°04'10,9"	13°36'11,0"	1701	Gl(19)	Cal, Wmca, Qtz	9	0.24	0.07	9	0.27	0.05	520	16.0	519	24.3	551	16.6	536	40.3
14	AS70	47°03'18,8"	13°36'05,1"	1853	KQ(11)	Qtz, Wmca, Chl	15	0.36	0.05	15	0.39	0.04	469	8.8	438	14.9	472	11.1	456	10.4
14	AS70	47°03'18,8"	13°36'05,1"	1853	KQ(11)	Qtz, Wmca, Chl	3	0.30	0.08	3	0.24	0.04	536		574		542		526	
15	AS71	47°03'18,8"	13°36'05,1"	1853	KQ(11)	Wmca, Ab, Qtz	17	0.14	0.08	17	0.14	0.08	579	17.5	632	30.3	605	18.9	593	20.4
16	AS78	47°06'00,1"	13°36'24,9"	1075	Gl(19)	Cal, Wmca, Qtz	20	0.43	0.11	20	0.39	0.05	467	11.2	443	14.0	466	9.5	452	11
17	AS80	46°59'52,9"	13°31'44,4"	2139	KQ(11)	Qtz, Wmca	7	0.41	0.02	7	0.41	0.02	458		457		462		447	
17	AS80	46°59'52,9"	13°31'44,4"	2139	KQ(11)	Qtz, Wmca	13	0.30	0.04	13	0.30	0.04	508	11.0	508	19.6	518	12.3	501	12.4
18	AS87	46°58'04,2"	13°30'04,1"	1480	Mo(20)	Qtz, Wmca, Ab, Czo, Chl, Ep	18	2.81	0.64	18	0.65	0.02	350	3.9	299	24.4	351	3.9	350	3.05
19	AS89	47°09'11,0"	13°22'47,4"	2017	Gl/Ma	Qtz, Wmca, Ab	16	0.52	0.14	16	0.41	0.05	457	11.3	439	12.4	459	10.9	444	10.2
20	AS90	47°09'37,5"	13°23'10,6"	2505	Ma(17)	Cal, Qtz, Wmca	19	1.56	0.32	19	0.61	0.01	372	2.9	389	4.3	373	2.9	368	2.42
21	AS91	47°11'12,2"	13°25'44,5"	1429	Ma(17)	Cal, Wmca, Qtz, Ab	20	1.63	0.22	20	0.62	0.03	365	6.1	380	9.3	366	6.2	362	5.08
22	AS93	47°16'47,5"	13°04'34,2"	1075	Ma(17)	Cal, Qtz	20	2.17	0.09	20	0.66	0.01	348	2.7	351	7.8	349	2.6	348	2.08
23	AS94	47°12'49,3"	13°06'57,4"	901	Gl(19)	Cal, Qtz, Ab	20	0.69	0.12	20	0.46	0.04	437	8.9	425	10.7	440	9.7	427	8.98
24	AS95	47°16'16,2"	13°12'11,8"	974	Ma(17)	Qtz, Wmca, Ab	16	1.71	0.45	16	0.58	0.06	382	13.5	396	21.0	388	10.9	381	9.12

Table A-1: continued

#	Sample	GPS coordinates		elev.	Tectonic		#	R1		#	R2		a		b		c		d	
	name	N	E	[m]	unit	Mineral assemblage	spec. R1	Mean	SD	spec. R2	Mean	SD	T(°C)	CI	T(°C)	CI	T(°C)	CI	T(°C)	CI
25	AS96	47°11'29,4"	13°24'02,1"	1756	Ma(17)	Qtz, Wmca, Ab	21	1.69	0.08	21	0.63	0.02	361	5.0	378	11.0	362	4.9	359	4.05
26	AS-Ka103	47°03'08,4"	13°34'38,1"	2097	Mo(20)	Qtz, Wmca, Ab, Chl, Bt, Tur	20	0.38	0.07	20	0.38	0.04	471	8.2	440	11.7	477	8.9	462	8.52
27	AS-Ka104	47°03'08,4"	13°34'38,1"	2097	Mo(20)	Cal, Qtz, Wmca	20	0.55	0.06	20	0.44	0.02	445	4.1	421	3.4	449	4.5	435	4.18
28	AS-Ka105	47°03'07,3"	13°34'50,6"	2062	Mo(20)	Qtz, Wmca, Chl	20	0.37	0.07	20	0.36	0.05	483	9.5	465	16.0	490	10.6	475	10.5
29	AS-Ka106	47°03'08,4"	13°34'54,6"	2049	Mo(20)	Cal, Qtz, Wmca	2	0.32	0.06	2	0.35	0.05	484		455		491		475	
30	AS-Ka108	47°03'11,2"	13°35'01,5"	2004	Gl/Rw	Qtz, Wmca, Ab	5	0.36	0.04	5	0.35	0.02	484		468		492		476	
31	AS-Ka109	47°03'14,3"	13°35'11,6"	1966	Gl(19)	Qtz, Wmca, Ab	19	0.42	0.05	19	0.38	0.02	473	5.0	455	7.1	479	5.6	463	5.42
32	AS-Ka110	47°03'16,5"	13°35'31,5"	1945	Gl(19)	Qtz, Wmca, Ab	20	0.63	0.04	20	0.44	0.01	444	2.7	436	2.9	448	2.9	434	2.67
33	AS-Ka113	47°03'38,6"	13°35'29,8"	1881	Gl(19)	Qtz, Wmca, Ab	20	0.45	0.06	20	0.40	0.03	462	6.1	436	8.4	467	6.6	452	6.38
34	AS-Ka114	47°03'47,1"	13°35'25,1"	1842	Gl/Rw	Qtz, Wmca, Cal	20	0.44	0.08	20	0.40	0.04	464	7.7	439	10.0	470	8.4	454	8.05
35	AS-Ka115	47°03'58,2"	13°35'33,9"	1831	Gl/Rw	Qtz, Wmca, Chl, Grt	14	0.42	0.10	14	0.39	0.05	469	12.5	446	16.7	476	13.8	460	13.2
36	AS-Ka116	47°04'02,6"	13°35'33,3"	1800	Gl/Rw	Qtz, Wmca, Ab, Chl	20	0.42	0.04	20	0.38	0.02	470	4.3	448	6.0	476	4.7	461	4.54
37	AS-Mu117	47°07'35,7"	13°20'12,0"	2347	Si(23)	Qtz, Wmca, Bt	11	0.34	0.06	11	0.35	0.04	485	12.4	463	20.0	492	13.7	476	13.4
37	AS-Mu117	47°07'35,7"	13°20'12,0"	2347	Si(23)	Qtz, Wmca, Bt	9	0.12	0.04	9	0.16	0.05	568	16.6	598	30.5	587	19.7	574	21.2
38	AS-Mu118	47°07'41,6"	13°20'11,6"	2341	Si(23)	Qtz, Wmca	18	0.13	0.06	18	0.18	0.06	559	13.7	583	24.7	578	16.0	564	17
39	AS-Mu121	47°08'10,8"	13°20'21,9"	2215	Mo(20)	Qtz, Wmca, Ab, Bt	19	0.23	0.05	19	0.26	0.05	524	10.6	526	18.2	537	12.1	521	12.4
40	AS-Mu122	47°07'59,6"	13°20'12,7"	2309	Mo(20)	Qtz, Wmca	16	0.21	0.03	16	0.15	0.03	547	7.8	558	14.3	563	8.7	548	9.4
41	AS-Mu123	47°08'02,2"	13°20'10,6"	2295	Mo(20)	Qtz, Wmca, Bt	17	0.40	0.11	17	0.34	0.05	489	12.1	487	14.4	497	13.4	481	13.3
42	AS-Mu124	47°08'18,8"	13°20'20,0"	2284	Gl(19)	Qtz, Cal, Ab, Wm	20	0.55	0.06	20	0.42	0.02	455	5.0	444	5.4	459	5.4	444	5.06
43	AS-Mu125	47°08'50,6"	13°21'15,0"	2262	Gl(19)	Qtz	3	0.33	0.03	3	0.35	0.02	485		458		492		476	
43	AS-Mu125	47°08'50,6"	13°21'15,0"	2262	Gl(19)	Qtz	17	0.13	0.05	17	0.17	0.05	564	12.3	592	21.4	582	14.5	569	15.4
44	AS-Mu126	47°09'13,0"	13°21'54,6"	2161	Ma(17)	Qtz, Wmca, Cal, Chl	19	1.09	0.12	19	0.53	0.03	404	6.8	425	10.1	407	7.0	396	6.22
45	AS-Mu127	47°09'10,8"	13°22'48,4"	2020	Ma(17)	Qtz, Wmca, Ab, Chl, Czo	11	0.69	0.08	11	0.46	0.03	437	9.0	432	14.4	441	9.5	427	8.77
45	AS-Mu127	47°09'10,8"	13°22'48,4"	2020	Ma(17)	Qtz, Wmca, Ab, Chl, Czo	9	0.46	0.10	9	0.34	0.34	489	11.0	503	23.8	497	12.2	480	12.1
46	AS-Mu128	47°08'57,3"	13°22'40,0"	1795	Gl(19)	Qtz, Wmca, Ab, Chl	16	0.40	0.08	16	0.35	0.03	485	7.8	478	9.0	480	8.4	464	8.15
47	AS-Mu129	47°08'46,1"	13°23'06,2"	1722	Gl(19)	Cal, Qtz, Ab, Wm	20	0.52	0.05	20	0.41	0.03	459	5.6	445	9.0	464	6.1	448	5.72
48	AS-Mu130	47°08'23,1'	13°23'22,5"	1666	Mo(20)	Wmca, Ab, Qtz, Chl, Tur	11	0.43	0.04	11	0.39	0.02	466	7.1	441	11.1	472	7.7	456	7.36
48	AS-Mu130	47°08'23,1'	13°23'22,5"	1666	Mo(20)	Wmca, Ab, Qtz, Chl, Tur	9	0.22	0.08	9	0.26	0.06	527	19.4	531	29.8	540	22.1	524	22.7
49	AS-Mu131	47°08'07,2"	13°23'44,9"	1689	Mo(20)	Qtz, Wmca, Ab, Bt	18	0.24	0.05	18	0.28	0.03	514	7.3	506	11.3	525	8.2	509	8.35
50	AS-Ste132	47°00'58,1"	13°32'13,9"	2249	Gl(19)	Cal, Qtz, Wmca, Ab, Bt	17	0.24	0.05	17	0.28	0.04	514	9.9	506	16.6	526	11.2	509	11.4

Table A-1: continued

#	Sample	GPS coordinates		elev.	Tectonic		#	R1		#	R2		a		b		c		d	
	name	N	E	[m]	unit	Mineral assemblage	spec. R1	Mean	SD	spec. R2	Mean	SD	T(°C)	CI	T(°C)	CI	T(°C)	CI	T(°C)	CI
51	AS-Ste133	47°00'51,4"	13°32'02,9"	2226	Gl(19)	Qtz, Wmca ,Cal, Ab, Bt	20	0.34	0.04	20	0.35	0.02	484	4.9	461	8.2	491	5.4	475	5.32
52	AS-Ste134	47°00'40,9"	13°32'40,6"	2021	Gl(19)	Cal, Qtz, Wmca, Ab	15	0.54	0.08	15	0.43	0.03	449	7.8	427	9.7	454	8.4	439	7.88
53	AS-Ste135	47°00'42,9"	13°32'54,1"	1982	Gl(19)	Qtz, Wm, Cal, Ab	15	0.33	0.09	15	0.34	0.04	492	9.7	477	11.6	500	10.8	484	10.6
54	AS-Ste136	47°00'47,2"	13°33'16,4"	1905	Gl(19)	Qtz, Wmca, Ab, Cal, Tur, Chl	17	0.51	0.08	17	0.41	0.03	460	7.0	446	11.3	465	7.5	450	7.12
55	AS-Ste137	47°01'03,9"	13°33'55,5"	1676	Gl(19)	Cal, Wmca, Qtz, Ab	20	0.44	0.07	20	0.38	0.03	470	6.6	452	8.2	476	7.2	460	6.89
56	AS-Ste138	47°01'39,0'	13°34'51,1"	1476	Gl(19)	Qtz, Wmca, Cal, Ab	17	0.44	0.12	17	0.39	0.04	468	9.3	448	9.5	474	10.2	458	9.78
57	AS-Ste139	47°01'35,6"	13°35'01,8"	1367	Gl(19)	Qtz, Cal, Wm, Ab	20	0.58	0.11	20	0.45	0.03	441	7.1	418	6.9	445	7.6	431	7.09
58	AS-Kal40	47°02'15,5"	13°35'51,6"	1489	KQ(11)	Qtz, Wmca, Ab, Chl	18	0.47	0.12	18	0.41	0.05	460	11.3	435	14.1	465	12.2	450	11.6
59	AS-Kal41	47°03'27,0"	13°36'46,8"	1669	KQ(11)	Qtz, Wmca, Ab, Chl, Bt	19	0.37	0.05	19	0.36	0.03	480	6.4	458	9.2	487	7.0	471	6.83
60	AS-Kal42	47°05'26,8"	13°36'39,2"	1075	Gl(19)	Cal, Qtz, Wmca	8	0.45	0.07	8	0.39	0.02	467	8.4	448	7.9	472	9.2	457	8.8
60	AS-Kal42	47°05'26,8"	13°36'39,2"	1075	Gl(19)	Cal, Qtz, Wmca	10	0.21	0.04	10	0.27	0.03	523	9.7	519	14.7	535	11.0	519	11.2
61	AS-Kal46	47°04'55,8"	13°37'11,7"	1315	Ma(17)	Cal, Qtz, Wmca	19	0.39	0.04	19	0.37	0.03	475	6.1	450	10.6	481	6.7	465	6.49
62	AS-Kal49	47°06'09,3"	13°37'14,8'	1162	Gl(19)	Qtz, Wm, Cal, Tur	10	0.35	0.07	10	0.35	0.03	487	9.0	471	9.9	495	10.0	479	9.79
62	AS-Kal49	47°06'09,3"	13°37'14,8'	1162	Gl(19)	Qtz, Wmca, Cal, Tur	10	0.16	0.07	10	0.21	0.06	545	19.5	559	32.6	561	22.7	546	23.8
63	AS-Sp150	47°07'39,0"	13°37'28,7"	2416	HN(16)	Cal, Qtz, Wmca	17	0.42	0.07	17	0.37	0.03	477	7.7	465	11.1	484	8.4	468	8.18
64	AS-Sp151	47°07'34,1"	13°37'18,7	2298	Ma(17)	Qtz, Wmca, Chl, Ab, Bt	9	0.28	0.02	9	0.33	0.01	496	5.0	473	11.1	504	5.5	488	5.49
64	AS-Sp151	47°07'34,1"	13°37'18,7	2298	Ma(17)	Qtz, Wmca, Chl, Ab, Bt	9	0.19	0.03	9	0.24	0.02	533	8.1	536	13.5	547	9.3	531	9.69
65	AS-Sp153	47°07'20,2"	13°36'27,3"	1899	Gl(19)	Qtz, Wmca, Ab, Chl	17	0.46	0.06	17	0.38	0.02	473	5.4	467	6.3	480	5.9	464	5.74
66	AS-Sp154	47°07'00,5"	13°37'32,0"	1889	Ma(17)	Qtz, Wmca, Ab, Chl	10	0.77	0.09	10	0.48	0.03	428	9.0	426	16.6	431	9.4	418	8.53
66	AS-Sp154	47°07'00,5"	13°37'32,0"	1889	Ma(17)	Qtz, Wmca, Ab, Chl	10	0.42	0.11	10	0.37	0.03	475	11.0	461	21.4	482	12.2	466	11.9
67	AS-Sp156	47°06'27,7"	13°37'29,7"	1494	Gl(19)	Qtz, Wmca, Cal, Chl	19	0.61	0.04	19	0.43	0.02	451	4.6	448	8.3	456	5.0	441	4.67
68	AS-Sp159	47°07'22,9"	13°35'31,8"	1426	Gl(19)	Cal, Wmca, Qtz	16	0.53	0.05	16	0.40	0.02	462	5.8	455	9.3	467	6.3	452	5.83
69	AS-Sp160	47°07'52,2"	13°36'08,8"	1609	Gl(19)	Qtz, Cal, Wmca, Chl	10	0.44	0.07	10	0.40	0.04	462	11.9	434	15.9	467	12.9	452	12.3
69	AS-Sp160	47°07'52,2"	13°36'08,8"	1609	Gl(19)	Qtz, Cal, Wmca, Chl	10	0.25	0.06	10	0.28	0.04	518	12.7	517	19.6	529	14.5	513	14.8
70	AS-Sp161	47°07'55,0"	13°36'29,6"	1774	Gl(19)	Cal, Qtz, Wmca	20	0.55	0.07	20	0.43	0.02	450	4.8	433	5.6	455	5.2	440	4.92
71	AS-Sp162	47°07'35,7"	13°36'46,6"	2062	Ma(17)	Qtz, Wmca, Ab, Chl	19	0.53	0.12	19	0.39	0.05	466	9.9	464	13.3	470	10.8	453	10.1
72	AS-Sp163	47°07'05,4"	13°36'27,7"	1841	Gl(19)	Wmca, Qtz, Ab, Chl	20	0.57	0.09	20	0.42	0.03	455	6.2	448	5.3	460	6.7	445	6.36
73	AS-Sp165	47°06'52,5"	13°36'24,1"	1624	Gl(19)	Qtz, Wmca, Cal, Ab, Chl	20	0.55	0.08	20	0.43	0.04	450	7.4	431	9.7	454	8.0	439	7.58
74	AS-Sp166	47°06'25,3"	13°36'08,4"	1353	Gl(19)	Cal, Qtz, Wmca, Ab, Chl	20	0.48	0.10	20	0.41	0.04	457	7.3	433	8.0	462	7.8	447	7.33
75	AS-Zed167	47°07'58,3"	13°34'02,3"	1275	Gl(19)	Qtz, Cal, Wmca	14	0.42	0.07	14	0.39	0.03	469	8.7	447	10.4	475	9.5	459	9.17

Table A-1: continued

#	Sample	GPS coordinates		elev.	Tectonic		#	R1		#	R2		a		b		c		d	
	name	N	E	[m]	unit	Mineral assemblage	spec. R1	Mean	SD	spec. R2	Mean	SD	T(°C)	CI	T(°C)	CI	T(°C)	CI	T(°C)	CI
76	AS-Zed168	47°09'10,9"	13°34'24,5"	1705	Gl(19)	Cal, Qtz, Wmca	19	0.71	0.09	19	0.46	0.02	436	5.2	432	3.7	439	5.5	426	5.09
77	AS-Zed170	47°08'48,6"	13°33'46,2"	1969	Gl(19)	Qtz, Wmca, Chl	17	0.49	0.10	17	0.41	0.04	459	9.1	439	10.7	464	9.9	449	9.28
78	AS-Zed171	47°08'27,6"	13°34'00,2"	1706	Gl(19)	Qtz, Cal, Wmca, Ab, Chl	20	0.57	0.08	20	0.44	0.04	446	7.3	425	9.9	450	7.9	435	7.41
79	AS-Zed172	47°08'29,4"	13°34'06,3"	1605	Gl(19)	Cal, Wmca, Qtz	18	0.52	0.05	18	0.40	0.02	461	3.9	451	8.5	464	4.2	449	4.01
80	AS-Zed173	48°08'10,1"	13°33'59,3"	1519	Gl(19)	Cal, Wmca, Qtz, Ab	20	0.70	0.06	20	0.47	0.02	432	3.8	421	3.1	435	4.0	422	3.63
81	AS-Zed174	47°08'12,9"	13°34'12,0"	1430	Gl(19)	Cal, Qtz, Wmca, Ab, Chl	19	0.51	0.11	19	0.41	0.04	460	8.0	447	7.7	465	8.6	450	8.16
82	AS-Zed175	47°08'14,7"	13°31'58,3"	1264	Gl(19)	Cal, Qtz, Wmca	14	0.48	0.09	14	0.42	0.03	453	8.2	422	8.6	457	8.8	443	8.22
83	AS-Zed176	47°08'08,4"	13°31'44,2"	1392	Gl(19)	Cal, Qtz, Wmca	20	0.57	0.06	20	0.44	0.02	447	4.8	430	5.2	451	5.2	437	4.82
84	AS-Zed177	47°08'02,3"	13°31'23,2"	1529	Gl(19)	Qtz, Wmca, Ab, Chl	18	0.53	0.09	18	0.43	0.04	451	9.8	429	14.1	456	10.6	441	9.92
85	AS-Zed178	47°07'48,9"	13°31'10,6"	1650	Gl(19)	Qtz, Wm, Ab, Chl, Tur	18	0.51	0.09	18	0.42	0.03	454	6.6	432	6.7	459	7.2	444	6.75
86	AS-Zed179	47°07'32,7"	13°30'59,5"	1852	Mo(20)	Qtz, Wmca, Ab, Chl	20	0.39	0.06	20	0.36	0.03	480	6.2	463	8.2	487	6.8	471	6.64
87	AS-Zed180	47°07'28,1"	13°30'46,0"	1959	Mo(20)	Qtz, Wmca, Ab, Bt, Chl	15	0.49	0.04	15	0.41	0.01	460	2.8	441	5.1	465	3.1	450	2.91
88	AS-Zed181	47°07'14,6"	13°30'07,8"	2263	Mo(20)	Qtz, Ab, Wmca, Chl, Bt	11	0.32	0.06	11	0.33	0.03	494	7.9	478	9.4	502	8.8	486	8.69
89	AS-Zed182	47°07'22,0"	13°29'56,7"	2128	Mo(20)	Ab, Wmca, Qtz, Chl, Tur	17	0.39	0.07	17	0.37	0.03	478	7.3	460	8.7	485	8.0	469	7.76
90	AS-Li183	47°04'03,4"	13°28'29,4"	1659	Si(23)	Qtz, Cal, Ab, Wmca, Bt, Czo, Chl	20	0.23	0.02	20	0.28	0.02	516	3.7	507	6.7	527	4.2	511	4.26
91	AS-Li184	47°04'03,4"	13°28'29,4"	1659	Si(23)	Qtz, Cal, Ab, Wmca, Chl, Czo	18	0.30	0.04	18	0.34	0.03	491	6.1	466	9.6	499	6.8	483	6.71
92	AS-Mu185	47°07'47,2"	13°22'09,6"	2339	Si(23)	Qtz, Wmca, Chl, Grt	19	0.24	0.06	19	0.31	0.03	505	6.9	484	11.0	515	7.8	499	7.79
93	AS-Mu187	47°08'07,6"	13°22'15,5"	2308	Mo(20)	Qtz, Wmca, Chl	20	0.28	0.05	20	0.31	0.04	503	8.2	491	13.4	513	9.2	497	9.22
94	AS-Mu188	47°08'37,7"	13°22'29,9"	1978	Gl(19)	Cal, Qtz, Wmca, Ab	20	0.58	0.07	20	0.43	0.02	452	5.1	441	6.3	456	5.4	441	5.08
95	AS-Mö189	46°52'34,0"	13°20'21,3"	1100	Gl(19)	Cal, Qtz, Wm, Ab, Bt	20	0.38	0.05	20	0.36	0.03	481	5.2	465	6.9	489	5.8	472	5.62
96	AS-Mö190	46°52'21,7"	13°20'43,9"	1028	Gl(19)	Qtz, Wmca, Cal, Bt, Ab	19	0.34	0.05	19	0.35	0.04	485	8.1	463	12.8	493	9.0	477	8.79
97	AS-Mö191	46°52'21,5"	13°20'25,9"	963	Gl(19)	Qtz, Wmca, Cal, Ab, Cld, Pl, Czo	20	0.33	0.04	20	0.35	0.02	487	4.8	464	6.6	495	5.3	478	5.23
98	AS-Mö193	46°50'37,8"	13°23'03,1"	613	KWN(10)	Wmca, Qtz, Grt, Tur, Chl, Bt	14	0.28	0.06	14	0.33	0.04	492	11.1	464	17.3	497	11.2	481	11
99	AS-Zed194	47°09'39,1"	13°21'56,2"	2404	Ma(17)	Qtz, Wmca, Chl	19	1.03	0.09	19	0.53	0.02	406	3.6	419	6.3	408	3.7	398	3.25
100	AS-Zed195	47°09'42,0"	13°22'13,8"	2265	Ma(17)	Qtz, Wmca, Ab, Chl	20	1.03	0.08	20	0.52	0.03	410	6.0	428	14.6	412	6.3	401	5.6
101	AS-Zed196	47°09'45,8"	13°22'11,8"	2259	Ma(17)	Qtz, Wmca, Chl	20	1.16	0.09	20	0.55	0.01	395	2.9	412	1.9	397	2.9	388	2.54
102	AS-Zed197	47°09'48,7"	13°22'06,1"	2248	Ma(17)	Qtz, Wmca, Ab, Chl	19	0.97	0.07	19	0.51	0.03	415	5.4	431	8.2	417	5.6	406	5.03
103	AS-Zed198	47°09'51,4"	13°21'57,5"	2244	Ma(17)	Qtz, Wmca	20	1.12	0.09	20	0.55	0.01	395	2.5	405	1.6	396	2.6	387	2.2
104	AS-Zed199	47°10'07,8"	13°22'06,9"	2201	Ma(17)	Qtz, Wmca	20	1.23	0.12	20	0.56	0.02	391	4.7	411	5.2	393	4.8	384	4.2
105	AS-Zed200	47°10'13,3"	13°22'05,5"	2193	Ma(17)	Qtz, Wmca	20	0.92	0.13	20	0.49	0.03	421	6.8	436	10.8	424	7.1	411	6.43

Table A-1: continued

#	Sample	GPS coordinates		elev.	Tectonic		#	R1		#	R2		a		b		c		d	
	name	N	E	[m]	unit	Mineral assemblage	spec. R1	Mean	SD	spec. R2	Mean	SD	T(°C)	CI	T(°C)	CI	T(°C)	CI	T(°C)	CI
106	AS-Zed201	47°10'21,3"	13°22'02,9"	2194	Ma(17)	Qtz, Wmca, Ab	18	0.85	0.08	18	0.50	0.02	417	4.6	416	4.5	420	4.8	408	4.3
107	AS-Ma202	47°10'00,9"	13°21'28,1"	2029	Gl(19)	Cal, Qtz, Wmca, Ab	20	0.46	0.08	20	0.40	0.04	464	7.6	445	8.7	470	8.4	454	8.05
108	AS-Ma203	46°58'06,8"	13°30'25,3"	1503	Gl(19)	Cal, Qtz, Wmca, Ab	20	0.62	0.04	20	0.42	0.01	455	2.9	437	3.1	460	3.1	444	2.95
109	AS-Ma204	46°58'03,9"	13°30'20,9"	1507	Mo(20)	Cal, Qtz, Wmca, Ab	20	0.41	0.03	20	0.39	0.01	468	2.9	441	4.2	474	3.2	458	3.08
110	AS-Ma205	46°58'00,3"	13°30'11,0"	1505	Mo(20)	Qtz, Wmca, Ab, Chl, Bt	19	0.24	0.02	19	0.29	0.02	511	3.6	498	6.0	522	4.0	505	4.07
111	AS-Ma206	46°58'00,7"	13°30'05,7"	1489	Mo(20)	Qtz, Ab, Wm, Tur, Chl, Bt	20	0.24	0.06	20	0.29	0.05	513	9.6	505	15.4	524	10.9	508	11.1
112	AS-Ma207	46°58'03,2"	13°30'04,6"	1496	KQ(11)	Qtz, Wmca, Ab, Pl, Bt	16	0.28	0.08	16	0.32	0.05	498	11.4	480	16.1	508	12.7	491	12.4
112	AS-Ma207	46°58'03,2"	13°30'04,6"	1496	KQ(11)	Qtz, Wmca, Ab, Pl, Bt	4	0.12	0.09	4	0.16	0.10	569		603		590		577	
113	AS-Ma208	46°57'51,8"	13°30'53,4"	1213	Gl(19)	Cal, Wmca, Qtz, Ab	20	0.56	0.10	20	0.43	0.04	450	7.4	435	7.2	455	7.9	440	7.33
114	AS-Ma209	46°57'35,7"	13°30'29,7"	1088	Gl(19)	Cal, Qtz, Wmca, Ab	20	0.45	0.05	20	0.39	0.02	468	5.0	449	7.0	474	5.5	458	5.28
115	AS-Ma210	46°57'33,0"	13°30'29,5"	1020	Gl(19)	Qtz, Wmca, Cal, Ab, Chl	19	0.36	0.03	19	0.36	0.02	481	3.3	458	5.3	486	5.4	470	5.23
116	AS-Ma212	46°57'32,4"	13°30'25,2"	982	Mo(20)	Ab, Wmca, Qtz, Chl, Tur	12	0.34	0.02	10	0.29	0.06	491	6.0	473	9.8	500	6.6	483	6.57
117	AS-Zed213	47°09'55,6"	13°24'59,9"	2168	Ma(17)	Qtz, Wmca	20	0.56	0.01	20	1.22	0.07	394	3.0	416	3.7	396	3.1	387	2.65
118	AS-Zed214	47°09'36,4"	13°24'49,3"	2060	Ma(17)	Qtz, Wmca	20	0.79	0.09	20	0.47	0.03	430	5.7	434	6.4	433	6.0	420	5.45
119	AS-Zed215	47°09'41,8"	13°26'30,3"	1548	Ma(17)	Qtz, Wmca	19	0.82	0.10	19	0.48	0.03	429	6.8	437	8.8	432	7.2	419	6.52
120	AS-Mu229	47°07'39,5"	13°20'10,8"	2344	Si(23)	Qtz, Wmca, Bt, Chl	15	0.17	0.02	20	0.23	0.02	539	4.0	544	7.7	553	4.6	537	4.77
121	AS-Ma230	46°55'59,4"	13°29'24,1"	1440	Gl(19)	Cal, Qtz, Wmca	18	0.34	0.02	18	0.35	0.04	488	5.3	473	7.8	497	5.9	480	5.84
122	AS-Ma231	46°56'02,6"	13°29'16,3"	1469	Gl(19)	Qtz, Wmca, Ab, Chl	13	0.36	0.03	13	0.38	0.07	480	8.4	461	10.5	482	9.1	466	8.83
123	AS-Ra234	46°56'05,0"	13°29'16,3"	1270	Gl(19)	Qtz, Wmca, Ab, Cal, Chl	18	0.32	0.04	18	0.27	0.05	500	8.0	480	12.6	510	9.0	493	8.95
124	AS-Ra235	46°54'31,7"	13°29'22,7"	1240	Gl(19)	Qtz, Wmca	20	0.27	0.04	20	0.31	0.03	503	5.5	488	7.8	512	6.8	496	6.13
125	AS-Ra236	46°54'30,3"	13°29'35,5"	1223	Gl(19)	Qtz, Wmca, Chl	19	0.47	0.06	19	0.39	0.03	465	5.9	450	8.9	471	6.4	455	6.17
126	AS-Gm238	46°53'15,4"	13°29'01,0"	1392	Gl(19)	Qtz, Wmca, Cal, Ab	20	0.41	0.03	20	0.50	0.07	458	5.9	438	7.2	462	6.3	447	5.94
127	AS-Gm240	46°53'19,6"	13°28'47,3"	1537	Gl(19)	Cal, Qtz, Wmca	20	0.40	0.10	20	0.38	0.02	470	7.1	442	10.5	476	7.7	460	7.37
128	AS-Gm241	46°52'57,5"	13°29'00,5"	1600	Gl(19)	Cal, Qtz, Wmca	20	0.40	0.10	20	0.36	0.06	479	6.2	457	9.4	486	6.8	470	6.54
129	AS-Gm242	46°53'29,2"	13°28'37,5"	1668	Gl(19)	Cal, Ab, Qtz, Wmca	22	0.44	0.02	22	0.43	0.03	443	3.3	386	6.3	447	3.5	433	3.26
130	AS-Gm243	46°53'44,6"	13°27'34,8"	2113	Mo(20)	Ab, Qtz, Wmca, Chl, Bt, Czo	17	0.36	0.03	17	0.33	0.07	481	7.8	449	11.4	488	8.5	471	9.05
131	AS-Gm244	46°53'18,4"	13°28'23,8"	1715	Gl(19)	Qtz, Wmca	20	0.35	0.00	20	0.36	0.01	482	4.9	460	7.6	489	5.4	473	5.26
132	AS-Gm245	46°52'56,5"	13°29'29,9"	1058	Gl(19)	Cal, Qtz, Wmca	20	0.44	0.03	20	0.58	0.08	443	5.6	421	6.2	447	6.0	433	5.57
133	AS-Gm246	46°51'44,8"	13°28'48,5"	1153	KQ(11)	Wmca, Qtz	15	0.36	0.03	15	0.31	0.05	480	8.6	443	13.5	487	9.5	471	9.33
134	AS-Gm247	46°52'59,6"	13°27'11,8"	2000	Gl(19)	Qtz, Wmca, Ab	20	0.31	0.02	20	0.27	0.03	502	5.1	486	8.4	511	5.8	495	5.8

Table A-1: continued

#	Sample	GPS coordinates		elev.	Tectonic		#	R1		#	R2		a		b		c		d	
	name	N	E	[m]	unit	Mineral assemblage	spec. R1	Mean	SD	spec. R2	Mean	SD	T(°C)	CI	T(°C)	CI	T(°C)	CI	T(°C)	CI
135	AS-Gm248	46°53'16,9"	13°26'45,9"	2120	Mo(20)	Qtz, Wmca, Bt, Ab	18	0.31	0.05	18	0.27	0.06	502	10.0	484	15.4	511	11.2	495	11.3
136	AS-Gm249	46°52'08,3"	13°27'29,3"	1616	Gl(19)	Cal, Qtz, Wmca	20	0.41	0.03	20	0.46	0.06	457	6.9	426	10.5	462	7.4	447	7.03
137	AS-Gm250	46°51'48,1"	13°27'53,4"	1290	KQ(11)	Qtz, Cal, Wmca	20	0.44	0.02	20	0.37	0.01	477	7.8	469	13.0	483	8.6	467	8.33
138	AS-Gm251	46°51'48,1"	13°27'53,4"	1290	Gl(19)	Cal, Qtz, Wmca	18	0.41	0.02	18	0.47	0.06	457	5.3	428	9.1	462	5.7	447	5.4
139	AS-Gm252	46°51'29,3"	13°27'09,5"	1251	Gl(19)	Cal, Qtz, Wmca	19	0.45	0.03	19	0.56	0.07	443	5.5	415	6.0	447	5.8	433	5.41
140	AS-Gm253	46°51'28,5"	13°26'58,8"	1244	Gl(19)	Cal, Qtz, Wmca, Ab	20	0.42	0.03	20	0.52	0.08	454	6.6	435	7.5	459	7.1	444	6.69
141	AS-Gm254	46°51'27,4"	13°26'54,2"	1242	Gl(19)	Qtz, Cal, Wmca	19	0.40	0.05	19	0.39	0.04	468	8.7	437	16.1	474	9.5	458	9.11
142	AS-Gm255	46°51'28,8"	13°27'07,8"	1167	Gl(19)	Cal, Qtz, Wmca, Ab	21	0.41	0.04	21	0.49	0.09	457	8.1	435	10.8	463	8.8	447	8.26
143	AS-Mz257	46°56'28,4"	13°11'00,6"	810	Mo(20)	Qtz, Cal, Wmca, Chl	16	0.26	0.05	16	0.31	0.04	503	9.8	487	15.8	513	10.9	497	10.9
144	AS-Gm258	46°51'00,8"	13°27'01,7"	1160	KQ(11)	Qtz, Wmca	16	0.31	0.03	16	0.25	0.03	505	6.8	486	11.7	514	7.7	498	7.74
145	AS-Gm259	46°51'20,9"	13°26'25,5"	1263	Gl(19)	Qtz, Wmca, Cal	16	0.43	0.02	16	0.52	0.03	450	3.6	424	5.6	455	3.8	440	3.55
146	AS-Gm260	46°51'29,2"	13°26'17,3"	1285	Gl(19)	Qtz, Wmca	19	0.38	0.04	19	0.39	0.03	468	5.7	434	9.3	474	6.2	459	5.89
147	AS-Gm261	46°51'57,4"	13°25'30,7"	1430	Gl(19)	Ab, Wmca, Qtz, Cal	19	0.36	0.02	19	0.35	0.04	482	4.5	457	6.4	489	4.9	473	4.76
148	AS-Gm262	46°51'49,2"	13°25'29,5"	1520	Gl(19)	Qtz, Wmca, Grt, Ab	20	0.34	0.04	19	0.33	0.06	490	8.5	466	10.2	495	8.0	479	7.89
149	AS-Gm263	46°51'37,6"	13°25'30,6"	1565	Gl(19)	Cal, Ab, Wmca, Qtz	18	0.38	0.04	18	0.41	0.09	473	9.4	452	11.6	479	10.3	463	9.99
150	AS-Gm264	46°51'33,2"	13°25'21,8"	1555	Gl(19)	Cal, Wmca, Qtz, Ab	18	0.34	0.03	18	0.30	0.05	490	7.4	463	11.2	498	8.25	481	8.12
151	AS-Gm265	46°51'20,2"	13°25'49,6"	1449	Gl(19)	Qtz, Wmca, Ab	19	0.42	0.04	19	0.40	0.03	464	5.4	435	9.0	473	8.8	454	5.69
152	AS-Gm266	46°51'21,0"	13°26'11,3"	1433	Gl(19)	Qtz, Ab, Wmca, Chl	20	0.49	0.03	20	0.39	0.01	466	2.9	455	3.9	472	3.2	456	3.05
153	AS-Pl267	46°52'12,1"	13°21'04,4"	958	Gl(19)	Cal, Qtz, Wmca	17	0.34	0.06	17	0.35	0.03	485	8.0	463	11.9	492	8.8	476	8.59
154	AS-Pl271	46°52'24,0"	13°22'24,0"	1611	Gl(19)	Qtz, Cal, Wmca, Ab	14	0.33	0.03	14	0.28	0.04	496	7.5	474	11.8	505	8.3	489	8.26
155	AS-Pl272	46°52'16,2"	13°22'10,5"	1584	Gl(19)	Qtz, Wmca, Bt, Ab	17	0.33	0.02	17	0.29	0.29	493	4.0	470	6.9	500	5.2	484	5.1
156	AS-Pl273	46°52'19,2"	13°21'46,6"	1550	Gl(19)	Bt, Wmca, Qtz, Grt	6	0.31	0.03	6	0.26	0.04	505	13.1	488	18.1	515	14.7	498	14.8
156	AS-Pl273	46°52'19,2"	13°21'46,6"	1550	Gl(19)	Bt, Wmca, Qtz, Grt	14	0.19	0.04	14	0.14	0.04	557	11.2	577	20.3	574	13.2	560	13.9
157	AS-Pl274	46°52'16,7"	13°21'31,7"	1342	Gl(19)	Qtz, Wmca, Chl, Bt, Cal, Ab	17	0.31	0.03	17	0.29	0.04	503	6.0	494	9.3	513	6.5	497	6.52
158	AS-Pl275	46°51'57,9"	13°21'38,7"	1080	Gl(19)	Ab, Wmca, Qtz, Bt, Cal	18	0.33	0.02	18	0.31	0.03	492	5.1	472	8.9	500	5.7	484	5.66
159	AS-Pl276	46°51'40,2"	13°21'51,8"	900	Gl/Rw	Qtz, Wmca, Ab, Tur	20	0.26	0.04	20	0.32	0.03	497	6.1	471	10.6	506	6.8	490	6.82
160	AS-Bu277	46°53'09,6"	13°20'28,7"	1592	Gl(19)	Ab, Wmca, Qtz, Cal	18	0.34	0.03	19	0.28	0.04	492	6.2	464	9.2	499	7.0	483	6.91
161	AS-Bu278	46°53'07,3"	13°20'21,4"	1513	Gl(19)	Qtz, Ab, Wmca, Cal, Bt	19	0.33	0.04	17	0.27	0.04	495	9.3	468	13.3	503	10.7	487	10.7
162	AS-Bu280	46°52'58,7"	13°20'30,3"	1477	Gl(19)	Cal, Qtz, Wmca, Ab	18	0.32	0.05	15	0.25	0.02	497	9.7	468	8.7	501	9.9	485	9.01
163	AS-Bu281	46°52'47,4"	13°20'35,6"	1382	Gl(19)	Qtz, Wmca, Bt, Grt	15	0.31	0.05	12	0.23	0.03	504	11.5	478	11.1	510	8.5	494	8.45

Table A-1: continued

#	Sample	GPS coordinates		elev.	Tectonic		#	R1		#	R2		a		b		c		d	
	name	N	E	[m]	unit	Mineral assemblage	spec. R1	Mean	SD	spec. R2	Mean	SD	T(°C)	CI	T(°C)	CI	T(°C)	CI	T(°C)	CI
164	AS-Bu282	46°52'46,1"	13°20'19,0"	1280	Gl(19)	Cal, Qtz, Ab, Bt, Wmca	18	0.31	0.03	13	0.27	0.03	503	7.7	487	10.2	513	8.7	497	9.67
165	AS-Bu283	46°52'50,2"	13°20'08,5"	1270	Gl(19)	Qtz, Wmca, Ab, Grt, Pl, Bt	17	0.28	0.05	9	0.27	0.05	514	10.8	477	23.0	526	12.2	509	12.3
166	AS-Bu284	46°52'36,3"	13°20'36,5"	1225	Gl(19)	Wmca, Qtz, Ab, Bt	16	0.38	0.02	16	0.36	0.04	471	5.7	434	8.7	478	6.2	462	5.93
167	AS-Bu285	46°52'30,8"	13°20'38,0"	1146	Gl(19)	Cal, Qtz, Wmca, Bt, Czo	20	0.41	0.07	20	0.38	0.04	474	7.3	453	9.4	480	8.0	464	7.68
168	AS-Bu286	46°52'19,6"	13°20'29,9"	958	Gl(19)	Cal,Wmca, Qtz, Ab, Bt	18	0.35	0.03	18	0.35	0.05	485	7.4	456	12.5	490	7.0	474	6.89
169	AS-Bu287	46°52'20,3"	13°20'12,3"	872	Gl/Rw	Qtz, Wmca, Cal	19	0.32	0.04	19	0.27	0.05	500	8.3	479	13.4	509	9.3	493	9.23
170	AS-Bu288	46°52'15,3"	13°20'15,6"	820	Mo(20)	Qtz,Wmca, Chl, Ab	14	0.32	0.06	14	0.23	0.07	500	14.6	489	26.8	509	16.4	493	16.2
171	AS-Re290	46°53'38,1"	13°18'31,8"	1114	Gl(19)	Cal, Qtz, Ab, Wmca, Ep, Bt	10	0.32	0.03	10	0.30	0.05	497	8.6	479	12.2	500	9.4	483	9.27
172	AS-Re291	46°53'28,9"	13°18'24,1"	1072	Gl(19)	Qtz, Wmca, Cal	18	0.32	0.05	18	0.30	0.07	500	11.0	486	17.4	509	12.3	493	12.2
173	AS-Re292	46°53'18,7"	13°18'20,3"	999	Gl/Rw	Cal, Qtz, Wmca	18	0.40	0.05	18	0.39	0.03	466	6.8	434	10.4	472	7.5	456	7.18
174	AS-Re293	46°53'12,7"	13°18'25,5"	944	Gl(19)	Cal, Wmca, Qtz	12	0.34	0.03	12	0.29	0.04	491	8.9	465	14.5	500	9.9	483	9.74
175	AS-Gm295	46°50'50,1"	13°25'29,0"	883	KQ(11)	Cal, Qtz, Wmca	20	0.32	0.06	17	0.32	0.11	501	11.9	479	14.1	510	13.2	494	13.1
176	AS-Ke296	46°55'00,9"	13°16'48,6"	1827	Gl(19)	Cal, Wmca, Qtz	10	0.50	0.04	10	0.71	0.13	416	11.7	385	9.7	425	17.2	413	15.8
176	AS-Ke296	46°55'00,9"	13°16'48,6"	1827	Gl(19)	Cal, Wmca, Qtz	10	0.31	0.04	10	0.26	0.05	501	12.4	481	17.4	515	11.6	498	11.7
177	AS-Ke299	46°54'59,6"	13°16'08,2"	1457	Gl(19)	Cal, Wmca, Bt, Ab, Qtz	20	0.34	0.03	20	0.30	0.05	490	7.1	463	11.4	498	7.9	482	7.8
178	AS-Ke300	46°55'08,8"	13°16'02,8"	1300	Gl(19)	Ab, Bt, Cal, Qtz, Wmca	20	0.31	0.04	20	0.28	0.05	502	7.7	487	12.2	512	8.6	496	8.62
179	AS-Ke301	46°54'29,0"	13°16'18,6"	1202	Gl(19)	Qtz, Wmca, Ab	15	0.31	0.03	15	0.27	0.05	505	8.6	488	12.9	515	9.6	499	9.62
180	AS-Ke302	46°54'31,0"	13°16'09,8"	1122	Gl(19)	Cal, Qtz, Ab, Wmca, Bt	20	0.32	0.03	20	0.29	0.05	500	6.6	487	9.6	510	7.4	493	7.43
181	AS-Ka303	47°03'04,2"	13°35'42,6"	1889	KQ(11)	Wmca, Qtz, Ab	20	0.37	0.03	20	0.40	0.06	476	6.1	455	7.1	482	6.8	466	6.59
182	AS-Zed304	47°12'05,5"	13°25'14,5"	1996	Ma(17)	Cal, Qtz, Wmca	20	0.63	0.02	20	1.78	0.16	360	3.3	378	5.0	362	3.2	358	2.67
183	AS-Zed305	47°11'57,8"	13°25'22,3"	2010	Ma(17)	Qtz, Wmca, Ab	20	0.62	0.01	20	1.77	0.13	365	2.4	390	4.1	366	2.4	362	2.01
184	AS-Zed307	47°11'25,7"	13°24'04,7"	1704	Ma(17)	Wmca, Qtz	20	0.53	0.02	20	1.08	0.11	406	5.0	426	6.6	408	5.2	398	4.56
185	AS-Zed308	47°11'10,7"	13°24'52,6"	1537	Ma(17)	Wmca, Qtz	20	0.57	0.01	20	1.29	0.08	387	2.8	408	4.6	389	2.9	381	2.44
186	AS-Zed309	47°10'57,7"	13°26'12,8"	1376	Ma(17)	Qtz, Wmca, Cal	13	0.58	0.04	13	1.32	0.32	384	9.1	403	9.1	386	9.7	378	8.28
187	AS-GrA312	47°14'00,2"	13°11'24,4"	960	Ma(17)	Qtz, Wmca	20	1.00	0.14	20	0.53	0.03	406	5.6	413	3.0	408	5.7	397	5.04
188	AS-GrA313	47°14'01,6"	13°11'22,9"	1061	Ma(17)	Cal, Qtz, Wmca	20	1.08	0.18	20	0.53	0.03	404	6.1	423	3.3	406	6.3	396	5.49
189	AS-GrA314	47°16'37,1"	13°11'45,9"	1335	Ma(17)	Qtz, Wmca, Ab	20	0.63	0.02	20	1.90	0.27	360	3.2	376	8.6	361	3.1	358	2.51
190	AS-GrA316	47°18'59,2"	13°12'01,9"	871	GW(4)	very fine-grained	20	0.57	0.01	20	1.28	0.09	389	3.1	412	3.3	391	3.2	383	2.71
191	AS-Gas318	47°08'04,1"	13°04'18,2"	1444	Gl(19)	Qtz, Ab, Wmca, Cal, Chl	20	0.38	0.02	20	0.39	0.04	471	3.9	444	5.2	477	4.3	461	4.15
192	AS-Gas319	47°08'04,8"	13°04'18,9"	1525	Gl(19)	Ab, Wmca, Cal, Qtz, Chl, Bt	20	0.51	0.04	20	0.77	0.03	489	5.4	468	8.7	497	6.0	480	5.9

Table A-1: continued

#	Sample	GPS coordinates		elev.	Tectonic		#	R1		#	R2		a		b		c		d	
	name	N	E	[m]	unit	Mineral assemblage	spec. R1	Mean	SD	spec. R2	Mean	SD	T(°C)	CI	T(°C)	CI	T(°C)	CI	T(°C)	CI
193	AS-Gas320	47°11'57,8"	13°06'39,8"	1012	Gl(19)	Cal, Wmca, Qtz, Bt	20	0.67	0.13	20	0.46	0.04	436	6.0	425	5.4	440	6.3	426	5.77
194	AS-Gas321	47°14'58,0"	13°06'38,8"	989	Ma(17)	Qtz, Wmca	20	0.54	0.03	20	1.07	0.17	400	6.1	408	5.1	402	6.2	393	5.37
195	AS-Gas322	47°15'30,9"	13°04'40,3"	891	Ma(17)	Qtz, Wmca	18	0.51	0.03	18	0.92	0.17	413	5.8	415	3.7	415	6.1	404	5.39
196	AS-Gös323	46°59'53,6"	13°19'45,1"	2417	Si(23)	Wmca, Bt, Grt, Qtz, Chl	14	0.07	0.04	14	0.04	0.03	612	11.5	680	23.3	640	14.0	632	15.5
197	AS-Glo325	47°05'03,1"	12°44'33,6"	2440	Gl(19)	Qtz, Wmca	15	0.27	0.07	15	0.31	0.05	503	12.3	488	19.6	513	13.9	497	14
198	AS-Glo326	47°05'04,7"	12°44'30,8"	2458	Gl(19)	Wmca, Bt, Grt, Qtz, Chl	20	0.30	0.01	20	0.32	0.01	499	6.3	484	9.7	508	7.0	492	6.97
199	AS-Glo327	47°03'09,9"	12°50'29,5"	1987	Gl/Rw	Qtz, Wmca, Chl, Grt	19	0.21	0.03	19	0.28	0.01	519	7.6	508	12.1	530	8.6	514	8.67
200	MH-286b	47°04'58,6"	12°50'09,7"	2695	Mo(20)	Qtz, Wmca, Grt, Chl, Bt	8	0.26	0.05	8	0.31	0.03	503	10.8	484	15.6	512	12.0	496	11.9
200	MH-286b	47°04'58,6"	12°50'09,7"	2695	Mo(20)	Qtz, Wmca, Grt, Chl, Bt	12	0.14	0.02	12	0.20	0.03	554	8.0	571	15.4	571	9.4	556	10.1

A-1.2 Method

Five different first-order Raman peaks or bands are observed, four of which so-called defect bands (D1-D4) and the fifth, is the graphite or G band (Tunistra and Koenig 1970, Beyssac et al. 2002a, 2003a, Nasdala et al. 2004). D4 is observable only at high degrees of disorder (Sadezky et al. 2005, Lahfid et al. 2010). In general, poor ordering of carbonaceous material (CM) is characterized by a prominent D1 (c. 1350 cm^{-1}), a smaller D2 (c. 1620 cm^{-1}) located on the shoulder of G (c. 1580 cm^{-1}) towards higher Raman shift, a very broad D3 (c. 1500 cm^{-1}) especially at temperatures below 350° C, and a D4 (c. 1200 cm^{-1}) on the D1 shoulder (towards lower Raman shift) (Dippel and Heintzenberg 1999, Gruber et al. 1994, Tuinstra and Koenig 1970, Lespade et al. 1984, Wang et al. 1990, Cuesta et al. 1994, Sze et al. 2001, Jawhari et al. 1995, Dippel et al. 1999, Nakamura et al. 1990). None of our samples contained D3 and D4 bands, indicating that the degree of ordering of CM is relatively high and that peak temperatures everywhere exceeded 350° C. In the Eastern Tauern Subdome (ETD), lower G peaks and higher D1 and D2 peaks characterize the lower greenschist-facies, whereas the opposite peak intensities are typical of the amphibolite-facies core of the ETD (Fig. A-1).

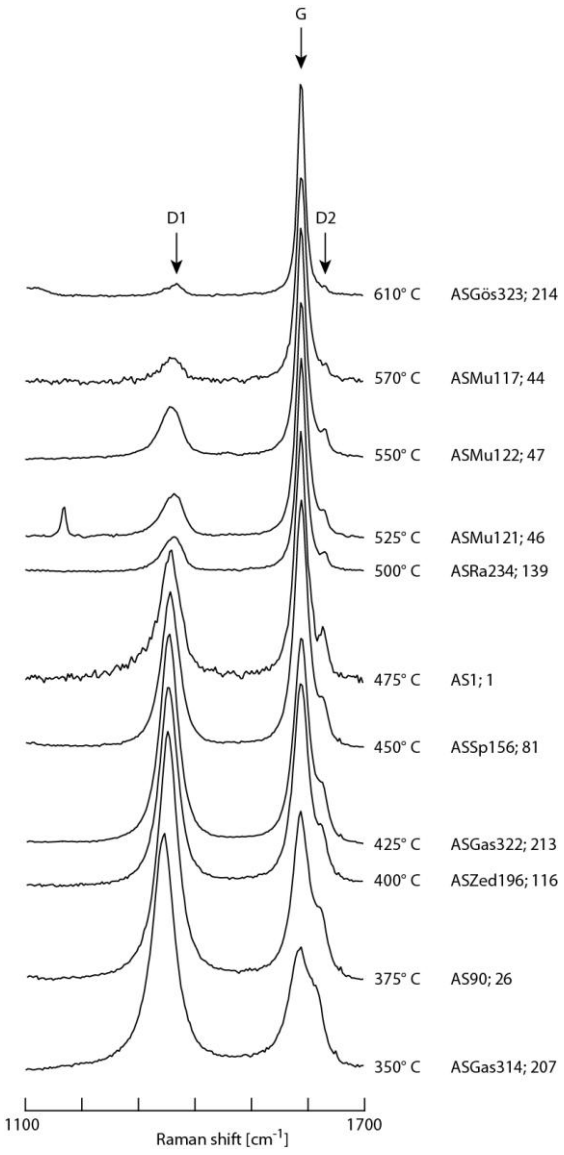

Figure A-1: Typical first-order Raman bands showing increasing order of carbonaceous material from bottom to top with increasing peak temperature. Sample numbers correspond to the listing in Table A-1 and the localities in Figure 3.3. G, D1 and D2 positions are marked with arrows. To facilitate comparison, the bands are normalized to the G band. Spectra at the top are from the core of the Eastern Tauern Subdome, whereas spectra further down pertain to localities away from the European basement of the Tauern Window, i.e., towards the Austroalpine units.

A-1.3 Compilation of observations used to draw the isograde and peak-temperature contours

Figure 3.2a shows the distribution of Alpine metamorphic minerals (own mapping), the Bt + St isograd (Droop 1981, 1985) and the 500 and 550° C isotemperature lines after Hoinkes et al. (1999). An amphibolite-facies mineral assemblage characterizes the core of the Hochalm Dome (Höck 1980, stop 196; AS-Gös323, Table A-1, Fig. 3.3). Staurolite is preserved in the Permo-Mesozoic cover between the Hochalm- and Storz nappes (stop 38, sample AS-Mu118, Table A-1, Fig. 3.3) and in the Glockner Nappe System of the Möll Valley (Höck 1980). We observed biotite and garnet in the Modereck- and Glockner nappe system adjacent to the Subpenninic basement (The only exemption is in the area of Mauterndorf, there biotites and garnets are common as shown in Figure 3.2a). Chloritoid is common in the Möll Valley and the Upper Muhr Valley, as originally observed by Höck (1980). High-pressure mineral assemblages are restricted to the vicinity of the Grossglockner Pass (e.g., Dachs and Proyer 2001, Kurz et al. 2008, Pollington and Baxter 2010).

A-1.4 Comparison of the calibrations

We plotted temperature calibrations b, c and d (Table 3.1) against the calibration of Beyssac et al. (2002b) in order to search for systematic variations in temperature estimates. Thus, a diagonal line in the T-T field represents a perfect match in the temperature calibrations. However, a glance at these figures shows that this is never the case, and we discuss some of these variations below.

A-1.4.1 Beyssac et al. 2002b versus Rahl et al. 2005 (Fig. A-2)

For the temperature range of 350° C to 575° C, the difference in estimated peak temperatures is less then ± 30° C, much less than the ± 50° C absolute error (Beyssac et al. 2002b). This is almost identical to the behavior that Wiederkehr et al. (2011) described for the Lepontine area at a similar range of peak temperatures (350° C to 575° C). At three points along the diagonal, the calibrations yield the same peak temperatures (350°, 425°, 530° C). At peak temperatures above 575°C, the difference in peak-temperature estimates increases markedly to about 68° C in the Göss Nappe, where the Rahl et al. (2005) calibration yields 680° C. The calibration of Rahl et al. (2005) has a much greater CI value than that of Beyssac et al. (2002b), primarily due to its more complex formula (Table 3.1). However, the relative uncertainty in the method of Beyssac et al. (2002b) is better than that of Rahl et al. (2005), especially at peak temperatures above 575° C. Wiederkehr et al. (2011) detected an inter-sample variation of c. 10-15° C. Our inter-sample variations are of the same order, but at temperatures above 575° C are greater than 15° C.

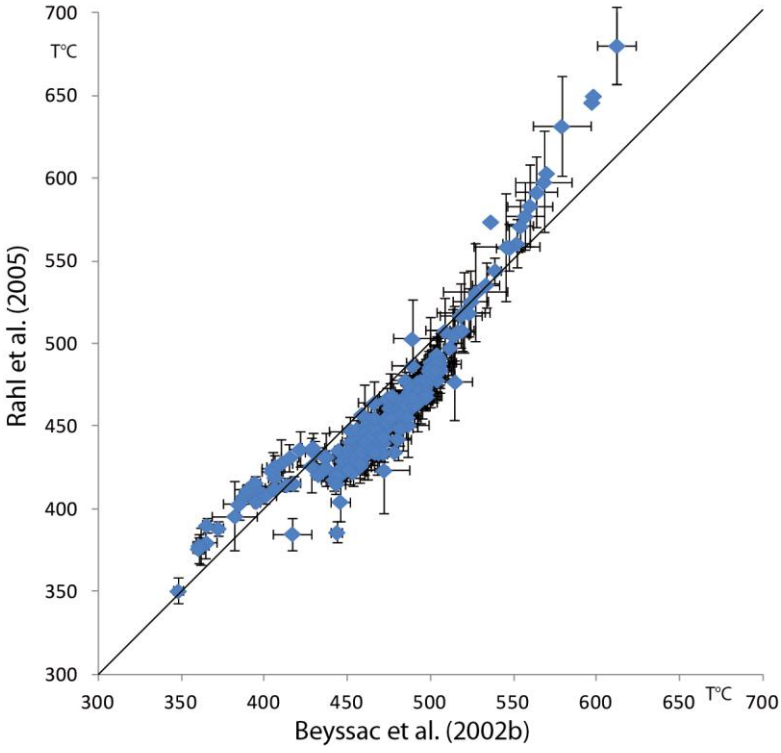

Figure A-2: Calibration plots of peak temperatures according to Beyssac et al. (2002b) and Rahl et al. (2005) with bars marking uncertainties.

A-1.4.2 Beyssac et al. 2002b versus Aoya et al. 2010 (calibration c, Fig. A-3)

These calibrations yield an almost linear systematic difference in temperature estimates over the entire temperature range from 350° C to greater than 600° C. The estimates for both are well below the ± 50° C uncertainty. There is almost no difference in peak temperatures from 350° C to 450° C. A slightly linear increase can be observed from 450° C to 625° C. At 550° C the difference is about 15° C. The maximum difference (28° C) coincides with the highest temperature (612° C Beyssac et al. 2002b; 640° C Aoya et al. 2010). The Aoya et al. (2010) calibration yields a systematically higher peak temperature at temperatures greater than 450° C. Even though the calibration of Aoya et al. (2010) is more complex (Table 3.1, bimodal coefficient), the uncertainty is similar or even somewhat greater than the calibration of Beyssac et al. (2002b). Thus, the peak-temperatures estimated with the calibration of Aoya et al. 2010 (calibration c of Table 3.1) are similar to those of Beyssac et al. (2002b) with inter-sample variations of 10-15° C over the whole temperature range from 350° C to 625° C. We note that even though contact metamorphic rocks were used for the calibration of Aoya et al. (2010), the similarity of the estimates provided by both calibrations indicate that kinetic effects had no significant influence.

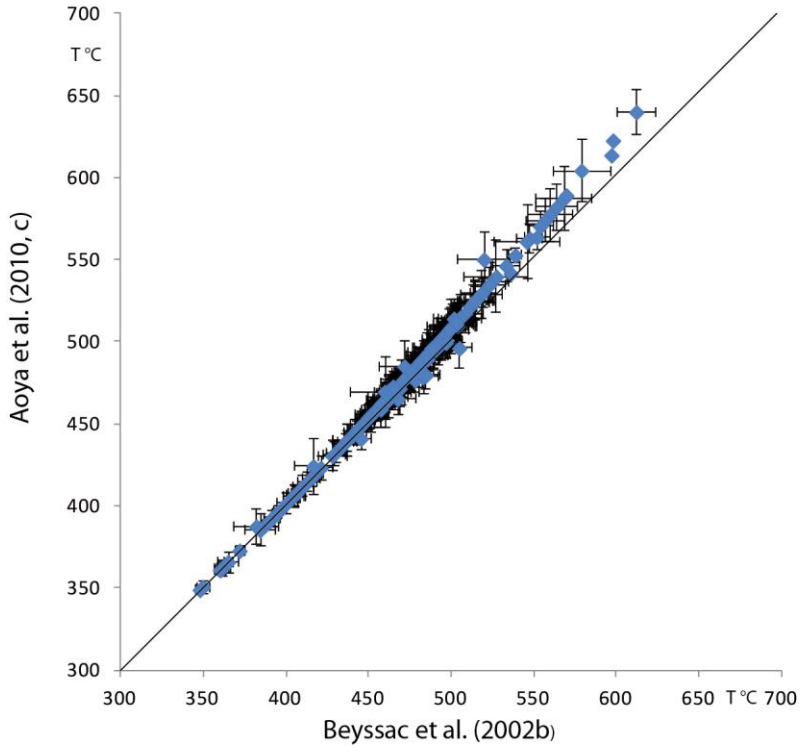

Figure A-3: Comparison plots of peak temperatures according to Beyssac et al. (2002b) and Aoya et al. (2010, calibration c in Table 3.1) with bars marking uncertainties.

A-1.4.3 Beyssac et al. 2002b versus Aoya et al. 2010 (calibration d, Fig. A-4)

Both calibrations are well below the ± 50° C uncertainty. At peak temperatures in the ranges of 350-375° C and 550-575° C, the calibrations yield the same estimates. Between these two coincident peak-temperature ranges (at 475° C), the peak temperatures of Aoya et al. 2010 are systematically lower and the difference in the maximum peak temperature is about 25° C. Above 575° C, the peak-temperature difference increases to 20° C, with the peak temperatures of Aoya et al. 2010 systematically higher (632° C) than of Beyssac et al. 2002b (612° C). As above, the peak temperatures obtained with the Aoya et al. 2010 calibration (d in Table 3.1) are similar to the Beyssac et al. (2002b) calibration. The inter-sample variations are in the range of 10-15° C over the entire temperature range of 350° C to 625° C.

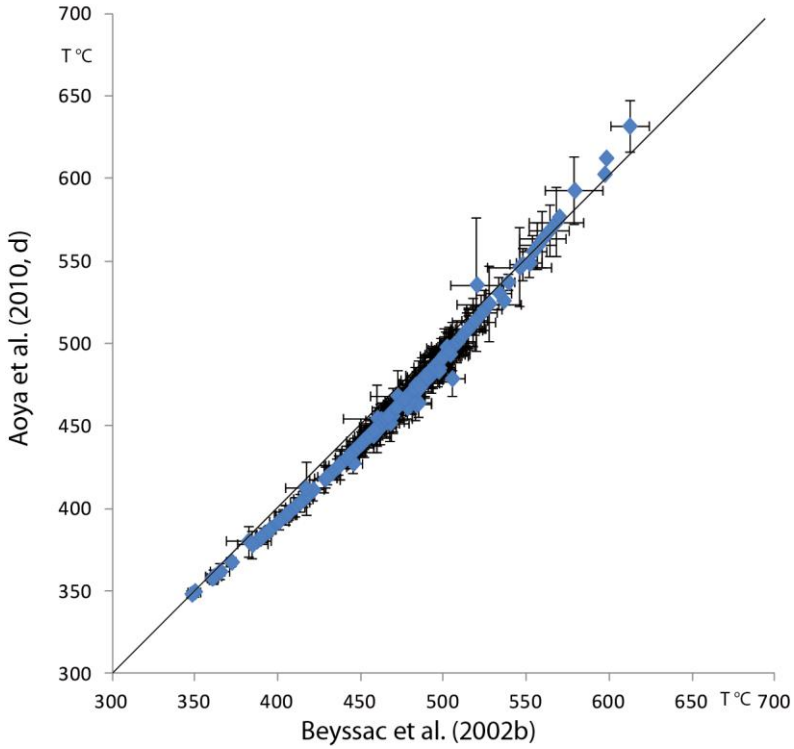

Figure A-4: Comparison plots of peak temperatures according to Beyssac et al. (2002b) and Aoya et al. (2010, calibration d in Table 3.1) with bars marking uncertainties.

A-1.5 Alternative RSCM peak-temperature contours

Figures A-5 to A-7 depicts the contours of peak temperatures in the study area according to the calibrations of Rahl et al. (2005) and Aoya et al. (2010, both calibrations) as listen b-d in Table 3.1 in contrast to the presented results of the calibration of Beyssac et al. (2002b) in Figure 3.4.

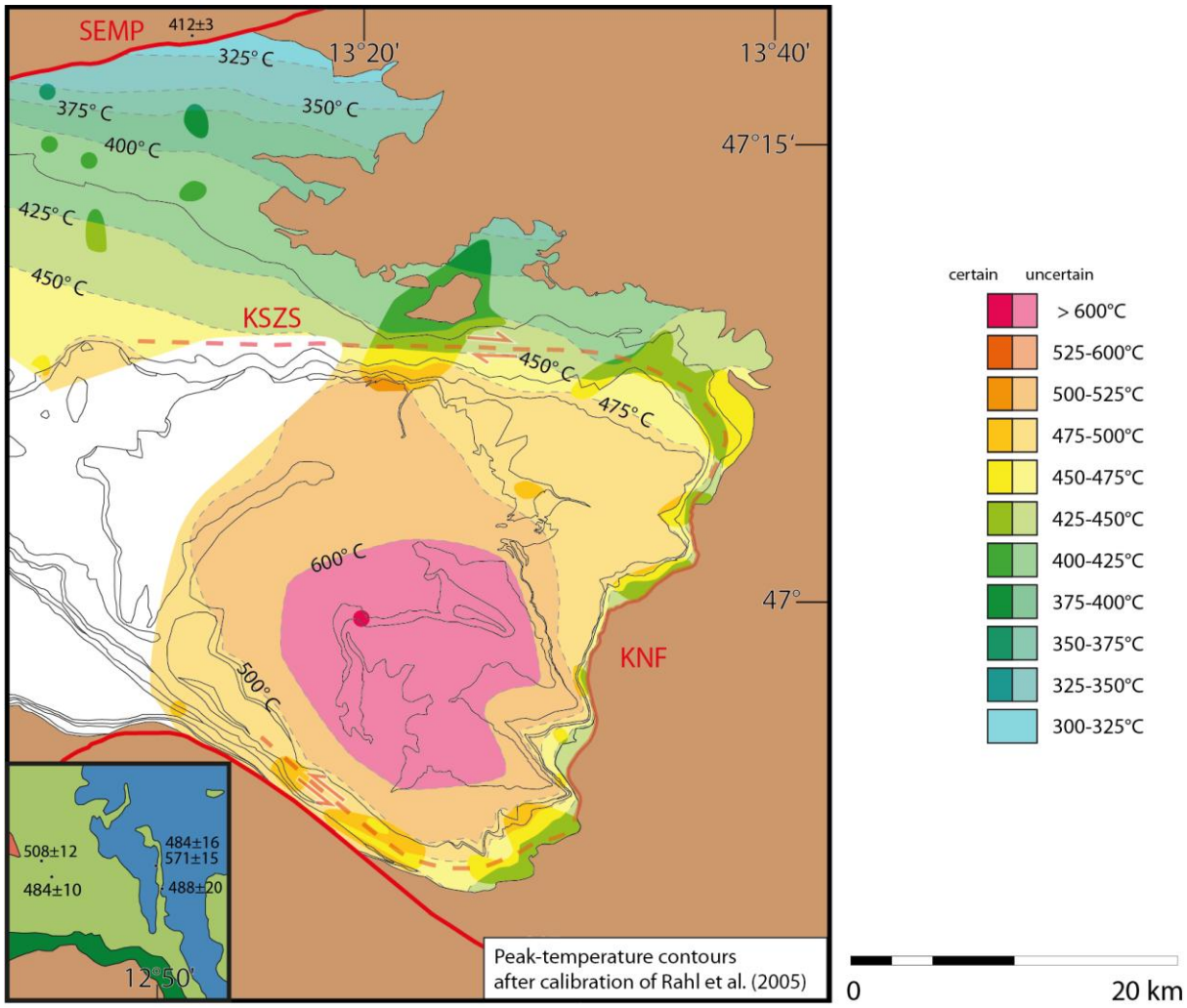

Figure A-5: Peak temperature contours in fabric domains 1 and 3 (Fig. 3.2b) are based on the calibration of Rahl et al. (2005). Transparent colours and dashed lines indicate areas and contours where the sample density is low. Brown colours indicate Austroalpine Units. Grey lines indicate tectonic contacts separating units of the Tauern Window as taken from Schmid et al. (submitted), Chapter 5. Inset shows estimated peak temperatures from the 4 samples in fabric domain 2. Sample locations and data in Figure 3.3 and Table A-1.

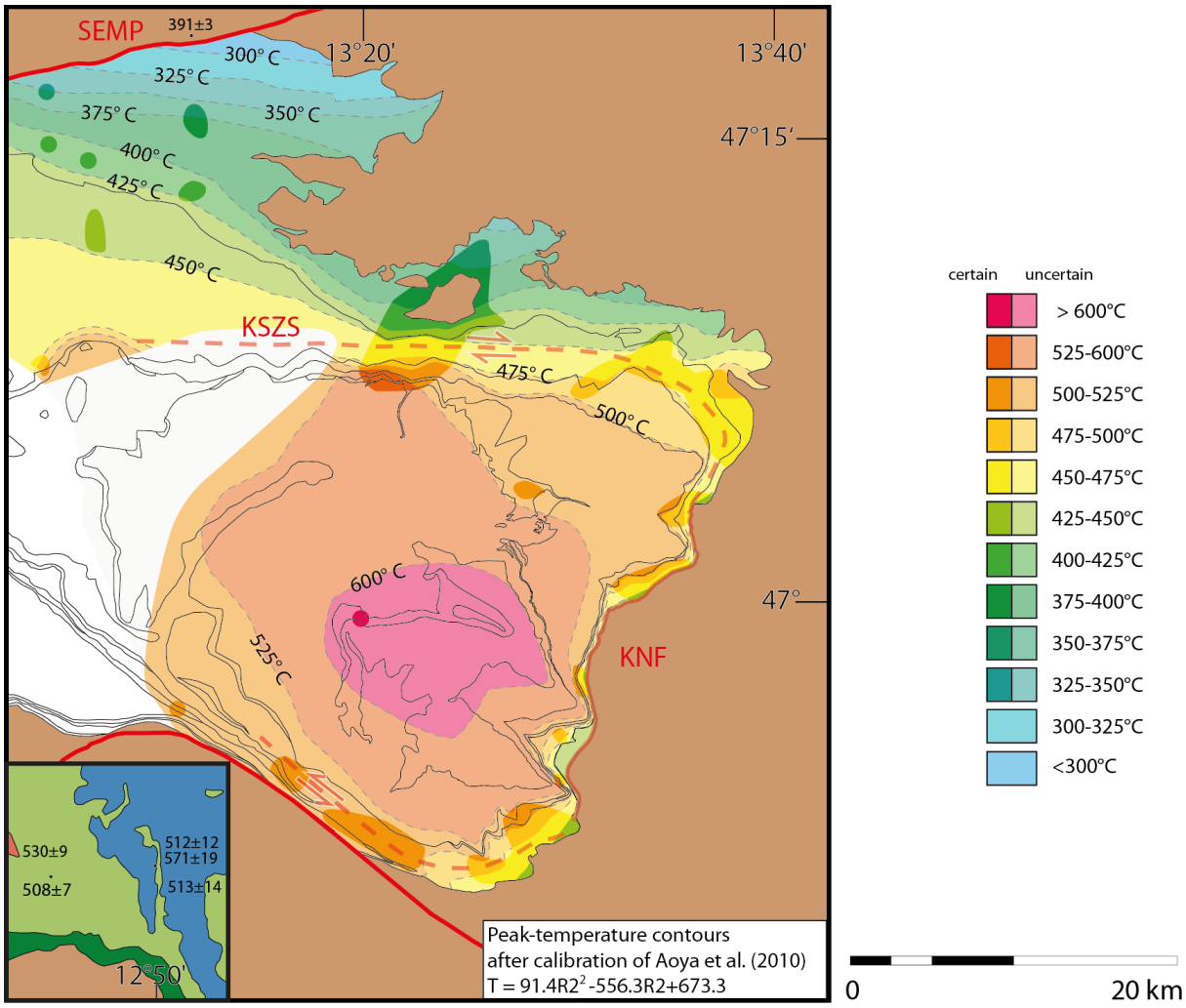

Figure A-6: Peak temperature contours in fabric domains 1 and 3 (Fig. 3,2b) are based on the calibration of Aoya et al. 2010, c in Table 3.1. Transparent colours and dashed lines indicate areas and contours where the sample density is low. Brown colours indicate Austroalpine Units. Grey lines indicate tectonic contacts separating units of the Tauern Window as taken from Schmid et al. (submitted), Chapter 5. Inset shows estimated peak temperatures from the 4 samples in fabric domain 2. Sample locations and data in Figure 3.3 and Table A-1.

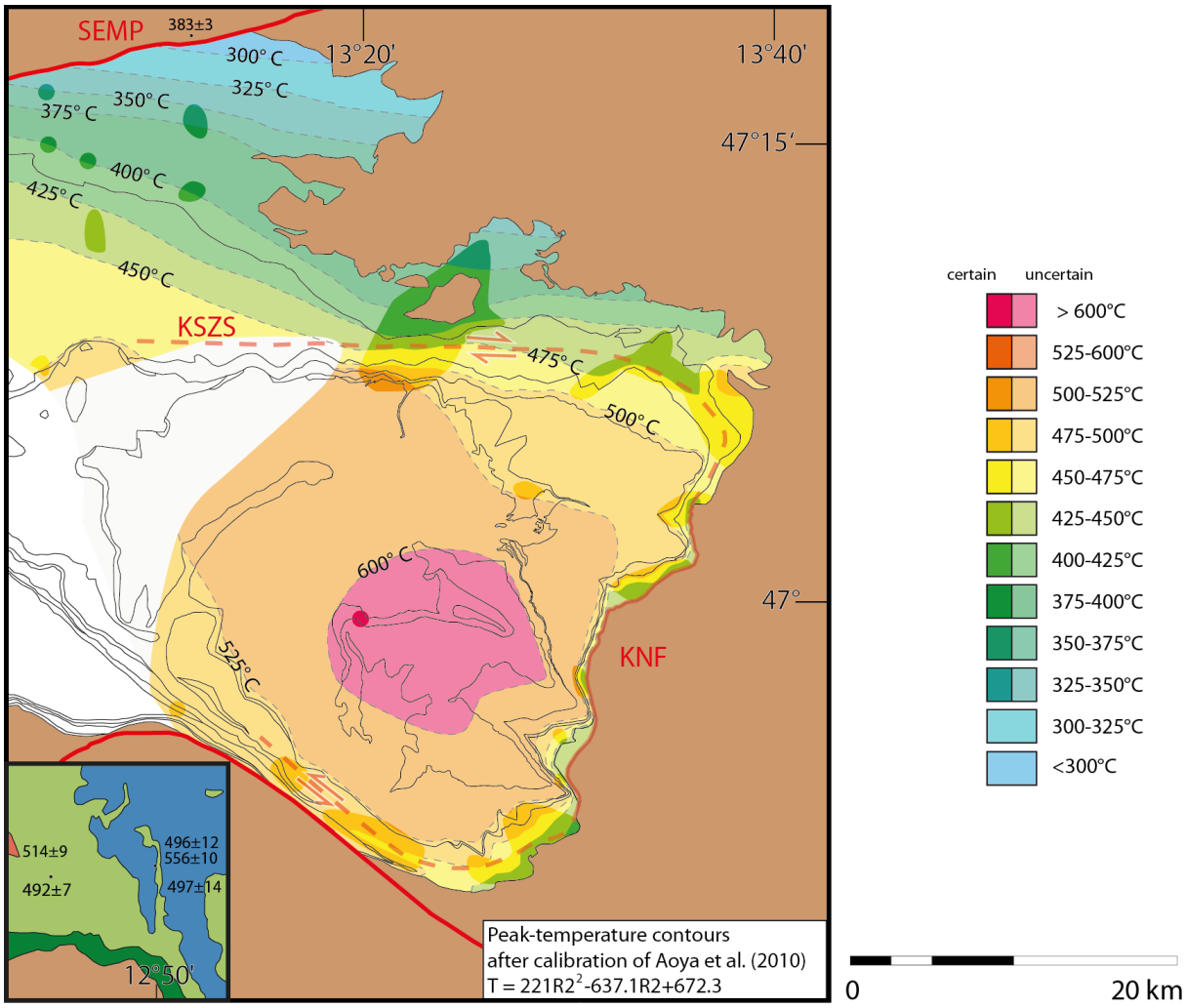

Figure A-7: Peak temperature contours in fabric domains 1 and 3 (Fig. 3.2b) are based on the calibration of Aoya et al. 2010, d in Table 3.1. Transparent colours and dashed lines indicate areas and contours where the sample density is low. Brown colours indicate Austroalpine Units. Grey lines indicate tectonic contacts separating units of the Tauern Window as taken from Schmid et al. (submitted), Chapter 5. Inset shows estimated peak temperatures from the 4 samples in fabric domain 2. Sample locations and data in Figure 3.3 and Table A-1.

A-2 Additional information to Chapter 4

A-2.1 Microprobe analyses of white micas

Microprobe analyses of the white mica composition are report in Chapter 4.4.1 and Table A-2. Table A-2 shows the summary of the white mica compositions of the nine samples including their different microfabrics used in this study. Note that the values are average values.

Table A-2: Summary mica composition

sample	AS1		AS27	AS36	AS41		AS46	AS51		AS52	AS63	AS74	
lithology	mica schist		mica schist	mica schist	mica schist		mica schist	mica schist		mica schist	mica schist	mica schist	
tectonic unit	Gl		Gl	KWN	Mo		Mo	St		St	Si	Si	
mineral	ms	ms	ms	ms	ms	ms	ms	ms	pg	ms	ms	ms	ms
microfabric	= sm	> sm	= sm	no sm	= sm	C'	= sm	= sm	C'	= sm	no sm	< sm	= sm
# analyses	32	17	13	38	3	2	25	23	3	15	56	17	14
SiO_2	49.46	49.32	52.81	49.63	49.82	49.78	49.66	48.11	47.37	50.54	49.92	49.44	49.64
TiO_2	0.11	0.12	0.14	0.19	0.13	0.14	0.15	0.22	0.25	0.21	0.18	0.12	0.12
Al_2O_3	31.77	30.50	26.95	31.07	30.22	32.22	31.64	27.21	28.27	29.47	30.94	30.87	30.58
FeO	2.60	2.17	1.35	2.53	3.39	2.80	1.68	2.37	2.45	3.00	1.52	3.64	3.56
MgO	1.37	1.18	2.85	1.51	1.19	0.91	1.01	2.06	1.72	1.85	1.34	0.92	1.00
CaO	0.01	0.00	0.00	0.00	0.00	0.01	0.00	0.00	0.00	0.00	0.27	0.01	0.01
Na_2O	0.37	0.33	0.02	0.30	0.38	0.53	0.37	0.23	0.23	0.29	0.34	0.39	0.31
K_2O	9.35	9.86	12.19	10.34	10.29	9.90	9.74	10.26	10.41	10.60	9.75	10.34	10.60
Total	95.05	93.49	96.31	95.58	95.43	96.30	94.26	90.46	90.69	95.97	94.26	95.73	95.82
Si	3.33	3.38	3.50	3.32	3.35	3.31	3.37	3.40	3.34	3.38	3.39	3.32	3.33
Ti	0.01	0.01	0.01	0.01	0.01	0.01	0.01	0.01	0.01	0.01	0.01	0.01	0.01
Al	2.52	2.46	2.10	2.45	2.40	2.53	2.53	2.27	2.35	2.32	2.47	2.44	2.42
Fe^{3+}	0.15	0.12	0.07	0.14	0.19	0.16	0.10	0.14	0.14	0.17	0.09	0.20	0.20
Mg	0.14	0.12	0.28	0.15	0.12	0.09	0.10	0.22	0.18	0.18	0.14	0.09	0.10
Ca	0.00	0.00	0.00	0.00	0.00	0.00	0.00	0.00	0.00	0.00	0.02	0.00	0.00
Na	0.05	0.04	0.00	0.04	0.05	0.07	0.05	0.03	0.03	0.04	0.04	0.05	0.04
K	0.80	0.86	1.03	0.88	0.88	0.84	0.84	0.93	0.94	0.90	0.84	0.89	0.91
H	2.00	2.00	2.00	2.00	2.00	2.00	2.00	2.00	2.00	2.00	2.00	2.00	2.00
Total	7.00	7.00	7.00	7.00	7.00	7.00	7.00	7.00	7.00	7.00	7.00	7.00	7.00

Gl – Glockner Nappe System; KWN – Koralpe Wölz Nappe System; Mo – Modereck Nappe System; Si – Silberck Unit (post-Variscan cover); St – Storz Nappe; ms – muscovite; pg – paragonite; > sm – folded white micas (micas are older than the Katschberg-related main foliation); = sm – orientation of the white micas paralle to the Katschberg-related main foliation; C' – shear band associated with the Katschberg-related main foliation; < sm – white micas growing over the Katschberg-related main foliation (micas are younger than the main foliation); no sm – no main foliation could be observed (annealed fabric). See discussion in Chapter 4.4.5.

Curriculum Vitae

For reasons of data protection,
the curriculum vitae is not included in the online version

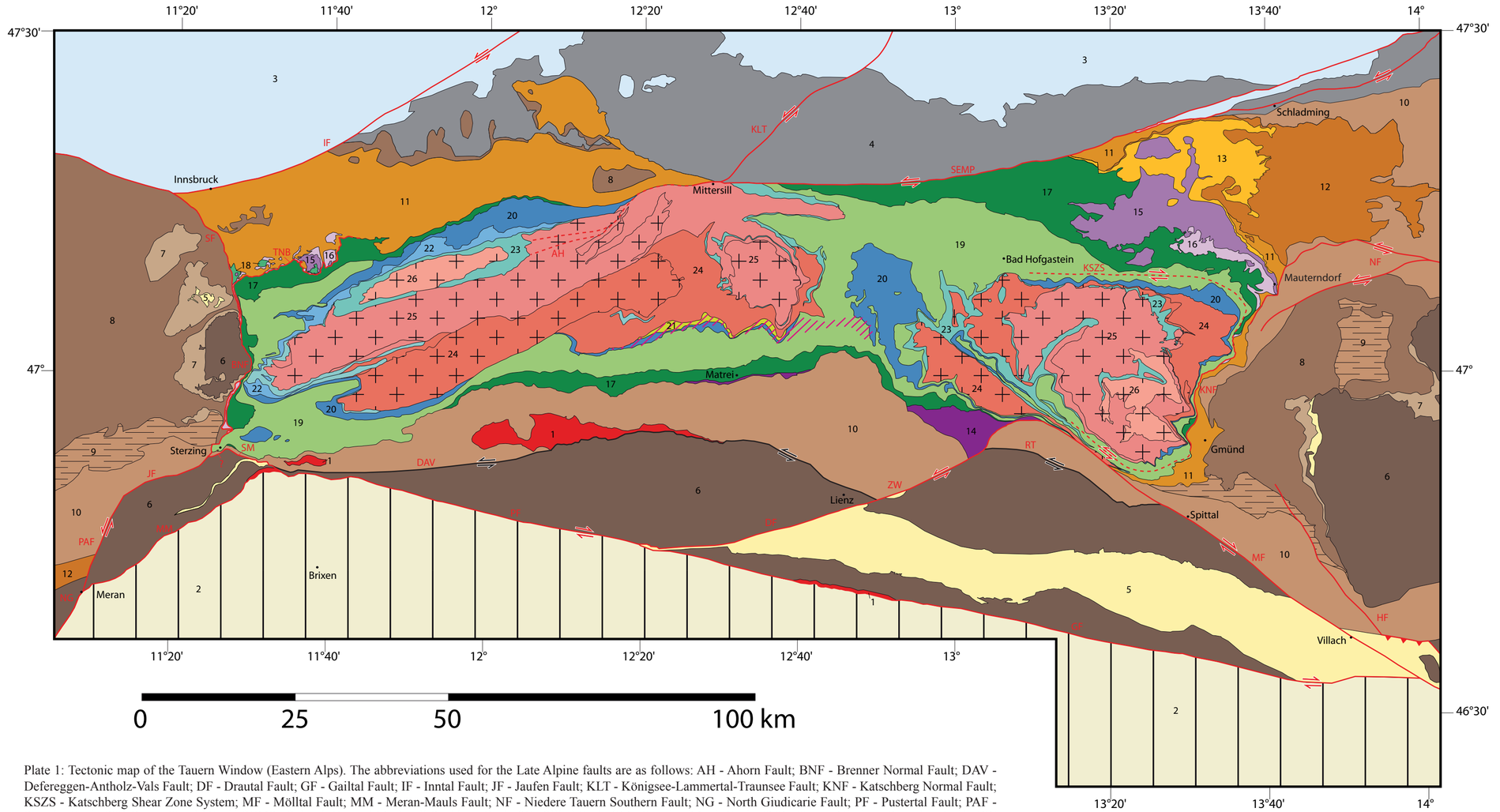

Plate 1: Tectonic map of the Tauern Window (Eastern Alps). The abbreviations used for the Late Alpine faults are as follows: AH - Ahorn Fault; BNF - Brenner Normal Fault; DAV - Defereggen-Antholz-Vals Fault; DF - Drautal Fault; GF - Gailtal Fault; IF - Inntal Fault; JF - Jaufen Fault; KLT - Königsee-Lammertal-Traunsee Fault; KNF - Katschberg Normal Fault; KSZS - Katschberg Shear Zone System; MF - Mölltal Fault; MM - Meran-Mauls Fault; NF - Niedere Tauern Southern Fault; NG - North Giudicarie Fault; PF - Pustertal Fault; PAF - Passeier Fault; RT - Ragga-Teuchl Fault; SEMP - Salzach-Ennstal-Mariazell-Puchberg Fault; SF - Silltal Fault; SM - Sterzing-Mauls Fault; TNB - Tauern Northern Boundary Fault; ZW - Zwischenbergen-Wöllatratten Fault.

1 Periadriatic plutons (Oligocene)
2 Southern Alps

Upper Austroalpine - far-travelled cover nappes
3 Northern Calcareous Alps (Mesozoic)
4 Grauwackenzone (Paleozoic)

Upper Austroalpine - basement and cover nappes
Drauzug-Gurktal Nappe System
5 Mesozoic cover (Blaser Nappe, Mauls Triassic, Drauzug)
6 Basement complexes (Steinach Nappe, South Defregg Units, Gurktal Nappe)
Ötztal-Bundschuh Nappe System
7 Mesozoic cover (Brenner Mesozoic, Stangalm Mesozoic)
8 Variscan basement
Koralpe-Wölz Nappe System
9 Schneeberg-Radenthein Units
10 Texel-Millstatt-Wölz Units
Silvretta-Seckau Nappe System
11 Innsbruck-Wagrain-Katschberg Quartzphyllite Units
12 High-grade Variscan basement (Campo and Schladming nappes)
13 Schladming Nappe - overturned Permo-Mesozoic cover

Lower Austroalpine nappes
14 Lower Austroalpine unit south of the Tauern Window
15 Reckner Nappe including Main Nappe Group of Radstatt Tauern
16 Hippold Nappe including Hochfeind Nappe

Ophiolite-bearing units (Penninic nappes)
17 Matrei Zone (mélange of units derived from Piemont-Liguria Ocean and Austroalpine blocks)
18 Reckner Ophiolitic Complex (Piemont-Liguria Ocean)
19 Glockner Nappe System (prasinites and calcschists, Valais Ocean

Units derived from the distal European margin (Subpenninic nappes)
Units in the hangingwall of the Venediger Duplex
20 Modereck Nappe System
21 Eclogite Zone
22 Wolfendorn Nappe
Venediger Duplex
23 Post-Variscan cover (Permo-Carboniferous and Mesozoic) of nappes in the Venediger Duplex
Permo-Carboniferous intrusions into Variscan basement
24 Zillertal-Riffl, Sonnblick-Romate and Mureck-Storz nappes
25 Tux-Granatspitz and Hochalm nappes
26 Ahorn and Göss nappes

Area of eclogite-facies overprint within the Tauern Window
First-order Mio- Pliocene fault; ductile and brittle; thrusts
First-order Mio- Pliocene fault; ductile
Major Oligocene-age ductile fault

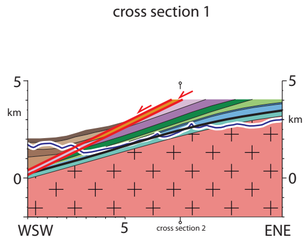

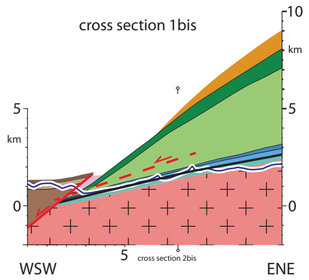

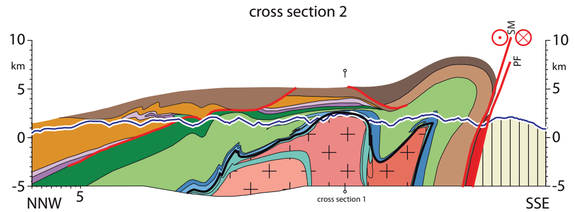

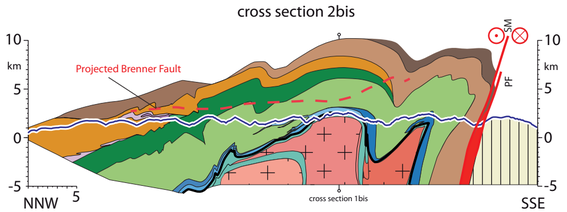

Large parts of cross sections 2 and 2bis follow a profile published by Brandner et al. (2008) and unpublished data from Töchterle (2011); all others are constructed according to published and unpublished maps of the Geologische Bundesanstalt of Austria, as well as own data that include extrapolations based on contouring of the most important tectonic boundaries. In case of profiles 1 and 2 extrapolations above the earth's surface were constructed based on the views expressed in Fügenschuh et al. (2012), while profiles 1bis and 2bis are constructed according to the interpretation by Rosenberg and Garcia (2011). Section 1 depicts two flat-lying brittle normal-fault offsets at the base and the top of the Hippold Unit, squeezed between Matrei Zone and Upper Austroalpine basement; Matrei Zone and units below, down to the top-part of the Subpenninic basement, are mylonitized due to normal-fault-related ductile shearing; based on the work of Töchterle (2011). Later-stage high-angle brittle faulting is regarded as relatively insignificant and hence, not shown in section 1. Section 1bis depicts the top of the Brenner Mylonites that primarily accommodate differential folding of the Tauern Window with respect to the Austroalpine units west of the Brenner Normal Fault (broken red line) as well as a steeper brittle fault (solid line) as contoured in Rosenberg and Garcia (2012). The thickness of the Glockner Nappe System is obtained by projecting upward the 40° west-dip of the contact Matrei Zone to Glockner Nappe System that can be contoured immediately NNE of Sterzing (Plate 1). Note that the scale of the along-strike profiles 1, 1bis, 9 and 10 is twice that of the rest of the profiles oriented perpendicular to strike. See Fig. 5.2 for the cross-section traces.

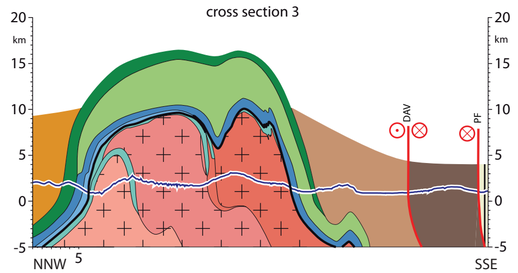

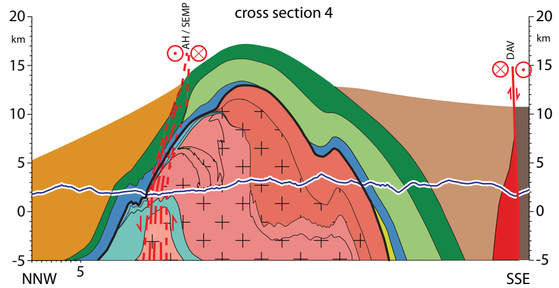

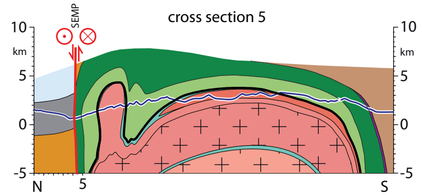

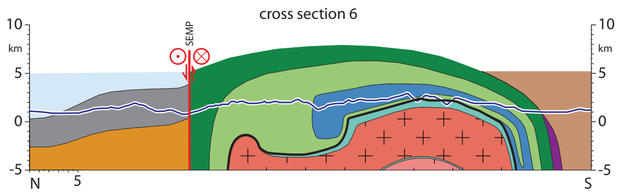

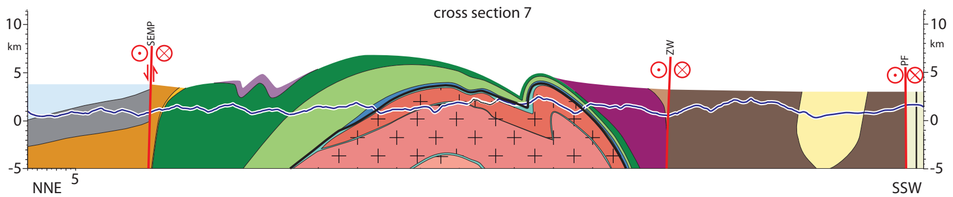

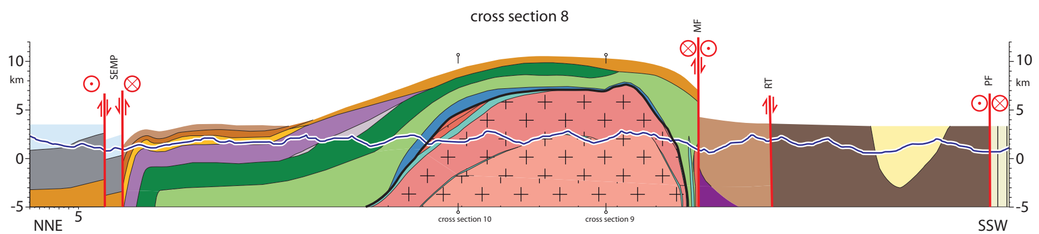

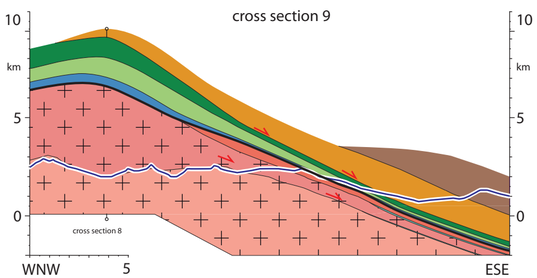

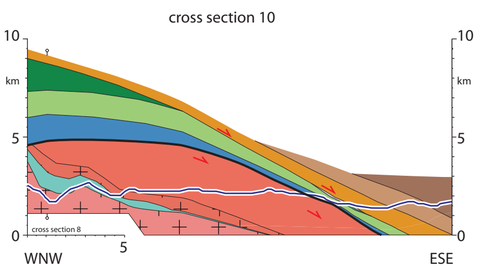

Plate 2: Orogen-perpendicular and -parallel cross sections, illustrating the crustal architecture of the Tauern Window.